RADIO ENGINEERING and ELECTRONIC PHYSICS

English Edition of

РАДИОТЕХНИКА И ЭЛЕКТРОНИКА

Published by the American Institute of Electrical Engineers
with the aid of a grant from the National Science Foundation

No.12 December 1961

Translated and Produced by Royer and Roger, Inc.

AMERICAN INSTITUTE OF ELECTRICAL ENGINEERS

Established 1884

345 East Forty-Seventh Street
New York 17, N.Y.

Warren H. Chase, President
N.S. Hibshman, Executive Secretary
C.E. Dean, Technical Vice President, Communications
W.F. Denkhaus, Director of Publications
L.G. Abraham, Chairman, Communications Division

The English edition of RADIO ENGINEERING AND ELECTRONIC PHYSICS is published by the American Institute of Electrical Engineers with the aid of a grant from the National Science Foundation. © 1961 by American Institute of Electrical Engineers. Also published under the same arrangement are the Russian electronic journals RADIO ENGINEERING and TELECOMMUNICATIONS.

RADIO ENGINEERING AND ELECTRONIC PHYSICS

(РАДИОТЕХНИКА И ЭЛЕКТРОНИКА)

Publication of the Institute of Radio Engineering and Electronic Physics,
Academy of Sciences of the USSR

Translated and Produced
by
Royer and Roger, Inc.

Translation Editor: Ivo Herzer, Columbia University

AIEE REVIEW COMMITTEE FOR RADIO ENGINEERING AND ELECTRONIC PHYSICS
Leonard S. Schwartz
New York University College of Engineering
Chairman

A.W. Bickley
W.P. Birkemeier
T.T.W. Bucher
J.L. Callahan
G.R. Cooper
W.A. Depp
R.S. Enticknap
A. Burr Fontaine
F.E. Froelich
Paul H. Gleichauf
G.S. Glinski
Bernard Harris
R.K. Hellmann
D.E. Higginbotham
B.A. Lengyel
W. Miller
Harry Rowe Mimno
W.W. Peterson
B. Reiffen
W.G. Schmidt
Herbert Sherman
D.L. Solomon
C.A. Stutt
G.Z. Sziklai
Joseph Vogelman
G.M. White
C.H. Wilcox
F.B. Wood
H.L. Yudkin

Subscriptions to Radio Engineering and Electronic Physics should be sent to AIEE
Special Subscription Department
41 East 28th Street, New York 16, New York

1961 Subscription rates:

	$	£
Individuals	28.50	10
Libraries, institutes, govt. agencies	57.00	20

12 issues per annum comprising approximately 1900 pages

INVESTIGATION OF THE RADIATION CHARACTERISTICS OF HIGHLY DIRECTIONAL MIRROR ANTENNAS WITH REFLECTOR OF ALTERNATING PROFILE

N.A. Esepkina, N.L. Kaidanovskii, B.G. Kuznetsov,
G.V. Kuznetsova, S.E. Khaikin

Expressions are derived for the directivity pattern of an antenna with a reflector of alternative profile. It is shown that the form of the in-phase aperture of the antenna under consideration varies with the elevation angle of the principal maximum of the diagram, and this leads to a corresponding change in the width of the diagram in the vertical plane without a change in the antenna gain. The question of parasitic polarization in an antenna with alternating-profile reflector is also considered.

INTRODUCTION

It became clear recently that reflectors of centimeter-wave antennas, with large effective areas, can be constructed of individual elements that are not mechanically connected with each other. This circumstance makes it possible to ensure a greater relative accuracy in such antennas than in antennas with a continuous reflector.

One of the ways of constructing an antenna with divided reflector is to construct an antenna with a reflector of alternating profile. The operating principle of such an antenna and some of its features are considered in references [1, 2, 3, 4, 5].

The purpose of the present investigation was to examine the radiation characteristics of an antenna with an alternating-profile reflector. In this antenna, unlike ordinary antennas with moving pattern, the radiation characteristic in the vertical plane changes with the elevation angle. It is characteristic that this change in the pattern width does not involve a decrease in the gain of the antenna. This feature of the alternating-profile antenna is due to the method employed in this antenna to displace the diagram in space. The directivity diagram is rotated not by moving the entire reflector as a whole, as in ordinary parabolic antennas, but by changing the shape of the reflector.

Together with varying the shape of the reflector, one changes not only the orientation of the in-phase aperture in space, but also the form of the aperture itself. As a result the width of the pattern of an antenna moving in a vertical plane changes in the same plane. The displacement of the main beam of the diagram in azimuth does not change the shape of the beam.

The directivity characteristics of the antenna are determined below both from the value of the field in its in-phase aperture, and from the electric currents in the reflector. Principal attention is paid to an investigation of the antenna field in the forward half space. The side and backward radiation in an antenna having a reflector with alternating profile have approximately the same structure as in ordinary parabolic antennas and can be determined by known methods.

1. FORM OF IN-PHASE APERTURE

The reflector of the antenna described converts a plane wave incoming at an angle Θ_0 into a cylindrical wave with vertical generatrix (or vice versa). By locating any linear radiator in the focus of the reflector, it is possible to focus the converging cylindrical wave to a point.

As described in [1, 2, 3, 4], the reflecting surface of the antenna consists of individual plane elements of height h and width a.

In order for the fields from all elements to add up in phase in the Θ_0 direction, the locus of their centers in the horizontal plane passing through the focus should be the following curve (see Fig. 1)

$$\rho = \frac{p}{1 + \cos\Theta_0 \cos\varphi} = \frac{R_0 - a_0 \cos\Theta_0}{1 + \cos\Theta_0 \cos\varphi}, \tag{1}$$

where p — parameter of the line joining the centers of the elements; Θ_0 — principal direction of the antenna or the angle of elevation of the radiation sources; R_0 — radius of initial circle, on which are situated the elements during the adjustment (or during observation in the zenith); a_0 — constant dependent on the maximum possible displacement of the elements ($a_0/R_0 \ll 1$).

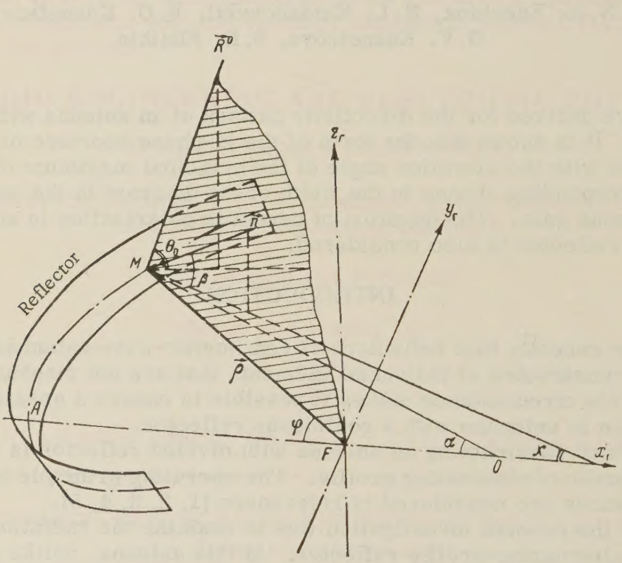

Fig. 1. Profile of reflector.

Equation (1) is the equation of a conic section in a polar system of coordinates with pole at the focus of this section. The eccentricity of the cross section is $\cos\Theta_0$. Inasmuch as $0 \le \cos\Theta_0 \le 1$ $(0 \le \Theta_0 \le \pi/2)$, this is the equation of an ellipse with parameter p, while when $\Theta_0 = 0$ and $\Theta_0 = \pi/2$ we get the equations of a parabola and a circle, respectively.

The equation of the line joining the centers of the elements has in Cartesian coordinates the form

$$y_h^2 + x_h^2 \sin^2\Theta_0 - 2px_h \cos\Theta_0 - p^2 = 0. \tag{1a}$$

The distance from a radiator located at the focus F to the reflector (focal distance) varies in accordance with

$$f = AF = \frac{p}{1 + \cos\Theta_0} = \frac{R_0 - a_0 \cos\Theta_0}{1 + \cos\Theta_0}. \tag{2}$$

The angle of inclination of the normal to the shield ($\vec{n}$) to the horizontal plane (β), or the angle of inclination of the reflecting element to the vertical, is given by [2]

$$\sin\beta = \frac{\sin\Theta_0}{\sqrt{2(1+\cos\Theta_0\cos\varphi)}}.$$

The angle χ between the projection of the normal on the horizontal plane and the axis x_h, which angle characterizes the rotation of the reflecting element relative to the vertical axis, is given by the following expression [3]

$$\operatorname{tg}\chi = \frac{\sin\varphi}{\cos\Theta_0+\cos\varphi}. \tag{4}$$

Let us determine the form of the in-phase aperture of the antenna; for this purpose we project the line joining the centers of the elements on the aperture plane, i.e., on a plane perpendicular to the principal direction (Fig. 2). We align the plane $x_h z_h$ of the horizontal system of coordinates (see Fig. 2), whose origin is at the focus F, with the principal antenna radiation direction (AB).

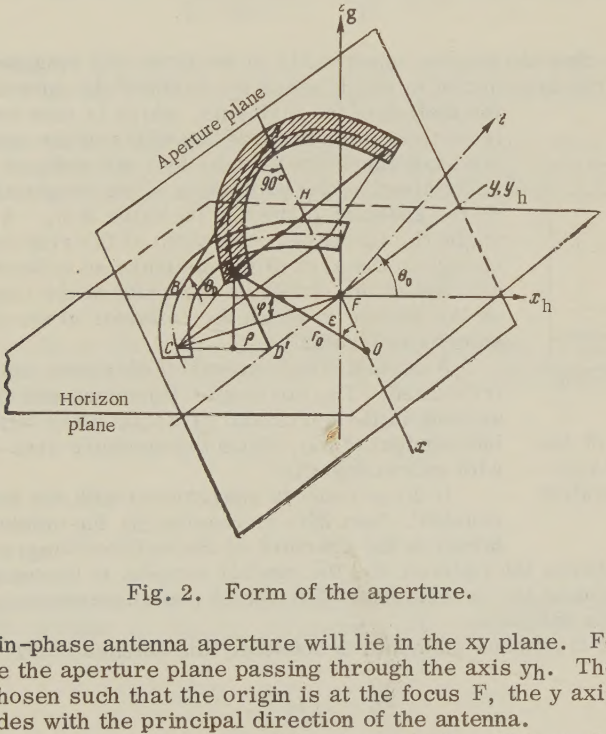

Fig. 2. Form of the aperture.

In this case the in-phase antenna aperture will lie in the xy plane. For convenience in calculation we choose the aperture plane passing through the axis y_h. The coordinates in the aperture plane are chosen such that the origin is at the focus F, the y axis coincides with y_h, and the c axis coincides with the principal direction of the antenna.

Projecting the line joining the centers of the elements (see (1a)) on the xy plane (the aperture plane) and recognizing that

$$y = y_h,\quad x_h = \frac{x}{\sin\Theta_0}, \tag{5}$$

we obtain

$$y^2 + \left(x - p\,\frac{\cos\Theta_0}{\sin\Theta_0}\right)^2 = \frac{p^2}{\sin^2\Theta_0}. \tag{6}$$

This is the equation of a circle with center on the x axis and radius $r = p/\sin\Theta_0$. Figure 3 shows the dependence of r/p on the angle of elevation Θ_0.

The projection of the line joining the centers of the elements is thus for the case $\Theta_0 > 0$ a circle whose radius and center location depend on the angle Θ_0. When $\Theta_0 = 0$ the projection of the line of centers is a straight line. Let us relate the polar angle φ in the horizontal plane with the correspond angle ϵ in the aperture plane, the latter angle being measured between the x axis and the radius drawn from the center of the aperture circle. It is seen from Fig. 2 that

$$OD = r_0 = \frac{p}{\sin\Theta_0}, \quad DH = y = y_h = \rho\sin\varphi = \frac{p\sin\varphi}{1+\cos\Theta_0\cos\varphi},$$

since

$$\rho = \frac{p}{1+\cos\Theta_0\cos\varphi}.$$

Then

$$\sin\varepsilon = \frac{DH}{OD} = \frac{\sin\varphi\sin\Theta_0}{1+\cos\Theta_0\cos\varphi}. \tag{7}$$

We shall assume that the antenna aperture is in the form of a ring and that its width is independent of ϵ. This assumption is valid, since the width of the aperture depends on the inclination of the elements, which in turn varies slightly (≤ 2°) from the center towards the edges of the antenna [see (3)]. We shall therefore assume that the width of the aperture is determined by the projection of the height of the center element on the aperture plane and its value is $h_r = h\cos(\Theta_2/2)$. As the angle Θ_0 increases, the width of the ring decreases. The change in the area of the aperture as a function of Θ_0 is due not only to the change in the width of the ring, but depends also on the method in which the reflector of the alternating-profile antenna is irradiated.

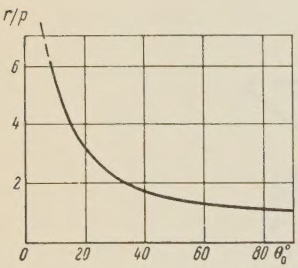

Fig. 3. Dependence of the relative radius of the aperture circle on the elevation angle Θ_0.

A certain fixed number of elements can be installed and irradiated. The horizontal dimension and the resolution of the antenna in the horizontal principal plane will in this case be independent of Θ_0, while the aperture area starts to decrease with increasing Θ_0.

If the antenna is constructed with the radiation angle kept constant, then with increasing Θ_0 the number of elements contained in the aperture of the radiator diagram will increase, since the distance between the radiator and the central element is increased [see (2)]. Consequently the resolution of the antenna in the horizontal plane increases with increasing Θ_0, as does the area of the aperture.

When the number of antenna elements is constant, the antenna horizontal dimension is

$$D_1 = 2p\,\mathrm{tg}\frac{\varphi_0}{2}. \tag{8}$$

Accordingly, for the case when the radiation angle is maintained constant, we have

$$D_2 = 2p\frac{\sin\varphi_0}{1+\cos\Theta_0\cos\varphi_0}, \tag{9}$$

where φ_0 is the angle between the central and outermost elements at $\Theta_0 = 0$ in the former case and the angle determined by the radiator diagram in the latter case.

Fig. 4 shows the dependence of ϵ_0 on Θ_0 for the case of constant aperture 1 and constant irradiation angle 2; ϵ_0 corresponds to the angle between the central and extreme elements in the aperture plane. In both cases $\varphi_0 = 60°$.

Fig. 5 shows the dependence of the horizontal dimension of the antenna on the elevation angle for the same cases.

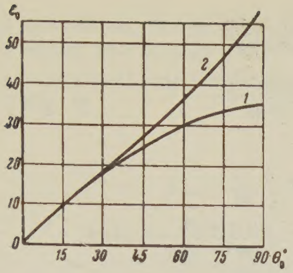

Fig. 4. Dependence of angular length of the arc ϵ_0 in the aperture on the elevation angle Θ_0.

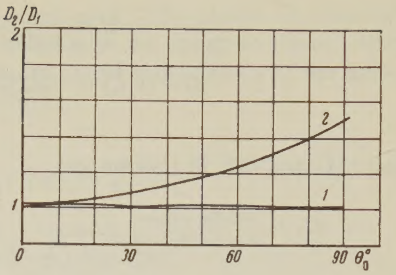

Fig. 5. Increase in horizontal dimension of the antenna due to increasing elevation angle at constant radiation angle.

Thus, the in-phase aperture of an alternating-profile antenna, for all elevation angles ($\Theta_0 \neq 0$), is part of a ring whose width, radius, and central angle vary with the elevation angle Θ_0.

2. DISTRIBUTION OF FIELD IN THE APERTURE OF AN ALTERNATING-PROFILE ANTENNA FOR DIFFERENT POLARIZATIONS OF THE RADIATOR FIELD

We determine the field in the aperture by geometrical optics. It is necessary to assume here that the reflecting surface consists of plane perfectly conducting elements. In this case the well known boundary conditions should be satisfied on the surface of the reflecting elements:

$$[\vec{n}\vec{E}_i] = -[\vec{n}\vec{E}_r], \quad (\vec{n}\vec{E}_i) = (\vec{n}\vec{E}_r), \tag{10}$$

where $\vec{n}$ — normal to the reflecting element; $\vec{E}_i$ — incoming field or radiator field; $\vec{E}_r$ — sought reflected field or field in the aperture. We first consider the case when the radiator field is vertically polarized:

$$\vec{E}_i = A\vec{E}_i^0 = A\vec{i}_{z_h}, \qquad \vec{E}_r = A\vec{E}_r^0$$

In our system of coordinates we have

$$E_{ix}^0 = -\cos\Theta_0, \quad E_{iy}^0 = 0, \quad E_{iz}^0 = \sin\Theta_0. \tag{11}$$

Let us find the components of the normal unit vector in the coordinate system x, y, z, knowing its components in the system x_h, y_h, z_h. It is seen from Figs. 1 and 2 that

$$\begin{gathered} n_{z\,h} = \sin\beta, \qquad \vec{i}_{x\,h} = \vec{i}_z\cos\Theta_0 + \vec{i}_x\sin\Theta_0, \\ n_{x\,h} = \cos\beta\cos\chi, \qquad \vec{i}_{y\,h} = \vec{i}_y, \\ n_{y\,h} = \cos\beta\sin\chi, \qquad \vec{i}_{z\,h} = \vec{i}_z\sin\Theta_0 - \vec{i}_x\cos\Theta_0, \\ \vec{n} = n_{x\,h}\vec{i}_{x\,h} + n_{y\,h}\vec{i}_{y\,h} + n_{z\,h}\vec{i}_{z\,h}, \end{gathered} \tag{12}$$

$\vec{i}_{xh}$, $\vec{i}_{yh}$, $\vec{i}_{zh}$, and $\vec{i}_x$, $\vec{i}_y$, $\vec{i}_z$ = unit vectors along the axes x_h, y_h, z_h and x, y, z respectively.

Using (3), (4), and (12), we obtain

$$n_x = (\vec{n}\vec{i}_x) = \frac{\sin\Theta_0\cos\varphi}{\sqrt{2 + (1 + \cos\Theta_0\cos\varphi)}},$$

$$n_y = (\vec{n}\,\vec{i}_y) = \frac{\sin\varphi}{\sqrt{2(1+\cos\Theta_0\cos\varphi)}},$$

$$n_z = (\vec{n}\,\vec{i}_z) = \frac{1+\cos\Theta_0\cos\varphi}{\sqrt{2(1+\cos\Theta_0\cos\varphi)}}. \tag{13}$$

Substituting (11) and (13) in (10) we get

$$E^0_{rx} = \frac{\cos\Theta_0+\cos\varphi}{1+\cos\Theta_0\cos\varphi} = \cos\varepsilon, \qquad E^0_{ry} = \frac{\sin\varphi\sin\Theta_0}{1+\cos\Theta_0\cos\varphi} = \sin\varepsilon, \tag{14}$$

$$E^0_{rz} = 0, \quad \text{i.e.,} \quad \vec{E}^0_r = -\vec{r}^0.$$

($\vec{r}^0$ — unit vector along the radius from the center of the aperture circle, $r^0_x = -\cos\epsilon$, $r^0_y = -\sin\epsilon$.

It is seen from (14) that in the case of normal (vertical) polarization of the radiator field, the field in the aperture is directed along the radius drawn from the center of the aperture.

In the case of horizontal polarization of the radiator field we have for the incoming field

$$E^0_{ix} = \sin\varphi\sin\Theta_0, \qquad E^0_{iy} = -\cos\varphi, \; E^0_{iz} = \sin\varphi\cos\Theta_0. \tag{15}$$

Substituting (15) and (13) in (10) we obtain

$$E^0_{ry} = \frac{\cos\Theta_0+\cos\varphi}{1+\cos\Theta_0\cos\varphi} = \cos\varepsilon,$$

$$E^0_{rx} = \frac{\sin\varphi\sin\Theta_0}{1+\cos\Theta_0\cos\varphi} = -\sin\varepsilon, \tag{16}$$

i.e.,

$$(\vec{E}^0_r\,\vec{r}^0) = 0.$$

Consequently, in the case of horizontal polarization of the radiator field, the field in the aperture is directed along the tangent to the aperture circle.

Fig. 6 shows the distribution of the field on the aperture in the case of vertical and horizontal radiator polarizations.

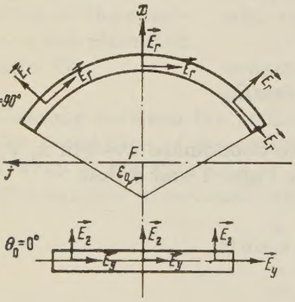

Fig. 6. Character of distribution of field on the aperture in the case of horizontal and vertical polarization.

(vectors along the aperture: $\vec{E}_T$)

3. CALCULATION OF DIRECTIVITY PATTERN

Knowing the form of the aperture and the field distribution on the aperture, we can determine the directivity pattern of the antenna. Let us find the field in the far zone of the antenna, using an approximate diffraction formula [7], which is valid when $i/kr \ll 1$, which in our case holds true

$$\vec{E} = \frac{ik}{2\pi}\int_S [[\vec{n}\vec{E}_1]\,\vec{R}^0]\,\frac{e^{-ikR}}{R}\,ds, \tag{17}$$

where $\vec{n}$ — normal to the aperture plane; $\vec{E}_1$ — field on the aperture; $\vec{R}^0$ — unit vector of the direction to the point of observation; R — distance to the point of observation; S — surface on which the field is specified, in our case the aperture area. No energy is radiated through the side surfaces which can be drawn from the antenna to the aperture plane, since on these surfaces $[\vec{n} \times \vec{E}] = 0$ (vertical polarization). The spherical components of the antenna field in the far zone are (Fig. 7)

$$E_\Theta = \frac{ik}{2\pi}\int\limits_S ([[\vec{n},\ \vec{E}_1]\,\vec{R}^0]\vec{\Theta}_0)\,\frac{e^{-ikR}}{R}\,ds,$$

$$E_\psi = \frac{ik}{2\pi}\int\limits_S ([[\vec{n}\vec{E}_1]\,\vec{R}^0]\,\vec{\psi}_0)\,\frac{e^{-ikR}}{R}\,ds. \tag{18}$$

It is seen from Fig. 7 that

$$n_x = n_y = 0, \qquad n_z = 1,$$
$$R_x^0 = \sin\Theta\cos\psi, \qquad R_y^0 = \sin\Theta\sin\psi,$$
$$R_z^0 = \cos\Theta, \qquad R = R_1 - \vec{r}\vec{R}^0, \qquad \vec{r} = \vec{r}^0 r, \tag{19}$$

Fig. 7. Toward calculation of far-zone field.

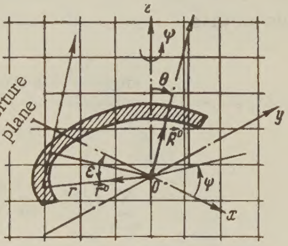

where r — distance from the origin to the element ds on the aperture; R_1 — distance from the point O to the point of observation

$$r_x^0 = -\cos\varepsilon, \qquad r_y^0 = -\sin\varepsilon, \qquad r_z^0 = 0,$$
$$(\vec{r}\vec{R}^0) = -\left(\frac{p}{\sin\Theta_0} + u\right)\sin\Theta\cos(\varepsilon - \psi); \tag{20}$$
$$ds \simeq \frac{p}{\sin\Theta_0}\,du\,d\varepsilon, \tag{21}$$

u varies from $h_r/2$ to $-h_r/2$.

We shall assume that the amplitude distribution of the field in the aperture over the angle ϵ is cosinusoidal and that the distribution along the radius is uniform:

$$\vec{E}_1 = \cos\gamma\varepsilon\vec{E}_1^0\,. \tag{22}$$

Substituting (19), (20), (21), and (22) in (18) and also using formula (14) or (16) for the field on the aperture, we obtain for a radiator with vertically polarized field the following expression

$$E_{\Theta v} = \frac{ik}{2\pi R_1}\,e^{-ikR_1}\,\frac{p}{\sin\Theta_0}\int\limits_S \cos(\varepsilon - \psi)\cos\gamma\varepsilon\, e^{-ik\left(\frac{p}{\sin\Theta_0} + u\right)\sin\Theta\cos(\varepsilon-\psi)}\,du\,d\varepsilon =$$
$$= \frac{A}{\sin\Theta_0}\int\limits_{-\varepsilon_0}^{\varepsilon_0} \cos(\varepsilon - \psi)\cos\gamma\varepsilon\, e^{-ikp\frac{\sin\Theta}{\sin\Theta_0}\cos(\varepsilon-\psi)}\,d\varepsilon \int\limits_{-\frac{h_\Gamma}{2}}^{\frac{h_\Gamma}{2}} e^{-iku\sin\Theta\cos(\varepsilon-\psi)}\,du, \tag{23}$$

$$E_{\psi_{\mathrm{V}}} = -\frac{ik}{2\pi R_1} e^{-ikR_1} \frac{p\cos\Theta}{\sin\Theta_0} \int\limits_{-\varepsilon_0}^{\varepsilon_0} \sin(\varepsilon+\psi)\cos\gamma\varepsilon e^{-ikp\frac{\sin\Theta}{\sin\Theta_0}\cos(\varepsilon-\psi)} d\varepsilon \times$$

$$\times \int\limits_{-\frac{h_{\mathrm{r}}}{2}}^{\frac{h_{\mathrm{r}}}{2}} e^{-iku\sin\Theta\cos(\varepsilon-\psi)}\, du. \tag{24}$$

It is seen from (23) and (24) that the directivity pattern contains the main polarization and parasitic polarization.

For a radiator field with horizontal polarization we can obtain formulas similar to (23) and (24); in this case it is necessary to use (16).

The integrals in (23) and (24) cannot be evaluated exactly. We therefore use for their determination the known expansion

$$e^{-ikp\frac{\sin\Theta}{\sin\Theta_0}\cos(\varepsilon-\psi)} = I_0\left(kp\frac{\sin\Theta}{\sin\Theta_0}\right) + 2\sum_{n=1}^{\infty} I_n\left(kp\frac{\sin\Theta}{\sin\Theta_0}\right) i^{-n}\cos n(\varepsilon-\psi). \tag{25}$$

After integration we obtain

$$E_\Theta = A\frac{1}{\sin\Theta_0}\frac{\sin\left[\frac{kh_{\mathrm{r}}}{2}\sin\Theta\cos\psi\right]}{\frac{kh_{\mathrm{r}}}{2}\sin\Theta\cos\psi}\left\{\cos\psi\left[I_0\left(kp\frac{\sin\Theta}{\sin\Theta_0}\right)f_1(\gamma\varepsilon_0) + \right.\right.$$

$$\left. + \sum_{n=1}^{\infty} J_n\left(kp\frac{\sin\Theta}{\sin\Theta_0}\right) i^{-n}\cos n\psi f_2(n,\gamma,\varepsilon_0)\right] +$$

$$\left. + \sin\psi\left[\sum_{n=1}^{\infty} J_n\left(kp\frac{\sin\Theta}{\sin\Theta_0}\right) i^{-n}\sin n\psi f_3(n,\gamma,\varepsilon_0)\right]\right\}, \tag{26}$$

$$E_\psi = -B\frac{\cos\Theta}{\sin\Theta_0}\frac{\sin\left[\frac{kh_{\mathrm{r}}}{2}\sin\Theta\cos\psi\right]}{\frac{kh_{\mathrm{r}}}{2}\sin\Theta\cos\psi}\left\{\sin\psi\left[J_0\left(kp\frac{\sin\Theta}{\sin\Theta_0}\right)f_1(\gamma\varepsilon_0) + \right.\right.$$

$$\left. + \Sigma J_n\left(kp\frac{\sin\Theta}{\sin\Theta_0}\right)(i)^{-n}\cos n\psi f_2(n,\gamma,\varepsilon_0)\right] +$$

$$\left. + \cos\psi\left[\sum_{n=1}^{\infty} J_n\left(kp\frac{\sin\Theta}{\sin\Theta_0}\right) i^{-n}\sin n\psi f_3(n,\gamma,\varepsilon_0)\right]\right\}, \tag{27}$$

where

$$f_1 = \frac{\sin(\gamma-1)\varepsilon_0}{\gamma-1} + \frac{\sin(\gamma+1)\varepsilon_0}{\gamma+1};$$

$$f_2 = \frac{\sin(n-\gamma-1)\varepsilon_0}{n-\gamma-1} + \frac{\sin(n-\gamma+1)\varepsilon_0}{n-\gamma+1} + \frac{\sin(n+\gamma+1)\varepsilon_0}{n+\gamma+1} + \frac{\sin(n+\gamma-1)\varepsilon_0}{n+\gamma-1};$$

$$f_3 = \frac{\sin(n-\gamma-1)\varepsilon_0}{n-\gamma-1} - \frac{\sin(n-\gamma+1)\varepsilon_0}{n-\gamma+1} - \frac{\sin(n+\gamma+1)\varepsilon_0}{n+\gamma+1} + \frac{\sin(n+\gamma-1)\varepsilon_0}{n+\gamma-1}.$$

In integrating (23) and (24) we assumed that

$$\frac{\sin\left[\frac{kh_{\mathrm{r}}}{2}\sin\Theta\cos(\varepsilon-\psi)\right]}{\frac{kh_{\mathrm{r}}}{2}\sin\Theta\cos(\varepsilon-\psi)} \approx \frac{\sin\left[\frac{kh_{\mathrm{r}}}{2}\sin\Theta\cos\psi\right]}{\frac{kh_{\mathrm{r}}}{2}\sin\Theta\cos\psi}.$$

This assumption is valid, for the dependence on ϵ is weak in our expression ($0 \leq \epsilon \leq 60°$) and manifests itself only at large values of $\sin \Theta$, i.e., in the side lobes.

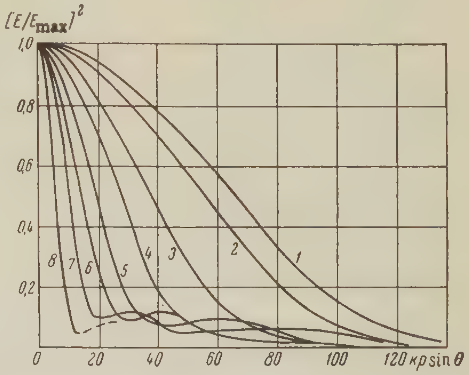

Fig. 8. Vertical antenna diagrams at different elevation angles and constant radiation angle:

$1 - \Theta_0 = 0°$; $2 - \Theta_0 = 10°$; $3 - \Theta_0 = 20°$; $4 - \Theta_0 = 30°$; $5 - \Theta_0 = 40°$; $6 - \Theta_0 = 50°$; $7 - \Theta_0 = 60°$; $8 - \Theta_0 = 90°$.

Figures 8, 9, and 10 show vertical ($\psi = 0$) and horizontal ($\psi = \pi/2$) directivity diagrams for different angles Θ_0 with a fixed number of elements and a constant radiation angle. The diagrams were calculated for a constant distribution of the field in the aperture ($\gamma = 0$).

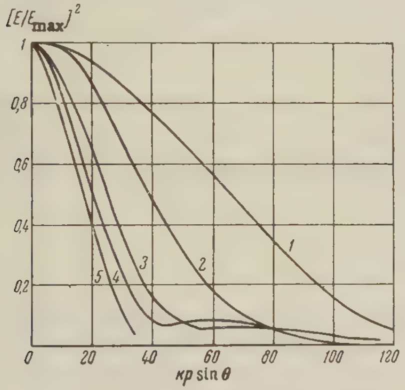

Fig. 9. Vertical antenna diagrams for different elevation angles and constant horizontal dimension:

$1 - \Theta_0 = 0°$; $2 - \Theta_0 = 20°$; $3 - \Theta_0 = 40°$; $4 - \Theta_0 = 60°$; $5 - \Theta_0 = 90°$.

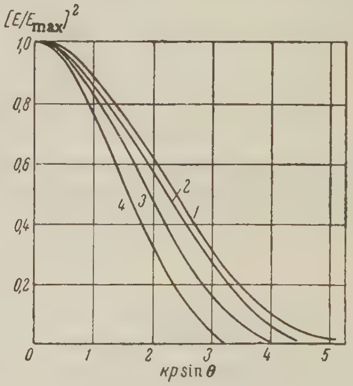

Fig. 10. Horizontal antenna diagrams for different elevation angles and constant radiation angle:

$$D = 2p \left(\frac{\sin \varphi_0}{1 + \cos \varphi_0 \cos \Theta_0}\right):$$

$1 - \Theta_0 = 0°$; $2 - \Theta_0 = 30°$; $3 - \Theta_0 = 60°$; $4 - \Theta_0 = 90°$.

Expressions (26) and (27) determine the field of the antenna for all elevation angles different from zero ($90° \leq \Theta_0 \leq 0$). But as the angle Θ_0 increases, these expressions turn out to be useless for calculation, since the form of the aperture approaches rectangular and the convergence of the series worsens.

It must be noted that the formulas given are not valid when $\Theta_0 = 0$. In this case the in-phase aperture has the form of a rectangle, and the directivity patterns are determined by the known formulas.

From (26) and (27) and from the curves shown in Figs. 8, 9, and 10 we see two features of the directivity patterns of an alternating-profile antenna: the variation of the width of the vertical diagram with the angle Θ_0, and the presence of parasitic polarization.

The vertical diagram depends on the angle of observation Θ_0. Whereas the antenna has a

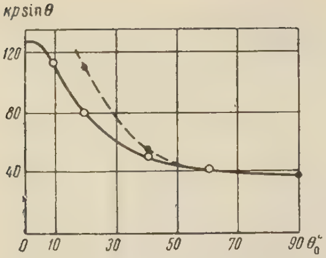

Fig. 11. Dependence of the width of the vertical antenna diagram at the 0.5 P_{max} level on the elevation angle at constant horizontal dimension.

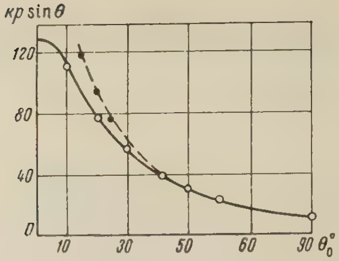

Fig. 12. Dependence of the width of the vertical antenna diagram at the 0.5 P_{max} level on the elevation angle at constant angle of radiation.

knife-like diagram when $\Theta_0 = 0$, the directivity pattern becomes closer to needle-like when $\Theta_0 = 90°$. This is due to the influence of the depth on the in-phase aperture H, equal to the segment AH (see Fig. 2). At small elevation angles $0 < \Theta_0 \leq 10°$, when the depth of the aperture, which is equal to the projection of the antenna depth H_0 on the aperture ($H = H_0 \sin \Theta_0$), is either commensurate with the height h of the element or smaller than this height, so that the diagram is determined by the dimension of the element. When $\Theta_0 > 10°$, the diagram is determined essentially by the depth of the aperture and becomes narrower with increasing elevation angle, i.e., with increasing depth. The width of the vertical diagram at the half-power level ($\Theta_{0.5P_{max}}$) varies approximately as

$$\Theta_{0.5\,P_{\max}} \sim \frac{\lambda}{H_0 \sin \Theta_0}. \tag{28}$$

In the case of an antenna with a fixed number of elements, H_0 is constant and given for an antenna with a fixed radiation angle by the formula

$$H_0 = p\left[\frac{1}{1+\cos\Theta_0} - \frac{1}{2+\cos\Theta_0}\right], \quad \varphi_0 = 60°. \tag{29}$$

Figures 11 and 12 show the width of the vertical diagram determined from the curves of Figs. 8 and 9 for various angles Θ_0. The same figures show dashed the width of the vertical diagram determined from (28) and (29). The agreement between the curves indicates that the width of the vertical diagram is actually determined by the depth of the aperture.

The variation of the horizontal diagram with the elevation angle is due to the increase in the horizontal dimension of the antenna and occurs only at a constant radiation angle.

The narrowness of the vertical diagram of an alternating-profile antenna is due to the curving of the aperture and not to the increase in its area; this narrowing therefore does not increase the gain. This question will be discussed later on in greater detail.

The narrowing of the diagram at the 0.5 P_{max} level is offset by the appearance of a small radiation level distributed in a large solid angle.

Fig. 13 shows sections of the directivity pattern for $\Theta_0 = 90°$, taken at planes parallel to the aperture plane at levels 0.5 P_{max} and 0.05 P_{max}. The points for these sections are taken from Fig. 14, which shows the azimuthal cross sections through the diagrams, i.e., intersections with planes passing through the optical axis of the antenna system. As can be seen from Figs. 13 and 14, at high elevation angles ($\Theta_0 \to 90°$) the narrowing of the principal lobe of the diagram is accompanied by a redistribution of the radiated energy to lateral directions that are close to the principal direction. As a result "tails" appear in the principal lobe of the diagram, and contain a large fraction of the radiated energy. This is why the antenna gain does not increase as $\Theta_0 \to 90°$.

It must be noted that at radiation angles outside the directivity pattern of each individual element ("shield") the level of the side bands is comparatively small and does not exceed 0.5 percent of P_{max}.

It is seen from (26) and (27) that lobes with parasitic polarization appear in the antenna diagram. The size of these lobes increases with increase of Θ_0 (see Fig. 15). The shaded areas in Fig. 13 indicate the directions of parasitic polarization (cross polarization) exceed 5 percent of P_{max}. As can be seen from Fig. 13, lobes with parasitic polarization are concentrated toward the horizontal main section of the diagram ($\psi = \pi/2$). This is precisely the difference between an antenna having an alternating-profile reflector and an ordinary antenna of the type of paraboloid of revolution, in which the lobes of the parasitic polarization make an angle of 45° to the principal planes of the antenna.

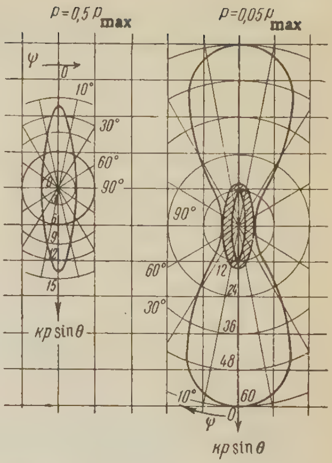

Fig. 13. Cross section through the three-dimensional diagram ($\Theta_0 = 90°$) taken at planes perpendicular to the optical axis, at the levels 0.5 P_{max} and 0.05 P_{max}. The shaded area shows where the level of parasitic polarization exceeds five percent.

The field in the parasitic lobes of the alternating-profile antenna has a phase shift $\pi/2$ relative to the main polarization. Consequently the polarization of the signal in the lateral directions, in an antenna with alternating profile, will be elliptical, while for definite angles Θ, for which the main and cross polarization components are equal, the polarization will be circular.

The presence of parasitic polarization makes it difficult to carry out polarization observations with an alternating-profile antenna, and also decreases somewhat the utilization coefficient, particularly at large Θ_0. It is therefore desirable to eliminate this polarization. For this purpose it is necessary to construct the antenna radiator with a definite polarization directivity pattern. The dependence of the polarization of the radiator field on the angle φ should be such that the polarization on the aperture be constant throughout the aperture (horizontal or vertical). In this case there will be no parasitic circular polarization. Such a radiator can be constructed. Some ways of constructing such a radiator are considered in reference [8].

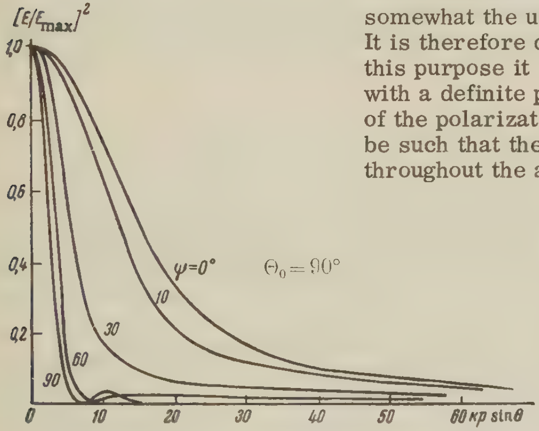

Fig. 14. Section through the three-dimensional diagram ($\Theta_0 = 90°$) at planes passing through the optical axis (vertical diagram when $\Psi = 0°$ and horizontal diagram when $\Psi_0 = 90°$).

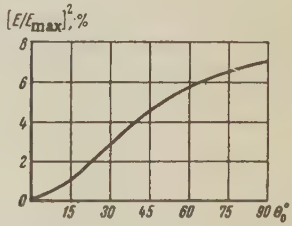

Fig. 15. Dependence of the relative power in the lobes with parasitic polarization on the elevation angle.

Formulas (26) and (27) were used to calculate diagrams for a cosinusoidal field distribution on the aperture (the case $E_{\epsilon = \epsilon_0} = 0.3\ E_{max}$).

In this case the diagrams still have the features indicated above. The falling-off distribution broadens the horizontal diagram by approximately 1.2 times and the vertical diagram by 1.4 times, and the level of the parasitic-polarization lobes is reduced thereby.

Directivity patterns were also calculated from the currents in the reflector. In this case the expression obtained for the main component of the field in vertical polarization of the radiator field and uniform radiation of the reflector is

$$E_\theta = A \int_{-\varphi_0}^{\varphi_0} V_1(\Theta, \varphi, \psi) V_2(\Theta, \varphi, \psi) e^{-ikp\Phi(\Theta, \varphi, \psi)} \, d\varphi, \tag{30}$$

where

$$V_1(\Theta, \varphi, \psi) = \frac{\sin\Theta \sin\Theta_0 \cos\varphi + \cos\Theta\,(1 + \cos\Theta_0 \cos\varphi)}{\sqrt{1 + \cos\Theta_0 \cos\varphi}\,\sqrt{(1 + \cos\Theta_0 \cos\varphi)^2 + \sin^2\Theta_0}};$$

$$V_2(\Theta, \varphi, \psi) = \int_{-h/2}^{h/2} e^{-ikuF(\Theta, \varphi, \psi)} \, du;$$

$$\Phi(\Theta, \varphi, \psi) = \frac{1 + \sin\varphi \sin\psi + \cos\Theta \cos\varphi \cos\psi}{1 + \cos\Theta_0 \cos\varphi};$$

$$F(\Theta, \varphi, \psi) = \frac{\sin\Theta_0\,(1 + \cos\varphi \cos\Theta \cos\psi + \sin\varphi \sin\psi) - (1 + \cos\Theta_0 \cos\varphi) \cos\psi \sin\Theta}{\sqrt{(1 + \cos\Theta_0 \cos\varphi)^2 + \sin^2\Theta_0}}$$

It is seen from (30) that in the principal direction $\Theta = \Theta_0$, $\psi = 0$, the fields from all the elements of the alternating-profile antenna add up in phase for all values of Θ_0. Indeed

$$F(\Theta_0, \varphi, 0) = 0,$$

$$\Phi(\Theta_0, \varphi, 0) = \frac{1 + \sin\varphi \sin\psi + \cos\Theta \cos\varphi \cos\psi}{1 + \cos\Theta_0 \cos\varphi} = \frac{1 + \cos\Theta_0 \cos\varphi}{1 + \cos\Theta_0 \cos\varphi} = 1.$$

The reason for it is that in an alternating-profile antenna the curve joining the centers of the elements ($\rho = p/(1 + \cos\theta_0 \cos\varphi)$ varies, whereas in an ordinary parabolic cylinder with electric beam rocking by a considerable amount ($\Theta_0 \neq 0$) the fields from the individual parts of the antenna do not add up in phase in the principal direction, and this results in distortion of the diagram. In this case

$$\Phi = \left. \frac{1 + \sin\varphi \sin\psi + \cos\Theta \cos\varphi \cos\psi}{1 + \cos\Theta_0 \cos\varphi} \right|_{\psi=0,\ \Theta=\Theta_0} = \frac{1 + \cos\Theta_0 \cos\varphi}{1 + \cos\varphi} \neq \text{const},$$

since $\rho = p/(1 + \cos\varphi)$. Expression (30) cannot be integrated exactly except when $\Theta_0 = 90°$. Under certain assumptions, expression (30) can be approximately integrated, while when $\Theta_0 \leq 60°$ rather simple expressions are obtained for the directivity pattern. The directivity patterns were calculated for different Θ_0 and were found to be similar to the diagrams of Figs. 8, 9, and 10.

4. COEFFICIENT OF UTILIZATION OF THE APERTURE SURFACE OF AN ALTERNATING-PROFILE ANTENNA

Let us determine the coefficient of utilization of the aperture surface of an alternating-profile antenna for different observation angles Θ_0. We shall assume that the antenna is ideal, i.e., there are no phase errors on the aperture of the antenna. Consequently in this case the utilization coefficient will be determined only by the distribution of the field amplitude on the aperture and by the magnitude of the parasitic polarization component. The gain of the in-phase aperture is [9]

$$G = \frac{4\pi}{\lambda^2} \frac{\left| \int_S F_{\text{main}}(\xi, \eta) \, ds \right|^2}{\int_S F^2(\xi, \eta) \, ds},$$

where $F(\xi, \eta) = \sqrt{F^2_{\text{main}} + F^2_{\text{par}}}$ – amplitude distribution of the field over the aperture;

$F_{\text{main}}(\xi, \eta)$ – amplitude distribution of the main polarization over the field aperture;

$F_{\text{par}}(\xi, \eta)$ — amplitude distribution of the cross-polarization field over the aperture.

In the calculations we have assumed everywhere that the field distribution over the height of the element (width of the aperture is hk) is uniform; therefore

$$F = f(\varepsilon) = \cos\gamma\varepsilon,$$
$$F_{\text{main}} = \cos\gamma\varepsilon\cos\varepsilon, \qquad F_{\text{par}} = \cos\gamma\varepsilon\sin\varepsilon,$$
$$F^2 = F^2_{\text{main}} + F^2_{\text{par}} = \cos^2\gamma\varepsilon\,(\sin^2\varepsilon + \cos^2\varepsilon) = \cos^2\gamma\varepsilon.$$

Then

$$G = \frac{4\pi}{\lambda^2}\,\frac{\left|\displaystyle\int\limits_{r_0-\frac{h}{2}\cos\frac{\Theta_0}{2}}^{r_0+\frac{h}{2}\cos\frac{\Theta_0}{2}}\int\limits_{-\varepsilon_0}^{\varepsilon_0}\cos\gamma\varepsilon\cos\varepsilon r\,dr\,d\varepsilon\right|^2}{\displaystyle\int\limits_{r_0-\frac{h}{2}\cos\frac{\Theta_0}{2}}^{r_0+\frac{h}{2}\cos\frac{\Theta_0}{2}}\int\limits_{-\varepsilon_0}^{\varepsilon_0}\cos^2\gamma\varepsilon\,[\sin^2\varepsilon + \cos^2\varepsilon]\,r\,dr\,d\varepsilon}, \tag{31}$$

where $r_0 = p/\sin\Theta_0$ — radius of the in-phase aperture. Integrating (31) we obtain

$$G = \frac{4\pi}{\lambda^2}\,2r_0\varepsilon_0 h\cos\frac{\Theta_0}{2}\,\frac{\left[\frac{\sin(\gamma-1)\varepsilon_0}{\gamma-1} + \frac{\sin(\gamma+1)\varepsilon_0}{\gamma+1}\right]^2}{\varepsilon_0^2\,2\left[1 + \frac{\sin 2\gamma\varepsilon_0}{2\gamma\varepsilon_0}\right]} = \frac{4\pi}{\lambda}\,S_{\text{aper}}\,\eta, \tag{32}$$

where

$$\eta = \frac{\left[\frac{\sin(\gamma-1)\varepsilon_0}{\gamma-1} + \frac{\sin(\gamma+1)\varepsilon_0}{\gamma+1}\right]^2}{2\left(1 + \frac{\sin 2\gamma\varepsilon_0}{2\gamma\varepsilon_0}\right)\varepsilon_0^2}; \qquad S_{\text{aper}} = 2r_0\varepsilon_0 h\cos\frac{\Theta_0}{2}; \tag{33}$$

η — utilization coefficient.

It is seen from (32) that the gain changes with the angle Θ_0, both because of the change in the utilization coefficient η, and the change in the aperture area.

Let us see how the utilization coefficient varies with Θ_0. It is seen from (33) that in the case of uniform radiation ($\gamma = 0$) the utilization coefficient is

$$\eta = \left(\frac{\sin\varepsilon_0}{\varepsilon_0}\right)^2. \tag{34}$$

Θ_0°	$\gamma = 0$		$\gamma\varepsilon_0 = \frac{\pi}{2}$	
	η_1	η_2	η_1	η_2
20	1	1	0,81	0,81
30	0,96	0,96	0,79	0,79
45	0,94	0,92	0,77	0,76
60	0,90	0,85	0,76	0,74
90	0,87	0,69	0,75	0,71

In a cosinusoidal distribution when $\gamma\epsilon_0 = \pi/2$ (the field is equal to zero on the edge of the aperture for all Θ_0) we have

$$\eta = \frac{1}{2}\left[\frac{\sin\left(\frac{\pi}{2} - \varepsilon_0\right)}{\frac{\pi}{2} - \varepsilon_0} + \frac{\sin\left(\frac{\pi}{2} + \varepsilon_0\right)}{\frac{\pi}{2} + \varepsilon_0}\right]^2. \tag{35}$$

The table lists the utilization coefficients calculated from (34) and (35) for a constant horizontal antenna dimension (η_1) and for a constant radiation angle $\varphi_0 = 60°$ (η_2). In the calculation we make use of the dependence $\epsilon_0 = f(\Theta_0)$ shown in Fig. 4.

It is seen from the table that in the case of a falling-off distribution the utilization coefficient changes little with changing Θ_0.

In conclusion, the authors are grateful to B.V. Braude for valuable hints and for participation in the discussion of the results.

REFERENCES

1. S.E. Khaikin, N.L. Kaidanovskii. Instruments and Measurement Techniques. 1959, 2, 19.
2. N.A. Esepkina. Abstract of Candidate Dissertation, Kalinin Leningrad Polytechnic Institute, 1958.
3. Investigation of the feasibility of a radiotelescope with alternating reflector profile with output aperture 10,000–20,000 m^2 for centimeter waves. Report of Kalinin Leningrad Polytechnic Institute, 1959.
4. S.E. Khaikin, N.L. Kaidanovskii, N.A. Esepkina, O.N. Shivris. News of the Main Astronomical Observatory, 1960, 21, issue 5, no. 164, 3.
5. B.V. Braude, N.A. Esepkina, N.L. Kaidanovskii, S.E. Khaikin. Radiotekhnika i Elektronika, 1960, 5, 4, 584.
6. V.Yu. Petrun'kin. Candidate dissertation, Kalinin Leningrad Polytechnic Institute, 1953.
7. V.Yu. Petrun'kin. Transactions Kalinin Leningrad Polytechnic Institute, 1955, no. 181, page 75.
8. N.S. Soboleva, G.V. Kuznetsova. Paper delivered at the expanded plenum of the commission on radioastronomy. Astronomic Council of the Academy of Sciences USSR, Moscow, 1960.
9. Microwave Antennas (translated from the English). Vol. 1, Soviet Radio Press, 1950.

Received by editor 22 February 1961

FLUCTUATIONS OF THE THERMAL RADIATION OF THE ATMOSPERE AT CENTIMETER AND MILLIMETER WAVELENGTHS

N.A. Armand

The fluctuations of thermal radiation of the atmosphere are theoretically investigated. Formulas are obtained for the dispersion of the brightness temperature of an antenna in the case of cloudless atmosphere and in the case when a statistically uniform cloud layer is present in the atmosphere. Calculations are made of the angular correlation of the thermal radiation of the atmosphere.

INTRODUCTION

A widely used observation method in radioastronomy is to detect astronomic objects by their own radiation. This radiation, naturally, is observed against the background of the thermal radiation of the atmosphere. Consequently an investigation of the characteristics of the atmosphere's thermal radiation is of great significance. At present the most detailed investigations concerned the mean values of the thermal radiation of the atmosphere [1—4]. Little study has been made of the fluctuation properties of this radiation. As far as this author knows, only one article [7] contains estimates of the intensity of the fluctuations of the brightness temperature of an antenna used to register the thermal radiation of the atmosphere, obtained on the basis of the spectral method. It is assumed in this paper, first, that the brightness temperature of the antenna is much less than the thermodynamic temperature of the atmosphere, and that the fluctuations of the radiation of the atmosphere are due essentially to fluctuations in temperature. In addition, the author of [7] transfers quite arbitrarily, in our opinion, the statistical properties of the temperature T of the atmosphere to a quantity αT (our notation), where α is the coefficient of absorption of the atmosphere and T its temperature.

The analysis presented below is free of these assumptions and enables us to investigate strong absorption of radiation in the atmosphere, to take into account fluctuations in the humidity, which manifest themselves most effectively at millimeter wavelengths. Although the numerical results are approximately the same in the corresponding portions of the radio band under identical conditions (cloudless atmosphere), nonetheless the results are qualitatively different. The difference lies, in particular, in the fact that in our calculations the square of the antenna temperature dispersion is proportional to the first power of the external scale of the turbulence fluctuations, whereas in [7] the square of the temperature dispersion of the antenna is proportional to the cube of this scale. In our opinion, the reason for this difference lies in the fact that the author of [7] used for the three-dimensional spectral density a formula in the form $k^{-11/3}$, whereas the sense of the transport equation calls for the use of a one-dimensional spectral density in the form $k^{-5/3}$.

Our paper consists of three parts. The first establishes the statistical property of the coefficient of absorption of radiation in air and in clouds. Regarding the latter, we note that the statistical properties of the coefficient of absorption in clouds are determined by the statistical properties of the water content. These properties, unfortunately, have not been thoroughly investigated, and we are therefore forced to make certain special assumptions.

By virtue of this, the corresponding results must be regarded as tentative.

In the second part we investigate the fluctuations of the brightness temperature of the antenna. The case of cloudless atmosphere is considered here as a particular case of cloudy atmosphere.

Finally, in the third part we establish the angular correlation connections between the fluctuations of the thermal radiation of an atmosphere free of clouds.

1. STATISTICAL CHARACTERISTICS OF THE COEFFICIENT OF ABSORPTION OF RADIOWAVES IN AIR

As is known, the absorption of electromagnetic wave in the centimeter and millimeter bands in air is due essentially to the absorption in oxygen and in the water vapor. Therefore the coefficient of absorption in air is represented in the form of the sum

$$\alpha = \alpha_1 + \alpha_2, \tag{1}$$

where α_1 – coefficient of absorption in oxygen and α_2 – coefficient of absorption in water vapor. As shown in [2, 3], α_1 and α_2 vary exponentially with height and

$$\alpha(z) = \alpha_{10} e^{-z/H_1} + \alpha_{20} e^{-z/H_2}, \tag{2}$$

where $H_1 \simeq 5.3 \cdot 10^3$ m and $H_2 \simeq 2.1 \cdot 10^3$ m. We shall henceforth assume for simplicity

$$\alpha(z) = \alpha_0 e^{-z/H}, \tag{3}$$

where α_0 and H are determined by equating (2) and (3) and their first derivatives at z = 0, i.e.,

$$\begin{gathered} \alpha_0 = \alpha_{10} + \alpha_{20}, \\ \frac{\alpha_0}{H} = \frac{\alpha_{10}}{H_1} + \frac{\alpha_{20}}{H_2}. \end{gathered} \tag{4}$$

With the aid of data given in [1] we can readily calculate α_0 and H, which are presented in Table 1 for various wavelengths.

Table 1

Values of α_1, α_2, α_0 and H

λ, см	α_1, 1/м	α_2, 1/м	$\alpha_0 = \alpha_1 + \alpha_2$	H, м
10	$0.15 \cdot 10^{-5}$	$0.005 \cdot 10^{-5}$	$0.15 \cdot 10^{-5}$	$5.0 \cdot 10^3$
3	$0.16 \cdot 10^{-5}$	$0.07 \cdot 10^{-5}$	$0.23 \cdot 10^{-5}$	$3.7 \cdot 10^3$
1.5	$0.20 \cdot 10^{-5}$	$1.90 \cdot 10^{-5}$	$2.10 \cdot 10^{-5}$	$2.2 \cdot 10^3$
1.0	$0.32 \cdot 10^{-5}$	$1.02 \cdot 10^{-5}$	$1.34 \cdot 10^{-5}$	$2.5 \cdot 10^{-3}$
0.667	$1.75 \cdot 10^{-5}$	$0.71 \cdot 10^{-5}$	$2.45 \cdot 10^{-5}$	$3.7 \cdot 10^3$

The absorption coefficient is a function of the meteorological parameters, namely the temperature T, the pressure p, and the humidity ρ (water-vapor content). We represent this relationship, away from the resonance lines, in the following form [1]

$$\alpha = \beta_1 \frac{p^2}{T^{5/2}} + \rho p \left[\beta_2^{(1)} \frac{e^{-\frac{280}{T}}}{T^2} + \frac{\beta_2^{(2)}}{T^{3/2}} \right], \tag{5}$$

where β_1, $\beta_2^{(1)}$, and $\beta_2^{(2)}$ depend on the internal properties of the molecules (magnetic and electric moments, magnitudes of the terms, etc.). We shall henceforth use formula (5); i.e., we confine ourselves to the non-resonant frequency ranges.

Since T, p, and ρ are random quantities, α is also random. The mean value of α is known, and its altitude dependence is determined from (3). The dispersion of the absorption coefficient can be determined from (5) by differentiating (since the fluctuations of T, p, and ρ are small), squaring, and averaging. We assume here that the fluctuations of T, p, and ρ are statistically independent and are adiabatic. (The fluctuations of T and p are related by the adiabatic equation.) Then

$$\sigma_\alpha^2 = \overline{\Delta\alpha^2} = (\bar{\alpha}_2)^2 \frac{\sigma_\rho^2}{(\bar{\rho})^2} + f^2(\bar{\alpha}_1, \bar{\alpha}_2) \frac{\sigma_T^2}{(\bar{T})^2}. \tag{6}$$

Here

$$f(\bar{\alpha}_1, \bar{\alpha}_2) = \frac{\mu}{\mu - 1}(2\bar{\alpha}_1 + \bar{\alpha}_2) - \frac{5}{2}\bar{\alpha}_1 - \frac{3}{2}\bar{\alpha}_2^{(2)} - \left(\frac{280}{\bar{T}} + 2\right)\bar{\alpha}_2^{(1)}; \tag{7}$$

$$\bar{\alpha}_1 = \beta_1 \frac{(\bar{p})^2}{(\bar{T})^{5/2}}; \tag{8}$$

$$\bar{\alpha}_2^{(1)} = \bar{\rho}\bar{p}\beta_2^{(1)} \frac{e^{-\frac{280}{T}}}{(\bar{T})^2}; \tag{9}$$

$$\bar{\alpha}_2^{(2)} = \bar{\rho}\bar{p}\beta_2^{(2)} \frac{1}{(\bar{T})^{3/2}}; \tag{10}$$

$$\bar{\alpha}_2 = \bar{\alpha}_2^{(1)} + \bar{\alpha}_2^{(2)}; \tag{11}$$

$\mu = 1.41$ is the adiabatic exponent of air; σ_ρ and σ_T — dispersion of the fluctuations of humidity and pressure; α_1 characterizes the absorption in oxygen; $\alpha_2^{(1)}$ corresponds to the absorption edge of water vapor near the 1.35 cm line, and $\alpha_2^{(2)}$ corresponds to the edges of the remaining absorption lines. These quantities are known [1] and the calculation of $f(\bar{\alpha}_1, \bar{\alpha}_2)$ entails no difficulty. For example, for $\lambda = 8$ mm, $\bar{\rho} = 7$ g/m^3, and $\bar{T} = 293$° K we have $f(\alpha_1, \alpha_2) = 4.27 \cdot 10^{-5}$ 1/m. For the remaining wavelengths the values are listed in Table 2.

Table 2

Values of $f(\bar{\alpha}_1, \bar{\alpha}_2)$ ($\bar{T} = 293$° K, $\bar{\rho} = 7.5$ g/m^3)

λ, см	10	3	1,5	1,0	0,667
$f(\bar{\alpha}_1, \bar{\alpha}_2)$	$0{,}66 \cdot 10^{-5}$	$0{,}89 \cdot 10^{-5}$	$2{,}18 \cdot 10^{-5}$	$2{,}19 \cdot 10^{-4}$	$8{,}71 \cdot 10^{-5}$

Table 3

Dispersion of the Absorption Coefficient ($\bar{T} = 293$° K, $\bar{\rho} = 7.5$ g/m^3)

λ, см	$\sigma_\alpha/\bar{\alpha}$
10	$0.47 \cdot 10^{-2}$
3	$1.36 \cdot 10^{-2}$
1.5	$4{,}00 \cdot 10^{-2}$
1,0	$3.36 \cdot 10^{-2}$
0,667	$1.30 \cdot 10^{-2}$

It follows from the averaged values given in [5] that $\sigma_\rho \simeq 0.33$ g/m^3 and $\sigma_T \simeq 0.3$° K. If we use these data as a basis, we obtain for $\lambda = 8$ mm, $\bar{\rho} = 7.5$ g/m^3 and T = 293° K (these meteorological parameters will henceforth be referred to as standard) a value $\sigma_\alpha/\bar{\alpha} \simeq 1.97 \cdot 10^{-2}$. For the remaining wavelengths the corresponding information is listed in Table 3. As can be seen from the estimates, for a wavelength $\lambda < 3$ cm the fluctuations of the absorption coefficient are essentially due to fluctuations of the humidity. Since $\bar{\alpha}_1$ and $\bar{\alpha}_2$ decrease with altitude, σ_α also decreases with altitude. We shall assume that this decrease is described by a function

$$\sigma_\alpha(z) = \sigma_\alpha(0) e^{-z/L} \tag{12}$$

and that in order of magnitude $L \simeq H$.

We further assume that the fluctuations of the coefficient of absorption are isotropic locally. This means that the fluctuations at two points are described by a correlation function in the form

$$\overline{\Delta\alpha(\vec{r}_1)\,\Delta\alpha(\vec{r}_2)} = R_\alpha(\vec{r}_1, \vec{r}_2) = \sigma_\alpha\left(\frac{\vec{r}_1+\vec{r}_2}{2}\right)\rho_\alpha(|\vec{r}_2-\vec{r}_1|), \tag{13}$$

where $\rho_\alpha(|\vec{r}_2 - \vec{r}_1|)$ – normalized autocorrelation function of the fluctuations of α. For simplicity we present $\rho_\alpha(x)$ in Taylor's form, i.e.,

$$\rho_\alpha(x) = e^{-x/l_\alpha}, \tag{14}$$

where l_α – external scale of the fluctuations.* It is natural to assume that this scale is equal to the external scale of the fluctuations of the refractive index and amounts to approximately 100 meters. We note also that since σ_α is a function of the height only, we have

$$\sigma_\alpha\left(\frac{\vec{r}_1+\vec{r}_2}{2}\right) = \sigma_\alpha\left(\frac{z_1+z_2}{2}\right). \tag{15}$$

2. STATISTICAL CHARACTERISTICS OF THE ABSORPTION COEFFICIENT IN CLOUDS

The absorption of electromagnetic radiation at centimeter wavelengths in clouds is due essentially to absorption in water vapor, which can be regarded as saturated in the clouds, and to Joule heat losses in the water droplets. The latter is described by an absorption coefficient [1]

$$\gamma = \int_0^\infty n(a)\,Q(a, \lambda)\,da, \tag{16}$$

where n(a)da is the number of drops per unit volume, the radii of the drops lying in the interval [a, a + da]; Q(a, λ) – effective diameter of scattering. Since $a \simeq 7-10\ \mu$ in clouds, we can use at centimeter wavelengths the following approximation

$$Q(a, \lambda) = \frac{4\pi^2 c a^3}{\lambda}, \tag{17}$$

where the coefficient c depends on the real and imaginary parts of the dielectric constant of the water. It is possible to calculate this coefficient on the basis of the data given in [1], from which it follows, for example, that c = 0.12 when λ = 8 mm and $\overline{T} = 293°$ K. Since the volume of the sphere V(a) is proportional to the cube of its radius, formula (16) can be rewritten as

$$\gamma = \frac{3\pi c}{\lambda}\int_0^\infty n(a)\,V(a)\,da = \frac{3\pi c}{\lambda\tilde{\rho}}W, \tag{18}$$

where W – water contents of the clouds, $\tilde{\rho}$ – density of the water. The water content of the clouds is on the order of 0.5–1.0 g/m^3 [6]. It follows therefore that for λ = 8 mm we have

---

*We should have used the Kolmogorov-Obukhov law for the choice of the correlation function. This would, however, complicate the calculations without changing appreciably the final result.

Table 4

Coefficient of Absorption in a Cloud and Its Fluctuations
($\overline{T}$ = 293° K, $\overline{\rho}$ = 17 g/m^3, $\overline{W}$ = 0.71 g/cm^3)

λ, см	$\frac{3\pi c_1}{\lambda}$, 1/м	$\overline{\gamma}$, 1/м	$\overline{\alpha}$, 1/м	$\overline{\beta}=\overline{\alpha}+\overline{\gamma}$
10	0.94	$0.0067 \cdot 10^{-4}$	$0.016 \cdot 10^{-4}$	$0.023 \cdot 10^{-4}$
3	10.1	$0.076 \cdot 10^{-4}$	$0.032 \cdot 10^{-4}$	$0.11 \cdot 10^{-4}$
1.5	42.1	$0.30 \cdot 10^{-4}$	$0.45 \cdot 10^{-4}$	$0.75 \cdot 10^{-4}$
1.0	94.1	$0.67 \cdot 10^{-4}$	$0.25 \cdot 10^{-4}$	$0.93 \cdot 10^{-4}$
0.667	206.0	$1.46 \cdot 10^{-4}$	$0.34 \cdot 10^{-4}$	$1.80 \cdot 10^{-4}$

λ, см	$\sigma_{\gamma\lambda}$, 1/м	σ_{α}, 1/м	σ_{β}, 1/м	$\sigma_{\beta}/\overline{\beta}$
10	$0.032 \cdot 10^{-5}$	$0.0008 \cdot 10^{-5}$	$0.032 \cdot 10^{-5}$	0.14
3	$0.07 \cdot 10^{-5}$	$0.0071 \cdot 10^{-5}$	$0.37 \cdot 10^{-5}$	0.34
1.5	$1.40 \cdot 10^{-5}$	$0.20 \cdot 10^{-5}$	$1.41 \cdot 10^{-5}$	0.19
1.0	$3.20 \cdot 10^{-5}$	$0.12 \cdot 10^{-5}$	$3.20 \cdot 10^{-5}$	0.34
0.667	$7.0 \cdot 10^{-5}$	$0.14 \cdot 10^{-5}$	$7.0 \cdot 10^{-5}$	0.37

$\gamma \simeq (0.7 - 1.4) \times 10^{-4}$ 1/m. The coefficient of absorption in the water vapor of the clouds under standard meteorological parameters ($\rho \approx 17$ g/m^3) is $\alpha \simeq 3.1 \cdot 10^{-5}$ 1/m for $\lambda = 8$ mm. Thus, the absorption in the droplets of the clouds exceeds the absorption in the water vapor.

The dispersion of γ is obviously

$$\sigma_{\gamma} = \frac{3\pi c}{\lambda \tilde{\rho}} \sigma_{W}, \tag{19}$$

where σ_W is the dispersion of the water contents. As far as we know, there is no information concerning the latter quantity, and it is therefore difficult to estimate σ_γ with any degree of reliability. One can, however, proceed in the following fashion. In [6] are given certain data on the altitude distribution of the mean water contents in cumulus clouds. These data will be regarded as the possible range of values of the water content. Then $\overline{W} = 0.71$ g/m^3, and $\sigma_W \simeq 0.34$ g/m^3. Consequently, for $\lambda = 8$ mm we have $\sigma_\gamma = 4.8 \cdot 10^{-5}$ 1/m, and $\sigma_\gamma / \overline{\gamma} = 0.48$. The data on $\overline{\gamma}$ and σ_γ for other wavelengths are listed in Table 4.

The over-all absorption coefficient in the clouds is

$$\beta = \alpha + \gamma, \tag{20}$$

and its dispersion, assuming the fluctuations of the water contents and of the humidity to be independent, is

$$\sigma_\beta^2 = \sigma_\alpha^2 + \sigma_\gamma^2. \tag{21}$$

We shall assume further that the fluctuations of β are isotropic and that the normalized autocorrelation function has a Taylor form. However, for the correlation radius l_β we use the estimate $l_\beta = 10$ meters in accordance with refractometric measurements in clouds [10].

3. BRIGHTNESS TEMPERATURE OF THE ANTENNA

Our problem is to calculate the brightness temperature that the antenna acquires under the influence of the thermal radiation of the atmosphere. We consider the general case, when the atmosphere contains in the height interval from h_1 to h_2 a cloud layer of thickness

$$d = h_2 - h_1. \tag{22}$$

For this purpose we use the transport equations for radiant energy [8], which in our case have the form

$$\begin{aligned} \frac{dI_1}{dz} - \frac{\alpha}{\sin\psi} I_1 &= -\frac{2\,\alpha k T_1}{\lambda^2 \sin\psi} \quad \text{for} \quad 0 < z \leqslant h_1, \\ \frac{dI_2}{dz} - \frac{\beta}{\sin\psi} I_2 &= -\frac{2\beta k T_2}{\lambda^2 \sin\psi} \quad \text{for} \quad h_1 \leqslant z \leqslant h_2, \\ \frac{dI_3}{dz} - \frac{\alpha}{\sin\psi} I_3 &= -\frac{2\,\alpha k T_3}{\lambda^2 \sin\psi} \quad \text{for} \quad z \geqslant h_2. \end{aligned} \tag{23}$$

Here I_1, I_2, I_3 — intensity of radiant energy in the space under the cloud, in the cloud, and above the cloud respectively; T_1, T_2, T_3 — temperatures in the same regions; $k = 1.38 \cdot 10^{-16}$ erg/deg—Boltzmann's constant; ψ — elevation angle of the beam at the point z. The group of equations (23) must be solved subject to continuity of the flux of electromagnetic radiation on the boundaries of the cloud* and the vanishing of this flux as $z \to \infty$. Under these conditions the solution has the form

$$I_1(z) = \frac{2k}{\lambda^2}\left\{\int_z^{h_1} \frac{T_1(\zeta)\,\alpha(\zeta)\,e^{-\tau(\zeta)}\,d\zeta}{\sin\psi} + e^{\eta(h_1)-\tau(h_1)}\left[\int_{h_1}^{h_2} \frac{T_2(\zeta)\,\beta(\zeta)\,e^{-\eta(\zeta)}\,d\zeta}{\sin\psi} + \right.\right.$$
$$\left.\left. + e^{\tau(h_2)-\eta(h_2)} \int_{h_2}^{\infty} \frac{T_3(\zeta)\,\alpha(\zeta)\,e^{-\tau(\zeta)}\,d\zeta}{\sin\psi}\right]\right\} e^{\tau(z)}, \tag{24}$$

where

$$\tau(z) = \int_0^z \frac{\alpha(\zeta)}{\sin\psi}\,d\zeta \tag{25}$$

is called the optical depth of the atmosphere and

$$\eta(\zeta) = \int_0^z \frac{\beta(\zeta)}{\sin\psi}\,d\zeta \tag{26}$$

the optical depth of the cloud. From (24) it follows that the brightness temperature of the antenna (z = 0) is

$$T_A = \int_0^{h_1} \frac{T_1(\zeta)\,\alpha(\zeta)\,e^{-\tau(\zeta)}\,d\zeta}{\sin\psi} + e^{\eta(h_1)-\tau(h_1)}\left[\int_{h_1}^{h_2} \frac{T_2(\zeta)\,\rho(\zeta)\,e^{-\eta(\zeta)}\,d\zeta}{\sin\psi} + \right.$$
$$\left. + e^{\tau(h_2)-\eta(h_2)} \int_{h_2}^{\infty} \frac{T_3(\zeta)\,\alpha(\zeta)\,e^{-\tau(\zeta)}\,d\zeta}{\sin\psi}\right]. \tag{27}$$

It is important for what follows that, as shown by more detailed calculations, the fluctuations of the temperature of the atmosphere and of the cloud do not exert any appreciable influence on the fluctuations of the brightness temperature of the antenna. Consequently we can replace T_1, T_2, and T_3 in the integrals of (27) by their mean values. In addition, since the temperature varies very slowly with altitude, T_1, T_2, and T_3 can be replaced by the mean value of the temperature of the atmosphere at the earth's surface, $\overline{T}_0$. Then, recognizing that $d\tau/dz = \alpha/\sin\psi$ and $d\eta/dz = \beta/\sin\psi$, we obtain

$$T_A = \overline{T}_0\,(1 - e^{-r}), \tag{28}$$

---

*We neglect refraction of the rays on the boundaries of the cloud, owing to the smallness of this effect.

where

$$r = \eta(h_2) - \eta(h_1) + \tau(h_1) + \tau(\infty) - \tau(h_2) \tag{29}$$

has the meaning of total optical depth. It follows from (28) that the statistical properties of the brightness temperature of the antenna are determined by the statistical characteristics of the total optical thickness.

4. MEAN VALUE OF THE TOTAL OPTICAL THICKNESS

It is obvious that the mean value of the total optical thickness is

$$\bar{r} = \overline{\eta(h_2) - \eta(h_1)} + \overline{\tau(h_1)} + \overline{\tau(\infty) - \tau(h_2)}. \tag{30}$$

As shown in [3], at elevation angles $\psi \geq 5°$ we can neglect refraction and assume the angle ψ to be the same everywhere. In addition, we assume that the fluctuations in the cloud are spatially homogeneous. Then

$$\overline{\eta(h_2) - \eta(h_1)} = \int_{h_1}^{h_2} \frac{\overline{\beta(\zeta)}\, d\zeta}{\sin\psi} = \frac{\bar{\beta} d}{\sin\psi} \tag{31}$$

and with account of (3)

$$\bar{\tau}(z) = \frac{\bar{\alpha}_0 H}{\sin\psi}\left(1 - e^{-\frac{z}{H}}\right). \tag{32}$$

If we introduce the mean height of the cloud $h = (h_1 + h_2)/2$, we can obtain for $\bar{r}$

$$\bar{r} = \frac{1}{\sin\psi}\left[\bar{\beta} d + \bar{\alpha}_0 H \left(1 - 2e^{-\frac{h}{H}} \operatorname{sh} \frac{d}{2H}\right)\right]. \tag{33}$$

We note that in the absence of a cloud (d = 0) we have

$$\bar{r} = \frac{\alpha_0 H}{\sin\psi}. \tag{34}$$

A very frequent case is when $d/2H \ll 1$ and therefore

$$\bar{r} = \frac{\bar{\beta} d + \bar{\alpha}_0 H}{\sin\psi}. \tag{35}$$

We shall use this formula from now on.

Let us estimate the numerator in (35) for $\lambda = 8$ mm. If we take $d = 10^3$ m, we get $\bar{\beta} d + \bar{\alpha}_0 H = 0.18$.

5. FLUCTUATIONS OF THE TOTAL OPTICAL DEPTH

Since the fluctuations under the cloud, inside the cloud, and above the cloud can be regarded as statistically independent, the dispersion of the total optical thickness is determined by the sum

$$\sigma_r^2 = \sigma^2_{\tau(h_1)} + \sigma^2_{\eta(h_2) - \eta(h_1)} + \sigma^2_{\tau(\infty) - \tau(h_2)}, \tag{36}$$

where

$$\sigma^2_{\tau(h_1)} = \frac{1}{\sin^2\psi} \int_0^{h_1}\int_0^{h_1} R_\alpha(\zeta, \zeta')\, d\zeta\, d\zeta'; \tag{37}$$

$$\sigma^2_{\eta(h_2)-\eta(h_1)} = \frac{1}{\sin^2\psi}\int_{h_1}^{h_2}\int_{h_1}^{h_2} R_\beta(\zeta,\zeta')\,d\zeta\,d\zeta'; \tag{38}$$

$$\sigma^2_{\tau(\infty)-\tau(h_1)} = \frac{1}{\sin^2\psi}\int_{h_2}^{\infty}\int_{h_2}^{\infty} R_\alpha(\zeta,\zeta')\,d\zeta\,d\zeta'. \tag{39}$$

Let us calculate first $\sigma^2_\tau(h_1)$. For this purpose we use formulas (13), (14), and (15). In addition, we introduce in the integral of (37) the new variables

$$x = \frac{\zeta+\zeta'}{2}, \quad y = |\vec{r}_2 - \vec{r}_1| = \frac{\zeta-\zeta'}{\sin\psi} \tag{40}$$

and take into account the parity of the autocorrelation function. As a result we get

$$\sin\psi\,\sigma^2_{\tau(h_1)} = 2\int_0^{h_1} \rho_\alpha(y)\,dy \int_{\frac{y\sin\psi}{2}}^{h_1-\frac{y\sin\psi}{2}} \sigma^2_\alpha(x)\,dx, \tag{41}$$

σ^2_α (x) changes appreciably over the interval $x \sim L/2$. The internal integral also changes on this interval; ρ_α(y) changes appreciably over the interval l_α. Since $l_\alpha \ll L$, we can put y = 0 in the internal integral. In addition, since usually $h_1 \gg l_\alpha$, the upper limit in the external integral can be made infinite. As a result we obtain

$$\sin\psi\,\sigma^2_{\tau(h_1)} = 2\int_0^{h_1} \sigma_\alpha{}^2(x)\,dx \int_0^{\infty} \rho_\alpha(y)\,dy. \tag{42}$$

We now substitute here formulas (12) and (14), and obtain

$$\sigma^2_{\tau(h_1)} = \frac{\sigma^2_\alpha(0)\,l_\alpha\,L\,(1-e^{-\frac{2h_1}{L}})}{\sin\psi}. \tag{43}$$

Similar calculations lead to

$$\sin\psi\,\sigma^2_{\eta(h_2)-\eta(h_1)} = 2\int_0^{\infty} \rho_\beta(y)\,dy \int_{h_1}^{h_2} \sigma^2_\beta(x)\,dx \tag{44}$$

or

$$\sigma^2_{\eta(h_2)-\eta(h_1)} = \frac{2dl_\beta\,\sigma^2_\beta}{\sin\psi}. \tag{45}$$

In order to calculate the third term in (36) we must replace β in (44) by α, h_1 by h_2, and h_2 by ∞.
Then

$$\sigma^2_{\tau(\infty)-\tau(h_2)} = 2\int_0^{\infty} \rho_\alpha(y)\,dy \int_{h_2}^{\infty} \sigma_\alpha{}^2(x)\,dx. \tag{46}$$

Substituting (12) and (14) in the last formula, we obtain ultimately

$$\sigma^2_{\tau(\infty)-\tau(h_2)} = \frac{\sigma_\alpha^2(0)\, l_\alpha L}{\sin\psi}\, e^{-\frac{2h_2}{L}}. \tag{47}$$

The net result is

$$\sigma_r^2 = \frac{1}{\sin\psi}\left\{2dl_\beta\sigma_\beta^2 + \sigma_\alpha^2(0)\, l_\alpha L\left(1-2e^{-\frac{2h}{L}}\operatorname{sh}\frac{d}{L}\right)\right]. \tag{48}$$

If there are no clouds (d = 0), then

$$\sigma_r^2 = \frac{\sigma_\alpha^2(0)\, l_\alpha L}{\sin\psi}. \tag{49}$$

In the presence of a cloud layer the first term of (48) is usually much greater than the second, so that $\sigma_\beta^2 \gg \sigma_\alpha^2(0)$. Therefore, in the presence of a cloud layer we get approximately

$$\sigma_r^2 = \frac{2dl_\beta\sigma_\beta^2}{\sin\psi}. \tag{50}$$

Table 5

Values of the Relative Fluctuations of the Antenna Temperature as a Function of the Elevation Angle (λ = 8 mm)

$\psi°$	10	20	30	40	50	60	70	80	90
$\sigma_{T_A}/\bar{T}_A$	$1.21\cdot10^{-3}$	$1.86\cdot10^{-3}$	$2.32\cdot10^{-3}$	$2.67\cdot10^{-3}$	$2.92\cdot10^{-3}$	$3.14\cdot10^{-3}$	$3.26\cdot10^{-3}$	$3.33\cdot10^{-3}$	$3.36\cdot10^{-3}$

For λ = 8 mm and d = 10^3 m we get

$$\sigma_r^2 = \frac{4{,}06\cdot10^{-5}}{\sin\psi}.$$

Consequently we have for the same wavelength

$$\frac{\sigma_r^2}{r} \approx 2.26\cdot10^{-4} \ll 1. \tag{51}$$

6. FLUCTUATIONS OF THE ANTENNA BRIGHTNESS TEMPERATURE

Inequality (51) enables us to assume that $\overline{e^{-r}} \simeq e^{-\bar{r}}$ and $\sigma_{e^{-r}} \simeq \sigma_r e^{-\bar{r}}$. Therefore the following well-known formula holds for the mean value of the antenna brightness temperature

$$\bar{T}_A = \bar{T}_0(1-e^{-\bar{r}}). \tag{52}$$

The dispersion of the brightness temperature of the antenna is

$$\sigma_{T_A} = \bar{T}_0\sigma_r e^{-\bar{r}}. \tag{53}$$

Finally, the relative dispersion is

$$\frac{\sigma_{T_A}}{T_A} = \frac{\sigma_r}{e^{\bar{r}} - 1} . \tag{54}$$

It is further convenient to analyze separately the cases of a cloudless atmosphere and an atmosphere with a cloud layer.

In the former case we must use (49) for σ_r. Then

$$\frac{\sigma_{T_A}}{\bar{T}_A} = \frac{\sigma_\alpha(0)\sqrt{l_\alpha L}}{\sqrt{\sin\psi}\,(e^{\bar{r}} - 1)} . \tag{55}$$

We shall henceforth assume L = H. If $\bar{r} \ll 1$, which is quite frequent, we get

$$\frac{\sigma_{T_A}}{\bar{T}_A} \simeq \frac{\sigma_\alpha(0)}{\bar{\alpha}_0}\sqrt{\frac{l_\alpha}{H}\sin\psi} . \tag{56}$$

By way of an example of the applicability of the resultant formulas, let us calculate the relative dispersion of the antenna temperature at different elevation angles for the 8 mm band. The results of these calculations are listed in Table 5.

In the case when the atmosphere contains a layer of clouds, we must use for σ_r formula (50). In this case

$$\frac{\sigma_{T_A}}{\bar{T}_A}\sqrt{\frac{2\,dl_\beta}{\sin\psi}}\,\frac{\sigma_\beta}{e^{\bar{r}}-1} . \tag{57}$$

Table 6

Values of the Relative Fluctuations of the Antenna Temperature as a Function of the Elevation Angle at Different Values of the Cloud Thickness

(λ = 8 mm, $\overline{\mathrm{T}}$ = 293°K, $\overline{\mathrm{W}}$ = 0.71 g/m^3, ρ = 17.0 g/m^3)

ψ°	d, м					
	100	200	500	1000	1500	2000
10	$0.98 \cdot 10^{-2}$	$1.18 \cdot 10^{-2}$	$1.17 \cdot 10^{-2}$	$0.91 \cdot 10^{-2}$	$0.68 \cdot 10^{-2}$	$0.51 \cdot 10^{-2}$
20	$1.71 \cdot 10^{-2}$	$1.91 \cdot 10^{-2}$	$1.95 \cdot 10^{-2}$	$1.70 \cdot 10^{-2}$	$1.43 \cdot 10^{-2}$	$1.20 \cdot 10^{-2}$
30	$2.12 \cdot 10^{-2}$	$2.56 \cdot 10^{-2}$	$2.54 \cdot 10^{-2}$	$2.23 \cdot 10^{-2}$	$1.96 \cdot 10^{-2}$	$1.69 \cdot 10^{-2}$
40	$2.38 \cdot 10^{-2}$	$2.91 \cdot 10^{-2}$	$2.16 \cdot 10^{-2}$	$2.66 \cdot 10^{-2}$	$2.37 \cdot 10^{-2}$	$2.10 \cdot 10^{-2}$
50	$2.53 \cdot 10^{-2}$	$3.18 \cdot 10^{-2}$	$3.48 \cdot 10^{-2}$	$2.97 \cdot 10^{-2}$	$2.66 \cdot 10^{-2}$	$2.27 \cdot 10^{-2}$
60	$2.71 \cdot 10^{-2}$	$3.37 \cdot 10^{-2}$	$3.76 \cdot 10^{-2}$	$3.48 \cdot 10^{-2}$	$2.85 \cdot 10^{-2}$	$2.55 \cdot 10^{-2}$
70	$2.80 \cdot 10^{-2}$	$3.49 \cdot 10^{-2}$	$3.98 \cdot 10^{-2}$	$3.64 \cdot 10^{-2}$	$3.04 \cdot 10^{-2}$	$2.75 \cdot 10^{-2}$
80	$2.90 \cdot 10^{-2}$	$3.61 \cdot 10^{-2}$	$3.98 \cdot 10^{-2}$	$3.82 \cdot 10^{-2}$	$3.10 \cdot 10^{-2}$	$2.76 \cdot 10^{-2}$
90	$2.90 \cdot 10^{-2}$	$3.61 \cdot 10^{-2}$	$3.98 \cdot 10^{-2}$	$3.82 \cdot 10^{-2}$	$3.10 \cdot 10^{-2}$	$2.76 \cdot 10^{-2}$

When $\bar{r} \ll 1$ we can use formula (35) and write

$$\frac{\sigma_{T_A}}{\bar{T}_A} = \frac{\sigma_\beta\sqrt{2\,dl_\beta\sin\psi}}{\bar{\beta}d + \bar{\alpha}_0 H} . \tag{58}$$

Table 6 lists the calculated values of the dispersion of the brightness temperature of the antenna as a function of the elevation angle for different values of the cloud layer thickness at λ = 8 mm. From a comparison of this table with Table 5 we see that the presence of the cloud layer increases the intensity of the thermal-radiation fluctuations of the atmosphere by one order of magnitude compared with the free atmosphere.

7. ANGULAR CORRELATION OF THE FLUCTUATIONS OF THE BRIGHTNESS TEMPERATURE OF AN ANTENNA

The mean value of the antenna brightness temperature and the intensity of the temperature fluctuations are functions of the elevation angle. Therefore a study of the correlation relations between the fluctuations of the thermal radiation of the atmosphere, arriving at the antenna from different directions, is of interest.

Assume that two beams propagate at elevation angles ψ_1 and ψ_2 and azimuth angles φ_1 and φ_2, and strike two corresponding antennas. Then the temperature of the first antenna, in accordance with (28), will be

$$T_A(\psi_1, \varphi_1) = \overline{T}_0 [1 - e^{-r(\psi_1, \varphi_1)}]$$

and that of the second

$$T_A(\psi_2, \varphi_2) = \overline{T}_0 [1 - e^{-r(\psi_2, \varphi_2)}].$$

Accordingly, the correlation function is

$$R_{T_A}(\psi_1, \varphi_1; \psi_2, \varphi_2) = (\overline{T}_0)^2 R_r(\psi_1, \varphi_1; \; \psi_2, \varphi_2)\, e^{-r(\psi_1, \varphi_1) - r(\psi_2, \varphi_2)}, \tag{59}$$

where

$$R_r(\psi_1, \varphi_1; \psi_2, \varphi_2) = \int_0^\infty \int_0^\infty \frac{R_\alpha(\zeta, \zeta')}{\sin\psi_1 \sin\psi_2}\, d\zeta\, d\zeta' \tag{60}$$

is a normalized correlation function of the antenna brightness temperature. We use formulas (13)–(15) for $R_\alpha(\zeta, \zeta')$. The main difficulty in the calculations that follow lies in the fact that now $|\vec{r}_2 - \vec{r}_1|$ is not proportional to $\zeta - \zeta'$, but is determined by the formula

$$|\vec{r}_2 - \vec{r}_1| = \frac{\sqrt{\sin^2\psi_2 \zeta^2 + \sin^2\psi_1 \zeta'^2 - 2\zeta\zeta' \sin\psi_1 \sin\psi_2 \cos\theta}}{\sin\psi_1 \sin\psi_2}, \tag{61}$$

where

$$\cos\theta = \sin\psi_1 \sin\psi_2 + \cos\psi_1 \cos\psi_2 \cos(\varphi_2 - \varphi_1); \tag{62}$$

θ is the angle between the beams.

To overcome this difficulty, we first rewrite (60) in the form

$$\sin\psi_1 \sin\psi_2 R_r(\psi_1, \varphi_1; \psi_2, \varphi_2) = \int_0^\infty \int_0^\zeta R_\alpha(\zeta, \zeta')\, d\zeta\, d\zeta' + \int_0^{\zeta'} \int_0^\infty R_\alpha(\zeta, \zeta')\, d\zeta\, d\zeta', \tag{63}$$

and then introduce new variables

$$x = \frac{\zeta + \zeta'}{2}, \qquad y = |\vec{r}_2 - \vec{r}_1|. \tag{64}$$

As a result we obtain

$$R_r(\psi_1, \varphi_1; \quad \psi_2, \varphi_2) = 2\int_0^{\infty} y\rho_\alpha(y)\, dy \left\{ \int_{\frac{y \sin\psi_1}{2}}^{\frac{y \sin\psi_1 \sin\psi_2}{A_1}} \frac{\sigma_\alpha^2(x)\, dx}{\sqrt{A_2^2 y^2 - 4x^2 \sin^2\theta}} + \right.$$

$$\left. + \int_{\frac{y \sin\psi_2}{2}}^{\frac{y \sin\psi_1 \sin\psi_2}{A_1}} \frac{\sigma_\alpha^2(x)\, dx}{\sqrt{A_2^2 y^2 - 4x^2 \sin^2\theta}} \right\}, \tag{65}$$

where

$$A_1 = \sqrt{\sin^2\psi_1 + \sin^2\psi_2 - 2\sin\psi_1 \sin\psi_2 \cos\theta};$$
$$A_2 = \sqrt{\sin^2\psi_1 + \sin^2\psi_2 + 2\sin\psi_1 \sin\psi_2 \cos\theta}. \tag{66}$$

A more thorough calculation shows that the lower limits in the internal integrals can be set equal to zero and the two integrals can be unified. If we now introduce a new variable

$$S = \frac{2x \sin\theta}{A_2 y}, \tag{67}$$

then the internal integral becomes independent of y. Thus the first integral, with account of (12) and (14), can be determined without particular difficulty and the end result is

$$R_r(\psi_1, \varphi_1; \psi_2, \varphi_2) = \frac{2\sigma_\alpha^2(0)}{\sin\theta} \int_0^{\frac{2\sin\psi_1 \sin\psi_2 \sin\theta}{A_1 A_2}} \frac{dS}{\left(\frac{1}{l_\alpha} + pS\right)^2 \sqrt{1 - S^2}}, \tag{68}$$

where

$$p = \frac{A_2}{L \sin\theta}. \tag{69}$$

We note that the last formula is valid only for a cloudless atmosphere. We confine ourselves to an analysis of this case. The last integral can be calculated by using the substitution S = sin t [9]. We obtain

$$R_r(\psi_1, \varphi_1; \psi_2, \varphi_2) = \frac{2\sigma_\alpha^2(0)\, l_\alpha L}{A_2(1 - q^2)} \left\{ 1 - \frac{q \cos t_0}{9 + \sin t_0} + \right.$$

$$\left. + \frac{q^2}{\sqrt{1 - q^2}} \ln \left[\frac{q + \operatorname{tg}\frac{t_0}{2} - \operatorname{tg}\frac{t_0}{2}\sqrt{1 - q^2}}{q + \operatorname{tg}\frac{t_0}{2} + \operatorname{tg}\frac{t_0}{2}\sqrt{1 - q^2}} \right] \right\}, \tag{70}$$

where

$$\sin t_0 = \frac{2\sin\theta \sin\psi_1 \sin\psi_2}{A_1 A_2}, \tag{71}$$

$$q = \frac{L \sin\theta}{l_\alpha A_2}. \tag{72}$$

Formula (70) can be used when q < 1. When q = 0 we can obtain from this formula, by going to the limit,

$$R_r = \frac{4}{3} \frac{\sigma_\alpha^2(0)\, l_\alpha L}{A_2} \left[1 - \frac{1 - \operatorname{tg}^3\frac{t_0}{2}}{\left(1 + \operatorname{tg}\frac{t_0}{2}\right)^3} \right]. \tag{73}$$

When q > 1 the logarithm is best replaced by the arctangent

$$R_r(\psi_1, \varphi_1; \psi_2, \varphi_2) = \frac{2\sigma_\alpha^2(0)\, l_\alpha L}{A_2(a^2-1)} \left\{ \frac{q \cos t_0}{q + \sin t_0} + \frac{2q^2}{\sqrt{q^2-1}} \operatorname{arctg} \frac{\operatorname{tg}\frac{t_0}{2}\sqrt{q^2-1}}{q + \operatorname{tg}\frac{t_0}{2}} - 1 \right\}. \quad (74)$$

We now consider particular cases of azimuthal correlation and correlation in the elevation angle. In the first case $\psi_1 = \psi_2 = \psi$ and $t_0 = \pi/2$. Therefore

$$R_r(\varphi_1; \varphi_2) = \frac{2\sigma_\alpha^2(0)\, l_\alpha L}{A_2(1-q^2)} \left\{ 1 + \frac{q^2}{\sqrt{1-q^2}} \ln \left[\frac{q+1-\sqrt{1-q^2}}{q+1+\sqrt{1-q^2}} \right] \right\} \text{ for } q < 1, \quad (75)$$

$$R_r(\varphi_1, \varphi_2) = \frac{4}{3} \frac{\sigma_\alpha^2(0)\, l_\alpha L}{A_2} \quad \text{for } q = 1; \quad (76)$$

$$R_r(\varphi_1, \varphi_2) = \frac{2\sigma_\alpha^2(0)\, l_\alpha L}{A_2(q^2-1)} \left\{ \frac{2q^2}{\sqrt{q^2-1}} \operatorname{arctg} \frac{\sqrt{q^2-1}}{q+1} - 1 \right\} \text{ for } q > 1. \quad (77)$$

Estimates show that in the 8 mm band a change in the elevation angle from 10 to 45° brings about a change in the angular radius of the azimuthal correlation approximately from 2.5 to 15.5°. By angular radius of correlation we mean here that value of the angular distance between rays at which the correlation function decreases to one third of its value at zero angular distance.

In the case of correlation in the elevation angle $\varphi_1 = \varphi_2$ and $t_0 = \psi$, where $\psi = (\psi_1 + \psi_2)/2$, provided the angular spacing is small. In this case the angular radius of correlation changes approximately from 1 to 11.5° as the elevation angle changes from 20 to 80°.

FUNDAMENTAL CONCLUSIONS

1. The relative fluctuations of the brightness temperature of an antenna registering the thermal radiation of the atmosphere, on the order of $10^{-2} - 10^{-3}$, are proportional to the intensity of the fluctuations of the absorption coefficient and decrease with decrease in elevation angle.
2. These fluctuations should increase sharply when clouds are present in the atmosphere.
3. The angular radius of correlation in azimuth and in elevation angle increases with increase in elevation angle.

REFERENCES

1. Propagation of UHF Waves. Translated from the English, edited by B.A. Shillerov, Soviet Radio Press, 1954.
2. S.A. Zhevakin, V.S. Troitskii, N.M. Tseitlin. News of the Universities, Ministry of Higher Education USSR, Radiophysics, 1958, 1, 2.
3. S.A. Zhevakin, V.S. Troitskii. Radiotekhnika i Elektronika, 1959, 4, 1, 21.
4. A.E. Salomonovich, O.M. Ataev. News of the Universities. Radiophysics, 1960, 3, 4.
5. E.E. Gossard. IRE Trans., 1960, AP-8, 2.
6. A.Kh. Khrgian. Physics of the Atmosphere. GIMFL, 2958.
7. K.S. Stankevich. News of the Universities. Radiophysics, 1960, 3, 6, 968.
8. V.V. Sobolev. Transport of Radiant Energy in the Atmospheres of Stars and Planets, GITTL, 1956.
9. H.B. Dwight. Tables of Integrals (Russian translation). IL, 1948.
10. C.M. Crain. Proc. IRE, 1955, 43, 10.

Received by editor 27 April 1961

USE OF THE METHOD OF SLOWLY VARYING PARAMETERS FOR AN INVESTIGATION OF NONLINEAR SELF-OSCILLATING SYSTEMS WITH DELAY

V.N. Yakovlev

The possibility is considered of using the method of slowly varying parameters for an investigation of nonlinear self-oscillating systems with delay. The effectiveness of the method proposed in this paper is illustrated with an example wherein a high-frequency self-oscillator with delay is analyzed.

INTRODUCTION

Self-oscillating nonlinear systems with delay are finding an ever increasing application in radio. These include pulse generators with delayed feedback and high-frequency generators with delay. Some problems in the theory of pulse generators with delay are considered in [6].

Problems in the theory of high-frequency self-oscillators with delayed feedback have been treated in greatest detail in [1, 2]. Foregoing an account of the details of the volt-ampere characteristics of the amplifying element of the generator, and representing the generator in the form of an ideal limiter, the author of these papers avoided the need for solving a nonlinear differential equation with delayed argument and investigated rather simply, clearly, and at the same time quite rigorously the stationary mode of a self-oscillator with delay, and the transient leading to this stationary mode.

In the present paper we analyze a self-oscillator with delayed feedback by investigating the nonlinear differential-difference equation of the generator, obtained with account of the real volt-ampere characteristic of its nonlinear element.

In this connection, we have used the method of slowly varying amplitudes (the Van der Pol method [3, 4, 5]) to devise a method for a quantitative analysis of nonlinear systems with delay. This method, when applied to systems that are so nearly linear and conservative that the wave form distortion of the generated oscillations can be disregarded in the specific technical problem, makes it possible to disclose the presence of many frequencies in oscillations with delay systems, and also to determine the frequency and the amplitude of the oscillations in the stationary mode.

1. METHOD OF SLOWLY VARYING PARAMETERS FOR THE ANALYSIS OF NONLINEAR SYSTEMS WITH DELAY

Let us proceed to examine the gist of the proposed method for investigating nonlinear systems with delayed feedback.

Assume that a nonlinear self-oscillating system with delay is described by an equation of the form

$$\ddot{u}(t) + 2\delta\dot{u}(t) - 2q\dot{u}(t-\tau) + \omega_0^2 u(t) = \mu f[u(t), \dot{u}(t), u(t-\tau), \ddot{u}(t-\tau)], \tag{1}$$

where τ — delay time; $\mu > 0$ — dimensionless quantity, small compared with unity. Here and below the differentiation is denoted by a superior dot

$$\dot{u}(t) = \frac{du}{dt}, \quad \dot{u}(t-\tau) = \frac{du}{dt}(t-\tau), \text{ etc.}$$

The equation of a near-harmonic self-oscillator without delay, as is well known, has the form

$$\ddot{u}(t) + \omega_0^2 u(t) = \mu f[u(t), \dot{u}(t)]. \tag{2}$$

The integral of equation (2) is determined in the following manner, using the well known methods of analysis of nearly linear nonlinear systems [3], for example, the method of slowly varying amplitudes (the Van der Pol method). We first determine the solution of (2) for $\mu = 0$ (the generating solution). We then take into account the effect of the right half of (2) with $\mu = 0$ on this solution. This effect, as is well known, reduces to the appearance of overtones and to a dependence of the instantaneous frequency on the oscillation amplitude. An account of the right half of (2) makes it possible at the same time to determine the amplitude and frequency of the stationary oscillations, and also their transient. Let us attempt to proceed analogously with equation (1), the left half of which contains all the linear terms of the equation of a system with and without delayed argument. An examination of equation (1) in precisely this form is due to the necessity for determining the frequencies of all the possible oscillations in the linearized system with delay (with $\mu = 0$).

When the second-order system under consideration is close to linear, it is natural to assume that the integral of (1) with $\mu > 0$ differs only slightly from the integral of equation (1) with $\mu = 0$. This circumstance makes it possible, as in the case of (2), to find first the solution of equation (1) with $\mu = 0$ (generating solution), and then take into account the influence of the right half of (1) on this solution.

Let us proceed now to determine the periodic solutions of equation (1) with $\mu = 0$:

$$\ddot{u}(t) + 2\delta\dot{u}(t) - 2q\dot{u}(t-\tau) + \omega_0^2 u(t) = 0. \tag{3}$$

In order to find the periodic solutions of (3), we use the Krylov and Bogolyubov method of harmonic linearization [4, 7] to make for the steady state an equivalent replacement of the function with delay $\dot{u}(t-\tau)$ by means of a function without delay in the form

$$\dot{u}(t-\tau) = a_1\dot{u}(t) + a_2\ddot{u}(t), \tag{4}$$

where a_1 and a_2 are coefficients still unknown.

We now assume that in the first approximation $\dot{u}(t)$ varies sinusoidally,

$$\dot{u}(t) = a\cos\omega t, \quad \ddot{u}(t) = -a\omega\sin\omega t. \tag{5}$$

After substituting (5) in (4) we obtain by using the formula for the cosine of the difference of two angles

$$a_1 = \cos\omega\tau, \quad a_2 = -\frac{\sin\omega\tau}{\omega}. \tag{6}$$

Equation (3) with account of (4) and (6) is now rewritten as

$$\ddot{u}(t) + \frac{2\delta - 2q\cos\omega\tau}{1 + \frac{2q}{\omega}\sin\omega\tau}\dot{u}(t) + \frac{\omega_0^2}{1 + \frac{2q}{\omega}\sin\omega\tau}u(t) = 0. \tag{7}$$

The system described by equation (7) is on the borderline of stability, and will support undamped periodic oscillations if

$$2q\cos\omega\tau - 2\delta = 0. \tag{8}$$

The frequency of the periodic oscillations is determined from the formula

$$\omega^2 = \frac{\omega_0^2}{1 + \frac{2q}{\omega} \sin \omega\tau}, \tag{9}$$

hence

$$\sin \omega\tau = \frac{\omega_0^2}{2q\omega} - \frac{\omega}{2q}. \tag{10}$$

The frequencies of the periodic oscillations can be determined by graphic solution of equation (10), which is transcendental in ω. For this purpose we represent equation (10) in the form

$$\sin \omega\tau = \frac{\omega_0^2 \tau}{2q\omega\tau} - \frac{\omega\tau}{2q\tau} = p_1 - p_2. \tag{11}$$

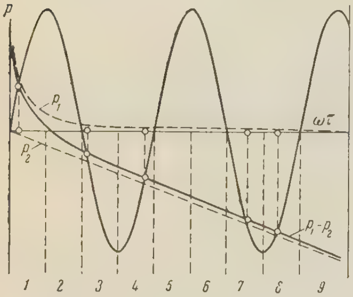

Fig. 1. Illustrating the determination of the oscillation frequencies of a linearized system with delay.

The first term p_1 of the right half of (11) is an equilateral hyperbola, the asymptotes of which are the axes p and $\omega\tau$ (Fig. 1), while the second term is the straight line p_2. The frequencies of the periodic solutions are determined by the abscissas of certain points of intersection (Fig. 1) between the curve of $p_1 - p_2 = \varphi(\omega\tau)$ and a sinusoidal curve. The points of intersection, as can be seen from Fig. 1, lie in the first, second, fourth, sixth, etc. quadrants. Oscillations will exist, however, only for frequencies for which (with $2q > 0$, $2\delta > 0$), in accordance with (8), the inequality $\cos \omega\tau > 0$ is satisfied, and in accordance with (10), $-\omega > \omega_0$. From this we get on the basis of (9)

$$\sin \omega\tau < 0,$$

$$1 + \frac{2q}{\omega} \sin \omega\tau > 0.$$

The conditions for the occurrence of periodic oscillations in a system with delay are consequently

$$\sin \omega\tau < 0, \quad \cos \omega\tau > 0. \tag{12}$$

If we now recognize that $\cos \omega\tau > 0$ and $\sin \omega\tau < 0$ only in the fourth quadrant, we can state that oscillations are possible only with frequencies determined by the abscissas of the point of intersection (Fig. 1) in the fourth, eighth, etc. quadrants.

It is also seen from Fig. 1 that the number of possible oscillations is limited, since the number of points of intersection is finite. The greater the coefficient 2q (the lower the Q of the resonance system and the broader its resonance characteristic), the more points of intersection there will be. However, not all oscillations with frequencies corresponding to these point of intersection will exist. The only oscillations that occur are those for which condition (8) is satisfied. Self-resonance is also possible when $\omega\tau = 2\pi + 2\pi n$, where $n = 0, 1, 2, \ldots$. In this case the oscillation frequencies will be equal to and multiples of the system frequency ω_0.

Periodic solutions of (3) corresponding to the values of the frequency ω as defined in (11) have the form

$$u_1(t) = A_1 \cos \psi_1, \; u_2(t) = A_2 \cos \psi_2, \ldots u_n(t) = A_n \cos \psi_n, \ldots u_i(t) = A_i \cos \psi_i,$$

where $\psi_n = \omega_n t + \theta_n$.

The frequency ω_i denotes here the highest frequency at which conditions (8) and (12) are still satisfied.

The amplitudes A_n and the phases θ_n are quantities that are constant in time and that depend on the initial conditions.

The general solution of (3), in accordance with the Schmidt theorem [7, 8], is equal to the sum of the particular solutions

$$u(t) = \sum_{n=1}^{i} A_n \cos \psi_n. \tag{13}$$

On the basis of the existence and uniqueness theorem [9] we can state that if equation (1) has a periodic solution (13) when $\mu = 0$, then a unique solution $u(t, \mu)$ exists when the condition $|\mu| < \mu_0$ is satisfied, where μ_0 is a certain positive constant.

Let us proceed now to a determination of $u(t, \mu)$, which is a solution of the equation

$$\ddot{u}(t) + \omega^2 u(t) = \mu F[u(t), \dot{u}(t), u(t-\tau), \dot{u}(t-\tau)], \tag{14}$$

obtained from (1) and (7).

The function $F(t, \tau)$ in the right half of (14) differs from the function $f(t, \tau)$ of equation (1) in that it contains a term transferred from the left half of equation (7)

$$\frac{2\delta - 2q\cos\omega\tau}{1 + \frac{2q}{\omega}\sin\omega\tau}\dot{u}(t),$$

in the linearized system with condition (8) satisfied; this term is equal to zero.

An investigation of equation (3), which describes a linearized system with delay, enables us to conclude that in the analysis of the linear problem we deal with a large number of self-excited oscillations. In practice, however, in nonlinear systems with delay, by virtue of the "small signal discrimination" [1, 11], an oscillation with a single frequency, having a maximum amplitude, is the only one observed. Only under certain conditions can oscillations occur at several frequencies in systems with several resonances [1]. Therefore in the case of a single-loop system, which we are considering, the solution of equation (14) for $\mu = 0$ can be written as

$$u(t) = A\cos\psi, \tag{15}$$

$$\dot{u}(t) = -\omega A \sin\psi. \tag{16}$$

It must be kept in mind here that in the case of a symmetrical resonance characteristic the only existing oscillation is the one with a frequency close to ω_0.

The solution of (14) with $\mu > 0$ will be sought, as in the case of $\mu = 0$, in the form

$$u(t) = A\cos\psi = A\cos(\omega t + \theta), \tag{17}$$

where A and θ are no longer constants, but certain functions of the time.

We shall now regard equation (17) as a certain change in variables; A and θ, which are the amplitude and phase of the oscillation, will be assumed to be new unknown functions of the time, the determination of which on the basis of (17) will yield the sought function $u(t)$. Differentiation of (17) with respect to the time yields

$$\dot{u}(t) = \dot{A}(t)\cos\psi - A(t)\dot{\theta}(t)\sin\psi - \omega A\sin\psi. \tag{18}$$

Taking (17) into account, we obtain from (18)

$$\dot{A}(t)\cos\psi - A(t)\dot{\theta}(t)\sin\psi = 0. \tag{19}$$

Differentiation of (17) yields

$$\ddot{u}(t) = -\omega\dot{A}(t)\sin\psi - \omega A(t)\dot{\theta}(t)\cos\psi - \omega^2 A\cos\psi. \tag{20}$$

Substituting now in (14) the values u(t), $\dot u$(t), and $\ddot u$(t) defined by formulas (15), (16), and (20), we get

$$\begin{gathered} -\omega\dot{A}(t)\sin\psi - \omega A(t)\dot{\theta}(t)\cos\psi = \mu F[A\cos\psi, \\ -\omega A\sin\psi,\ A\cos(\psi-\omega\tau),\ -\omega A\sin(\psi-\omega\tau)]. \end{gathered} \tag{21}$$

Solving (19) and (21) with respect to $\dot A$ and $\dot\theta$ we get

$$\begin{gathered} \dot{A}(t) = -\frac{\mu}{\omega}F[A\cos\psi,\ -\omega A\sin\psi,\ A\cos(\psi-\omega\tau), \\ -\omega A\sin(\psi-\omega\tau)]\sin\varphi, \end{gathered} \tag{22}$$

$$\begin{gathered} \dot{\theta}(t) = -\frac{\mu}{\omega A}F[A\cos\psi,\ -\omega A\sin\psi,\ A\cos(\psi-\omega\tau), \\ -\omega A\sin(\psi-\omega\tau)]\cos\psi. \end{gathered} \tag{23}$$

Equations (22) and (23) are of first order and contain in their right halves periodically varying quantities. The time derivatives $\dot A$ and $\dot\theta$ are proportional to the small parameter μ. For this reason the amplitude A(t)$\dot\theta$ and the phase θ(t) of the oscillations can be regarded, as in the case of nonlinear systems without delay, as slowly varying functions of the time. Thus, the functions A(t) and θ(t) can be assumed constant over the duration of a single period $2\pi/\omega$ when it comes to solving (22) and (23), and in determining the values of $\dot A$(t) and $\dot\theta$(t) with the aid of these equations we can use in place of the instantaneous values of the functions F sin ψ and F cos ψ the values of these functions averaged over the period. Then, changing over to the total phase of the oscillations $\psi = \omega t + \theta$, we obtain in place of (22) and (23)

$$\begin{gathered} \dot{A}(t) = -\frac{\mu}{2\pi\omega}\int_0^{2\pi} F[A\cos\psi, -\omega A\sin\psi, A\cos(\psi-\omega\tau), \\ -\omega A\sin(\psi-\omega\tau)]\sin\psi d\psi, \end{gathered} \tag{24}$$

$$\begin{gathered} \dot{\theta}(t) = \omega - \frac{\mu}{2\pi\omega A}\int_0^{2\pi} F[A\cos\varphi, -\omega A\sin\psi, A\cos(\psi-\omega\tau), \\ -\omega A\sin(\psi-\omega\tau)]\cos\psi d\psi. \end{gathered} \tag{25}$$

Expressions (24) and (25) differ from similar equations for nonlinear systems without delay only in that the integrands contain terms with delayed argument.

Putting $\dot A$(t) = 0 and $\dot\psi$(t) = 0 we can readily determine with the aid of (24) and (25) the approximate values of the amplitude and the frequency of the oscillation established in the system.

In order to obtain the second-approximation equations, which yield A and θ accurate to second order of smallness inclusive, we can use the recommendations given in reference [4].

2. ANALYSIS OF SELF-OSCILLATOR WITH DELAY

By way of an example of the application of the method, let us analyze a self-oscillator with a tuned grid circuit and with a delay line (Fig. 2). According to the symbols used in Fig. 2, neglecting the plate reaction of the tube, we obtain the following system of equations:

$$\begin{gathered} C\dot{u} + i_L + i = 0, \\ L\dot{i}_L + ri_L = u - M\dot{i}_a, \\ i_a = S(u_g)u_g, \end{gathered} \tag{26}$$

where $S(u_g)$ is the transconductance of the tube, which depends on the grid voltage; M — coefficient of mutual conduction.

We assume that the delay line has ideal amplitude-frequency and phase-frequency characteristics and is matched on the tube grid side. Then

$$u_g = u(t-\tau), \quad u = i\rho, \tag{27}$$

where τ — delay time, ρ — wave resistance of the line.

Solving the system (26) and (27) for u, we obtain when $\rho \gg r$ the following nonlinear differential-difference equation of the oscillator:

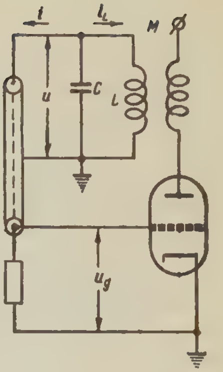

Fig. 2. Principal diagram of high-frequency self-oscillator with delay.

the following nonlinear differential-difference equation of the oscillator:

$$LC\ddot{u}(t) + \left(\frac{L}{\rho} + rC\right)\dot{u}(t) - S[u(t-\tau)]M\dot{u}(t-\tau) + u(t) = 0. \tag{28}$$

To be specific we represent the dependence of the dynamic transconductance on the grid voltage $u_g(t) = u(t-\tau)$, in the case when the operating point is chosen near the point of maximum transconductance, in the following simplified form [5]:

$$S[u(t-\tau)] = S_0 - S_2 u^2(t-\tau). \tag{29}$$

This case, as is well known, corresponds to a soft oscillator mode.

Substituting (29) into (28) and taking (4), (5), and (6) into account, we arrive at an equation of the form (14):

$$\ddot{u}(t) + \omega^2 u(t) = -\mu\left[\frac{S_2\omega_0}{S_0}\dot{u}(t-\tau)u^2(t-\tau) + \frac{1}{\mu}\frac{2\delta - 2q\cos\omega\tau}{1+\frac{2q}{\omega}\sin\omega\tau}\dot{u}(t)\right], \tag{30}$$

where

$$2\delta = \omega_0^2\left(\frac{L}{\rho} + rC\right); \quad 2q = \omega_0^2 S_0 M; \quad \mu = S_0 M\omega_0; \tag{31}$$

$$\omega^2 = \frac{\omega_0^2}{1 + \frac{\omega_0^2 S_0 M}{\omega}\sin\omega\tau}.$$

Bearing in mind that the sought solution $u(t) = A\cos\psi$, we obtain with the aid of (24)

$$\dot{A}(t) = -\frac{\mu A^3\omega_0 S_2}{2\pi S_0}\int_0^{2\pi}\sin(\psi-\omega\tau)\cos^2(\psi-\omega\tau)\sin\psi\,d\psi - {}$$
$$- \frac{A}{2\pi}\frac{2\delta - 2q\cos\omega\tau}{1+\frac{2q}{\omega}\sin\omega\tau}\int_0^{2\pi}\sin^2\psi\,d\psi. \tag{32}$$

Using the formulas for the sine and cosine of the difference of two angles, we can realize (32) and (25) in the form

$$\dot{A}(t) = \frac{\mu A^3\omega_0 S_2}{2\pi S_0}\left[(3\sin^2\omega\tau - 1)\cos\omega\tau J_1 + (1 - 3\cos^2\omega\tau)\sin\omega\tau J_2 - \right.$$

$$-\sin^2\omega\tau\cos\omega\tau J_3 + \sin\omega\tau\cos^2\omega\tau J_4] - \frac{A}{2\pi}\,\frac{2\delta - 2q\cos\omega\tau}{1+\frac{2q}{\omega}\sin\omega\tau}\,J_5, \tag{33}$$

$$\dot{\psi}(t) = \omega + \frac{\mu A^2\omega_0 S_2}{2\pi S_0}\,[(3\sin^2\omega\tau - 1)\cos\omega\tau J_4 + (1 - 3\cos^2\omega\tau)\sin\omega\tau J_1 -$$

$$-\sin^2\omega\tau\cos\omega\tau J_2 + \sin\omega\tau\cos^2\omega\tau J_6] - \frac{A}{2\pi}\,\frac{2\delta - 2q\cos\omega\tau}{1+\frac{2q}{\omega}\sin\omega\tau}\,J_7, \tag{34}$$

where

$$J_1 = \int_0^{2\pi}\sin^2\psi\cos^2\psi\,d\psi; \qquad J_2 = \int_0^{2\pi}\sin^3\psi\cos\psi\,d\psi; \qquad J_3 = \int_0^{2\pi}\sin^4\psi\,d\psi;$$

$$J_4 = \int_0^{2\pi}\sin\psi\cos^3\psi\,d\psi; \qquad J_5 = \int_0^{2\pi}\sin^2\psi\,d\psi; \qquad J_6 = \int_0^{2\pi}\cos^4\psi\,d\psi;$$

$$J_7 = \int_0^{2\pi}\sin\psi\cos\psi\,d\psi.$$

After determining $J_1 = \pi/4$, $J_2 = J_4 = J_7 = 0$, $J_3 = J_6 = \frac{3}{4}\pi$, $J_5 = \pi$ we obtain from (33) and (34) respectively

$$\dot{A}(t) = -\frac{\mu\omega_0 A^3 S_2}{8S_0}\cos\omega\tau - \frac{A}{2}\,\frac{2\delta - 2q\cos\omega\tau}{1+\frac{2q}{\omega}\sin\omega\tau}, \tag{35}$$

$$\dot{\psi}(t) = \omega + \frac{\mu A^2\omega_0 S_2}{8S_0}\sin\omega\tau. \tag{36}$$

The amplitude of the steady-state oscillations in accordance with (35), with $\dot{A}(t) = 0$ and with account of (31), is

$$A_{s.s.} = 2\left[\frac{S_0 M\cos\omega\tau - \left(\frac{L}{\rho} + rC\right)}{S_2 M\cos\omega\tau\left(1 + \frac{\omega_0^2 S_0 M}{\omega}\sin\omega\tau\right)}\right]^{1/2}. \tag{37}$$

The frequency of the stationary oscillations is determined from (36)

$$\omega_{s.s.} = \omega + \frac{\mu A_y^2\omega_0 S_2}{8S_0}\sin\omega\tau = \omega + \frac{\omega_0^2\sin\omega\tau\left[S_0 M\cos\omega\tau - \left(\frac{L}{\rho} + rC\right)\right]}{2\cos\omega\tau\left(1 + \frac{\omega_0^2 S_0 M}{\omega}\sin\omega\tau\right)}. \tag{38}$$

The nonlinear correction to the frequency, as can be seen from (38), is proportional to the small parameter μ. It will be all the greater, the stronger the inequality

$$S_0 M\cos\omega\tau > \frac{L}{\rho} + rC, \tag{39}$$

which, in accordance with (37), is the condition for the self-excitation of the oscillator.

Approximately, accurate to a quantity on the order of μ, we can assume $\omega_{s.s.} = \omega$.

CONCLUSIONS

The method described for investigating nonlinear systems with delay enables us to detect multiple frequencies in oscillators with delayed feedback, determine the frequencies of the possible oscillations, determine the amplitude and frequency of the stationary oscillations, and finally obtain the conditions for self-oscillation.

REFERENCES

1. I.S. Gonorovskii. Contribution to the theory of high-frequency self-oscillators with delayed feedback. Radiotekhnika, 1958, 13, 5, 25.
2. I.S. Gonorovskii. On the establishment of self-oscillations in a high-frequency oscillator with delayed feedback. Ibid., 1958, 14, 1, 15.
3. A.A. Andronov, A.A. Vitt, S.E. Khaikin. Theory of oscillations. GIFML, 1959.
4. N.N. Bogolyubov, Yu.A. Mitropol'skii. Asymptotic methods in the theory of nonlinear oscillations. GIFML, 1958.
5. I.M. Kapchinskii. Methods of the theory of oscillations in radio engineering. GEI, 1954.
6. C.C. Cutler. The regenerative pulse generator. Proc. IRE, 1955, 43, 2, 140.
7. V.S. Kislyakov. Use of the Krylov and Bogolyubov method for constructing asymptotic approximations for the investigation of systems with delay. Automation and remote control. 1960, 21, 4, 442.
8. V.S. Kilyakov. Motivation of the use method of harmonic linearization for the investigation of periodic oscillations of a system with delay. Ibid., 1960, 21, 11, 1480.
9. N.N. Krasovskii. Periodic solutions of differential equations with time delay. Proceedings Academy of Sciences USSR, 1957, 114, 2, 252.
10. N. Minorsky. Self-excited oscillations in dynamical systems possessing retarded actions. Trans. ASME, 1942, 64, 1, 65.
11. V. Met. On multimode oscillators with constant time delay. Proc. IRE, 1957, 45, 8, 1119.

Received by editor 11 January 1961

SMALLEST NUMBER OF CONTROLLABLE ELEMENTS IN AN ANTENNA WITH ELECTRIC BEAM SCANNING

M.I. Kontorovich, V.Yu. Petrun'kin

The question is considered of the number of independent antenna elements necessary to ensure beam scanning in the necessary three-dimensional angle. A relation is derived between the number of elements and the directivity coefficient of the antenna. Linear beam scanning is considered by way of a particular example.

INTRODUCTION

As is well known, electric displacement of the antenna pattern in space can be realized with the aid of a system consisting of a series of radiators, fed with currents (or voltages) with suitable chosen amplitudes and phases. A particular case of such a system is a linear grid of radiators, in which the orientation of the diagram in space is produced by choosing the phases of the currents and individual elements with the amplitudes remaining constant.

In this connection, Vendik [1] has shown that for a specified beam scanning angle Θ_0 and for a specified diagram width $\Delta\cdot\Theta$ of the array, the smallest number of the array elements n independently controlled in phase is determined by the condition

$$n = \frac{\Theta_0}{\Delta\Theta} + 1.$$

In another paper [2], Vendik extends this relation to include a broader class of antennas.

The present article is also devoted to the question of the smallest number of elements in a system that realizes displacement of the directivity pattern in a given three-dimensional angle; we shall attempt, however, to relate the number n not with the width of the diagram, but with the directivity coefficient of the antenna, which, it seems to us, describes the antenna more completely in most cases (although not always).

As can be seen from the derivation given below, the relations obtained in the present article pertain to antenna systems of arbitrary form, provided that neither the antenna itself, nor the surrounding medium contain nonlinear (or time dependent) elements; if such elements are present, they can be regarded only as controlling elements, which do not influence the character of the partial diagrams.

1. ON THE SMALLEST VALUE OF ONE QUADRATIC FORM

We consider in a spherical frame r, φ, Θ, a system of functions $P_i(\varphi, \Theta)$ (i = 1, 4, ..., n) which in general are complex and depend only on φ and Θ.

We assume that the P_i on the surface of a sphere of unit radius are orthogonal and normalized in the sense that the following conditions are satisfied

$$\int_S P_i(\varphi, \Theta)\, P_k^*(\varphi, \Theta)\, ds = 0, \quad \int_S |P_i(\varphi, \Theta)|^2\, ds = 1, \tag{1}$$

where the integration is taken over the sphere of unit radius and P_k^* is the complex conjugate of P_k.

We now set up the function

$$\Phi = \sum_{i=1}^{n} C_i P_i (\varphi, \Theta), \tag{2}$$

which is a linear combination of the functions P_i with coefficients C_i independent of φ or of Θ. In addition, we stipulate that for a certain fixed direction φ_0, Θ_0, the following equation is satisfied

$$\Phi (\varphi_0, \Theta_0) = \sum_{i=1}^{n} C_i P_i (\varphi_0, \Theta_0) = \alpha, \tag{3}$$

where α is a certain real number.

We now set up the quantity

$$Q = \int_S |\Phi^2| \, ds,$$

where the integral is taken over the entire surface of the unit circle. In accordance with (1) we obtain

$$Q = \sum_{i=1}^{n} C_i C_i^* = \sum_{i=1}^{n} |C_i|^2, \tag{4}$$

where C_i^* is the complex conjugate of C_i.

The choice of coefficients C_i was heretofore not limited at all, except for condition (3), and consequently we can specify arbitrarily n - 1 out of the n coefficients; for example, we can choose arbitrarily C_i for all i except i = 1.

Of all the possible systems of coefficients, we now separate one system, defined by the relationships

$$C_{i0} = \alpha \frac{P_i^*}{\sum_{i=1}^{n} |P_i|^2}, \tag{5}$$

and all the quantities are taken here for values $\varphi = \varphi_0$ and $\Theta = \Theta_0$.

It is easy to verify by simple substitution that C_{i0} satisfies relation (3); in addition, it is seen directly that the following equations hold true

$$C_{i0} P_1^* = C_{10} P_i^*. \tag{6}$$

If we now turn to formula (4) and calculate for this case $Q = Q_0$, we obtain

$$Q_0 = |\alpha|^2 \frac{1}{\sum_{i=1}^{n} |P_i|^2}. \tag{7}$$

Let us show now that the value $Q = Q_0$ which we obtained and which corresponds to the coefficients $C_i = C_{i0}$ will be the smallest of all the possible values, subject to the condition, of course, that any system of coefficients satisfies the relation (3).

For this purpose we set up the difference

$$Q - Q_0 = \sum_{i=1}^{n} [|C_i|^2 - |C_{i0}|^2]$$

and make the following transformations:

$$|C_i|^2 = C_i C_i^* = (C_i - C_{i0} + C_{i0})(C_i^* - C_{i0}^* + C_{i0}^*) =$$
$$= (C_i - C_{i0})(C_i^* - C_{i0}^*) + C_{i0}(C_i^* - C_{i0}^*) + C_{i0}^*(C_i - C_{i0}) + C_{i0}C_{i0}^*$$

so that consequently

$$|C_i|^2 - |C_{i0}|^2 = |C_i - C_{i0}|^2 + C_{i0}(C_i^* - C_{i0}^*) + C_{i0}^*(C_i - C_{i0}).$$

Thus

$$Q - Q_0 = \sum_{i=1}^{n} |C_i - C_{i0}|^2 + \sum_{i=0}^{n} [C_{i0}(C_i^* - C_{i0}^*) + C_{i0}^*(C_i - C_{i0})]. \tag{8}$$

From (3) we readily obtain the relation

$$\sum_{i=1}^{n} P_i (C_i - C_{i0}) = 0, \tag{9}$$

and also the complex conjugate relation

$$\sum_{i=1}^{n} P_i^* (C_i^* - C_{i0}^*) = 0. \tag{10}$$

Multiplying now (9) and (10) by C_{10}^*/P_1 and C_{10}/P_1^* respectively and subtracting from (8), we obtain

$$Q - Q_0 = \sum_{i=1}^{n} |C_i - C_{i0}|^2 + \sum_{i=1}^{n} \left[(C_i - C_{i0}) \left(C_{i0}^* - \frac{P_i}{P_1} C_{10}^* \right) + \right.$$
$$\left. + (C_i^* - C_{i0}^*) \left(C_{i0} - \frac{P_i^*}{P_1^*} C_{10} \right) \right].$$

However, on the basis of (6) the last sum vanishes, and consequently

$$Q - Q_0 = \sum_{i=1}^{n} |C_i - C_{i0}|^2 \geqslant 0, \tag{11}$$

from which follows directly the foregoing statement that Q_0 will be the smallest of all the possible Q.

2. ON THE NUMBER OF CONTROLLABLE ELEMENTS WHICH ENSURE BEAM SCANNING WITH THE REQUIRED GAIN

The results obtained above enable us to establish a connection between the number of controlled elements in the radiating system and the beam scanning angle and the directivity coefficient of the antenna.

Let us assume that on the surface of a unit-radius sphere* there is produced an electric field whose tangential component is $E(\varphi, \Theta)$. We now assume that at the point $\varphi_0\Theta_0$ under consideration (the direction of the principal maximum of the antenna pattern) the field is E_0

---

*The radius is chosen sufficiently large to be able to consider the antenna field in the far zone.

$$E(\varphi_0, \Theta_0) = E_0.$$

Assuming the field to be linearly polarized, we can write for the radiation power

$$W = \frac{c}{4\pi} \int\limits_S |E|^2 ds. \tag{12}$$

Then the directivity coefficient of the antenna in the direction φ_0, Θ_0 is given by

$$D = \frac{cE_0^2}{W}. \tag{13}$$

We now consider a radiating system consisting of radiators, each of which produces a field E_i, so that $E = \sum_{i=1}^{n} E_i$.

Since the field produced by each individual radiator is proportional to the intensity of excitation (current, voltage, or some other factor causing a proportional change in the field), we can put

$$E_i = C_i P_i,$$

where P_i — functions that depend on φ and Θ (partial diagrams) and which obey conditions (1)*; C_i — coefficients that do not depend on φ or Θ, and which are determined by the excitation condition of the antenna in such a way that $\alpha = E_0$ [condition (3)].

Thus, we can write

$$E = \sum_{i=1}^{n} C_i P_i. \tag{14}$$

Now, starting with (12), we can write

$$W = \frac{c}{4\pi} \sum_{i=1}^{n} |C_i|^2$$

and in accordance with (7) we obtain the estimate

$$W \geqslant \frac{c}{4\pi} \frac{E_0^2}{\sum\limits_{i=1}^{n} |P_i|^2}.$$

Consequently,

$$D \leqslant 4\pi \sum_{i=1}^{n} |P_i|^2. \tag{15}$$

We now consider D as a function of the coordinates φ_0, Θ_0 (a function of the position of the principal antenna beam in space), and integrate (15) over the surface of the sphere.

---

*Thus, the partial diagrams are assumed orthogonal. It will be shown below that this is not a necessary condition.

Taking into account the normalization (1) of the functions P_i, we obtain

$$\int_S D ds \leqslant 4\pi \sum_{i=1}^{n} \int_S |P_i|^2 ds = 4\pi n$$

or

$$n \geqslant \frac{1}{4\pi} \int_S D ds. \tag{16}$$

Thus, for a given value of D as a function of φ_0 and Θ_0 (i.e., during the process of scanning the beam) the necessary number of partial radiators which make up the antenna and are controlled independently of each other should be not less than the right half of (16). When the coefficients C_i in (14) are chosen equal to C_{i0}, as follows from the preceding, the inequality (16) turns into the equation

$$n = \frac{1}{4\pi} \int_S D ds. \tag{17}$$

Thus, recognizing that the lower limit of inequality (16) can be reached in at least one case, we should assume that the smallest value of n is determined by the equation (17).

We now proceed to an examination of the case when the scanning of the beam is in a certain region S_Ω, corresponding to a solid angle Ω, and attempt to determine the minimum number of controllable elements of the antenna for this case. Leaving aside the question of the physical realizability of the corresponding fields, we first set D equal to zero everywhere except in the region S_Ω; this obviously must be done in order to minimize the integral (17). Thus, we can write

$$n = \frac{1}{4\pi} \int_{S_\Omega} D ds. \tag{18}$$

If D is not constant in the region S_Ω and assumes a maximum value D_{max} and a minimum value D_{min}, we obtain from (18) the inequalities

$$n > \frac{\Omega}{4\pi} D_{\mathbf{min}}, \quad n < \frac{\Omega}{4\pi} D_{\mathbf{max}}. \tag{19}$$

If D is constant in the region S_Ω, we obtain in place of (19)

$$n = \frac{\Omega}{4\pi} D. \tag{20}$$

Thus, if during the process of the beam scanning the gain changes within the limits

$$D_{\mathbf{min}} < D < D_{\mathbf{max}},$$

then the minimum value of n lies in the range defined by (19); if D is constant, then the smallest n that ensures the chosen value of D is given by (20).

3. GENERALIZATION OF THE RESULTS OBTAINED TO THE CASE OF NON-ORTHOGONAL FUNCTIONS

We assumed in the preceding arguments that the functions P_i form an orthogonal system in the sense of relations (1). The results obtained, however, remain in force if the orthogonality condition is not satisfied. This can be seen from the following considerations. If the functions P_i are not orthogonal, then we can employ the known process of orthogonalization and set up a new system of orthogonal functions q_i [3], each of which represents a linear combination of P_i, i.e.,

$$q_i = \sum_{s=1}^{n} \mu_{is} P_s, \tag{21}$$

where $\mu_{i,s}$ are constant coefficients, which in general are complex.

Solving (21) with respect to P_s we get

$$P_i = \sum_{s=1}^{n} \nu_{is} q_s,$$

where $\nu_{i,s}$ are coefficients expressed in terms of the $\mu_{i,s}$. Thus, relation (14) can be rewritten as

$$E = \sum_{i=1}^{n} \sum_{s=1}^{n} C_i \nu_{is} q_s = \sum_{i=1}^{n} d_i q_i, \tag{22}$$

where

$$d_s = \sum_{s=1}^{n} C_s \nu_{st}.$$

Repeating all the preceding arguments with respect to relation (22), which is a linear combination of the functions q_i, obeying the orthogonality conditions, we arrive directly at the previous conclusions.

4. CASE OF LINEAR BEAM SCANNING

The general relations (16) and (20) which we obtained above enable us also to consider the special case when the field depends only on a single coordinate, say φ. In this case, obviously, the displacement can only be along the single line, and in this sense we can speak of a linear beam scanning. It is precisely the case of linear scanning that has until now been considered in the literature [1, 2].

We assume accordingly that the displacement of the beam is in the azimuthal direction and that its position is determined by the angle φ_0.

The characteristic of the directivity of the radiating system is, for each φ_0, a function of φ and is independent of the polar angle Θ. Accordingly, the electric field (on the sphere considered above) can be represented as

$$E = E_0 A(\varphi, \varphi_0),$$

where $A(\varphi, \varphi_0)$ is a function of φ, which turns into unity when $\varphi = \varphi_0$.

Expression (12) now assumes the form

$$W = \frac{c}{4\pi} E_0^2 \int_0^{2\pi} |A|^2 d\varphi \int_0^{\pi} \sin\Theta \, d\Theta = \frac{cE_0^2}{2\pi} \int_0^{2\pi} |A|^2 d\varphi,$$

and consequently

$$D = \frac{cE_0^2}{W} = \frac{2\pi}{\int_0^{2\pi} |A|^2 d\varphi}.$$

Substituting in (17) this expression for D, we obtain

$$n = \frac{1}{2}\int_0^{2\pi} \frac{d\varphi_0}{\int_0^{2\pi} | A | (\varphi, \varphi_0) |^2 \, d\varphi} \int_0^{\pi} \sin \Theta_0 \, d\Theta_0 = \int_0^{2\pi} \frac{d\varphi_0}{\int_0^{2\pi} | A | (\varphi, \varphi_0) |^2 \, d\varphi} . \qquad (23)$$

If we introduce

$$D_\varphi = \frac{2\pi}{\int_0^{2\pi} | A (\varphi, \varphi_0) |^2 \, d\varphi} ,$$

then (23) assumes the form

$$n = \frac{1}{2\pi} \int_0^{2\pi} D_\varphi (\varphi_0) \, d\varphi_0 . \qquad (24)$$

This formula is similar to (17). The quantity D_φ contained here is the ratio of the square of the field intensity in the φ_0 direction to the mean value of the square of the field intensity on the arc of a great circle on the sphere, and is in this case the analog of the directivity coefficient D.

If we assume, as we did in Section 2, that the field beyond the limits of the scanning angle ($\varphi_1 < \varphi < \varphi_2$) vanishes and that D_φ remains constant within this range, we obtain the relation

$$n = \frac{\varphi_2 - \varphi_1}{2\pi} D_\varphi , \qquad (25)$$

which is an analog of (20).

It is interesting to note that in the case when the directivity characteristic of the radiator has the form

$$| A (\varphi, \varphi_0) | = \frac{\sin a (\varphi - \varphi_0)}{a (\varphi - \varphi_0)} ,$$

we obtain for D_φ the expression

$$D_\varphi \simeq \frac{5.6}{\Delta\varphi} ,$$

where $\Delta\varphi$ is the width of the diagram at the half-power points, and (25) yields

$$n \simeq \frac{\varphi_2 - \varphi_1}{\Delta\Theta} .$$

Thus, for this special case we obtain an expression which agrees approximately with the formula derived by Vendik.

In conclusion, it is interesting to point out that formulas (24) and (25) hold also for a somewhat more general case than that considered in the present section, namely when the directivity pattern can be represented in the form of a product of two functions, one dependent only on φ and the other dependeng on Θ, i.e., when

$$E = E_0 A (\varphi, \varphi_0) \frac{B (\Theta)}{B (\Theta_0)} .$$

REFERENCES

1. O.G. Vendik. Synthesis of linear array of radiator with non-mechanical beam scanning. News of the colleges. Ministry of Higher Education, USSR, Radio Engineering. 1960, 3, 1, 77.

2. O.G. Vendik. On the distribution of current in an antenna with non-mechanical beam scanning. Ibid., 1961, 4, 1, 64.
3. P.M. Morse, H. Feshbach. Methods of Theoretical Physics. McGraw-Hill, New York, 1953.

Received by editor 25 April 1961

ELECTROMAGNETIC WAVES IN A RECTANGULAR CROSS-SHAPED WAVEGUIDE

N.A. Kuz'min, T.V. Makarov

A variational method is used to find the eigenfunctions and eigenvalues of the waves of a regular ideally conducting cross-shaped waveguide. Numerical results are given.

1. FORMULATION OF THE PROBLEM

The determination of the fields and of the critical frequencies of electromagnetic waves (E and H modes) in a regular ideally conducting waveguide reduces to a solution of the scalar equations

$$\Delta \begin{Bmatrix} \tilde{\psi} \\ \psi \end{Bmatrix} + \begin{Bmatrix} \tilde{\varkappa} \\ \varkappa \end{Bmatrix}^2 \begin{Bmatrix} \tilde{\psi} \\ \psi \end{Bmatrix} = 0 \qquad (1)$$

under suitable boundary conditions:

a) for magnetic wave $\left.\frac{\partial \tilde{\psi}}{\partial n}\right|_{(L)} = 0,$ (2)

b) for electric wave $\psi|_{(L)} = 0$ (3)

on the contour (L) of the transverse cross section ($S_\perp$) of the waveguide. All the geometrical parameters of the cross-shaped waveguide are shown in Fig. 1. The operator Δ is the two-dimensional Laplace operator; $\tilde{\varkappa}$ and $\varkappa$ are the eigenvalues of the magnetic and electric waves, respectively; $\vec{n}$ is the outward normal to the contour; the functions $\tilde{\psi}$ and ψ are the longitudinal components of the magnetic and electric Hertz vectors, connected with the longitudinal components of the fields by the well known relationships

$$H_z = \tilde{\varkappa}^2 \tilde{\psi}, \quad E_z = \varkappa^2 \psi,$$

with

$$\begin{Bmatrix} \tilde{\varkappa} \\ \varkappa \end{Bmatrix}^2 = k^2 - \begin{pmatrix} \tilde{h} \\ h \end{pmatrix}^2,$$

$\tilde{h}$ and h are the propagation constants of the magnetic and electric waves, respectively.

As is well known, the extremal functionals, the Euler equations of which are represented by (1), have the form

$$\begin{Bmatrix}\tilde{\varkappa}\\ \varkappa\end{Bmatrix}^2 = \iint\limits_{S_\perp} \left(\nabla \begin{Bmatrix}\tilde{\psi}\\ \psi\end{Bmatrix}\right)^2 dS_\perp \tag{4}$$

subject to the condition that

$$\iint\limits_{S_\perp} \begin{Bmatrix}\tilde{\psi}\\ \psi\end{Bmatrix}^2 dS_\perp = 1, \tag{5}$$

where ∇ is the two-dimensional Hamiltonian operator.

To abbreviate the notation, we introduce the symbol u_n, which defines the approximate expressions for $\tilde{\psi}$ or ψ, subject to the suitable condition (2) or (3).

To determine the eigenvalues and eigenfunctions it is convenient to use the Ritz method, according to which the approximate solutions are constructed in the form of a series

$$u_n = \sum_{i=1}^{n} a_i \varphi_i, \tag{6}$$

where a_i are coefficients still unknown. The functions φ_i should, in accordance with the Ritz method, satisfy the boundary condition (3); if condition (2) obtains, the requirement on φ_i can be relaxed somewhat. The set of functions $\{\varphi_i\}$ should be a complete and linearly independent system. The coefficients a_i are chosen from the minimum condition (4) subject to condition (5). Thus, the problem reduces to finding the minimum of functions of n variables

$$(\nabla u_n, \nabla u_n) = \sum_{i,j=1}^{n} (\nabla\varphi_i, \nabla\varphi_j)\, a_i a_j,$$

where the parentheses denote the scalar products of the functions. Using the Lagrange method of indeterminate coefficients, we set up a functional

$$F = (\nabla u_n, \nabla u_n) - \begin{Bmatrix}\tilde{\varkappa}\\ \varkappa\end{Bmatrix}^2 (u_n, u_n)$$

and obtain from the condition $\partial F/\partial a_j = 0$ a symmetrical system

$$\sum_{i=1}^{n} a_i \left[(\nabla\varphi_i, \nabla\varphi_j) - \begin{Bmatrix}\tilde{\varkappa}\\ \varkappa\end{Bmatrix}^2 (\varphi_i, \varphi_j)\right] = 0; \quad j = 1, 2, 3, \ldots, n. \tag{7}$$

The system (7) is linear and homogeneous with respect to a_i. From the condition that its determinant must vanish, we obtain a characteristic equation for $\begin{Bmatrix}\tilde{\varkappa}\\ \varkappa\end{Bmatrix}^2$:

$$\begin{vmatrix}
(\nabla\varphi_1, \nabla\varphi_1) - \begin{Bmatrix}\tilde{\varkappa}\\ \varkappa\end{Bmatrix}^2 (\varphi_1, \varphi_1); & (\nabla\varphi_2, \nabla\varphi_1) - \begin{Bmatrix}\tilde{\varkappa}\\ \varkappa\end{Bmatrix}^2 (\varphi_2, \varphi_1); \ldots & (\nabla\varphi_n, \nabla\varphi_1) - \begin{Bmatrix}\tilde{\varkappa}\\ \varkappa\end{Bmatrix}^2 (\varphi_n, \varphi_1); \\
(\nabla\varphi_1, \nabla\varphi_2) - \begin{Bmatrix}\tilde{\varkappa}\\ \varkappa\end{Bmatrix}^2 (\varphi_1, \varphi_2); & (\nabla\varphi_2, \nabla\varphi_2) - \begin{Bmatrix}\tilde{\varkappa}\\ \varkappa\end{Bmatrix}^2 (\varphi_2, \varphi_2), \ldots & (\nabla\varphi_n, \nabla\varphi_2) - \begin{Bmatrix}\tilde{\varkappa}\\ \varkappa\end{Bmatrix}^2 (\varphi_n, \varphi_2); \\
\cdots & \cdots & \cdots \\
(\nabla\varphi_1, \nabla\varphi_n) - \begin{Bmatrix}\tilde{\varkappa}\\ \varkappa\end{Bmatrix}^2 (\varphi_1, \varphi_n); & (\nabla\varphi_2, \nabla\varphi_n) - \begin{Bmatrix}\tilde{\varkappa}\\ \varkappa\end{Bmatrix}^2 (\varphi_2, \varphi_n), \ldots & (\nabla\varphi_n, \nabla\varphi_n) - \begin{Bmatrix}\tilde{\varkappa}\\ \varkappa\end{Bmatrix}^2 (\varphi_n, \varphi_n);
\end{vmatrix} = 0 \tag{8}$$

The smallest of the roots of equation (8) is equal to the minimum of (4) subject to condition (5).

To find the approximate m-th eigenvalue [2] we must seek the minimum of expression (4) subject to the additional conditions

$$(u_m, u_m) = 1, \quad (u_m, u_k) = 0; \quad k = 1, 2, 3, \ldots, (m-1) \tag{9}$$

where u_k is the approximate value of the k-th normalized eigenfunction of the Laplace operator.

2. MAGNETIC WAVES

The first eigenvalue of equation (1) subject to condition (2) will correspond to the fundamental magnetic wave (Fig. 1a).

For the functions φ_i of the fundamental magnetic wave we choose the sequence

$$\varphi_{nm} = \sin\frac{n\pi x}{2a} - \sin\frac{m\pi y}{2a}; \quad n, m = 0, 1, 3, 5, \ldots.$$

We confine ourselves in our calculations to the functions

$$\varphi_1 = \sin\frac{\pi x}{2a}; \quad \varphi_2 = -\sin\frac{\pi y}{2a}; \quad \varphi_3 = \sin\frac{3\pi x}{2a}; \quad \varphi_4 = -\sin\frac{3\pi y}{2a}.$$

Then the approximate expression for the first eigenfunction is written in the form

$$\tilde{\psi}_1 = a_1 \sin\frac{\pi x}{2a} - a_2 \sin\frac{\pi y}{2a} + a_3 \sin\frac{3\pi x}{2a} - a_4 \sin\frac{3\pi y}{2a}.$$

From the vanishing of the first-order determinant in (8) we obtain the first approximation to the eigenvalue

$$\tilde{\varkappa}_1^{(1)} = \frac{\pi}{2a}\sqrt{\frac{1-(1-\sigma)^2+\frac{1}{\pi}(1-\sigma)\sin\pi\sigma}{1-(1-\sigma)^2-\frac{1}{\pi}(1-\sigma)\sin\pi\sigma}}, \tag{10}$$

where $\sigma = b/2a$; the superscript (1) denotes the degree of approximation. The higher the order of the determinant, the greater the accuracy of the eigenvalues and the closer they approach the true values. The calculations were carried out to the fourth-order approximation. The first eigenvalue and the coefficients of the first eigenfunction, expressed as a function of σ with $2a$ = const and normalized in accordance with (5), have been obtained by setting the fourth-order determinant equal to zero and are listed in Table 1. The same table shows for comparison the eigenvalue calculated by formula (10).

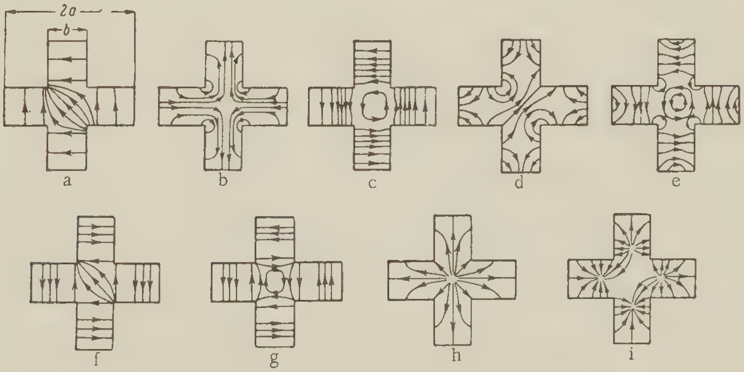

Fig. 1

Table 1

σ	1.0	0.75	0.50	0.25	0.10	0.05
$\tilde{\varkappa}_1^{(1)}\cdot 2a$	3.14	3.34	3.90	4.70	5.20	5.40
$\tilde{\varkappa}_1^{(4)}\cdot 2a$	3.14	3.33	3.88	4.06	3.44	3.60
$\tilde{\varkappa}_1^{(4)}\cdot 2a\,\sigma$	3.14	2.50	1.94	1.02	0.34	0.18
$a_1=a_2$	$\frac{0.5}{a}$	$\frac{0.53}{a}$	$\frac{0.66}{a}$	$\frac{0.97}{a}$	$\frac{1.56}{a}$	$\frac{2.17}{a}$
$a_3=a_4$	0	$\frac{0.0073}{a}$	$\frac{0.03}{a}$	$\frac{0.196}{a}$	$\frac{0.35}{a}$	$\frac{0.50}{a}$

As $\sigma \to 1$ the fundamental wave of the cross-shaped waveguide goes over into a sum of two fundamental degenerate H_{10} and H_{01} modes of a square waveguide with eigenvalues $\pi/2a$. When $\sigma < 1$ the field of the main wave is concentrated on the internal angles of the cross, and it is therefore more advantageous to normalize the eigenvalue of this wave to $2a\sigma$ (3rd row of Table 1). We designate the waves in the cross-shaped waveguide by the same indices as used for the waves of the rectangular waveguide, so that as $\sigma \to 1$ the corresponding wave goes over into the wave of the rectangular waveguide. It is therefore convenient to call the waves of the cross-shaped waveguide quasi-waves of the rectangular waveguide. Figure 2 shows the dependence of the eigenvalue of the quasi-(H_{10} + H_{01}) mode of the cross-shaped waveguide. The distribution of the electric field of this wave in the transverse cross section is shown in Fig. 1a.

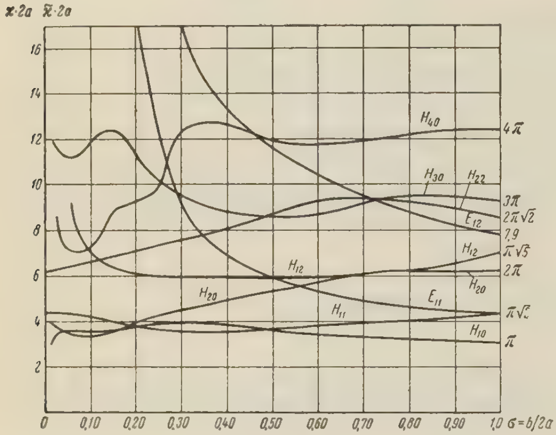

Fig. 2

The second eigenvalue of equation (1) subject to conditions (2) and (9) in a cross-shaped waveguide corresponds to the quasi-H_{11} wave (Fig. 1b). For this wave the functions φ_i have the form

$$\varphi_{nm} = \sin\frac{n\pi x}{2a}\cos\frac{n\pi y}{2a} + \cos\frac{m\pi x}{2a}\sin\frac{m\pi y}{2a}, \quad n, m = 0, 1, 3, 5, \ldots .$$

Confining ourselves to the functions

$$\varphi_1 = \sin\frac{\pi x}{2a}\cos\frac{\pi y}{2a}; \qquad \varphi_2 = \cos\frac{\pi x}{2a}\sin\frac{\pi y}{2a};$$

$$\varphi_3 = \sin\frac{3\pi x}{2a}\cos\frac{3\pi y}{2a}; \qquad \varphi_4 = \cos\frac{3\pi x}{2a}\sin\frac{3\pi y}{2a},$$

we obtain in the first approximation

$$\tilde{\varkappa}_2^{(1)} = \frac{\pi\sqrt{2}}{2a}\sqrt{\frac{1-(1-\sigma)^2-\frac{1}{\pi^2}\sin^2\pi\sigma}{1-(1-\sigma)^2-\frac{1}{\pi^2}\sin^2\pi\sigma}}. \tag{11}$$

The second eigenvalue and the coefficient of the normalized second eigenfunction as a function of σ, obtained from the vanishing of the fourth-order determinant, are listed in Table 2 (see also Fig. 2, curve H_{11}). The same table shows the value of $\tilde{\varkappa}_2^{(1)}$, calculated by formula (11). As $\sigma \to 1$ the quasi-H_{11} wave goes over into a superposition of two H_{11} modes of the square waveguide, the polarizations of which are turned 90° relative to each other, and the eigenvalues of which are $\pi\sqrt{2}/2a$.

Table 2

σ	1.0	0.75	0.50	0.25	0.10	0.05
$\tilde{\varkappa}_2^{(1)}\cdot 2a$	$\pi\sqrt{2}$	4.20	3.90	3.72	4.20	4.38
$\tilde{\varkappa}_2^{(4)}\cdot 2a$	$\pi\sqrt{2}$	4.00	3.62	3,68	4.20	4.38
$a_1=a_2$	$\frac{0.707}{a}$	$\frac{0.708}{a}$	$\frac{0.77}{a}$	$\frac{1.00}{a}$	$\frac{1.58}{a}$	$\frac{2.24}{a}$
$a_3=a_4$	0	$\frac{0.04}{a}$	$\frac{0.005}{a}$	$\frac{0.06}{a}$	$\frac{0,04}{a}$	$\frac{0.04}{a}$

The third eigenvalue of equation (1) subject to conditions (2) and (9) corresponds in a cross-shaped waveguide to a quasi-$(H_{20} + H_{02})$ mode (Fig. 1c). This wave, which is reminiscent of the H_{01} mode in a round waveguide, is described by function φ_i of the form

$$\varphi_{nm} = \cos\frac{n2\pi x}{2a} - \frac{\cos m2\pi y}{2a}; \quad n, m = 0, 1, 2, 3, \ldots.$$

Confining ourselves to the functions

$$\varphi_1 = \cos\frac{2\pi x}{2a}; \quad \varphi_2 = -\cos\frac{2\pi y}{2a}; \quad \varphi_3 = \cos\frac{4\pi x}{2a}; \quad \varphi_4 = -\cos\frac{4\pi y}{2a},$$

we obtain in first approximation

$$\tilde{\varkappa}_3^{(1)} = \frac{2\pi}{2a}\sqrt{\frac{1-(1-\sigma)^2-\frac{1}{2\pi}(1-\sigma)\sin 2\pi\sigma}{1-(1-\sigma)^2+\frac{1}{2\pi}(1-\sigma)\sin 2\pi\sigma}}. \tag{12}$$

The eigenvalue and the coefficients of the normalized eigenfunction as a function of σ, obtained from the vanishing of the fourth-order determinant, are listed in Table 3 (see also Fig. 2, curve H_{20}).

Table 3

σ	1.0	0.75	0.50	0.25	0.10	0.05
$\tilde{\varkappa}_3^{(1)}\cdot 2a$	2π	6.54	6.28	4.76	3.90	3.68
$\tilde{\varkappa}_3^{(4)}\cdot 2a$	2π	6.26	5.27	4.38	3.62	3.42
$a_1=a_2$	$\frac{0.50}{a}$	$\frac{0.53}{a}$	$\frac{0.57}{a}$	$\frac{0.67}{a}$	$\frac{0.92}{a}$	$\frac{1.18}{a}$
$a_3=a_4$	0	$-\frac{0.014}{a}$	$-\frac{0.08}{a}$	$-\frac{0.022}{a}$	$+\frac{0.056}{a}$	$+\frac{0.19}{a}$

The upper row of Table 3 shows the value of $\varkappa_3^{(1)} \cdot 2a$, calculated from formula (12). We see therefore that the maximum value of the parasitic component $a_3/a_1 = a_4/a_2$ will occur at $\sigma = 0.5$, and the minimum will occur at $\sigma \simeq 0.25$. When $\sigma = 0.5$ the internal angles of the cross are precisely in the antinode of the electric field, causing thereby a maximum perturbation of this wave. When $\sigma \to 1$, the quasi-$(H_{20} + H_{02})$ mode goes over into a superposition of two degenerate modes, H_{20} and H_{02}, with eigenvalues equal to $2\pi/2a$.

The quasi-$(H_{12} + H_{21})$ mode (Fig. 1d) is described by the following set of functions φ_i:

$$\varphi_1 = \sin\frac{\pi x}{2a}\cos\frac{2\pi y}{2a}; \qquad \varphi_2 = \cos\frac{2\pi x}{2a}\sin\frac{\pi y}{2a};$$

$$\varphi_3 = \sin\frac{3\pi x}{2a}\cos\frac{4\pi y}{2a}; \qquad \varphi_4 = \cos\frac{4\pi x}{2a}\sin\frac{3\pi y}{2a}.$$

The first approximation of the eigenvalue of the quasi-(H_{12} + H_{21}) mode is

$$\tilde{\varkappa}_4^{(1)} = \frac{\pi\sqrt{5}}{2a}\times$$
$$\times\sqrt{\frac{1-(1-\sigma)^2-\frac{3}{5\pi}(1-\sigma)\sin\pi\sigma-\frac{3}{10\pi}(1-\sigma)\sin 2\pi\sigma-\frac{1}{2\pi^2}\sin\pi\sigma\sin 2\pi\sigma}{1-(1-\sigma)^2+\frac{1}{2\pi}(1-\sigma)\sin\pi\sigma-\frac{1}{\pi}(1-\sigma)\sin 2\pi\sigma+\frac{1}{2\pi^2}\sin\pi\sigma\sin 2\pi\sigma}}. \tag{13}$$

The eigenvalue and the coefficients of the normalized eigenfunction as a function of σ, obtained from the vanishing of the fourth-order determinant, are listed in Table 4 (see also Fig. 2, curve H_{12}). The same table lists the values of $\tilde{\varkappa}_4^{(1)}$ calculated from formula (13). As $\sigma \to 1$ we obtain a superposition of two degenerate H_{21} and H_{12} modes, with eigenvalues $\pi\sqrt{5}/2a$.

Table 4

σ	1.0	0.75	0.50	0.25	0.10	0.05
$\tilde{\varkappa}_4^{(1)}\cdot 2a$	$\pi\sqrt{5}$	6.55	6.25	6.12	7.00	9.00
$\tilde{\varkappa}_4^{(4)}\cdot 2a$	$\pi\sqrt{5}$	6.30	6.00	6.00	7.00	11.7
$a_1=a_2$	$\frac{1.0}{a}$	$\frac{0.99}{a}$	$\frac{0.78}{a}$	$\frac{1.04}{a}$	$\frac{2.57}{a}$	$\frac{4.00}{a}$
$a_3=a_4$	0	$\frac{0.003}{a}$	$\frac{0.05}{a}$	$\frac{0.04}{a}$	$\frac{0.104}{a}$	$\frac{0.318}{a}$

For the fifth eigenvalue of the quasi-H_{22} mode (Fig. 1e), with functions φ_i of the form

$$\varphi_{nm} = \cos\frac{n2\pi x}{2a}\cos\frac{m2\pi y}{2a}; \quad n, m = 1, 2, 3, \ldots$$

the first approximation to $\tilde{\varkappa}_5$ is

$$\tilde{\varkappa}_5^{(1)} = \frac{2\pi\sqrt{2}}{2a}\sqrt{\frac{1-(1-\sigma)^2+\frac{1}{4\pi^2}\sin^2 2\pi\sigma}{1-(1-\sigma)^2+\frac{1}{\pi}(1-\sigma)\sin 2\pi\sigma-\frac{1}{4\pi^2}\sin^2 2\pi\sigma}}. \tag{14}$$

The eigenvalue of this wave is obtained with good accuracy already in the second approximation. Table 5 lists the eigenvalues of the first and second approximations and the coefficients of the normalized eigenfunction of second approximation as a function of σ (see also Fig. 2, curve H_{22}). As $\sigma \to 1$, the quasi-H_{22} mode goes over into a superposition of two H_{22} modes, the polarizations of which are turned 90° relative to each other and the eigenvalues of which are $2\pi\sqrt{2}/2a$.

For the quasi-(H_{30} + H_{03}) mode (Fig. 1f), the functions φ_i have the form

$$\varphi_{nm} = \sin\frac{n3\pi x}{2a} - \sin\frac{m3\pi y}{2a}; \quad n, m = 0, 1, 3, 5, \ldots$$

For

$$\varphi_1 = \sin\frac{3\pi x}{2a}; \quad \varphi_2 = -\sin\frac{3\pi y}{2a}; \quad \varphi_3 = \sin\frac{9\pi x}{2a}; \quad \varphi_4 = -\sin\frac{9\pi y}{2a}$$

the first approximation to $\tilde{\varkappa}_6$ is

$$\tilde{\varkappa}_6^{(1)} = \frac{3\pi}{2a}\sqrt{\frac{1-(1-\sigma)^2+\frac{1}{3\pi}(1-\sigma)\sin 3\pi\sigma}{1-(1-\sigma)^2-\frac{1}{3\pi}(1-\sigma)\sin 3\pi\sigma}}. \tag{15}$$

The eigenvalue and the coefficients of the normalized eigenfunction as a function of σ are listed in Table 6.

Table 5

σ	1.0	0.75	0.50	0.25	0.10	0.05
$\tilde{\varkappa}_5^{(1)}\cdot 2a$	$2\pi\sqrt{2}$	9.58	8.90	7.45	6.70	6.44
$\tilde{\varkappa}_5^{(2)}\cdot 2a$	$2\pi\sqrt{2}$	9.57	8.80	7.44	6.70	6.44
a_1	$\frac{1,0}{a}$	$\frac{1.09}{a}$	$\frac{1.16}{a}$	$\frac{1.23}{a}$	$\frac{1.70}{a}$	$\frac{2.39}{a}$
a_2	0	$-\frac{0.005}{a}$	$+\frac{0.07}{a}$	$+\frac{0.024}{a}$	$-\frac{0.042}{a}$	$-\frac{0.038}{a}$

Table 6

σ	1.0	0.75	0.50	0.25	0.10	0.05
$\tilde{\varkappa}_6^{(1)}\cdot 2a$	3π	9.65	8.70	10.7	14.5	15.7
$\tilde{\varkappa}_6^{(4)}\cdot 2a$	3π	9.50	8.60	10.2	12.0	11.3
$a_1=a_2$	$\frac{0.50}{a}$	$\frac{0.52}{a}$	$\frac{0.56}{a}$	$\frac{0.81}{a}$	$\frac{1.50}{a}$	$\frac{2.18}{a}$
$a_3=a_4$	0	$-\frac{0.006}{a}$	$+\frac{0.01}{a}$	$+\frac{0.014}{a}$	$-\frac{0.46}{a}$	$-\frac{0.51}{a}$

As $\sigma \to 1$, the quasi-($H_{30} + H_{03}$) mode goes over into a sum of two modes, H_{30} and H_{03}, with eigenvalues equal to $3\pi/2a$. It is interesting that (3) $\tilde{\varkappa}_6^{(4)} \cdot 2a = 3\pi$ and $a_3 = a_4 = 0$. When $\sigma = 0$, (6) and $\sigma = 0$. This means that the cross sections with such dimensions hardly perturb the sum of the modes H_{30} and H_{03} of the rectangular waveguide.

For the quasi-($H_{40} + H_{04}$) mode (Fig. 1g), which is similar in its character of field distribution to the H_{02} mode of a round waveguide,* the functions φ_i have the form

$$\varphi_{nm} = \cos\frac{n4\pi x}{2a} - \cos\frac{m4\pi y}{2a}; \quad n, m = 0.\ 1.\ 2.\ 3.\ldots.$$

For

$$\varphi_1 = \cos\frac{4\pi x}{2a}; \quad \varphi_2 = -\cos\frac{4\pi y}{2a}; \quad \varphi_3 = \cos\frac{8\pi x}{2a}; \quad \varphi_4 = -\cos\frac{8\pi y}{2a}$$

the first approximation to the eigenvalue of this wave is

---

*We note that the eigenvalue of this wave does not follow the eigenvalue of the quasi-($H_{30} + H_{03}$) mode. This wave must be taken into account in many cases when considering problems of matching regular round waveguides with bent waveguides of cross-shaped section in the propagation of a H_{01} mode in a round waveguide.

$$\tilde{\varkappa}^{(1)} = \frac{4\pi}{2a}\sqrt{\frac{1-(1-\sigma)^2-\frac{1}{4\pi}(1-\sigma)\sin 4\pi\sigma}{1-(1-\sigma)^2+\frac{1}{4\pi}(1-\sigma)\sin 4\pi\sigma}}. \tag{16}$$

The eigenvalue (Fig. 2) and the coefficients of the normalized eigenfunction of the quasi-(H_{40} + H_{04}) mode as a function of σ, obtained from the vanishing of the fourth-order determinant, are listed in Table 7. The same table shows for comparison the eigenvalue obtained from formula (16).

Table 7

σ	1.0	0.75	0.50	0.25	0.10	0.05
$\tilde{\varkappa}^{(1)}\cdot 2a$	4π	12.51	12.50	12.50	8,60	7,70
$\tilde{\varkappa}^{(4)}\cdot 2a$	4π	12.16	12.00	9.88	7,30	7,06
$a_1 = a_2$	$\frac{0.50}{a}$	$\frac{0.52}{a}$	$\frac{0.5}{a}$	$\frac{0.76}{a}$	$\frac{1,01}{a}$	$\frac{1,39}{a}$
$a_3 = a_4$	0	$-\frac{0.0364}{a}$	0	$-\frac{0.14}{a}$	$-\frac{0.05}{a}$	$-\frac{0,12}{a}$

As $\sigma \to 1$, the quasi-(H_{40} + H_{04}) mode goes over into the (H_{40} + H_{04}) mode of a rectangular waveguide, with eigenvalue $4\pi/2a$.

3. ELECTRICAL WAVES

The determination of the critical frequency of the first electric wave in the waveguide (quasi-E_{11}) (Fig. 1h) reduces to the calculation of the smallest nonvanishing eigenvalue of equation (1) subject to condition (3). For the functions φ_i(x, y) we can choose for this problem a system of functions made up of products of the function ω(x, y) by different combinations of trigonometric functions, where the function ω(x, y) is continuous, has finite and bounded partial derivatives $\partial\omega/\partial x$ and $\partial\omega/\partial y$ within the region S_1, and satisfies the conditions $\omega(x, y) > 0$ inside S_1 and $\omega(x, y) = 0$ on the contour L [3]. The trigonometric functions can be chosen to be

$$\cos\frac{n\pi x}{2a}\cos\frac{m\pi y}{2a}; \qquad n, m = 0, 1, 3, 5, \ldots.$$

For the "cross" region, the function ω(x, y) is defined in the form

$$\omega(x, y) = [|a^2\sigma^2 - x^2| + (a^2\sigma^2 - x^2) + |a^2\sigma^2 - y^2| + \\ + (a^2\sigma^2 - y^2)](a^2 - x^2)(a^2 - y^2). \tag{17}$$

Then the functions φ_i, which satisfy the condition (3) on the entire contour L, will be

$$\varphi_{nm} = \omega(x, y)\cos\frac{n\pi x}{2a}\cos\frac{m\pi y}{2a}; \quad n, m = 0, 1, 3, 5, \ldots.$$

Confining ourselves to the case n = m = 0, we obtain the first approximation to the eigenvalue

$$\varkappa_1^{(1)} = \frac{2}{a}\times$$

$$\times\sqrt{\frac{\frac{8}{45}\sigma^3+\frac{8}{75}\sigma^5+\frac{4}{9}\sigma^6+\frac{24}{4725}\sigma^7-\frac{4}{15}\sigma^8+\frac{8}{945}\sigma^9+\frac{116}{1575}\sigma^{10}-\frac{4}{525}\sigma^{12}}{\frac{64}{225}\sigma^5+\frac{4}{9}\sigma^6-\frac{128}{1575}\sigma^7-\frac{16}{45}\sigma^8+\frac{79}{4725}\sigma^9+\frac{2}{15}\sigma^{10}-\frac{16}{525}\sigma^{12}+\frac{4}{1225}\sigma^{14}}}. \tag{18}$$

The numerical value of $\varkappa_1^{(1)}$ and the coefficient a_0, normalized to the eigenfunction of the quasi-E_{11} mode as a function of σ, are listed in Table 8 (see also Fig. 2).

The determination of the critical frequency of the second electric quasi-($E_{12} + E_{21}$) mode (Fig. 1i) reduces to a calculation of the second eigenvalue of Equation (1) subject to boundary condition (3) and the supplementary condition (9).

Table 8

σ	1,0	0,75	0,50	0,25	0,10	0,05
$\varkappa_1^{(1)} \cdot 2a$	4.5	4,84	6.00	12.2	29.6	64.0
$a_0 a^7$	0,25	0.54	1.50	9.70	48.6	570

Table 9

σ	1,0	0,75	0,50	0,25
$\varkappa_2^{(1)} \cdot 2a$	7.9	9.32	11.74	29.2
$a_1 a^7$	0.29	0.57	1.26	9.48

For the functions φ_i we chose the system

$$\varphi_{nm} = \omega(x, y)\left(\sin\frac{n2\pi x}{2a} + \sin\frac{m2\pi y}{2a}\right); \quad n, m = 1, 2, 3, \ldots.$$

Table 9 lists the values of the coefficient of normalized approximate eigenfunction and the corresponding value of $\varkappa_2^{(1)}$ of the quasi-($E_{12} + E_{21}$) mode as a function of σ subject to the condition n = m = 1.

The formula for $\varkappa_2^{(1)}$ is very cumbersome and is not given here. As $\sigma \to 1$, the quasi-($E_{12} + E_{21}$) mode goes over into a superposition of the two degenerate modes E_{12} and E_{21}, with eigenvalues $\sim\pi\sqrt{5}/2a$. This wave of the cross-shaped waveguide can be represented as a transformed sum of the E_{11} modes of a round waveguide (one with even and the other with odd azimuthal dependences). Consequently, the transition from a round waveguide to a cross-shaped one lifts the degeneracy from the H_{01} and E_{11} modes (see the curves H_{20} and E_{12} respectively in Fig. 2). This makes it possible to make effective use of a cross-shaped waveguide in bends for the transmission of the H_{01} mode.

REFERENCES

1. S.G. Mikhlin. Direct Methods in Mathematical Physics. GITTL, 1950.
2. P. Frank and R. von Mises. Differential and Integral Equations of Mathematical Physics (German). Part II. 1937.
3. L.V. Kontorovich and V.I. Krylov. Approximate Methods of Higher Analysis. Third edition, GITTL, 1950.

Received by editor 13 April 1960

MAGNETOSTATIC OSCILLATIONS OF A SMALL GYROTROPIC SPHEROID MAGNETIZED PERPENDICULAR TO THE AXIS OF ROTATION

Hsu Yen-cheng

We consider a method of calculating the resonant conditions and the field configurations of magnetostatic oscillations of a small transversely magnetized spheroid. By way of example we give the calculations for simple modes corresponding to Walker oscillations (1, - 1) and (2, -1). It is shown that the results obtained can also be used to take into account the influence of the ellipticity of this sphere on the resonance conditions and the resonant fields. The case is considered of a transversely magnetized thin cylinder, and the spectrum of its magnetostatic oscillations is obtained.

INTRODUCTION

The problem of magnetostatic oscillations of a small gyrotropic spheroid, magnetized along the axis of rotation, was first considered by Walker [1]. In the present article we investigate the case of transverse magnetization, the limiting cases of which are a transversely magnetized cylinder and a tangentially magnetized disc. In principle such a problem must be solved with the aid of Lame functions, which have been studied little. However, we shall follow a different path and express the potentials and the field components in terms of series of spheroidal functions which we derive.

1. MAGNETOSTATIC OSCILLATIONS OF A SMALL GYROTROPIC SPHEROID, MAGNETIZED IN THE TRANSVERSE PLANE

The problem will be solved in a spheroidal system of coordinates, which is connected with the Cartesian system of coordinates in the following fashion:

$$\begin{aligned} x &= (a^2 - b^2)^{1/2}(1+\xi^2)^{1/2}(1-\eta^2)^{1/2}\cos\varphi, \\ y &= (a^2 - b^2)^{1/2}(1+\xi^2)^{1/2}(1-\eta^2)^{1/2}\sin\varphi, \\ z &= (a^2 - b^2)^{1/2}\xi\eta. \end{aligned} \tag{1}$$

We assume that the constant magnetic field is directed along the y axis, and that the z axis coincides with the axis of rotation of the spheroid (see Fig. 1).

The permeability of the gyrotropic spheroid is in the form of a tensor

$$\|\mu\| = \begin{vmatrix} \mu & 0 & -ik \\ 0 & 1 & 0 \\ ik & 0 & \mu \end{vmatrix}. \tag{2}$$

Taking into account the smallness of the sample dimensions compared with the wavelength, we can assume that

$$\vec{h} = \operatorname{grad} \psi. \tag{3}$$

Substituting this expression into the equation

$$\operatorname{div} \vec{B} = 0 \tag{4}$$

and taking (2) into account, we obtain a differential equation for the potential ψ_i inside the ferrite:

$$\mu \left(\frac{\partial^2}{\partial x^2} + \frac{\partial^2}{\partial z^2} \right) \psi_i + \frac{\partial^2}{\partial y^2} \psi_i = 0.$$

If we change the coordinate from y to $\sqrt{\mu}\, y'$ [1], this equation reduces to a Laplace equation the solution of which has the form [2]

$$\psi_{i_{n,m}} = P_n^m (i\xi') P_n^m (\eta') \begin{matrix} \cos m\varphi' \\ \sin m\varphi' \end{matrix} =$$

$$= A_{n,m} \int\limits_{-\pi}^{\pi} P_n \left(\frac{iz + x \cos\lambda + \sqrt{\mu}\, y \sin\lambda}{c} \right) \begin{matrix} \cos m\lambda \\ \sin m\lambda \end{matrix} d\lambda,$$

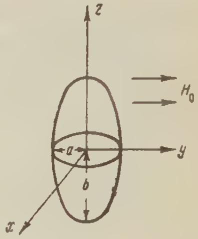

Fig. 1

where $c = (a^2 - b^2)^{1/2}$; ξ', η', and φ' are the modified spheroidal coordinates obtained after making the substitution $y = \sqrt{\mu}\, y'$.

The Legendre polynomial under the integral sign can be transformed in the following fashion:

$$P_n \left(\frac{iz + x \cos\lambda + \sqrt{\mu}\, y \sin\lambda}{c} \right) = P_n \left(\frac{iz + x \cos\lambda + y \sin\lambda}{c} + \frac{\sqrt{\mu} - 1}{c} y \sin\lambda \right) =$$

$$= P_n \left(\frac{iz + x \cos\lambda + y \sin\lambda}{c} \right) + P_n' \left(\frac{iz + x \cos\lambda + y \sin\lambda}{c} \right) \frac{\sqrt{\mu} - 1}{c} y \sin\lambda +$$

$$+ \frac{1}{2!} P_n'' \left(\frac{iz + x \cos\lambda + y \sin\lambda}{c} \right) \left(\frac{\sqrt{\mu} - 1}{c} y \sin\lambda \right)^2 + \ldots,$$

where the prime denotes differentiation with respect to the argument. It must be noted that the series is finite for any specified n.

It is also known that [3]

$$\sin^p \lambda = \begin{cases} \sum\limits_{s=0}^{p/2} A_s \cos (p - 2s) \lambda & \text{for even p,} \\ \sum\limits_{s=0}^{\frac{p-1}{2}} A_s' \sin (p - 2s) \lambda & \text{for odd p,} \end{cases}$$

$$P_n' = (2n - 1) P_{n-1} + (2n - 5) P_{n-3} + (2n - 9) P_{n-5} + \ldots .$$

Using the foregoing expressions, we obtain

$$\psi_{i_{n,m}} = A_{n,m} \sum_{p=0}^{n} y^p \int\limits_{-\pi}^{\pi} \sum_s A_{p,s} P_{n-p-2s} \left(\frac{iz + x \cos\lambda + y \sin\lambda}{c} \right) \times$$

$$\times \begin{matrix} \cos m\lambda \\ \sin m\lambda \end{matrix} \sin^p \lambda\, d\lambda = \sum_{p,q} f_{p,q} (\xi) P_{n-2p}^{n-2q} (\eta) \begin{matrix} \cos (n - 2q) \varphi \\ \sin (n - 2q) \varphi \end{matrix}, \tag{5}$$

where $A_{p,s}$ are certain numerical coefficients; $f_{p,q}(\xi)$ are certain functions of ξ.

The normal component of the induction has the form

$$B_{\xi\, i_{n,m}} = \mu (\operatorname{grad}_\xi \psi_{i_{n,m}}) - ik \left(\frac{\partial \psi_{i_{n,m}}}{\partial x} \cos\alpha_3 - \frac{\partial \psi_{i_{n,m}}}{\partial z} \cos\alpha_1 \right) -$$

$$-(\mu-1)\frac{\partial\psi_{i_{n,m}}}{\partial y}\cos\alpha_2,$$

where $\cos\alpha_1$, $\cos\alpha_2$, $\cos\alpha_3$ are direction cosines, with respective values

$$\left(\frac{1-\eta^2}{a^2}+\frac{\eta^2}{b^2}\right)^{-1/2}\left[\frac{(1-\eta^2)^{1/2}}{a}\cos\varphi,\ \frac{(1-\eta^2)^{1/2}}{a}\sin\varphi,\ \frac{\eta}{b}\right].$$

It is obvious that

$$B_{\xi\, i_{n,m}}=\sum_{u,v} g_{u,v}(\xi)\frac{P_{n-2u}^{n-v}(\eta)}{\left(\frac{1-\eta^2}{a}+\frac{\eta^2}{b^2}\right)^{1/2}}\begin{matrix}\cos(n-v)\varphi\\ \sin(n-v)\varphi\end{matrix}, \tag{6}$$

where $g_{n,\nu}(\xi)$ are certain functions of ξ.

From equations (5) and (6) we see that the boundary conditions cannot be satisfied for one arbitrarily prescribed combination on the indices n and m. To satisfy the boundary conditions for a specified value of n it is necessary to bring into consideration a group of modes whose indices are determined by the following rule:

$$\begin{gathered}\psi_{i_n}=\sum_{p=0}^{N}\sum_{m=0}^{n-2p}\psi_{i_{n-2p,m}}=\sum_{p=0}^{N}\sum_{m=0}^{n-2p}F_{p,m}(\xi)\,P_{n-2p}^{m}(\eta)\begin{matrix}\cos m\varphi\\ \sin m\varphi\end{matrix},\\ \psi_{e_n}=\sum_{p=0}^{N}\sum_{m=0}^{n-2p}Q_{n-2p}^{m}(i\xi)\,P_{n-2p}^{m}(\eta)\begin{matrix}\cos m\varphi\\ \sin m\varphi\end{matrix},\end{gathered} \tag{7}$$

where N = n/2 when n is even and N = (n - 1) / 2 when n is odd; $F_{p,m}(\xi)$ are certain functions of ξ_e; ψ_e is the potential outside the spheroid. We see that to construct the potentials of the natural modes of the spheroid we must take a series ψ_n with terms whose first indices take on all even values (if n is even) or odd values (if n is odd) smaller than n, while the second index runs through all the numbers less than the first index.

It is a very complicated manner to obtain the spectrum for all the modes by satisfying the boundary conditions in general form. Let us consider, by means of simple examples, how one can satisfy the boundary conditions and obtain the resonance conditions.

a) Homogeneous precession, n = 1.

$$\begin{gathered}\psi_i=\frac{c_1x-ic_2z}{(a^2-b^2)^{1/2}}=c_1(1+\xi^2)^{1/2}(1-\eta^2)^{1/2}\cos\varphi-ic_2\xi\eta,\\ \psi_e=c_3Q_1^1(i\xi)\,P_1^1(\eta)\cos\varphi+c_4Q_1(i\xi)\,P_1\eta,\\ B_{\xi i}\big|_{\xi=\xi_0}=\frac{(c_1\mu+c_2k)\,b}{(a^2-b^2)(\eta^2+\xi_0^2)^{1/2}}(1-\eta^2)^{1/2}\cos\varphi-\frac{i\,(c_2\mu+c_1k)\,a\eta}{(a^2-b^2)(\eta^2+\xi_0^2)^{1/2}},\\ B_{\xi e}\big|_{\xi=\xi_0}=\frac{i\xi_0\frac{a}{b}}{(a^2-b^2)(\eta^2+\xi_0^2)^{1/2}}\left[c_3Q_1^{1'}(i\xi_0)\,P_1^1(\eta)\cos\varphi+c_4Q_1'(i\xi_0)\,P_1(\eta)\right].\end{gathered}$$

The resonance condition has the form

$$k^2=\left(\mu-\frac{a^2}{b^2}\frac{i\xi_0Q_1^{1'}(i\xi_0)}{Q_1^1(i\xi_0)}\right)\left(\mu-\frac{i\xi_0Q_1'(i\xi_0)}{Q_1(i\xi_0)}\right). \tag{8}$$

b) Inhomogeneous precession, n = 2, dependence on φ = sin 2φ and sin φ.

$$\begin{gathered}\psi_i=\frac{y\,(c_1'x-ic_2'z)}{a^2-b^2}=\frac{c_1}{18}P_2^2(i\xi)\,P_2^2(\eta)\sin 2\varphi-\frac{c_2'}{9}P_2^1(i\xi)\,P_2^1(\eta)\sin\varphi,\\ \psi_e=c_3'Q_2^2(i\xi)\,P_2^2(\eta)\cos\varphi\sin\varphi+c_4'Q_2^1(i\xi)\,P_2^1(\eta)\sin\varphi.\end{gathered}$$

The resonance condition is

$$k^2 = \left(\mu + 1 - \frac{a^2}{b^2} \frac{i\xi_0 Q_2^{2'}(i\xi_0)}{Q_2^2(i\xi_0)}\right)\left(\frac{b^2}{a^2} + \mu - \frac{i\xi_0 Q_2^{1'}(i\xi_0)}{Q_2^1(i\xi_0)}\right). \tag{9}$$

After making the limiting transitions a → b, $\xi_0 \to \infty$ we obtain $k^2 = (\mu + 4)^2$, which corresponds to the Walker modes (2, -1).

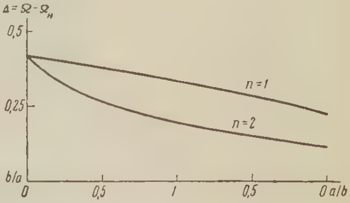

Fig. 2.

In the general case the field of the oscillations is elliptically polarized. The ellipticity of the field is determined by the ratios c_1/c_2 and c'_1/c'_2, the values of which can be readily calculated from the boundary conditions.

Fig. 2 shows the dependence of the roots Δ of equations (8) and (9) on the form of the spheroid when $\Omega_H = H_i/4\pi M_0 = 1$, where H_i is the intensity of the constant magnetic field inside the spheroid and M_0 is the saturation magnetization of the ferrite.

We note that with the aid of the results obtained above we can account for the influence of the ellipticity of the sphere on the resonant conditions of the magnetostatic oscillations. Let us assume that we have $a^2 = b^2 \pm \delta^2$, where δ^2 is a small quantity, i.e., $\delta^2/b^2 \ll 1$ and $|\xi_0^2| = b^2/\delta^2 \gg 1$. We expand the right half of (8) in powers of $1/\xi_0^2$ and confine ourselves to terms up to $(1/\xi_0^2)^2$ inclusive. We can readily calculate the resonant conditions for homogeneous precession

$$\Delta \simeq \frac{1}{3} \pm \frac{1}{30} \frac{\delta^2}{b^2},$$

where $\Delta = -1/(\mu - k - 1)$ (the same as obtained by Walker [1]).

Obviously, the correction (second term of the right half of this equation) is small.

As a consequence of the ellipticity of this sphere, ellipticity occurs in the resonant fields of the homogeneous precession

$$\frac{c_1}{c_2} \simeq 1 \mp \frac{9}{10k} \frac{\delta^2}{b^2}.$$

By the same method we can take into account the influence of the ellipticity of this sphere on the resonant conditions of other magnetostatic-oscillation modes.

2. OSCILLATION SPECTRUM OF TRANSVERSELY MAGNETIZED CYLINDER

In principle one can use the above-described method to determine the resonant conditions of all higher modes of the spheroid oscillations. Although it can be shown that to obtain the spectrum of the oscillations it is sufficient to take in (6) and (7) the terms having indices p = u = 0, the calculations for the higher modes remain very complicated. In practice it is of interest to consider a simpler case, that of a transversely magnetized cylinder.

The case of a longitudinally magnetized cylinder is considered in [4]. The result obtained in that reference differs in that account is taken in its derivation of the finite dimension of the specimen (i.e., the radius of the cylinder) and of the influence of the waveguide wall for the case of a sufficiently slow wave. Obviously, if we put $\chi_2 R \ll 1$, $\chi_0 R \ll 1$ and take only the first term of the expansions of the Bessel and Hankel functions, then equation (35) of [4] goes over into $\mu \pm k = -1$, i.e., into Kitell's resonance condition for the case of a cylinder, and all modes merge into one type. In the present paper, owing to the complexity of the problem, we assume the cylinder to be sufficiently thin; the results obtained here should coincide with that obtained in the preceding section after taking the limiting transition a/b → 0.

The coordinate system associated with the cylinder is shown in Fig. 3. Let us assume that a dependence of the field components on the coordinates has the form

$$f(r, \theta)\, e^{-ihz}. \tag{10}$$

We consider the case of a thin cylinder, i.e.,

$$|k_0 a| \ll 1, \qquad |k_0^2 a^2 \varepsilon\mu| \ll 1,$$
$$|ha| \ll 1, \qquad |k_0^2 a^2 \varepsilon k| \ll 1, \tag{11}$$

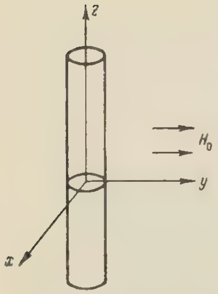

Fig. 3

where $k_0 = \frac{2\pi}{\lambda_0}$ — wave number in a vacuum; a — radius of the cylinder; ϵ — dielectric constant of the ferrite. For this case we can assume the problem to be quasi-static, i.e.,

$$\operatorname{rot} \vec{h} \simeq 0.$$

Consequently, we can put $\vec{h}_i = \operatorname{grad} \psi_i$.

From the equation div $\vec{B} = 0$ with account of relation (2) it follows that

$$\mu \frac{\partial^2}{\partial x^2} \psi_i + \mu \frac{\partial^2}{\partial z^2} \psi_i + \frac{\partial^2}{\partial y^2} \psi_i = 0.$$

Taking (10) and (11) into account, we can neglect the second term in the left half of this equation and obtain

$$\mu \frac{\partial^2}{\partial x^2} \psi_i + \frac{\partial^2}{\partial y^2} \psi_i = 0. \tag{12}$$

The solution of equation (12) assumes the form

$$\psi_i = r^{\pm n} (\cos\theta \pm i\sqrt{\mu}\sin\theta)^n.$$

For the fields inside the cylinder we need take only r^{+n}. It is easy to calculate the field components and the induction components:

$$h_{r_i} = \frac{\partial \psi_i}{\partial r} = n r^{n-1} (\cos\theta \pm i\sqrt{\mu}\sin\theta)^n,$$

$$h_{\theta_i} = \frac{1}{r}\frac{\partial \psi_i}{\partial \theta} = n r^{n-1} (\cos\theta \pm i\sqrt{\mu}\sin\theta)^{n-1} (-\sin\theta \pm i\sqrt{\mu}\cos\theta),$$

$$B_{r_i} = (\mu\cos^2\theta + \sin^2\theta) H_{r_i} + (1-\mu)\sin\theta\cos\theta H_{\theta_i} =$$
$$= n\mu r^{n-1} (\cos\theta \pm i\sqrt{\mu}\sin\theta)^{n-1} \left(\cos\theta \pm \frac{i\sin\theta}{\sqrt{\mu}}\right).$$

Consequently, in constructing the potentials of the natural modes of the cylinder, which should satisfy the boundary conditions on the surface of the cylinder, we must take the series

$$\psi_i = \sum_{p=0}^{N} \{A_{n-2p} r^{n-2p} (\cos\theta + i\sqrt{\mu}\sin\theta)^{n-2p} +$$
$$+ B_{n-2p} r^{n-2p} (\cos\theta - i\sqrt{\mu}\sin\theta)^{n-2p}\}.$$

The potential outside the cylinder has the form

$$\psi_e = \sum_{p=0}^{N} \{C_{n-2p} r^{-n+2p} (\cos\theta + i\sin\theta)^{n-2p} + D_{n-2p} r^{-n+2p} (\cos\theta - i\sin\theta)^{n-2p}\}.$$

To satisfy the boundary conditions we must equate ψ_i with ψ_e and B_{r_i} with B_{r_e} on the surface of the cylinder. Obviously, the resonance conditions are determined by the first terms, which contain $\cos^n\theta$ and $\sin\theta\cos^{n-1}\theta$. This follows from the fact that these terms contain only the coefficients A_n, B_n, C_n and D_n. Therefore, in satisfying the boundary conditions we obtain a system of four equations with four unknowns A_n, B_n, C_n, D_n, which determines completely the resonant conditions. The remaining equations do not influence the resonant conditions; they merely determine the coefficients A_{n-2p}, B_{n-2p}, C_{n-2p}, D_{n-2p} $(p = 1, 2, \ldots, N)$.

It is easy to show that

$$(\cos\theta \pm i\sqrt{\mu}\sin\theta)^n =$$

$$= \left(\sum_s C_n^{2s}\mu^s\right)\cos^n\theta \pm i\left(\sum_s C_n^{2s+1}\sqrt{\mu}\,\mu^s\right)\sin\theta\cos^{n-1}\theta + \text{ other terms},$$

$$\sum_s C_n^{2s}\mu^s = \frac{(1+\sqrt{\mu})^n + (1-\sqrt{\mu})^n}{2},$$

$$\sum_s C_n^{2s+1}\sqrt{\mu}\,\mu^s = \frac{(1+\sqrt{\mu})^n - (1-\sqrt{\mu})^n}{2}. \tag{13}$$

Then the expression for the potentials and the induction components can be transformed in the following fashion:

$$\psi_i = \frac{(A_n+B_n)}{2}[(1+\sqrt{\mu})^n + (1-\sqrt{\mu})^n]\,r^n\cos^n\theta +$$

$$+\frac{(A_n-B_n)\,i}{2}[(1+\sqrt{\mu})^n - (1-\sqrt{\mu})^n]\,r^n\sin\theta\cos^{n-1}\theta + \text{ other terms},$$

$$\psi_e = (C_n+D_n)\,r^{-n}2^{n-1}\cos^n\theta +$$

$$+(C_n-D_n)\,r^{-n}2^{n-1}\,i\sin\theta\cos^{n-1}\theta + \text{ other terms},$$

$$B_{r_e}|_{r=a} = n\sqrt{\mu}\,a^{n-1}\left[\frac{(A_n+B_n)}{2}\{(1+\sqrt{\mu})^n - (1-\sqrt{\mu})^n\}\cos^n\theta +\right.$$

$$\left.+\frac{i(A_n-B_n)}{2}\{(1+\sqrt{\mu})^n + (1-\sqrt{\mu})^n\}\sin\theta\cos^{n-1}\theta\right] + \text{ other terms},$$

$$B_{r_i}|_{r=a} = -na^{-n-1}2^{n-1}[(C_n+D_n)\cos^n\theta +$$

$$+i(C_n-D_n)\sin\theta\cos^{n-1}\theta] + \text{ other terms}.$$

After satisfying the boundary conditions, we obtain the resonance conditions:

a) when $A_n = B_n$

$$(1+\sqrt{\mu})^{n+1} + (1-\sqrt{\mu})^{n+1} = 0,$$

b) when $A_n = -B_n$

$$(1+\sqrt{\mu})^{n+1} - (1-\sqrt{\mu})^{n+1} = 0.$$

We can also combine these conditions

$$(1+\sqrt{\mu})^{n+1} \pm (1-\sqrt{\mu})^{n+1} = 0 \qquad (n \neq 0). \tag{14}$$

Formula (14) can be used to calculate the resonant conditions for any mode. It is important to note that the spectrum of the oscillations lies in the region of negative values of μ. We note also that when $n = 1$ we get $A_1 = B_1$ and the resultant resonant condition is of the form $\mu = -1$, which agrees with Kitell's result for homogeneous precession under suitable choice of the demagnetization coefficients.

If we put $n = 2$, $A_2 = -B_2$ then the resonant condition has the form $\mu = -3$, which coincides with solution (9) after making the limiting transition $a/b \rightarrow 0$.

In conclusion I am grateful to A.A. Pistol'kors for guiding this investigation.

I am greatly indebted to Ya.A. Monosov and A.V. Vashkovskii for many valuable hints.

REFERENCES

1. L.R. Walker. Phys. Rev., 1957, 105, 2, 390.
2. E.W. Hobson. Theory of Spherical and Ellipsoidal Functions (Russian translation), IL, 1952, p. 405 [original published by Cambridge Univ. Press, 1931].
3. I.N. Bronshtein, K.A. Semendyayev. Mathematics Handbook. GITTL, 1954. p. 184.
4. V.V. Nikol'skii. Radio Engineering and Electronic Physics. 1960, 5, 1, 39.

Received by editor 19 January 1961

PROPAGATION OF H_{0n} MODES IN ANNULAR WAVEGUIDE WITH DIELECTRIC SHEATH AND METAL BRAID

I.P. Kotik, A.N. Sivov

We determine the reflection and transmission coefficients for a plane electromagnetic wave obliquely incident on a flat grating in the case when the vector E is parallel to the wires of the grating. The period of the grating is assumed small compared with the wavelength. The shape of the wire and the dielectric filling are assumed to be, generally speaking, different on both sides of the grating and are taken into consideration. The fields near the conductors are determined. The equivalent boundary conditions obtained for this case are used for the analysis of the propagation of H_{0n} mode in an annular waveguide with dielectric sheath and metallic braid. The attenuation due to the losses in the dielectric layer is determined, along with the correction to the phase velocity, compared with a smooth tube. At dielectric thicknesses $d = m\frac{\lambda}{2}\frac{1}{\sqrt{\epsilon'-1}}$ $(m = 1, 2, \ldots)$ a sharp increase in attenuation is observed and is attributed to the occurrence of resonance in the region between the periodic structure and the braid.

1. FORMULATION AND SOLUTION OF THE PROBLEM FOR A PLANE GRATING

In reference [1] is considered a plane electromagnetic wave incident on a dense grating for the case when the vector $\vec{H}$ is parallel to the wires, and the dielectric filling is different on both sides of the grating.

In the present article we analyze a case in which the electric field in the wave incident on the grating is parallel to the wires. Assuming the period p to be small compared with the wavelength λ we must find the transmitted and reflected field, the fields near the conductors, and obtain the boundary conditions equivalent to the action of the grating.

We introduce a rectangular system of coordinates (x, ξ, y), connected with the grating in the following fashion. The ox axis is perpendicular to the wires, and lies in the plane of the grating; the oξ axis is directed along the wires and passes through the center of the cross section of one of the wires; oy coincides with the normal to the plane of the grating. The space above the grating (y > 0) and under the grating (y < 0) is filled with homogeneous dielectrics with dielectric constants ϵ_2 and ϵ_1. In all of space we have $\mu = 1$. The grating is made of parallel ideally conducting cylindrical conductors of arbitrary cross section, but this cross section has two symmetry axes ox and oy. The time dependence of the fields is assumed in the form $e^{i\omega t}$. Since the directions of propagation of the waves are perpendicular to the wires, and the grating is homogeneous in ξ direction, the fields are independent of the the coordinate ξ ($\partial \ldots/\partial \xi \equiv 0$) and the problem is a plane one. According to Maxwell's equations, the nonvanishing components of the field are expressed in terms of E_ξ in the following fashion:

$$H_x = -\frac{1}{ik}\frac{\partial E_\xi}{\partial y}, \quad H_y = \frac{1}{ik}\frac{\partial E_\xi}{\partial x}, \qquad k = \frac{2\pi}{\lambda}. \tag{1}$$

For E_ξ we obtain the Helmholtz equation $\nabla^2 E_\xi + k^2\epsilon_i E_\xi = 0$ with boundary conditions $E_\xi = 0$ on the contour of the wire. Fig. 1 shows a typical portion of the field, bounded by the contours Γ_1 (5' - 4' - 3' - 2 - 3 - 4 - 5) and Γ_2 (4 - 3 - $\bar{2}$' - - 3' - 4' - $\bar{5}$). A plane wave is incident on the grating from the side y' < 0 (see Fig. 1) at an angle φ_1. The reflected wave travels in the negative direction of the y'' axis, while the transmitted wave propagates at the refraction angle φ_2 ($\sin\varphi_2 = \sin\varphi_1 \sqrt{\frac{\varepsilon_1}{\varepsilon_2}}$) in the positive direction of the $\bar{y}$' axis. Portions 5' — 5 and $\bar{5}$' — $\bar{5}$ are sufficiently remote from the grating to guarantee formation of plane-wave fields.

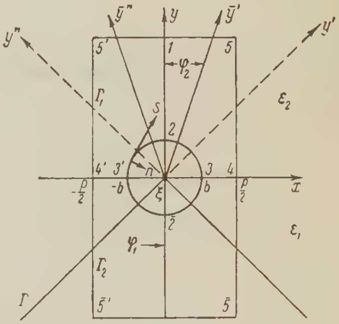

Fig. 1

a) Connection between the fields in the far zones and the fields on the contour of the wire and on the plane y = 0. To determine the connection between the fields in far zones (portions 5' — 5 and $\bar{5}$' — $\bar{5}$) and the fields near the conductors, we apply the Lorentz lemma (see, for example, [2]) to the contours Γ_1 and Γ_2. We choose for the auxiliary fields involved in the lemma the plane-wave fields in the space without the lattice, with a plane interface between dielectrics at y = 0. The directions of propagation of the auxiliary waves are chosen such as to make them "head-on" relative to the true fields; i.e., the field E^1, H^1 (which is head-on with respect to the transmitted wave) is the field of the wave incident on the interface from the opposite side in the negative direction of the y' axis (see Fig. 1). We put $\alpha_i = \sin\varphi_i$; $\beta_i = \cos\varphi_i$. Let us write the expressions for the true fields in the far zones and for the auxiliary fields

$$\begin{aligned}
&y > 0: \quad E_\xi = Te^{-ik\sqrt{\varepsilon_2}\,\bar{y}'},\\
&y < 0: \quad E_\xi = e^{-ik\sqrt{\varepsilon_1}\,y'} + Re^{ik\sqrt{\varepsilon_1}\,y''},\\
&y \geqslant 0: \quad E_\xi^1 = T_1 e^{-ik\sqrt{\varepsilon_2}\,\bar{y}''},\ E_\xi^2 = e^{ik\sqrt{\varepsilon_2}\,\bar{y}'} + R_2 e^{-ik\sqrt{\varepsilon_2}\,\bar{y}''},\\
&y \leqslant 0: \quad E_\xi^1 = e^{-ik\sqrt{\varepsilon_1}\,y''} + R_1 e^{ik\sqrt{\varepsilon_1}\,y'}, \quad E_\xi^2 = T_2 e^{ik\sqrt{\varepsilon_1}\,y'}.
\end{aligned} \tag{2}$$

Here R and T are the sought reflection and transmission coefficients; R_i and T_i are the reflection and transmission coefficients for the auxiliary fields, which are determined from the simple problem involving the incidence of a plane E-polarized wave on a plane interface between two homogeneous dielectrics

$$R_1 = \frac{\sqrt{\varepsilon_1}\beta_1 - \sqrt{\varepsilon_2}\beta_2}{\sqrt{\varepsilon_1}\beta_1 + \sqrt{\varepsilon_2}\beta_2}; \quad T_1 = \frac{2\sqrt{\varepsilon_1}\beta_1}{\sqrt{\varepsilon_1}\beta_1 + \sqrt{\varepsilon_2}\beta_2},$$

$$R_2 = -R_1; \qquad T_2 = T_1 \frac{\sqrt{\varepsilon_2\beta_2}}{\sqrt{\varepsilon_1\beta_1}}. \tag{3}$$

The following relations are satisfied on the lines $\bar{5}' - 5$ and $\bar{5} - 5$

$$\begin{gathered} H\left(\frac{p}{2}\right) = H\left(-\frac{p}{2}\right)e^{-\gamma}, \quad E\left(\frac{p}{2}\right) = E\left(-\frac{p}{2}\right)e^{-\gamma}, \\ H^i\left(\frac{p}{2}\right) = H^i\left(-\frac{p}{2}\right)e^{\gamma}, \quad E^i\left(\frac{p}{2}\right) = E^i\left(-\frac{p}{2}\right)e^{\gamma}, \\ \gamma = ik\sqrt{\varepsilon_1}\alpha_1 p. \end{gathered} \tag{4}$$

This leads to the vanishing of the integrals on the vertical portions. As a result we obtain the sought relations between the fields in the far zone and the fields near the conductors:

$$\begin{gathered} \int\limits_{(5'-5)} (E_\xi^i H_x - E_\xi H_x^i)\,dx = \int\limits_{(3'-2-3)} E_\xi^i H_s ds + \int\limits_{(4'-3'),\,(3-4)} (E_\xi^i H_x - E_\xi H_x^i)\,dx, \\ \int\limits_{(\bar{5}'-\bar{5})} (E_\xi H_x^i - E_\xi^i H_x)\,dx = \int\limits_{(3-\bar{2}-3')} E_\xi^i H_s ds - \int\limits_{(4'-3'),\,(3-4)} (E_\xi^i H_x - E_\xi H_x^i)\,dx. \end{gathered} \tag{5}$$

Substituting the expressions for the fields from (2) in the left halves of (5), we obtain

$$\begin{aligned} 0 &= \int\limits_{(3'-2-3)} E_\xi^1 H_s ds + \int\limits_{(4'-3'),\,(3-4)} (E_\xi^1 H_x - E_\xi H_x^1)\,dx, \\ 2\sqrt{\varepsilon_1}\beta_1 p\,(R_1 - R) &= \int\limits_{(3-\bar{2}-3')} E_\xi^1 H_s ds - \int\limits_{(4'-3'),\,(3-4)} (E_\xi^1 H_x - E_\xi H_x^1)\,dx, \\ -2\sqrt{\varepsilon_2}\beta_2 pT &= \int\limits_{(3'-2-3)} E_\xi^2 H_s ds + \int\limits_{(4'-3'),\,(3-4)} (E_\xi^2 H_x - E_\xi H_x^2)\,dx, \\ 2\sqrt{\varepsilon_1}\beta_1 pT_2 &= \int\limits_{(3-\bar{2}-3')} E_\xi^2 H_s ds - \int\limits_{(4'-3'),\,(3-4)} (E_\xi^2 H_x - E_\xi H_x^2)\,dx. \end{aligned} \tag{6}$$

Thus, the coefficients R and T are expressed in terms of the field on the contour of the wire:

$$\begin{gathered} 2\sqrt{\varepsilon_1}\beta_1 p\,(R_1 - R) = \oint\limits_C E_\xi^1 H_s ds, \\ 2\sqrt{\varepsilon_2}\beta_2 p\,(T_1 - T) = \oint\limits_C E_\xi^2 H_s ds. \end{gathered} \tag{7}$$

b) Field near the wires. The substitution of the Laplace equation for the wave equation leads in our case to an error on the order of $(kp)^2$; therefore, if we find the solution of the equation $\nabla^2 E = 0$ accurate to terms of order $(kp)^2$, we can assume that this solution is equivalent to the true field with the same degree of accuracy. This solution, as follows from (5), will be used only on the contour of the wire and on the line $y = 0$ between the wires. Thus, it is required to find a solution E_ξ of the Laplace equation accurate to terms of order $(kp)^2$, satisfying the following requirements: 1) the quantities E_ξ and $\partial E_\xi/\partial y$ are continuous on $(4' - 3')$, $(3 - 4)$; 2) $E_\xi = 0$ on the contour of the wire. Using the results of [3] [see formulas (25) — (28)], in which it is assumed that $\epsilon_2 = \epsilon_1 = 1$ (we note that the parameters of the dielectrics are not involved in our formulation), we can write an expression for the field near the conductors in terms of two constants A and B, which for the time being are arbitrary, in the form

$$E_\xi = (Ay_2 + By_3)(1 - ik\sqrt{\varepsilon_1}\alpha_1 x_2), \tag{8}$$

where $y_2(x, y)$, $y_3(x, y)$, $x_2(x, y)$ — imaginary and real parts of certain conformal mappings corresponding to the chosen shape of the wires (for a determination of the mappings see [3]).

c) Determination of the sought quantities. Substituting (8) into the first and fourth equations of (6), we obtain the constants A and B, after which, using the field near the conductors, which now is known, we obtain from (7) the sought reflection and transmission coefficients:

$$A = -\frac{2ik\sqrt{\varepsilon_1}\beta_1}{G_2}\,\frac{1}{\dfrac{G_1}{G_2}+\dfrac{D_1}{D_2}}, \qquad B = \frac{2ik\sqrt{\varepsilon_1}\beta_1}{D_2}\,\frac{1}{\dfrac{G_1}{G_2}+\dfrac{D_1}{D_2}}, \tag{9}$$

$$R = -\frac{\dfrac{\overline{G}_2}{G_2}+\dfrac{\overline{D}_2}{D_2}}{\dfrac{G_1}{G_2}+\dfrac{D_1}{D_2}}T_1 + R_1, \qquad T = \frac{\dfrac{\overline{G}_1}{G_2}-\dfrac{\overline{D}_1}{D_2}}{\dfrac{G_1}{G_2}+\dfrac{D_1}{D_2}}T_1. \tag{10}$$

Here

$$G_n = 1 + ik\sqrt{\varepsilon_n}\beta_n l_2, \qquad D_n = 1 + ik\sqrt{\varepsilon_n}\beta_n l_3,$$
$$\overline{G}_n = 1 - ik\sqrt{\varepsilon_n}\beta_n l_2, \qquad \overline{D}_n = 1 - ik\sqrt{\varepsilon_n}\beta_n l_3. \qquad n = 1, 2, \ldots .$$

The parameters l_2 and l_3, which depend on the shape and on the relative dimensions of the wires, are determined from the conformal mappings. For wires with round cross section the calculated values of the parameters l_2/p and l_3/p, obtained with the aid of the Bloch transformation [4], are shown in Fig. 2 as functions of the filling coefficient $q = 2b/p$. Let us consider the limiting cases of formulas (10).

1) When $\epsilon_1 = \epsilon_2 = 1$ expressions (9) and (10) go over into formulas (32) and (33) of [3] for the case where the fields are independent of the coordinate ξ.

2) When $q = 1$ (the grating is converted into a corrugated surface) $l_2 = l_3$ and we obtain

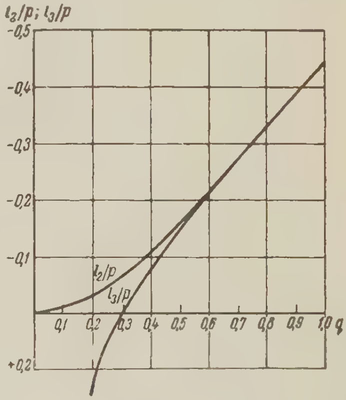

Fig. 2

$$R = -\frac{1 - ik\sqrt{\varepsilon_1}\beta_1 l_2}{1 + ik\sqrt{\varepsilon_1}\beta_1 l_2} \simeq -e^{-2ik\sqrt{\varepsilon_1}\beta_1 l_2}. \tag{11}$$

In this case $T = 0$, $|R| = 1$, as expected.

3) When $q = 0$ we have $l_2/p = 0$, $l_3/p = \infty$ and therefore $R = R_1$, $T = T_1$.

If we eliminate the region of small q, where the parameter l_3/p is large, then formulas (10) can in our approximation be rewritten in the form

$$R = -1 + ik\sqrt{\varepsilon_1}\beta_1(l_3 + l_2), \quad T = ik\sqrt{\varepsilon_1}\beta_1(l_3 - l_2). \tag{12}$$

We see that the coefficients R and T determined by these formulas are independent of the parameters of the outer dielectric, this being a consequence of the negligible [of order $kp\left(\frac{l_3}{p} - \frac{l_2}{p}\right)$] leakage of the field to the outer region. The determined reflection and transmission coefficients enable us to write boundary conditions, equivalent to the action of a real grating

$$E_{\xi 2} - E_{\xi 1} = ikl_2(H_{x2} + H_{x1}),$$
$$E_{\xi 2} + E_{\xi 1} = ikl_3(H_{x2} - H_{x1}). \tag{13}$$

The first boundary condition denotes the presence of a magnetic current along the x axis, while the second denotes the presence of an electric current along the ξ axis. As follows from a comparison with formula (34) of [3], the boundary conditions do not change their form if we consider the problem with a dielectric interface. Conditions (13) can be used to analyze the propagation of H_n modes in periodic waveguides.

2. H_{0n} MODES IN ANNULAR WAVEGUIDE WITH DIELECTRIC SHEATH AND METAL BRAID

To analyze the propagation of H_n modes in an annular waveguide with dielectric sheath and screen (Fig. 3), we make use of boundary conditions (13), written in the cylindrical coordinate system r, φ, z:

$$\begin{aligned} E_{\varphi 1} - E_{\varphi 2} &= ikl_2 (H_{z1} + H_{z2}), \\ E_{\varphi 1} + E_{\varphi 2} &= ikl_3 (H_{z1} - H_{z2}), \end{aligned} \tag{14}$$

which must be satisfied on the periodic structure, i.e., when r = a, and the conditions on the screen $E_{\varphi 2} = 0$ when r = b (b — a = d). In the region a < r < b the dielectric constant has a

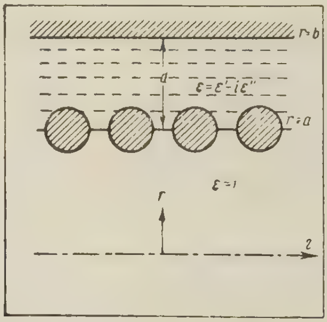

Fig. 3.

value $\epsilon = \epsilon' - i\epsilon$ for the internal region $(0 < r < a)$ $\epsilon = 1$. Substituting the expressions for the field components

$$\begin{aligned} H_{z1} &= \alpha^2 J_0 (\alpha r) A_1, \\ H_{z2} &= \beta^2 [A_2 J_0 (\beta r) + B_2 N_0 (\beta r)], \\ E_{\varphi 1} &= - ik\alpha J_1 (\alpha r) A_1, \\ E_{\varphi 2} &= - ik\beta [A_2 J_1 (\beta r) + B_2 N_1 (\beta r)] \end{aligned} \tag{15}$$

(here $\alpha = \sqrt{k^2 - h^2}$; $\beta = \sqrt{k^2\epsilon - h^2}$; $h = h' - ih''$ — the propagation constant) in the boundary conditions and eliminating the constants, we obtain the dispersion equation. Using the asymptotic representation of the special functions of arguments βa and βb, which is permissible for large ka and when $|\epsilon - 1| > 1$, we can write the dispersion equation in the form

$$\left(\frac{J_1 (\alpha a)}{J_0 (\alpha a)} + \alpha \frac{l_3 + l_2}{2}\right)\left(\operatorname{tg} \beta d + \beta \frac{l_3 + l_2}{2}\right) = \frac{(l_3 - l_2)^2}{4} \alpha\beta. \tag{16}$$

When q = 1 ($l_3 = l_2$) we obtain an equation for a corrugated waveguide with shallow corrugations

$$\frac{J_1 (\alpha a)}{J_0 (\alpha a)} = - \alpha l_2. \tag{17}$$

The phase constant, determined by perturbation theory, is

$$h = h_0 + \frac{p}{a}\frac{l_2}{p}\frac{\mu^2}{h_0 a^2}; \quad J_1(\mu) = 0; \quad h_0 = \sqrt{k^2 - \left(\frac{\mu}{a}\right)^2}. \tag{18}$$

Since the leakage of the field into the region a < r < b is usually negligible when q is not small [proportional to the small quantity $kp\left(\frac{l_3}{p} - \frac{l_2}{p}\right)$], it naturally makes a small contribution to the change in the phase constant. Therefore formula (18) holds also when $q \neq 1$. For attenuation due to losses in the dielectric, we obtain the formula

$$h'' = \frac{(l_3 - l_2)^2}{4}\frac{\mu^2}{h_0 a^4}\,\mathrm{Im}\left[\frac{\beta_0 a}{\mathrm{tg}\,\beta_0 d + \beta_0 l_2}\right], \qquad \beta_0 = \sqrt{k^2\varepsilon - h_0^2}. \tag{19}$$

As $d \to \infty$, we have $\tan \beta_0 d \to -i(\epsilon'' \neq 0)$ and formula (19) goes into formula (1) of reference [5], which determines the losses in an annular waveguide with infinite dielectric sheath. If we assume that $\epsilon'' \ll \epsilon' - 1$ and neglect the quantities μ^2, $\mu^2(l_2/a)^2$, $\mu^2(d/a)^2$ respectively, we can write the formula for the relative attenuation (with respect to the losses in an annular waveguide with infinite dielectric sheath) in the form

$$\eta = \frac{h''(d)}{h''(d = \infty)} = \frac{2}{x}\frac{Q\,(x\,\mathrm{sh}\,2yd - y\sin 2xd)}{[\sin 2xd + 2xl_2Q]^2 + [\mathrm{sh}\,2yd + 2yl_2Q]^2}, \tag{20}$$

$$x = k\sqrt{\varepsilon' - 1}, \quad y = k\frac{\varepsilon''}{2\sqrt{\varepsilon' - 1}}, \quad Q = \mathrm{sh}^2\,yd + \cos^2 xd.$$

The result of the calculations of the relative attenuation for parameter values a = 30 mm, λ = 8 mm, ϵ' = 3, ϵ'' = 0.1, q = 0.5, p = 0.3 mm are plotted in Fig. 4 as a function of d. At dielectric thicknesses $d = \frac{\lambda}{4}(2m + 1)\frac{1}{\sqrt{\epsilon' - 1}}$ we have minima at $\eta = \tanh yd$. When $d = \frac{\lambda}{2}m\frac{1}{\sqrt{\epsilon' - 1}}$ we have η = ~~tang~~ $yd/(l_2 x)^2 + (\tanh yd + l_2 y)^2$. At these points we observe an increase in the relative attenuation. This phenomenon can be explained in the following fashion. The tangential electric field is always equal to zero at r = 0 at r = b (wall of the braid) and is quite small at r = a, i.e., on the surface of the annular waveguide; when the thickness of the dielectric is such that an integral number of half wave lengths fit in the dielectric, resonance occurs in the region between the periodic structure and the screen, accompanied by an accumulation of energy in this region, and this leads to an increase in the attenuation. The considerable decrease in the relative attenuation when the dielectric thickness differs from the "resonant" value can be attributed to the additional return of energy to the internal region owing to multiple reflections in the dielectric layer, in spite of the small coupling between the regions.

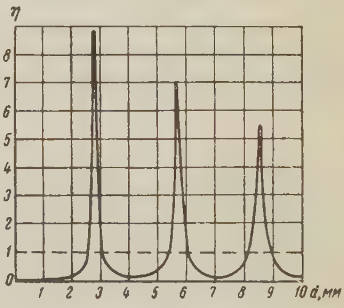

Fig. 4

In conclusion, the authors are deeply grateful to B.Z. Katsenelenbaum for valuable advice made during the performance of the report work.

REFERENCES

1. A.N. Sivov. Incidence of plane electromagnetic wave on a plane grating (case when the vector H is parallel to the wires). Radio Engineering and Electronic Physics. 1961, 6, 1, 58.
2. L.A. Vainshtein. Electromagnetic Waves. Soviet Radio Press, 1957, p. 418.

3. A.N. Sivov. Electrodynamic theory of dense plane grating made of dense plane wires. Radio Engineering and Electronic Physics. 1961, 6, 4, 483.
4. E. Blokh. Investigation of plane grating made up of theoretical profiles of finite thickness. Trudy TsAGI, 1947, no. 611.
5. B.Z. Katsenelenbaum. Attenuation of H_{0n} mode in a helical waveguide. Radio Engineering and Electronic Physics. 1959, 4, 3, 428.

Received by editor 17 April 1961

USE OF LORENTZ LEMMA FOR APPROXIMATE CALCULATION OF THE PROPAGATION CONSTANTS IN AN ELECTRONIC DEVICE SUCH AS A TUBE WITH TRANSVERSE INTERACTION

L.N. Loshakov

An approximate method is described for obtaining the characteristic equation for a tube with transverse interaction, the method being based on the application of the Lorentz lemma under assumptions similar to those previously used in the theory of traveling wave tubes.

INTRODUCTION

In papers [1, 2] we developed the theory of the waveguide model of a tube with transverse interaction (TTI), based on the use of a specific physical model of a slow-wave system in the form of a waveguide filled with dielectric. This theory has enabled us to establish many of the basic properties of the investigated device.

Certain interest, however, is attached to a derivation of more general relations, characterizing the operation of the TTI, and not rigidly connected with the specific type of the slow-wave system. Under certain assumptions, this more general TTI theory can be constructed with the aid of the Lorentz lemma (conjugate lemma) in analogy with the theory previously developed for a traveling wave tube (TWT) with interaction in the longitudinal direction [3, 4].

In the present article we describe the calculation, which has been carried out as applied to a class of slow-wave systems, in which the electromagnetic processes in the absence of an electron beam can be approximately described with the aid of a single harmonic wave propagating along the system. This means that the existence of an aggregate of spatial harmonics will not be taken into account. In spite of the foregoing limitation, the results developed below have a more general character compared with the theory of the waveguide model of the TTI.

1. DERIVATION OF FUNDAMENTAL EQUATION

For maximum simplification of the calculation we assume that the TTI has a slow-wave system, in which the wave propagation is best described in a rectangular coordinate frame. We shall assume that the z axis coincides with the direction of propagation of energy and that the electron beam moves along the transverse x axis.*

We neglect losses and apply the conjugate lemma

$$\int_S ([\vec{E}_I \vec{H}^*_{II}] + [\vec{E}^*_{II} \vec{H}_I])\,\vec{n}\,dS = -\int_V \vec{i}_I \vec{E}^*_{II}\,dV \tag{1}$$

to a small volume V = bdxdz, inside the slow-wave system, bounded by the surface S, assuming that the electron beam in the y axis direction occupies the portion from $y = b_1$ to $y = b_2$ (see the figure). In formula (1) $\vec{E}_I$ and $\vec{H}_I$ denote the electric and magnetic fields in the system in the presence of an electron beam with an ac component of current density $\vec{i}_I$; $\vec{E}_{II}$ and $\vec{H}_{II}$ denote the fields in the same slow-wave system in the absence of an electron beam; $\vec{n}$ is a unit outward normal vector to the surface S. Recognizing that the current density i_I has only one component i along the x axis, we obtain in this case on the basis of formula (1)

$$\frac{\partial}{\partial x}\left\{\int_z^{z+dz} dz \int_0^b ([\vec{E}_I \vec{H}^*_{II}] + [\vec{E}^*_{II} \vec{H}_I])\,\vec{n}_x dy\right\} dx + \\ + \frac{\partial}{\partial z}\left\{\int_x^{x+dx} dx \int_0^b ([\vec{E}_I \vec{H}^*_{II}] + [\vec{E}^*_{II} \vec{H}_I])\vec{n}_z dy\right\} dz = -\int_x^{x+dx} dx \int_z^{z+dz} dz \int_{b_1}^{b_2} iE^*_{IIx} dy. \tag{2}$$

From formula (2) follows the main initial relationship

$$\frac{\partial}{\partial x}\int_0^b ([\vec{E}_I \vec{H}^*_{II}]_x + [\vec{E}^*_{II} \vec{H}_I]_x)\,dy + \frac{\partial}{\partial z}\int_0^b ([\vec{E}_I \vec{H}^*_{II}]_z + [\vec{E}^*_{II} \vec{H}_I]_z)\,dy = -\int_{b_1}^{b_2} iE^*_{IIx}\,dy. \tag{3}$$

We shall assume the operating mode in the device under investigation to be a longitudinally magnetic wave LM_{mn} with $H_x = 0$ and $m \neq 0$, $n \neq 0$. A wave of this type has the field components necessary for interaction.

Specifying a harmonic dependence on the time t in the form $e^{j\omega t}$ with angular frequency ω, in analogy with the theory of the ordinary traveling wave tube [4], we assume for the unknown electric field in the system with electron beam the expressions

$$E_{Ix} = E_{2x} + j\frac{\Gamma}{\omega\varepsilon}\,i, \quad E_{Iy} = E_{2y}, \quad E_{Iz} = E_{2z}, \tag{4}$$

assuming the field component $\vec{E}_2$ to be vortical. In the foregoing expressions Γ is the dispersion coefficient with the aid of which we take into account the influence of the transverse dimensions of the electron beam on the space-charge field, ϵ — dielectric constant of the medium, and $j = \sqrt{-1}$. In the calculation we use the rational practical system of units.

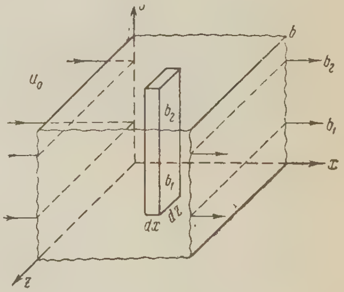

Relation (3) with account of formulas (4) can be rewritten

$$\frac{\partial}{\partial x}\int_0^b (E_{2y}H^*_{IIz} - E_{2z}H^*_{IIy} + E^*_{IIy}H_{Iz} - E^*_{IIz}H_{Iy})\,dy + \\ + \frac{\partial}{\partial z}\int_0^b (E_{Ix}H^*_{IIy} + E^*_{IIx}H_{Iy})\,dy = -\int_{b_1}^{b_2} iE^*_{IIx}dy. \tag{5}$$

---

*It is assumed that slow waves can propagate along the x axis or in both directions indicated.

The expression obtained will be used for approximate calculation in the presence of certain assumptions, similar to those assumed earlier in the theory of the ordinary traveling wave tube [3, 4].

We separate from the standing wave existing in the transverse cross section of the system without the electron beam the wave traveling in the direction of possible motion of the electrons, and characterize this wave by a field $\vec{E}_{II}$, $\vec{H}_{II}$, which we call the auxiliary field. Assuming that the field component E_{IIx} of this wave is described by the expression

$$E_{IIx} = E_{0x}(y)\, e^{j\omega t - j\beta_0 x - jw_0 z}, \tag{6}$$

we can, using the relations derived from Maxwell's equations

$$\begin{aligned} E_{IIy} &= \frac{1}{k^2-\beta_0^2}\frac{\partial^2 E_{IIx}}{\partial x\,\partial y}, \quad & E_{IIz} &= \frac{1}{k^2-\beta_0^2}\frac{\partial^2 E_{IIx}}{\partial x\,\partial z}, \\ H_{IIy} &= \frac{j\omega\varepsilon}{k^2-\beta_0^2}\frac{\partial E_{IIx}}{\partial z}, \quad & H_{IIz} &= -\frac{j\omega\varepsilon}{k^2-\beta_0^2}\frac{\partial E_{IIx}}{\partial y}, \end{aligned} \tag{7}$$

where $k = \omega\sqrt{\epsilon\,\mu}$ is the phase constant of the medium, express their remaining components of the auxiliary field in terms of E_{IIx}.*

The presence of an electron beam perturbs the auxiliary field, which results in the sought field $\vec{E}_I$, $\vec{H}_I$. Using for the previously introduced component E_{2x} of the sought field of the traveling perturbed wave the expression

$$E_{2x} = E_{0x}(y)\, e^{j\omega t + \nu x + \gamma z} \tag{8}$$

and confining ourselves to the case of small signals, we obtain from the electron-ballistics equations by the well known procedure [4]

$$i = \frac{j\omega\varepsilon q E_{2x}}{(\nu + jk_0)^2 + \Gamma q}, \qquad E_{1x} = E_{2x} - \frac{\Gamma q E_{2x}}{(\nu + jk_0)^2 + \Gamma q}. \tag{9}$$

In formulas (9) we use the notation

$$q = \frac{e i_0}{m\varepsilon u_0^3}, \qquad k_0 = \frac{\omega}{u_0}, \tag{10}$$

where e, m and u_0 are the charge, mass, and dc components of the electron velocity respectively; i_0 is the dc component of the electron current density.

Let us assume that the components $\vec{E}_2$ and $\vec{H}_I$ of the sought field can be expressed in terms of E_{2x} by means of formulas such as (7) subject to the condition that the field dependence on the coordinates is given by (8). We can then reduce relation (5), by using (6) — (9) and certain transformations that contain no approximations, to the form

$$\begin{aligned} &\frac{(\nu^2+\beta_0^2)\,\omega\varepsilon}{(k^2-\beta_0^2)^2}\int_0^b \left(\left|\frac{dE_{0x}}{dy}\right|^2 + j\gamma w_0 |E_{0x}|^2 \right) dy + \frac{(\gamma^2 + w_0^2)\,\omega\varepsilon}{k^2-\beta_0^2}\int_0^b |E_{0x}|^2\, dy + \\ &+ \frac{(j\gamma w_0 - w_0^2)\Gamma q}{(\nu + jk_0)^2 + \Gamma q}\,\frac{\omega\varepsilon}{k^2-\beta_0^2}\int_{b_1}^{b_2} |E_{0x}|^2\, dy + \frac{\omega\varepsilon q}{(\nu + jk_0)^2 + \Gamma q}\int_{b_1}^{b_2} |E_{0x}|^2\, dy = 0. \end{aligned} \tag{11}$$

We confine ourselves to an electron beam with sufficiently small current density (the perturbation that it introduces is small). In this case $\nu \simeq j\beta_0$, $\gamma \simeq jw_0$ and the product $j\gamma w_0$ under the integral sign in the first term of formula (11) can be replaced by w_0^2. Using the relations that hold true in the absence of the beam

---

*The wave traveling in the x-axis direction is an E mode.

$$\Pi_{0x} = \frac{1}{2}\,\mathrm{Re}\left(E_{IIy}H^{*}_{IIz} - E_{IIz}H^{*}_{IIy}\right),$$

$$P'_{0x} = \int_0^b \Pi_{0x}\,dy = \frac{\omega\varepsilon\beta_0}{2\left(k^2-\beta_0^2\right)^2}\int_0^b \left(\left|\frac{dE_{0x}}{dy}\right|^2 + w_0^2\,|E_{0x}|^2\right)dy, \tag{12}$$

$$\Pi_{0z} = \frac{1}{2}\,\mathrm{Re}\left(E_{IIx}H^{*}_{IIy}\right), \qquad P'_{0z} = \int_0^b \Pi_{0z}\,dy = \frac{\omega\varepsilon w_0}{2\left(k^2-\beta_0^2\right)}\int_0^b |E_{0x}|^2\,dy, \tag{13}$$

we can reduce (11) to the form

$$(\nu^2+\beta_0^2)\left[(\nu+jk_0)^2+\Gamma q\right] + (\gamma^2+w_0^2)(\nu+jk_0)^2 N + \\ + \left[(\gamma^2+w_0^2)N + (j\gamma w_0 - w_0^2)N_1\right]\Gamma q + q\,\frac{\omega\varepsilon\beta_0}{2P'_{0x}}\int_{b_1}^{b_2} |E_{0x}|^2\,dy = 0, \tag{14}$$

where

$$N = \frac{P'_{0z}}{P'_{0x}}\,\frac{\beta_0}{w_0}; \qquad N_1 = N\,\frac{\int_{b_1}^{b_2} |E_{0x}|^2\,dy}{\int_0^b |E_{0x}|^2\,dy}. \tag{15}$$

At small beam current densities the third term of (14) does not play an essential role and can be neglected. However, the similar term $(\nu^2 + \beta_0^2)\Gamma q$ must be retained because it may combine with the last term of the equation.

Taking the foregoing into account, we can rewrite (14) in the form

$$(\nu^2+\beta_0^2)\left[(\nu+jk_0)^2+\Gamma q\right] + (\gamma^2+w_0^2)(\nu+jk_0)^2 N + q\,\frac{\omega\varepsilon\beta_0}{2P'_{0x}}\int_{b_1}^{b_2} |E_{0x}|^2\,dy = 0. \tag{16}$$

This is the sought characteristic equation relating the unknown propagation constants ν and γ.

2. DISCUSSION OF EQUATION (16) AND ITS APPLICATION TO THE DETERMINATION OF THE PROPAGATION CONSTANTS

In order to verify (16), we first apply it to the waveguide model of the TTI, which previously has been analyzed sufficiently rigorously [1, 2], and which is characterized by the fact that the beam does not influence the dependence of the fields on the coordinate y, a lack of influence on which we based the above approximation. In this case $b_1 = 0$, $b_2 = b$

$$P'_{0x} = \frac{\omega\varepsilon\beta_0}{2\left(k^2-\beta_0^2\right)}\int_0^b |E_{0x}|^2\,dy; \; N = 1, \; \Gamma = 1, \tag{17}$$

and in place of (16) we obtain

$$(\nu^2+\beta_0^2)\left[(\nu+jk_0)^2+q\right] + (\gamma^2+w_0^2)(\nu+jk_0)^2 + q\left(k^2-\beta_0^2\right) = 0. \tag{18}$$

The last equation coincides with the characteristic equation obtained for the waveguide model of the TTI (in comparing equation (18) with equation (16) of article [1] we must put $\beta_0 = m\pi/a$, owing to the difference in notation).

We note that equation (18) points to the necessity of retaining the term $(\nu^2 + \beta_0^2)\Gamma q$ when equation (14) is simplified.

On introducing the dimensionless quantities with the aid of the relations

$$\nu = -j\beta_0 (1 + \delta), \qquad \gamma^2 = -w_0^2 (1 + 2\Theta), \tag{19}$$

$$\eta = \frac{k_0}{\beta_0}, \qquad M = \frac{q}{\beta_0^2}, \qquad R = \frac{w_0^2}{\beta_0^2} \tag{20}$$

equation (16) assumes the form

$$\begin{aligned} &\delta^4 + 2(2-\eta)\delta^3 + [4(1-\eta) + (1-\eta)^2 + 2NR\theta - \Gamma M]\delta^2 + 2[(1-\eta)^2 + \\ &+ (1-\eta)2NR\theta - \Gamma M]\delta + (1-\eta)^2 2NR\theta + MK_c = 0, \end{aligned} \tag{21}$$

where

$$K_c = \frac{\omega\varepsilon}{2\beta_0 P'_{0x}} \int_{b_1}^{b_2} |E_{0x}|^2 \, dy \tag{22}$$

is the coefficient of coupling between the electron beam and the slow-wave system. The coupling coefficient, defined by formula (22), is similar in meaning to the formula for the coupling coefficient of the ordinary traveling wave tube and the quantities contained in it can be regarded as being referred to a unit length of the system. A comparison shows that the more general characteristic equations of the TTI (21) differ formally from the corresponding equation of the waveguide model of the TTI (formulas (27) of article [1]) in the presence of factors N and Γ in some terms. In the case of the waveguide model of the TTI, as already noted, $n = \Gamma = 1$.

The value of Γ depends on the transverse dimensions of the electron beam and on its coupling with the slow-wave system. A sufficiently rigorous determination of Γ is a complicated matter and calls for special investigation. In the approximate calculations one can use in many cases (small coupling coefficients), apparently, values of Γ obtained for the natural modes in a free electron beam with specified dimensions [4].

The value of N depends on the structure of the slow-wave system. For complex structures, the value of N must be determined.

The characteristic equation of the TTI, unlike the case of the ordinary traveling wave tube, contains two unknown unknowns, namely the correction terms to the propagation constant Γ and θ. Therefore, to find the propagation constants we must solve this equation simultaneously with the boundary conditions, which must be specified on the transverse boundaries of the system. The calculation procedure proposed in [1] can be employed also in the more general case considered here. If the boundary conditions are identical with those of reference [1], the previously obtained formulas can be directly used after replacing $m\pi$, M, and R by $\beta_0 a$, ΓM, and NR respectively in all expressions, with the exception of the product MK_c (a = transverse dimension of the system).

In particular, for $\eta = 1$ it follows from formula (50) of article [1] and from formulas (15), (20), and (22) that

$$\operatorname{Re} \gamma = w_0 \frac{\beta_0 a M K_c}{16NR} = \frac{\beta_0 a M \omega\varepsilon}{32P'_{0z}} \int_{b_1}^{b_2} |E_{0x}|^2 \, dy. \tag{23}$$

The last expression does not contain the quantity P'_{0x}.

It can be assumed that the results previously obtained can be generalized to include cases when the periodic structure of the slow-wave system must be taken into account. For this purpose, in accord with the known traveling wave tube theory [5, 6], we must take P'_{0x} and P'_{0z} to mean the time-averaged power fluxes per unit length and width of the system respectively, produced by the aggregate of the spatial harmonics. In this case the sign of P'_{0x} and P'_{pz} may differ from the sign of the phase constant of the operating spatial harmonics in the corresponding direction.

REFERENCES

1. L.N. Loshakov. On the theory of an electronic microwave device with interaction in the transverse direction. Radio Engineering and Electronic Physics. 1960, 5, 9, 1448.
2. L.N. Loshakov. On the coupling coefficient between the electron beam and the slow-wave system in a microwave device with interaction in the transverse direction. Ibid. 1961, Technical Physics). 1956,
3. L.N. Loshakov. Approximate calculation of the propagation constant in transmission lines in the presence of an electron beam. ZhTF (Journal of Technical Physics). 1956, 26, 4, 809.
4. L.N. Loshakov. An account of the space-charge field in the calculation of the propagation constants in a slow wave system in the presence of an electron beam, using the Lorentz lemma. Radio Engineering and Electronic Physics. 1959, 4, 4, 688.
5. L.N. Lolhakov. Use of the Lorentz lemma for the determination of the propagation constant and the interaction between an electron beam and spatial harmonics. Ibid. 1957, 2, 4, 461.
6. L.N. Loshakov. Concerning a preferred form of the expression for the coupling coefficient in the interaction between an electron beam and the spatial harmonics of a slow-wave system. Ibid. 1961, 6, 10, 1685.

Received by editor 4 May 1961

COMBINATION NOISE IN A TRANSIT KLYSTRON

S.N. Kornilov

We analyze theoretically the influence of combination effects on the noise level of a transit klystron operating as a frequency multiplier or amplifier. The conclusions obtained are applicable for an estimate of the ratio of the signal power to the noise power in the case of a multiplier klystron, a two-cavity amplifier, and a cascade amplifier with synchronous tuning of the cavities. The conditions are discussed under which the ratio of these powers is maximal.

INTRODUCTION

The purpose of the present work was to estimate the influence of combination effects on the noise level in a transit klystron used as a frequency multiplier or an amplifier. This question is of interest from the point of view of the loss of stability of the amplified or frequency-converted oscillation. In the present article we consider the effect of fluctuations of the beam velocity in an electron gun, operating in the full space-charge mode, and fluctuations of the exciter voltage.

1. FORMULATION OF THE PROBLEM

Assume that the input to a two-cavity transit klystron is an oscillation in the form $U \sin \omega_n t_1 + V(t_1)$, where $V(t_1)$ is the random component of the voltage. The electron beam

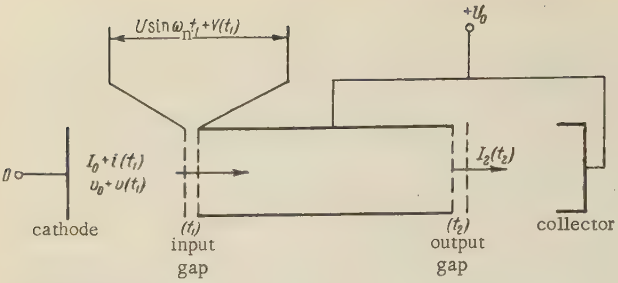

Fig. 1. Diagram to explain the conditions of the problem.

proceeding to the input cavity of the klystron also fluctuates; its current is $I_0 + i(t_1)$ and its velocity is $v_0 + v(t_1)$, where v_0 and I_0 are the dc components, while $v(t_1)$ and $i(t_1)$ are the fluctuating components (Fig. 1).

The distribution of all the fluctuating quantities at the input of the klystron will be assumed normal. It is our task to find the spectral density of the noise power at the output of the klystron operating in the nonlinear mode, i.e., at large values of the bunching parameter relative to the harmonic signal. The results obtained will thus be applicable to modes where the klystron operates as a power amplifier or a frequency multiplier. The analysis is made by the spectral method, and the system regarded as one-dimensional. The space charge in the drift space is disregarded.

2. INITIAL CONDITIONS

In order to know $i(t_1)$ and $v(t_1)$ we must specify a definite model of the noise process in the electron gun. Of greatest practical interest is operation in the space-charge mode. Under these conditions, the fluctuation occurring in the near-cathode region can be regarded as plane, so that the Llewellyn-Peterson formula [1] can be applied. We shall assume that the electron gun consists of two electrodes — a cathode and an anode — and operates in full space-charge mode.

Considering the fluctuation process in a limited time interval from $-T/2$ to $+T/2$, we can obtain with the aid of the Llewellyn equations the connection between the spectral components of the fluctuations at the anode and at the cathode:

$$i_T(\omega) = j\omega T_1 I_0 e^{j\varphi(\omega)} \frac{|v_{\kappa T}(\omega)|}{v_0}, \quad v_T(\omega) = -e^{j\varphi(\omega)} \frac{|v_{\kappa T}(\omega)|}{v_0}, \tag{1}$$

Here $i_T(\omega)$, $v_T(\omega)$, $v_{kT}(\omega)$ — spectral components of the functions, the instantaneous values of which we denote by $i(t_1)$, $v(t_1)$, $v_k(t_1)$; $i(t_1)$ and $v(t_1)$ are the random components of the current and velocity at the anode of the gun; $v_k(t_1)$ — random component of the velocity at the cathode; T_1 — mean transit time of the electrons from the cathode to the anode; it is assumed that $\omega T_1 \gg 3\pi$. The phase $\varphi(\omega)$ has an equiprobable distribution.

The spectral density of the mean square of the velocity fluctuations at the cathode

$$g_\kappa = \lim_{T\to\infty} \frac{2}{T} |v_{\kappa T}(\omega)|^2 = \frac{4-\pi}{I_0} \frac{e}{m} kT_\kappa. \tag{2}$$

Here k is Boltzmann's constant and T_k the cathode temperature. The electron gun may frequently have a complex construction, which can be approximated by a diode followed by a drift section. If the length of the latter is small compared with the effective wavelength of the plasma, then formulas (1) can be used also in this case, taking T_1 to mean the effective transit time, which is equal to the difference in the transit time in the diode and in the drift space: $T_1 = T_d - T_{dr}$.

In the case of deviations from such a construction and from such an operating mode, the fluctuations of the current and velocity at the output of the projector will be determined not only by the velocity noise but also by the current noise in the near-cathode region. However, the theory of fluctuation phenomena at the potential minimum is at present not sufficiently developed to take consistent account of the current noise. Therefore it would hardly be justified to complicate the formulation of the problem, since the number of unverified assumptions in the initial conditions is increased. As regards the behavior of the real devices with diode guns, from the point of view of the noise level the full space charge mode is favorable for such devices.

3. SPECTRUM OF THE CONVECTION CURRENT AT THE OUTPUT OF THE KLYSTRON AND SIGNAL TO NOISE POWER RATIO

The convection current at the output of the klystron is connected with the input current, as is well known, by a relation that follows from the charge-conservation principle:

$$I_2 = I_1 \sum_{k=1}^{k=L} \left|\frac{dt_1}{dt_2}\right|_k, \tag{3}$$

where L is the order of multi-valuedness of the dependence of the exit time t_1 on the entrance time t_2. If we confine ourselves to sufficiently small values of U/U_0, then t_2 is expressed in terms of t_1 in the following fashion:

$$t_2 = t_1 + T_0 - \frac{M_1 U T_0}{2U_0} \sin \omega_n t_1 - \frac{M_1 V(t_1) T_0}{2U_0} - \frac{M_1 V_i(t_1) T_0}{2U_0} - \frac{v(t_1) T_0}{v_0},$$

where U_0 — drift potential; M_1 — coefficient of electron interaction; T_0 — average transit time in the drift space; $V_i(t)$ is the voltage induced by the noise current of the gun in the gap of the input circuit. Let us represent I_2 in the form of a Fourier integral in the finite time interval T. Later on, after we derive the expression needed, we obtain the spectrum of the main square of I_2 by going to the limit $T \to \infty$. The inverse Fourier transformations, pertaining to functions specified on the interval from $-T/2$ to $+T/2$, will be designated by the subscript T. Thus, for the inverse transformation (spectrum) of the convection current I_2 we obtain

$$F_T(\omega) = \int_{-\frac{T}{2}}^{+\frac{T}{2}} I_1 \sum_{k=1}^{k=L} \left|\frac{dt_1}{dt_2}\right|_k e^{-j\omega t_2}\, dt_2. \tag{4}$$

Replacing the integration variable t_2 by t_1 and using the smallness of the fluctuating terms, we can represent (4) in a form more amenable to computations

$$F_T(\omega) = I_0 e^{-j\omega T_0} \int_{-\frac{T}{2}}^{+\frac{T}{2}} [1 + \beta(t_1)]\, e^{-j\left(\omega t_1 - \frac{\omega}{\omega_c} X \sin \omega_n t_1\right)}\, dt_1, \tag{5}$$

where

$$\beta(t_1) = \frac{i(t_1)}{I_0} + j\omega T_0 \frac{M_1 V(t_1)}{2U_0} + j\omega T_0 \frac{M_1 V_i(t_1)}{2U_0} + j\omega T_0 \frac{v(t_1)}{v_0}. \tag{6}$$

Representing $\beta(t_1)$ by means of a Fourier integral and expanding the integrand factor $e^{j\frac{\omega}{\omega_n} X \sin \omega_n t_1}$ in a Bessel-function series, we obtain

$$F_T(\omega) = I_0 e^{-j\omega T_0} \sum_{(n)} J_n\left(\frac{\omega}{\omega_n} X\right) \int_{-\frac{T}{2}}^{+\frac{T}{2}} \left[1 + \frac{1}{2\pi} \int_{-\infty}^{+\infty} f_T(\omega')\, e^{j\omega' t_1}\, d\omega'\right] e^{-j(\omega - n\omega_n) t_1}\, dt_1, \tag{7}$$

where $X = M_1 U \omega_n T_0 / 2U_0$ is the bunching parameter.

The summation extends over all integer values of n from $-\infty$ to $+\infty$. The function $f_T(\omega')$ is the spectrum of the process $\beta(t_1)$, considered in the interval from $-T/2$ to $+T/2$:

$$f_T(\omega') = \int_{-\frac{T}{2}}^{+\frac{T}{2}} \beta(t_1) e^{-j\omega' t_1} dt_1 = \frac{i_T(\omega')}{I_0} + j\omega' T_0 \frac{M_1 V_T(\omega')}{2U_0} + \\ + j\omega' T_0 \frac{M_1 V_{iT}(\omega')}{2U_0} + j\omega' T_0 \frac{v_T(\omega')}{v_0}, \tag{8}$$

where $i_T(\omega')$, $V_T(\omega')$, $V_{iT}(\omega')$, $v_T(\omega')$ — spectra of the corresponding random functions, considered in the finite time interval.

The spectrum of the exciter noise will be assumed, for the sake of being specific, to be uniform; after it is filtered by the input cavity it can be represented in the form $V_T(\omega') = \frac{|Z_1(\omega')|}{R_1} e^{j\varphi(\omega')} |V_T(\omega')|$. We assume that the phase $\psi(\omega')$ also has an equiprobable distribution. In the last formula R_1 is the equivalent resistance of the input resonator, and $Z_1(\omega')$ is its total impedance.

4. SPECTRAL DENSITY OF MEAN-SQUARE CONVECTION CURRENT

The sought spectral density is obviously represented in the following fashion

$$\overline{g_i(\omega)} = \overline{\lim_{T\to\infty} \frac{2}{T} [F_T(\omega) F_T^*(\omega)]}. \tag{9}$$

The superior bar denotes averaging over the ensemble, the need for which follows from the statistical nonstationary nature of the process under consideration. Changing the order of integration in (7) and substituting the resultant value in (9), we have

$$\frac{\overline{g_i(\omega)}}{I_0^2} = \overline{\sum_{(n)} \sum_{(n')} J_n\left(\frac{\omega}{\omega_n} X\right) J_{n'}\left(\frac{\omega}{\omega_n} X\right) \lim_{T\to\infty} \frac{2}{T} \Big\{ 2\pi\delta_T(\omega - n\omega_n) +} \\ \overline{+ \int_{-\infty}^{+\infty} f_T(\omega') \delta_T[\omega' - (\omega - n\omega_n)] d\omega' \Big\} \Big\{ 2\pi\delta_T(\omega - n'\omega_n) +} \\ \overline{+ \int_{-\infty}^{\infty} f_T^*(\omega') \delta_T[\omega' - (\omega - n'\omega_n)] d\omega' \Big\}}. \tag{10}$$

Here $\delta_T(\Omega) = \frac{1}{2\pi} \int_{-\frac{T}{2}}^{+\frac{T}{2}} e^{j\Omega t_1} dt_1$. The limit $\delta_T(\Omega)$ as $T \to \infty$ is equal to the delta-function $\delta(\Omega)$.

Since the cavity at the input of the klystron is as a rule tuned to one of the harmonics of the signal, practical interest is attached to an investigation of the noise spectrum near the frequency $N\omega_n$ where the N is the multiplicity of the harmonic filtered at the output. Within the limits of this band we can disregard all forms of frequency dependence, except resonance, i.e., we can put $J_\nu(\frac{\omega}{\omega_n} X) \simeq J_\nu(NX)$ and $\omega - \nu\omega_n \simeq (N - \nu)\omega_n$.

After several simplifications and averaging, which owing to the equiprobable distribution of the phases φ and ψ in the fluctuating part of the spectrum leaves only series terms with equal indices $n = n'$, the expression for $\overline{g_i(\omega)}$ assumes the following form

$$\frac{\overline{g_i(\omega)}}{I_0^2} = 4\pi^2 J_N^2(NX) \delta(\omega - N\omega_n) + \sum_{(n)} J_n^2(NX)(N-n)^2 p^2 g_k +$$

$$+ [J_{N-1}^2(NX) + J_{N+1}^2(NX)] \left| \frac{Z_1(\omega_c + \delta\omega)}{R_1} \right|^2 (q^2 g_V + s^2 g_K) +$$

$$+ [J_{N-1}^2(NX) - J_{N+1}^2(NX)] \left| \frac{Z_1(\omega_c + \delta\omega)}{R_1} \right| \cos\left(\arg Z_1 + \frac{\pi}{2}\right) p s g_K. \tag{11}$$

Here $\delta\omega = N\omega_n$, it being assumed that $|\delta\omega| \ll \omega_n$; $p = (\Theta_1 - \Theta_0)/v_0$; $q = (M_1\Phi_0)/2U_0$; $S = M_1^2 \Theta_0\Theta_1 R_1/2R_0 v_0$, where $\Theta_0 = \omega_n T_0$; $\Theta_1 = \omega_n T_1$; $R_0 = U_0/I_0$ is the beam resistance. The spectral density of the mean square of the velocity fluctuations at the cathode g_k is determined by the formula (2), and $g_V = \lim_{T\to\infty} \frac{2}{T} |V_T|^2$ is the spectral density of the mean square of the fluctuations of the exciter voltage.

In the derivation we make use of the fact that the terms containing the total impedance Z_1 of the input cavity as a factor have an appreciable value only in the vicinity of ω_n. The first term is proportional here to the power of the spectral line of the N-th harmonic of the determined signal. The second is proportional to the spectral density of the noise power at frequency ω, due to the corresponding portion of the broadband spectrum of the current and to a combination of the signal harmonics with the frequencies of the broadband noise spectrum. The third term gives the component of the spectral noise density, connected with the effect of the narrow-band bunching by means of the noise voltages acting in the input cavity. These voltages are, on the one hand, the noise voltages of the exciter, and on the other the voltages induced by the fluctuating current of the gun. The first term appeared as the result of the correlation between the fluctuation current and the velocity at the output of the gun. Depending on the sign of the detuning of the input cavity, this term can either increase or decrease the total noise power; i.e., the correlation brings about asymmetry of the spectrum.

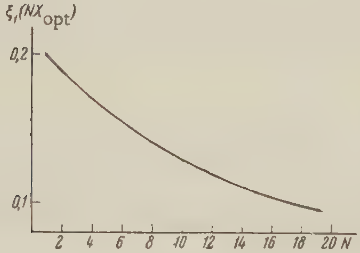

Fig. 2. Dependence of the function $\xi_1(NX)$ on N with the bunching parameter optimal for each N.

The sum of the infinite series in (11) can be calculated by using the Neuman expansion in in squares of Bessel functions

$$\sum_{n=-\infty}^{n=+\infty} J_n^2(z) = 1; \quad \sum_{n=-\infty}^{n=+\infty} n^2 J_n^2(z) = \frac{z^2}{2}.$$

We then obtain for the fluctuation part of the spectrum

$$\frac{\overline{g_{if}(\omega)}}{J_0^2} = \left(1 + \frac{X^2}{2}\right) N^2 p^2 g_K +$$

$$+ \frac{1}{1 + \left(2Q_1 \frac{\delta\omega}{\omega_n}\right)^2} \left[(q^2 g_V + s^2 g_K)\, \xi_1(NX) + 2Q_1 \frac{\delta\omega}{\omega_n} p s g_K\, \xi_2(NX) \right]. \tag{12}$$

Here

$$\xi_1(NX) = J_{N-1}^2(NX) + J_{N+1}^2(NX);$$

$$\xi_2(NX) = J_{N-1}^2(NX) - J_{N+1}^2(NX);$$

$Z_1(\omega_n + \delta\omega)$ is expressed in terms of the Q_1 of the input cavity and the relative detuning $\delta\omega/\omega_n$.

Fig. 2 shows the values of $\xi_1(NX)$ as functions of N under optimal choice of the bunching parameter X for each value of N; under these conditions $\xi_2(NX)$ vanishes for all N. We recall that $g_{if}(\omega)$ is considered in the vicinity of the harmonics of the signal, with the input cavity tuned to the signal frequency. Fig. 3 shows an approximate picture of the spectrum resulting from formula (12). The broadband part of the spectrum is characterized by an increase in the intensity with frequency (proportional to N^2). The narrow-band spectrum, due to the fluctuations and exciter noise induced in the input gap, decreases in intensity with increasing frequency. The spectral density of the mean square of the fluctuation voltage at the output gap is determined by the following expression

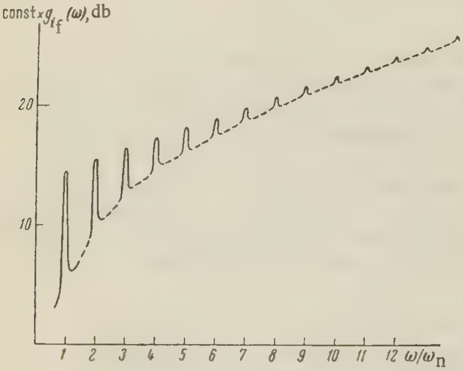

Fig. 3. Approximate form of the spectrum of the mean-square convection current at the output of the klystron. The dashed lines denote portions of the spectrum which are not accurately described by formula (12), which is derived under the assumption that ω/ω_n are close to integer values.

$$\overline{g_{uf}(\omega)} = \frac{M_2^2 \overline{g_{if}(\omega)} R_2^2}{1 + \left(2Q_2 \frac{\delta\omega}{N\omega_n}\right)^2} \tag{13}$$

Here M_2 is the coefficient of electron interaction of the gap; R_2 and Q_2 are the equivalent resistance and the Q of the output cavity, respectively. It is assumed that the cavity is tuned to the N-th harmonic of the signal. In addition to $\overline{g_{if}(\omega)}$ and $\overline{g_{uf}(\omega)}$, it is also interesting to consider the ratio of the signal power to the spectral power density of the noise at frequencies that are symmetrical with respect to the signal frequency:

$$\gamma = \frac{2 I_0^2 J_N^2(NX)\left[1 + \left(2Q_2 \frac{\delta\omega}{N\omega_n}\right)^2\right]}{\overline{g_{if}(N\omega_n + \delta\omega)} + \overline{g_{if}(N\omega_n - \delta\omega)}}. \tag{14}$$

5. DISCUSSION OF THE SOLUTION. NUMERICAL EXAMPLES: FREQUENCY MULTIPLIER, DOUBLY TUNED AMPLIFIER, CASCADE AMPLIFIER WITH SYNCHRONOUS TUNING

It follows from (12) that in the general case the noise spectrum is asymmetrical. This is the consequency of the effect of the input cavity on the phase of the narrow band fluctuations, which are correlated with the broadband fluctuations. The asymmetry is all the stronger, the farther the considered noise band from the resonant frequency; it vanishes when the bunching parameter is optimal for the given N, since $\xi_2(NX_{opt}) = 0$. The noise level of the klystron increases with increasing output frequency; if N is constant, then the broadband part of the noise increases in proportion to the square of the input frequency. The power of narrow band noise, as follows from (12), is proportional to the fourth power of the frequency. Actually, however, the frequency dependence is weaker, for the cavity parameters, the perveance, and the klystron geometry also change with changing range.

Practical interest attaches to two cases: in the first the specific nature of the operation of systems with klystrons is such that noise whose spectrum is concentrated near the carrier is of greatest importance. In the second case we are interested in noise bands situated at a distance of several tens of Mc from the carrier. We disregard in the analysis some specific low-frequency noise sources (flicker effect, vibration, rectifier ripple). The formulas are therefore not applicable to the calculation of the spectral density of noise very close to the carrier frequency. They do make it possible, however, to calculate the noise level in that part of the low-frequency spectrum where the effect of these sources becomes weaker, i.e., at distances on the order of $10^4 - 10^5$ cps). Let us assume that there is no exciter noise ($g_V = 0$). Then, using the smallness of $\delta\omega$, we can approximately write expression (12) for $\overline{g_{if}(\omega)}$:

$$\frac{\overline{g_{if}(\omega)}}{I_0^2} \simeq \left(1+\frac{X^2}{2}\right)N^2p^2g_K + \xi_1(NX)\,s^2g_K.$$

Substituting here the values of s, p, and g_k we obtain

$$\frac{\overline{g_{if}(\omega)}}{I_0^2} \simeq \left[\left(1+\frac{X^2}{2}\right)N^2(\Theta_1-\Theta_0)^2 + \xi_1(NX)\left(\frac{M_1^2\Theta_0\Theta_1R_1}{2R_0}\right)^2\right]\frac{(4-\pi)kT_K}{2R_0}. \tag{15}$$

Let us give a few specific examples.

a) Multiplier klystron. Let us consider the noise properties of a multiplier klystron as the multiplication factor is varied by retuning the input, at a constant setting of the output cavity ($N\omega_n$ = const). We specify parameters characteristic of the low-power multiplier klystron, operating in the three-centimeter band (see, for example, [2]): $U_0 = 2000$ v, $I_0 = 50$ ma, $N\theta_1 = 100$, $N\theta_0 = 35$, $R_1 = 50$ kohm, $M_1 = 0.95$, $Q_1 = 1000$, $Q_2 = 1000$. We allow certain arbitrariness in the computations, by assuming that R_1 and N_1 remain constant as the input frequency changes.

In Fig. 4 we show on a logarithmic scale the coefficients

$$a_1 = \left(1+\frac{X^2}{2}\right)N^2(\Theta_1-\Theta_0)^2,$$

$$a_2 = \xi_1\,(NX)\left(\frac{M_1^2\Theta_0\Theta_1R_1}{2R_0}\right)^2,$$

which characterize the relative shares of the broadband and narrow-band noise for different N; for each N we assume X to be optimal. We see that the influence of the narrow-band noise rapidly decreases with increasing multiplicity. Fig. 5 shows the ratio of the signal power to the spectral density of the noise power, calculated by formula (14). It is practically independent of N.

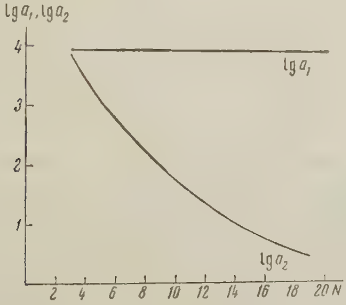

Fig. 4. Dependence of log a_1 and log a_2 on N, characterizing the relative share of the broadband and narrow band noise in a multiplier klystron at constant setting of the output cavity.

The dependence of γ on the bunching parameter X is shown in Fig. 6 for N = 10. The greatest signal to noise power ratio is obtained in the region of optimal values of the bunching parameter.

Let us see now how the multiplier converts the noise of the exciter. We assume that the exciter is the only source of noise; it then follows from (12) that

$$\frac{\gamma}{\gamma_e} = \frac{2 J_N^2(NX)}{X^2 \xi_1(NX)},$$

where $\gamma_e = \frac{U^2}{4g_V}$ is the ratio of the signal power to the spectral density of the noise power of the exciter. At optimal excitation, γ/γ_e is quite close to unity over a wide range of N; i.e., the signal/noise ratio of the exciter is transformed by the multiplier without modification, regardless of the multiplication parameters. In an analysis of noise far from the carrier, this statement becomes incorrect; in this case the signal/noise ratio may be improved by the filtering in the cavities.

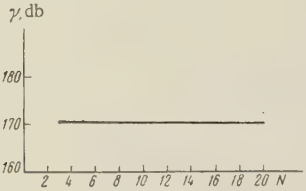

Fig. 5

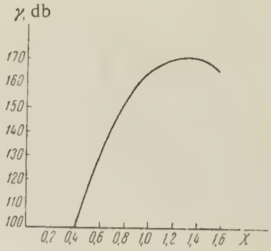

Fig. 6

Fig. 5. Dependence of the ratio of the signal power to the spectral density of the noise power on N at the output of a multiplier klystron at constant setting of the output cavity.

Fig. 6. Dependence of the ratio of the signal power to the spectral density of the noise power on the bunching parameters for a tenfold increase in frequency.

If the multiplier klystron operates as a heterodyne, it is required to know the absolute value of the noise power at a distance from the carrier equal to the intermediate frequency. With the bunching parameter optimal, the noise spectrum is symmetrical about the carrier; it is therefore sufficient to calculate the spectral density in one of the mirror points. For the klystron considered here, with $N = 10$ and $\delta f = 40$ Mc the noise power in a band of 1 Mc is on the order of 10^{-12} watt. This figure is obtained assuming optimum coupling between the output cavity and the load and optimum bunching parameter. The exciter noise is disregarded.

b) Two-cavity amplifying klystron. Let us specify typical parameters for an amplifier klystron of medium power in the three-centimeter band (we use data published in [3]):

$U_0 = 6000$ v, $I_0 = 450$ ma ($P_\sim = 400$ w), $R_1 = 50{,}000$ ohms, $M^2 = 0.55$, $\Theta_1 = 14$, $\Theta_0 = 16.5$.

Using formula (15) with $N = 1$, we calculate $g_{if}(\omega)$ near the carrier, assuming that the bunching parameter is optimal ($X = 1.84$).

The result is

$$\overline{g_{if}(\omega)} = (0.95 \cdot 10^{-23} + 0.48 \cdot 10^{-20}) \frac{a^2}{\text{cps}}.$$

The first term reflects the role of the broadband noise, while the second represents the narrowband noise. The spectral density of the narrowband noise is three orders of magnitude greater. This appreciable difference is due in this case to the closeness of Θ_1 and Θ_0, the difference between which determines the spectral density of the narrow-band noise. However, even if one of these angles is small compared with the other, the narrow-band noise remains one order of magnitude greater than the broadband noise. This is typical of an amplifier klystron. Corresponding to this value is $\gamma = 192$ db [formula (14)]. This figure is considerably better than in the multiplier example considered earlier. The reason for it is the high power rating of the device [the increase in the potential and current on the beam makes it possible to increase the signal power while retaining the same order of fluctuation power, as follows from formula (15)]. Fig. 7 shows the variation of γ as a function of the excitational level of the klystron. The transformation coefficient of the excited noise is close to unity in the case of the amplifier, just as it is in the case of the multiplier, for optimal excitation, independently of the values of the instrument parameters.

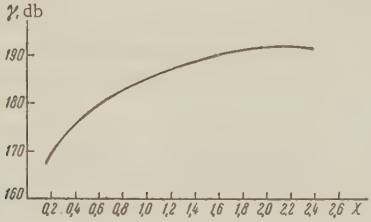

Fig. 7. Dependence of the ratio of the signal power to the spectral density of the noise power on the bunching parameter for a two-cavity amplifier klystron.

c) Cascade klystron in the synchronous-tuning mode. It was noted earlier that the narrowband noise component predominates in the amplitication mode. This enables us to use the derived formulas for the calculation of the combination noise in a synchronously tuned cascade klystron.

Neglecting all the current components induced in the output cavity, except the one existing as a result of the velocity modulation in the preceding gap, we can consider the output stage of the multi-circuit klystron as a two-cavity klystron, the current in the input gap of which has a fluctuating component that is amplified by a factor K_i compared with the component at the output of the gun, where K_i is the current gain of the stages preceding the final stage. Consequently, the ratio of the signal power to the spectral density of the noise power in a cascade klystron decreases as K_i^2:

$$\gamma_{\text{к}} = \frac{\gamma}{K_i^2}\,. \tag{16}$$

By way of illustration let us consider a cascade klystron having the same parameters as the two-cavity klystron considered above; we assume that when four cavities are used we have $K_i = 50$ db. This corresponds to $\gamma_k = 142$ db.

It is natural to ask: what should be done to guarantee a maximum signal to noise power ratio in these devices? Let us examine formula (14) from this point of view, with particular attention to the region of frequencies close to the carrier frequency, and assuming the exciter to be noiseless:

$$\gamma \simeq \frac{I_0^2 J_N^2(NX)}{g_i f(\omega)} = \frac{2 I_0 U_0 J_N^2(NX)}{(4-\pi)\, kT_{\text{к}} \left[\left(1-\frac{X^2}{2}\right) N^2 (\Theta_1-\Theta_0)^2 + \xi_1(NX)\left(\frac{M_1^2 \Theta_0 \Theta_1 R_1}{2 R_0}\right)^2\right]}\,.$$

An analysis of this formula, which is valid when the gun operates in the full-space-charge mode, leads to the following conclusions.

1) The more powerful klystrons (and consequently those with the higher voltages) guarantee a higher signal to noise power ratios than the less powerful ones.

2) It is desirable to use low-temperature cathodes.

3) In amplification, as indicated above, the decisive role is played by the narrow-band noise, the power of which is proportional to $M_1^2\Theta_0\Theta_1 R_1/R_0$. In designing a klystron for a specified power and gain, the quantities obtained in these expressions are sufficiently well defined, and it is therefore difficult to reduce the noise level by choosing these quantities without deteriorating the parameters of the amplifier. It is more convenient to change the construction of the gun in such a way as to guarantee a minimum of the convection noise current exciting the input cavity. This can be done by using the same principles as are used in traveling-wave tubes and in low-noise klystrons intended for preamplification [4].

4) In the case of frequency multiplication by a large factor, when the basic role is played

by the broadband noise, the noise can be reduced also in the case of a diode-type gun, by reducing the different $\Theta_1 - \Theta_0$. If the space charge in the drift region cannot be regarded as sufficiently weak so as to be able to use the derived formula directly, the qualitative picture nevertheless remains the same; in view of the difference in the signs of the velocity modulation at the cathode and at the anode of the gun, it is always possible to find a combination of Θ_1 and Θ_0 such as to guarantee a minimum noise.

A consistent account of the space charge in this problem is exceedingly difficult because it becomes necessary to regard the bunching of a broad spectrum of fluctuations in the presence of a strong signal and its harmonics. This gives rise to many problems which have not been solved at present even for the simpler cases.

Inasmuch as we are essentially interested in the signal to noise power ratio, it appears that an account of the repulsion should not greatly influence this result.

In real klystrons there can appear types of noise other than those considered above. These include ion noise, current distribution noise (which is particularly strong in tubes having grids), and secondary electron noise.

Consequently, before one improves the properties of the klystron from the point of view of noise due to current fluctuations and electron velocity of the cathode, it is essential to verify that everything has been done to get rid of the foregoing additional noise. The best, from this point of view, should be gridless klystrons with good current transmission.

REFERENCES

1. F.B. Llewellyn. Electron Inertia (translation), GTI (1946).
2. V.J. Norris. The frequency-multiplier klystron. J. Electronics, 1956, 1, 5, 477.
3. M.O. Bryant, C.P. Lea-Wilson. Some experiments on broad-band c-w klystron at x-band. J. Electronics and Control. 1959, 6, 6, 481.
4. F.M.H. Robinson. Microwave shot noise in electron beam and the minimum shot noise factor of TWT and klystrons. J. Brit. Instn. Radio Engrs., 1954, 14, 2, 79.

Received by editor 24 March 1961

FREQUENCY PROPERTIES OF NEGATIVELY BIASED GERMANIUM DIODES WITH WELDED CONTACTS

S.N. Ivanov, N.E. Skvortsova, Yu.F. Sokolov

The frequency properties of diodes of n and p germanium with welded contacts are experimentally investigated under inverse voltages. It is shown that the series resistance does not depend on the frequency in the microwave band, but does not agree with the low-frequency value. The leakage resistance differs from the low-frequency value of the barrier-layer resistance.

INTRODUCTION

Interest in the use of semiconductor diodes under inverse high-frequency voltages has recently increased appreciably [1, 2]. In most papers devoted to this question, the diode is represented by a capacitance C' in series with a resistance R_l (Fig. 1), where R_l is frequently identified with the series resistance r_s [3]. Such a representation is a rather crude approximation. It can be shown that if we start with the complete equivalent circuit of the contact (Fig. 2), where R is a resistance shunting the barrier-layer capacitance,* the value of which satisfies the inequality $R \gg 1/\omega C$ then

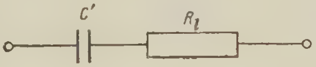

Fig. 1. Equivalent circuit of rectifying contact of the diode at microwave frequencies under negative bias.

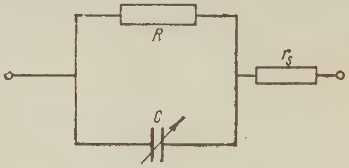

Fig. 2. Complete equivalent circuit of rectifying contact of diode at microwave frequencies.

$$R_l = r_s \left(1 + \frac{1}{\omega r_s C} \cdot \frac{1}{\omega R C} \right). \tag{1}$$

Under certain conditions, namely if $R \sim 10^3$ ohms in the microwave band, the second term in the parentheses of the right half of (1) can be comparable with unity, even if $R \gg 1/\omega C$.** In this case, according to (1), R_l should depend on the frequency. Experimental data on the frequency dependence of R_l, which are in good agreement with (1) if we assume that $R \sim 10^3$ ohms, are given in [4].

---

*Since the nature of this resistance remains undecided as will be shown below, we shall briefly call it the leakage resistance.

**When this inequality is satisfied we have $C \simeq C'$.

A few remarks should be made concerning the equivalent circuit of Fig. 2 and concerning expression (1). If we start the analysis of the magnitude and frequency dependence of R_l with equation (1) and assume that R is the resistance of the barrier layer, we must presuppose that R decreases sharply with increasing frequency. In fact, on dc we have $R_0 \sim 10^6 - 10^7$ ohms, which differs by three or four orders of magnitude from the value of R at microwave frequencies. In [4, 5] an attempt is made to attribute the low value of R to the effect of surface leakage in the microwave band.

We note also that nothing is mentioned in the papers known to us regarding the frequency dependence of r_s, and furthermore apparently so far there is no unified point of view on how r_s is to be defined at microwave frequencies.

It is clear from the foregoing that a systematic investigation of the frequency dependence and the dependence on the inverse bias of the contact parameters r_s, R, and C is a timely problem, for such investigations may help establish the physical causes that determine the value of R_l and cause it to be frequency dependent.

1. OBJECTS OF INVESTIGATION

In the present investigation we studied the frequency properties of diodes made of n or p type germanium with welded contacts (in hemispherical geometry), made in accordance with the technology described in [6]. In addition, we investigated diodes with ohmic contact,* made of p-type germanium in accordance with precisely the same technology as the n-type germanium diodes (i.e., we used material with the same specific resistivity, with contact wires made of the same batch, and under identical welding conditions). It can be assumed here that the geometry of the ohmic contacts and of the contacts with barrier layer was the same, i.e., the mean values of r_s determined for the ohmic contacts and for the barrier-layer contacts should coincide in the mean if the physical nature of the resistance r_s does correspond to the prevailing notions.

2. MEASUREMENT PROCEDURE

a) Low-frequency measurements. We determined the series resistance r_{si}^0 at low frequencies by extrapolating the dependence of the differential resistance in the forward direction

$$R_0(I) = r_{si}^0 + \frac{1}{\alpha I} \tag{2}$$

to $1/I \to 0$.

This method of determining r_{si}^0 can be subject to the following objection: if it is assumed that when the current flows through the barrier in the forward direction an important role is played by the injection of the minority carriers, then at large forward currents, when the injection level is high, "conduction modulation" of the semiconductor layer may start. If such an effect exists, one should observe a deviation of the function $R_0(1/I)$ from linear, and equation (2) no longer applies. However, no such deviation is observed in experiment as the current is varied from 100 to 5000 μa; i.e., the conduction modulation was insignificant in our research.

b) High frequency measurements. Measurements of the contact impedances Z at microwaves were carried out in the frequency range from $3 \cdot 10^9$ to $6 \cdot 10^{10}$ sec^{-1}. The procedure for measuring Z is described in [7, 8]. Determination of the contact parameters r_s, C, and R was in accordance with the equivalent circuit of Fig. 2. Since there are no descriptions in the literature of methods for determining r_s at microwaves, we shall discuss this question in greater detail. Three methods can be proposed for determining r_s at microwaves.

---

*By "diode with ohmic contact" we mean here a construction similar to an ordinary semiconductor diode, in which the barrier layer is replaced by an ohmic contact. More details about such diodes are found in [7].

1) Determination of r_s by measuring the impedance Z_{ohm} of diodes with ohmic contact. The prevailing notions concerning the nature of the series resistance of the contact lead to the following expression (for hemispherical contacts)

$$r_s = \frac{\rho}{\pi d}, \tag{3}$$

where d is the diameter of the contact and ρ is the specific resistivity.

The resistances $r_{s\ ohm}$ of diodes with ohmic contact should on the average be equal to the series resistance of the corresponding diodes with barrier layer. Since the active component of the resistance of the ohmic contact is $r_{s\ ohm}$, the latter is defined as $\mathrm{Re}\, Z_{ohm}$.

2) Determination of r_s by extrapolating Re Z to large currents. According to the equivalent circuit of Fig. 2

$$\mathrm{Re}\, Z = r_s + \frac{R}{1+\omega^2 C^2 R^2}. \tag{4}$$

The dependence R(I) is such that $R \to 0$ as $I \to \infty$ [9]. Starting from this, we can determine r_{si} if we plot Re Z vs. 1/I and extrapolate it to $1/I \to 0$. As regards the question of conduction modulation, the arguments advanced in item a) of the present section, in connection with the method for determining r^0_{si}, remain in force.

3) Determination of r_s from the value of the capacitance C. In the investigated diodes, the capacitance has the following dependence on the inverse voltage U:

$$C(U) = \frac{\pi d^2}{2}\sqrt{\frac{\varepsilon q N}{8\pi(\varphi_c + U)}}, \tag{5}$$

where ϵ — dielectric constant, q — electron charge, N — concentration of impurities in the n region, and φ_c — contact potential differences. From (3) and (5) it follows that

$$r_s\sqrt{C} = A\rho\sqrt[4]{\frac{N}{\varphi_c + U}}, \tag{6}$$

where A is a constant. For a given ρ, the values of N and φ_c are fixed and equation (6) with U = 0 assumes the form

$$r_s\sqrt{C} = \mathrm{const}. \tag{7}$$

From this we can determine r_{sc} from the measured value of C.

3. RESULTS

Experimental investigations of the frequency variation of contact resistances of diodes made of n and p germanium show that the character of the main relationships is the same for these diodes. It is therefore advantageous to describe the results obtained for the frequency and bias-voltage dependence of r_s, C, R, and R_l for both types of diodes simultaneously.

1) Series resistance. The determination of r_s was by the methods described in Section 2 (division b, items 2 and 3). For one series, analogous diodes (i.e., having the same ρ and d) with ohmic contact were investigated. In addition, we determined the value of r^0_{si} for all the diodes.

The experimental data are listed in Tables 1 and 2. Fig. 3 shows typical variation of Re Z with 1/I at different frequencies for one of the diodes.

The main results, as can be seen from the tables, are as follows:

1. The values of r_{si}, r_{sc}, and $r_{s\ ohm}$ are independent of the frequency in the investigated microwave band and are of the same magnitude, with good degree of accuracy.

2. The values of r^0_{si} for all diodes are less than corresponding values of r_{si} at microwaves, whereas $r_{s\ ohm}$ on dc and at microwave frequencies are in good agreement.

3. The values of r_s for diodes made of p germanium are higher for diodes made of n germanium for equal impurity concentrations and contact diameters.

Table 1

Series Resistances

ω, sec^{-1}	n-type Germanium $\rho = 0{,}05$ ohm · cm $C_0 \simeq 0{,}3$ $\mu\mu f$			p-type Germanium $\rho = 0{,}1$ ohm · cm $C_0 \simeq 1{,}5$ $\mu\mu f$	
	r_{si}	$r_{s\,ohm}$	$\overset{*}{r}_{sc}$	r_{si}	$\overset{*}{r}_{sc}$
0	8.3	11	—	6.5	—
$0.59 \cdot 10^{10}$	—	—	11.5	11.3	10
$1.23 \cdot 10^{10}$	10	11.4		—	
$1.94 \cdot 10^{10}$	11	12		11.5	
$5.9 \cdot 10^{10}$	13	14		11	

Note: The asterisk denotes the mean value of measurements made at different frequencies

Table 2

Comparison of Series Resistances of Contact Diodes Made of n and p Type Germanium

($N = 5 \cdot 10^{16}$ cm^{-3}, $d \sim 23$ $m\mu$)

	p Germanium	n Germanium
$\overset{*}{r}_s$	15	7

Note: The asterisk denotes the mean value of measurements made at different frequencies

2) Barrier layer capacitance and leakage resistance. Fig. 4 shows a typical dependence of the capacitance of the rectifying contact on the diode inverse voltage. Each point is the mean value of the capacitance obtained from measurements at seven frequencies in the microwave band ($\omega = 3 \cdot 10^9 \div 6 \cdot 10^{10}$ sec^{-1}). The dependence of $1/C^2$ on U_{inv} is shown in Fig. 5.

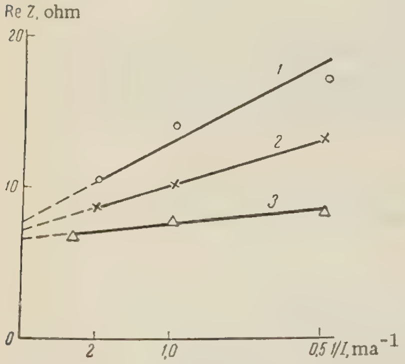

Fig. 3. Experimental dependence of Re Z on 1/I in the forward direction at different frequencies:
1 — $\omega = 0.63 \cdot 10^{10}$ sec^{-1};
2 — $\omega = 0.82 \cdot 10^{10}$ sec^{-1};
3 — $\omega = 5.9 \cdot 10^{10}$ sec^{-1}.

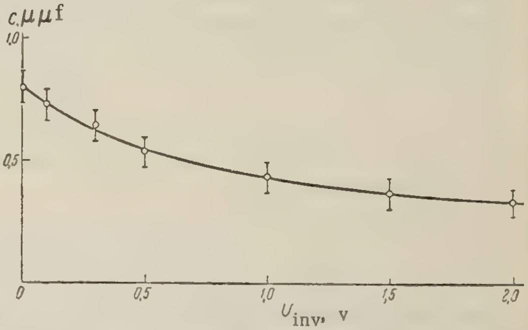

Fig. 4. Dependence of the contact capacitance on the inverse voltage.

It follows from the foregoing results that the capacitance of the rectifying contact is independent of the frequency and is proportional to $(\varphi_c + U_{inv})^{-1/2}$; i.e., as expected, this is a charge capacitance.

It is necessary to stipulate beforehand that R can be determined only for those diodes in which the loss resistance R_l is considerably greater than R_s. In the case when R_l and r_s are close in magnitude, the determination of R entails very great errors and was not carried out.

Fig. 6 shows the dependence of R on the inverse voltage at different frequencies. It follows from the curves in Fig. 6 that R increases with increasing inverse voltage, differs greatly from the low-frequency value of the barrier-layer resistance, and amounts to about 10^3 ohms in the investigated range for diodes made of n and p germanium. The data obtained agree with the results given in [4, 5]. The interpretation of the results proposed in these papers is in our opinion insufficiently convincing, for to explain the experimental data it becomes necessary to introduce a series of parameters which cannot be determined by independent observation and cannot explain the experimental results in a wide range of frequencies. Actually, if we start from the equivalent circuit of Fig. 3b of reference [4],

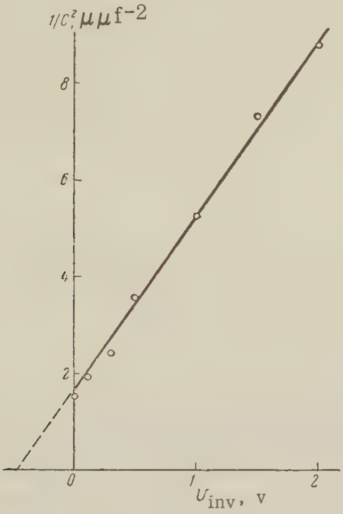

Fig. 5

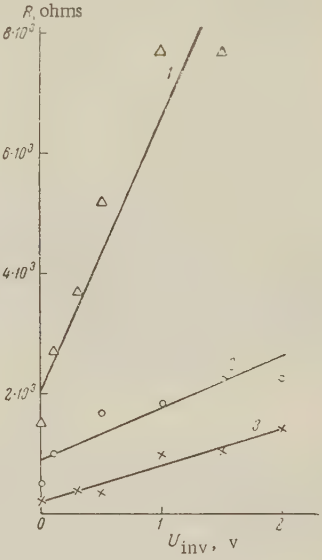

Fig. 6

Fig. 5. Dependence of $1/C^2$ on the inverse voltage.

Fig. 6. Dependence of the résistance R on the inverse voltage for different frequencies: $1 - \omega = 6.5 \cdot 10^9$ sec^{-1}; $2 - \omega = 2 \cdot 10^{10}$ sec^{-1}; $3 - \omega = 5.9 \cdot 10^{10}$ sec^{-1}.

then at sufficiently low frequencies ($\omega \sim 10^7 - 10^8$), when $R_{s1} \ll 1/\omega C_s$, the capacitance of the diode should be $C_s >> C_t$. This is not observed experimentally. Apparently, the data available at present are insufficient to establish the nature of the leakage resistance R.

3) Loss resistance. Fig. 7 shows the frequency dependence of R_l.* The dependence of R_l on the voltage for a diode with $C_0 \simeq 1$ $\mu\mu$f, at different frequencies is shown in Fig. 8. From an examination of the frequency and bias-voltage dependence of R_l it follows that for all the diodes:

1) R_l decreases with increasing frequency.

2) The smaller the initial capacitance of the rectifying contact, the greater the frequencies at which R_l is no longer dependent on the frequency. In the frequency region where R_l is independent of the frequency, it coincides with good accuracy with the series resistance r_s.

3) The loss resistance increases with increasing inverse voltage on the diode. This dependence is more strongly pronounced for the low-frequency region of the investigated range.

4) The loss resistance R_l has the same frequency dependence for diodes made of germanium with different types of conductivities.

---

*In Fig. 7 R_l corresponds to $U_{inv} = 0.5$ v, for at lower voltages errors are possible because the condition for small signal mode at microwave frequencies is not satisfied.

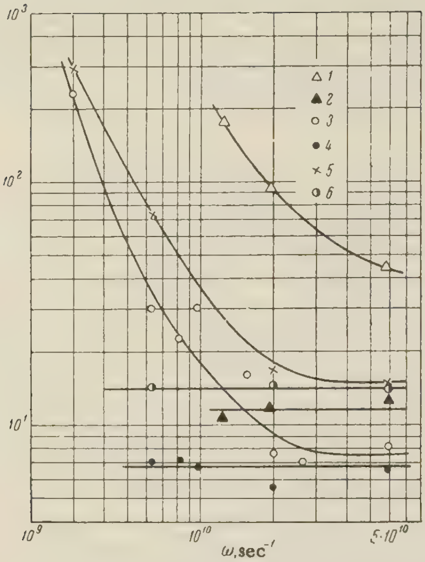

Fig. 7. Dependence of loss resistance on the frequency.

1) R_1; 2) r_{si} (1,2 — n Ge diode $C_0 \simeq 0.2$ μμf);
3) R_1; 4) r_{si} (3,4 — n Ge diode $C_0 \simeq 0.8$ μμf);
5) R_1; 6) r_{si} (5,6 — p Ge diode $C_0 \simeq 0.8$ μμf).

4. DISCUSSION OF RESULTS

1) Series resistance. As stated in the introduction, one of the main purposes of the experimental investigation consisted of determining the dependence of r_s on the frequency.

The results of item 1 of Section 3 show that, on the one hand, r_s is independent of the frequency of the microwave band, and on the other hand it differs from r_{si}^0. It is impossible to attribute this discrepancy to the conduction modulation of the layer of semiconductor, for two reasons. First, as is indicated in Section 2, this modulation was insignificant in the experiments described, and second, even if it did occur, it should manifest itself in equal measure at dc and at microwave frequencies.

Let us consider expression (3) for r_s:

$$r_s = \frac{\rho}{\pi d}.$$

It follows from this expression that r_s changes either when ρ is changed or when d is changed. Inasmuch as there is no modulation of ρ, it must be assumed that the change in r_s is due to the change in d. We shall attempt to explain qualitatively the cause of this change.

Essentially, r_s is the resistance of that region of the semiconductor in which the current is determined primarily by the drift component. The boundary of this region in those cases when the diffusion current comprises an appreciable fraction of the current through the junction does not coincide with the technological boundary of the rectifying contact, and is situated a distance on the order of the diffusion length L_0 from the latter. This diffusion length can be comparable with d (see Fig. 9). In fact, in a spherical layer of thickness

$$L_0 \sim \sqrt{D\tau},$$

where τ is the lifetime of the minority carriers, and D the diffusion coefficient, the current is essentially due to diffusion; i.e., this region makes no contribution to the series resistance. The expression for r_s should thus have the form

$$r_s = \frac{\rho}{\pi (d + 2L_0)}. \tag{8}$$

The picture should be different at microwave frequencies. The diffusion component of the microwave current is confined to the region near the technological boundary of the

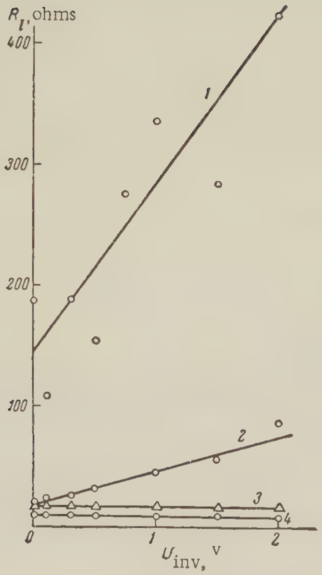

Fig. 8

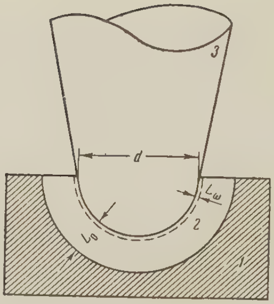

Fig. 9

Fig. 8. Dependence of the loss resistance on the inverse voltage on the diode (n type germanium, $C_0 \simeq 1$ $\mu\mu$f): 1 — $\omega = 3 \cdot 10^9$ sec^{-1}; 2 — $\omega \simeq 10^{10}$ sec^{-1}; 3 — $\omega = 1.55 \cdot 10^{10}$ sec^{-1}; 4 — $\omega = 5.9 \cdot 10^{10}$ sec^{-1}.

Fig. 9. Rectifying contact:

1 — layer of semiconductor; 2 — semiconductor region that does not contribute to the dc series resistance; 3 — contact whisker.

junction, with thickness $L_\omega \sim \sqrt{D/\omega}$ [10]. Estimates show that in the investigated band we have $L_\omega << d$, and thus r_s is determined by formula (3) (where d is the contact diameter) and is independent of ω.

Thus, the ratio of r_{si} measured at microwave frequencies to r^0_{si} should, in accordance with (3) and (8), be equal to

$$\frac{r_{si}}{r^0_{si}} = 1 + \frac{2L_0}{d}. \tag{9}$$

An estimate of the quantity L_0 and consequently τ leads, in accordance with (9), to values $\tau \sim 10^{-7} - 10^{-8}$ sec. Inasmuch as r_{sc} and $r_{s\ ohm}$ are determined by the same equation (3), the agreement between the experimental values of r_{si}, r_{sc}, and $r_{s\ ohm}$ as well as their independence of ω are quite legitimate.*

A comparison of r_s for specimens made of n and p type germanium with identical impurity concentrations and with identical contact diameters has shown, as expected, that r_s is smaller for n type germanium, since the mobility of the majority carriers in n type germanium is greater than in p type germanium.

2) Loss resistance. Let us see now what determines the frequency dependence of R_l — the frequency dependence of r_s, the dependence of R and C, or the dependence of all these quantities simultaneously.

---

*To confirm the validity of the proposed interpretation, it is interesting to investigate the frequency dependence of r_s near frequencies $\omega \sim 1/\tau$.

The frequency dependence of R_l and the difference between R_l and r_{si}^0 are due both to the fact that r_s has different values at high and at low frequencies, and by the frequency dependence of R (the strong decrease in R at microwave frequencies, compared with the low-frequency value R_0).

Inasmuch as R is of the same order of magnitude for all the diodes ($R \sim 10^3$ ohms), the second term in the parentheses in the right half of (1) should contribute to R_l up to high frequencies if C is small, compared with the case of large C. This is experimentally observed.

The authors are grateful to S.G. Kalashnikov for useful discussions and for critical remarks concerning this paper.

REFERENCES

1. A. Uhlir. Proc. IRE. 1958, 46, 6, 1099.
2. M. Uenohara. Proc. IRE. 1960, 48, 2, 169.
3. V.S. Etkin. Radio Electronic Industry. 1959, 9, 3.
4. S.T. Eng, R. Solomon. Proc. IRE. 1960, 48, 3, 358.
5. D.E. Sawyer. J. Appl. Phys. 1959, 30, 3, 1669.
6. S.N. Ivanov. N.E. Skvortsova, Yu.F. Sokolov. Radio Engineering and Electronic Physics. 1959, 4, 9, 1938.
7. Yu.F. Sokolov. Ibid. 1961, 6, 3, 399.
8. F.S. Rusin, N.E. Skvortsova, Yu.F. Sokolov. Collection, Semiconductor Devices and Their Applications. 1958, 3, 13.
9. N.A. Penin, N.S. Skvortsova. Radio Engineering and Electronic Physics. 1958, 3, 2, 267.
10. W. Shockley. Bell System Techn. J. 1949, 28, 3, 435.

Received by editor 14 February 1961

CAPACITANCE AND SERIES RESISTANCE OF GERMANIUM DIODES

V.S. Bagaev, A.A. Zherebtsova, V.A. Pavlenko

We give the results of measurement of capacity and resistance of germanium diodes, made by fusion and diffusion methods (fixed-impurity junction and diffused base diodes). The diode capacitances were measured at three frequencies: 130 kc, 40 Mc, and 1830 Mc, depending on the bias voltage, and are independent of the frequency within the limits of measurement accuracy. The series resistance of the diodes is independent of the bias voltage and has one and the same value at 40 as at 1830 mc for fusion p^+-n diodes etched in hydrogen peroxide and diffusion n^+-p diodes etched in SR-r, whereas in the case of diffusion diodes etched in hydrogen peroxide the values of the series resistance are 2 — 5 times larger at the lower frequency.

INTRODUCTION

The diode can be represented by means of an equivalent circuit (shown in Fig. 1), where r_s — series (base) resistance of the diode, C and R — capacitance and differential resistance of the p-n junction, L — inductance of the contact spring, C_c — capacitance of the cartridge (between the nipples). This circuit is applicable up to very high frequencies, so long as the linear dimensions of the diode are small compared with the wavelength. At low frequencies (100 kc) the circuit simplifies somewhat; i.e., the diode can be represented by the equivalent circuit shown in Fig. 2.

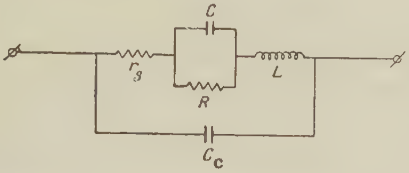

Fig. 1. Equivalent circuit of parametric diode.

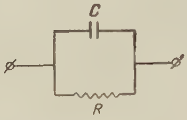

Fig. 2. Equivalent circuit of diode for low frequencies.

To determine the parameters of the circuit, we made measurements at 130 kc, 40 mc, and 1830 mc. The measurement at the highest frequency enables us to determine r_s, C, L, and C_c. The values of r_s and C were measured as functions of the inverse bias, assuming that $R \gg 1/\omega C$. We used here a method based on measuring the voltage standing wave coefficient and the shift of the minimum in a line terminated by a complex load. From the measured quantities we calculated Y_{in} — the input admittance of the diode, and also $Y_{nl} = j\omega C_c$ — input admittance at no load, and $Y_{sc} = j\omega C_c + 1/j\omega L$ — input admittance measured under short circuit conditions. The quantities r_s and C were determined from the relation

$$r_s - j\frac{1}{\omega C} = \frac{1}{Y_{in} - Y_{nl}} - \frac{1}{Y_{sc} - Y_{nl}}.$$

The accuracy with which r_s and C were determined was ± 10%.

A block diagram of the apparatus is shown in Fig. 3. The modulation frequency was set by means of audio oscillator (1) (ZG-10), which synchronized the operation of square wave generator (2) (GIP-1). From this generator the pulses were fed to the modulation input of the GSS-15 generator (3), and were also used as a reference voltage at the input of synchronous detector (8). The GSS-15 generator fed the measuring line (4), to the end of which was connected the investigated diode (5). The detected signal from the probe of the measuring line was fed to a 28 IM amplifier (7), and from there to a synchronous detector (8). The gain in sensitivity was due to the reduction in the noise bandwidth to 1 cps. The need for higher sensitivity was brought about by the large values of the measured VSWR.

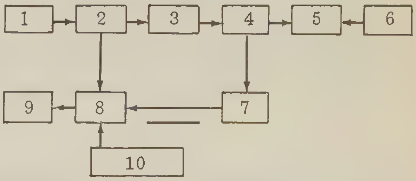

Fig. 3. Block diagram of apparatus for measurement of total input impedance of the diode: 1 — audio generator; 2 — pulse generator; 3 — microwave generator; 4 — measuring line; 5 — holder with diode; 6 — circuit for applying bias voltage to the diode; 7 — amplifier; 8 — synchronous detector; 9 — indicating instrument; 10 — stabilized rectifier.

At 130 kc, we determined C and R likewise as a function of the inverse voltage. The measurement was by means of a twin-T bridge with a capacitance measurement accuracy of 0.2 $\mu\mu$f. Measurements at 40 mc, which were made with a Q-meter of increased sensitivity, gave a certain idea of the frequency properties of the diode parameters R_s and C.

EXPERIMENTAL RESULTS AND THEIR DISCUSSION

A study of the static characteristics of the diodes was made in accord with the properties of the initial material, the manufacturing technology, and the geometrical dimensions of the diodes. Figs. 4 and 5 show a log-log plot of the capacitance on the applied inverse voltage for fusion and diffusion diodes at 130 kc and 1830 mc. The same figures show the values of the capacitance obtained with a bias of -2 volts at 40 mc. As can be seen from Figs. 4 and 5, at these frequencies the values of the capacitance agree for all the investigated diodes and are within the limits of measurement accuracy.

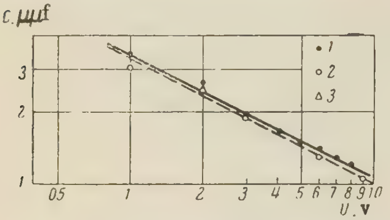

Fig. 4. Dependence of the capacitance on the inverse voltage for a fusion diode (diode No. 58, n = 2.05):
1 — measurement at 130 kc;
2 — measurements at 1830 Mc;
3 — measurements at 40 Mc.

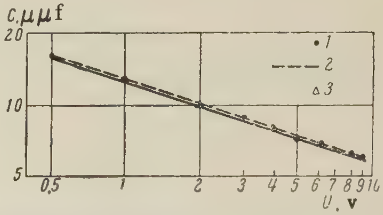

Fig. 5. Dependence of the capacitance on the inverse bias for a diffusion diode (diode No. 61a, n = 3.15):
1 — measurements at 130 kc;
2 — measurements at 1830 Mc;
3 — measurements at 40 Mc.

Using portions of the curves in the voltage region where $U > \varphi^*$ (U — external voltage and φ^* — additional potential difference [1]) we can determine the values of the exponent for $C = \alpha U^{-\frac{1}{n}}$. We can then use the plot of $C^{-n} = \beta' U$ to determine φ^*, as can be seen from Fig. 6.

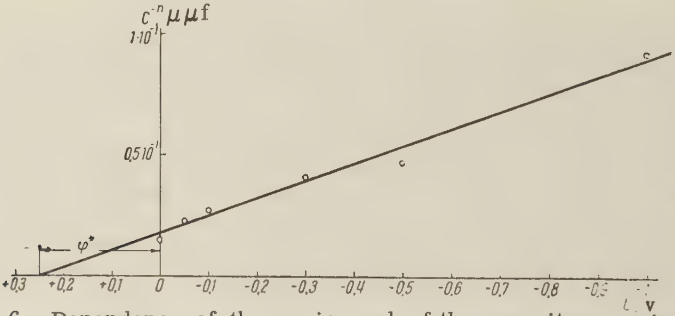

Fig. 6. Dependence of the reciprocal of the capacitance raised to the n-th power on the inverse voltage. Diode No. 56, n = 2.2.

The values of φ^* obtained from experiment and calculated from the formula [1]

$$\varphi^* = U_c - U_i = \frac{kT}{q} \ln \frac{\beta N_d^2}{n_i^2}$$

with account of the volume inversion layer at $\beta = 1$, are respectively 0.23 and 0.34 volts for fusion diodes (with $N_d = 2 \cdot 10^{16}$ cm^{-3}), and 0.28 and 0.37 volts for $N_d = 3.5 \cdot 10^{16}$ cm^{-3}. In this formula, U_c — contact potential difference, U_i — voltage drop across the inversion layer, k — Boltzmann's constant, T — absolute temperature, q — charge of the electron, N_d — excess concentration of the ionized impurity, n_i — intrinsic concentration of the carriers, β — factor indicating the relation between the concentrations of the mobile carriers in the inversion layer and in the volume. The foregoing formula is not valid for diffusion diodes.

The values of the series resistance of r_s, obtained by various methods, are summarized in Tables 1 and 2, which indicate the numbers of diodes, the breakdown voltages (v), the specific resistivity of the initial material (ohm-cm), the area of the p-n junction (cm^2), the thickness of the base (μ), the series resistance (ohm) calculated from the formula $r_s = \rho \cdot l/S$ (where l — thickness of base, S — area of the p-n junction) and measured at 1830 and 40 mc,

Table 1

No. of diode	U, v	ρ, ohm-cm	S, cm^2	l, μ	r_s, ohms (cal.)	r_s, ohms		C, μf (bias -2v)	Notes
						1830 Mc	40 Mc		
46	19	0,15	$3{,}6\cdot10^{-5}$	40	17	20	—	1,3	Fusion diodes etched in U_2O_2
49	19	0,15	$3{,}4\cdot10^{-5}$	40	18	13	—	0,6	
56	16	0,12	$8{,}2\cdot10^{-5}$	50	7	6,0	—	2,1	
57	17	0,12	$9{,}0\cdot10^{-5}$	50	7	6,5	4	2,5	
58	17,5	0,12	$7{,}3\cdot10^{-5}$	50	8	7,0	—	2,0	
59	17	0,12	$5{,}2\cdot10^{-5}$	50	6	7,5	6	2,3	
69	17	0,12	$4{,}7\cdot10^{-5}$	50	13	13,0	18	1,5	
62	11	0,07	$3{,}0\cdot10^{-5}$	35	8	7,0	9	1,0	
64	12	0,07	$3{,}2\cdot10^{-5}$	35	8	8,0	—	1,3	

and the capacitance of the p-n junction at a bias of -2 volts. The formula for r_s is valid for the employed technology of p-n junction production, within the framework of the accuracy of the measurement of r_s, for both fusion and diffusion diodes. The thickness of the base l for $d > l$, where d is the diameter of the p-n junction, was estimated from the cross section of the specimen perpendicular to the area of the p-n junction visually under the microscope for fusion diodes, and by the thermal-probe method for diffusion diodes.

The series resistance r_s, measured at 1830 Mc, remains constant at inverse biases ranging from 0 to 10 volts (Fig. 7). A possible explanation is that the broadening of the p-n junction is insignificant compared with the thickness of the base. As can be seen from Tables 1 and 2, satisfactory agreement is obtained between the measured and calculated values of r_s for fusion diodes. For diffusion diodes, some values of r_s agree with the calculated ones and others do not, and in the latter case the values of r_s at 40 Mc are 2 — 5 times greater than those measured at 1830 Mc for the same diodes. The frequency dependence of r_s was noted in [2]. Since we have assumed that r_s is the resistance of the base material, it is independent of the frequency. Consequently, in the case when the different values of r_s do not agree, we must say that we have measured a certain equivalent resistance $r_{s\,eq}$.

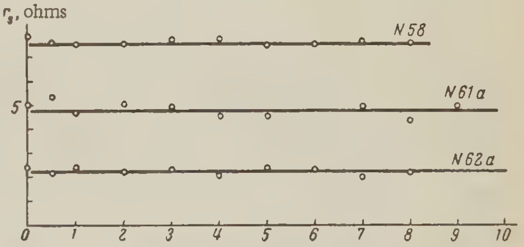

Fig. 7. Dependence of the series resistance r_s of the diode on the inverse voltage.

Replacement of r_s by $r_{s\,eq}$ for certain diodes can be explained in the following manner, using the experimental results. In fusion diodes with p^+-n junctions etched in hydrogen peroxide, and in diffusion n^+-p diodes etched in SR-4, no frequency dependence of r_s was observed (see Tables 1 and 2). When etching in hydrogen peroxide, an n-type surface is

Table 2

No. of diode	U, v	ρ, ohm-cm	S, cm^2	l, μ	r_s, ohms (cal.)	r_s, ohms		C, μf (bias -2v)	Notes
						1830 Mc	40 Mc		
19a	43	0,17	$6{,}7\cdot10^{-5}$	25	6	7,5	40	1,2	Diffusion diodes etched in SR-4 (19a-70a) and in U_2O_2 (13-20)
45a	43	0,17	$2{,}1\cdot10^{-4}$	30	2	7,0	14	2,7	
61a	12,5	0,013	$1{,}6\cdot10^{-4}$	150	—	4,8	14	5,8	
62a	12,5	0,013	$3{,}0\cdot10^{-4}$	150	0,65	2,2	9	10,0	
70a	12,5	0,013	$7{,}2\cdot10^{-5}$	25	0,3	3,7	6	2,2	
13	19	0,02	$5{,}3\cdot10^{-5}$	70	3	4,6	4	2,0	
14	19	0,02	$9{,}3\cdot10^{-5}$	70	2	2,5	3	3,7	
15	19	0,02	$2{,}3\cdot10^{-5}$	70	—	5,3	6	1,0	
20	19	0,02	$5{,}5\cdot10^{-5}$	150	—	6,5	5	2,0	

always formed on the germanium, whereas etching in SR-4 always produces a p-type surface [3]. Consequently however, we can assume that on the p-side of diffusion n^+ -p diodes etched in hydrogen peroxide there is formed a surface inversion layer, which enables us to explain the frequency dependence of $r_{s\ eq}$ [2]. In the case of fusion p^+ -n diodes etched in hydrogen peroxide and diffusion n^+ -p diodes etched in SR-4, apparently, no surface inversion layer is produced on the high-resistance side of the junction.

The authors are grateful to B. M. Vul for guidance of this project and for a discussion of the results. The authors are grateful to N. E. Skvortsova, Yu. F. Sokolov, and S. N. Ivanov for a discussion of the results. They also thank Yu.N. Koroleva, L.M. Novak, and G.P. Proshako for preparing the specimens.

REFERENCES

1. B.M. Vul, E.I. Zavaritskaya. ZhETF. (Journal of Experimental and Theoretical Physics). 1960, 38, 1, 10.
2. S.T. Eng, R. Solomon. Proc. IRE, 1960, 48, 3, 358; D.E. Sawyer, J. Appl. Phys. 1959, 30, 11, 1689.
3. A.V. Rzhanov, I.G. Neizvestnyi, V.V. Roslakov. ZhTF. (Journal of Technical Physics). 1956, 26, 10, 2142.

P.N. Lebedev Physics Institute,
Academy of Sciences, USSR

Received by editor 28 December 1960

VOLT-AMPERE CHARACTERISTIC OF TUNNEL DIODE

V.L. Bonch-Bruevich, P.S. Serebrennikov

Taking into account the inhomogeneity of the field in the junction and assuming complete degeneracy ($T = 0$), expressions are obtained for the volt-ampere characteristic of a tunnel diode both for direct transitions and for transitions with scattering on phonons and impurities.

INTRODUCTION

The investigation of the volt-ampere characteristic of a tunnel diode has already been the subject of several papers (see, for example, [1, 2, 3]). Nevertheless, in our opinion no completely satisfactory solution of the problem has yet been presented. In reference [1] is considered an intentionally simplified ("caricature") variant of the calculation, in which no account is taken of the dependence of the transition probability on the position of the electron in the band. This did not interfere with a determination of the point of the minimum current, but the expression for the maximum, as will be shown later on, turned out to be incorrect. In [2] the volt-ampere characteristic is calculated for the case of a homogeneous field, which, as we shall show, does not correspond to the nature of the system under consideration. In [3] the transition probability in an inhomogeneous field is calculated with the aid of a quasi-classical method. Such an approach, apparently, needs justification, even if the method itself is applicable; in the tunnel diode, however, the conditions for the applicability of the quasi-classical method are not satisfied; the field changes strongly over a distance equal to the typical wavelengths.

In the present paper we attempt to calculate the volt-ampere characteristic of a tunnel diode using, where possible, no hypotheses that cannot be directly verified by experiment. We note that the problem proposed encounters certain complications of principal character, characteristic of precisely this essentially quantum-mechanical system, which distinguish the tunnel diode from the ordinary diode with p-n junction.

First, the width of the p-n junction in the tunnel diode ($\sim 10^{-6}$ cm) is comparable with the mean electron wavelength. Consequently, the distribution of the field and of the charge cannot be calculated here by usual classical means. Certain customary notions (for example, the notion of a completely depleted layer) can lose their direct meaning thereby.

Second, the electric field in the junction is highly inhomogeneous; over the length of the junction the field intensity increases from 0 to approximately 10^6 v/cm and drops again to 0. This is an important circumstance, for the probability of tunnel penetration depends greatly on the intensity of the field, as a result of which different regions of the junction give sharply different contributions to the current. It is precisely for this reason that it seems to us that the calculation in [2] is not sufficiently convincing. An attempt to take into account the inhomogeneity by introducing some factor in the exponent does not solve anything, unless an unambiguous way of determining this factor is indicated. If we do not regard this factor as merely a "trimming" constant, the problem again reduces to an examination of the effect in an inhomogeneous field.

Third, it is precisely in the tunnel diode that an important role can be assumed by deviations of the real structure of the junction from the ideal structure usually considered in theory. Indeed, by virtue of the sharp dependence of the probability of tunnel penetration on the field intensity, local changes in the latter (connected, for example, with dislocations, fluctuations in the distribution of the impurity, etc.) can make noticeable contribution to the current.

Fourth, in the tunnel diode we unavoidably deal with strongly doped semiconductors. The energy spectrum of the latter is apparently more complicated than when the impurity concentration is low [1, 4, 5, 6, 7]. Actually, the impurity bands existing when the concentration of the impurity is about 10^{15}–10^{17} cm^{-3}* overlap with the "intrinsic" bands on further increase in the concentration (in the range of about $0.5 \cdot 10^{18}$ cm^{-3}). This gives rise to a spectrum of complicated structure consisting, generally speaking, of several branches. In addition, owing to the scattering of the carriers by the impurity atoms, states with specified quasi-momenta acquire a finite lifetime. This leads to an effective smearing of the edges of the band, and consequently one cannot speak of boundaries of the spectrum in the true sense of the word at all. It is therefore more correct to assume that in a strongly doped semiconductor the so-called "forbidden" band also contains allowed portions of energy, and different points of the band are characterized by a different state density, which decreases asymptotically as the center of the band is approached.** In other words, the notion of boundaries of "allowed" bands can be introduced only in a certain arbitrary sense, taking this to mean the values of the energy beyond which the density of the states becomes sufficiently small. It is precisely in this sense that this notion was used in [1] and will be used below.

In connection with the foregoing the calculation of the Fermi levels, either theoretically or by using Hall's data, becomes rather complicated. In the present paper we shall regard the Fermi level simply as a phenomenologically specified parameter subject to direct determination by experiment. It is also very difficult to calculate the probabilities of the tunnel penetration from the impurity portions of the spectrum. The existing theory of the tunnel effect in its literal form is not applicable here even in the case of a homogeneous field. We shall henceforth consider only transitions between the intrinsic bands; the results formally obtained for any value of the external voltage Φ will actually be valid here only in a region not too close to the point of the minimum tunnel current $\Phi_{\min}$ (approximately in the region $\Phi_{\min} \gtrsim 0.1 - 0.3$ v).

1. FORMULATION OF THE PROBLEM

Formally any completely rigorous solution of the problem should include also the calculation of the probability of tunnel transition in an inhomogeneous field. Such an approach, however, seems to us to be little justified, since the exceeding complexity of the involved calculations would unavoidably lead to many approximations, and the accuracy of the solutions would be illusory. This is all the more correct if one takes into account the unavoidable non-ideality of the object (see the introduction). We therefore use an approximate procedure, which is valid as soon as the length of the junction l greatly exceeds the atomic dimensions (in a typical diode this inequality is satisfied with a margin of two orders of magnitude). Under these conditions we can break up the p-n junction into portions small enough to make the field inside each of them practically homogeneous, and at the same time large enough to make the linear dimensions noticeably greater than the lattice constant. Then the ordinary theory of the tunnel effect will be applicable to each portion, and the resultant current will be obtained by integrating over the entire junction.

---

* The figures cited here and below pertain to germanium.

** These portions of the spectrum can be called somewhat arbitrarily "impurity portions."

To carry out this program we must specify an explicit form for the field intensity E as a function of the coordinate x (the Ox axis is perpendicular to the junction). At the present time the phenomenological approach appears to be the most advantageous. We put

$$E = \begin{cases} E_m\left\{1-\left(\frac{x}{l_1}\right)^{\gamma}\right\}, & 0 \leqslant x \leqslant l_1, \\ E_m\left\{1-\left(\frac{x}{-l_2}\right)^{\gamma}\right\}, & -l_2 \leqslant x \leqslant 0, \end{cases} \tag{1}$$

where E_m, γ, l_1, l_2 — parameters; $\gamma \geq 0$. It is obvious that the length of the junction is $l = l_1 + l_2$. With a small external voltage, this length is connected with the charge capacitance of the junction C by the relation

$$C = \frac{\varepsilon S}{4\pi l}, \tag{2}$$

where ϵ is the dielectric constant of the substance; S — area of the junction. The quantities l and consequently C depend on the external voltage Φ ($\Phi > 0$ in the forward direction). Using equations (1) and also the condition of the continuity of the potential at the point $x = 0$, we readily obtain

$$lE_m = \frac{\gamma+1}{\gamma}(U_c - \Phi),$$

where U_c is the contact difference of potentials between the n and p specimens.

Let us assume now that the capacitance of the junction changes when Φ varies only as a result of a change in the length of the junction. For ordinary junctions with depletion layer this is unconditionally correct. One might think that in our case this assumption would yield a reasonable approximation at sufficiently small values of Φ/U_c. Then formula (2) becomes valid not only when $\Phi \to 0$, and we obtain for l and E_m, using the Poisson equation* (see [8]),

$$l = l_0\left(1 - \frac{\Phi}{U_c}\right)^{\frac{1}{\gamma+1}}, \tag{3}$$

$$E_m = \frac{\gamma+1}{\gamma}\,\frac{U_c - \Phi}{l} = E_{m,0}\left(1 - \frac{\Phi}{U_c}\right)^{\frac{\gamma}{\gamma+1}}. \tag{4}$$

Here l_0 and $E_{m,0}$ are the length of the junction and the maximum field in the junction when $\Phi = 0$. We note also that

---

*The use of the Poisson equation does not mean that the quantum effects are neglected. As is well known, the Poisson equation is valid also for a quantum system of interacting particles: it determines the average potential of the electrostatic field, and its right half should contain the average space-charge density. It is precisely for a phenomenological calculation of the latter from formulas (1) that we are using Poisson's equation.

$$qU_c = \Delta E + \Delta_n + \Delta_p, \tag{5}$$

where q is the charge of the electron and ΔE — width of the forbidden band; the other symbols are clear from the figure.

It is clear from (2) — (4) that the parameters l and $E_{m,0}$ (the only parameters of importance for what is to follow) can be estimated by measuring the charge capacitance of the junction as a function of the voltage.

The tunnel current connected with the individual portion within which the field is homogeneous is calculated by the standard formulas. As is well known, it is necessary to distinguish here between three basic cases: direct transitions, indirect transitions with participation of phonons, and indirect transitions with scattering on the impurities.* The probabilities of the first and second processes have been calculated in [9 — 11], while transitions with scattering by impurities were recently considered by one of the authors [12].

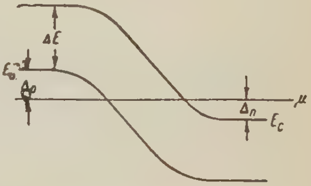

Diagram of the p-n tunnel junction (zero voltage on the junction): μ — Fermi level; E_c — bottom of the conduction band in the n region; E_v — top of the valence band in the p region.

The expressions for the tunnel current density contain the distribution functions for the conduction electrons and for the roles in the n and p regions, respectively. We confine ourselves in the present article to the case of complete degeneracy; i.e., we assume that $kT \ll \Delta_n$, $kT \ll \Delta_p$.

2. DIRECT TRANSITIONS

Transitions of this type (and likewise transitions with scattering on impurities) apparently play an appreciable role in germanium diodes [13]. As shown in [9], in the anisotropic case the transition probability contains a quantity with dimension of mass, determined by the behavior of the function $E_c(p) - E_v(p)$ near the branch point in the complex plane [$E_c(p)$, $E_v(p)$ — energy of the electron in the conduction band and the valence band respectively]. This circumstance introduces a certain uncertainty into the answer, which at present is difficult to eliminate. We shall therefore carry out the calculation in the isotropic approximation, characterizing the electron and the hole by means of scalar effective masses m_n and m_p. It must merely be kept in mind that the "width of the forbidden band" ϵ_0 must in this case be taken to mean the lower boundary of the intrinsic absorption of light in the given crystal (generally speaking, it exceeds the "thermal" width of the forbidden band; in germanium, however, this difference is small, making direct transitions possible in practice). For numerical estimates we should use values that are characteristic of germanium:
$m_n = 0.22\ m_0$, $m_p = 0.045\ m_0$ (light holes), $\epsilon_0 = 0.80$ ev.

We denote by d the lattice constant and by $p_\perp$ the two-dimensional vector formed by the quasi-momentum components perpendicular to the direction of the electric field. We introduce, further, the reduced mass $m_r = m_n m_p/(m_n + m_p)$ and put

$$E(p_\perp) = \frac{\pi \varepsilon_0^{1/2} (m_r \varepsilon_0 + p_\perp^2)}{2q\hbar m_r^{1/2}}. \tag{6}$$

The quantity $E(p_\perp)$ obviously has the dimension of electric field intensity. Then, according to [11], the probability of the tunnel transition in an homogeneous field E, referred to unit time, is

---

*Naturally, indirect transitions with participation of quasi-particles of some other type, such as plasma quanta, other conduction electrons or holes, or excitons are also possible. They deserve a special investigation, but are all the same less probable than those indicated above.

$$d\omega = \frac{2\pi}{\hbar}\frac{qEd}{36}e^{-\frac{E(p_\perp)}{E}}\,\delta(p'_\perp - p_\perp)\,\delta(W' - W)\,d^2p'_\perp\,dW', \tag{7}$$

where W — energy of the electron; the primed and unprimed quantities pertain to states before and after the tunnel transition; $d^2p'_\perp$ denotes a two-dimensional volume element in the space $p'_\perp$. To calculate the total electron current it is necessary to note that the number of states in the energy interval dW for a specified value of $p_\perp$ is dW/que. Taking this into consideration, we see that the electron currents from the conduction band into the valence band and back will be

$$i_{c\to v} = 2\int d\omega f_n(W)\,[1 - f_p(W)]\,\frac{d^2p_\perp dW}{(2\pi\hbar)^2 qEd}, \tag{8a}$$

$$i_{v\to c} = 2\int d\omega f_p(W)\,[1 - f_n(W)]\,\frac{d^2p_\perp dW}{(2\pi\hbar)^2 qEd}. \tag{8b}$$

Consequently, for the resultant current $i = i_{c\to v} - i_{v\to c}$ we obtain

$$i = \frac{1}{36\pi\hbar^3}\int \exp\left\{-\frac{E(p_\perp)}{E}\right\}\{f_n(W) - f_p(W)\}\times$$
$$\times\,\delta(p'_\perp - p_\perp)\,\delta(W' - W)\,d^2p'_\perp d^2p_\perp dW'\,dW \equiv i(x). \tag{9}$$

As indicated above, this expression must be considered as a current due to a small portion dx, over which the field E(x) can be regarded as homogeneous. The total current is obtained by integrating over the entire junction:

$$i = \int \frac{dx}{l}\,i(x). \tag{10}$$

In the calculation of the integral we shall assume the functions $f_n(W)$ and $f_p(W)$ to be independend of x. Actually, the length of the junction is in this case less than the mean free path; we can therefore assume that there are practically no collisions in the region of the junction.

Substituting (9) in (10) and using formulas (1) for E(x) we arrive at integrals of the form

$$I \equiv \int_0^{l_1} \exp\left\{-\frac{E(p_\perp)}{E_m\left[1 - \left(\frac{x}{l_1}\right)^\gamma\right]}\right\}dx. \tag{11}$$

Let us put for the time being

$$\frac{E(p_\perp)}{E_m} = a$$

and make a change of variables:

$$\frac{a}{1 - \left(\frac{x}{l_1}\right)^\gamma} - a = t.$$

We obtain

$$I = \frac{l_1 a}{\gamma}e^{-a}\int_0^\infty \frac{t^{\frac{1}{\gamma}-1}e^{-t}}{(a+t)^{\frac{1}{\gamma}+1}}\,dt.$$

We note now that

$$a=\frac{E(p_\perp)}{E_m}\geqslant\frac{\pi\varepsilon_0^{3/2}m_r^{1/2}}{2q\hbar E_m}=\frac{\pi\varepsilon_0^{3/2}m_r^{1/2}\gamma l}{2q\hbar(\gamma+1)(U_\mathrm{c}-\Phi)}=$$
$$=\frac{\pi\gamma}{2(\gamma+1)}\,\frac{\varepsilon_0}{q(U_\mathrm{c}-\Phi)}\sqrt{\frac{\varepsilon_0 m_r d^2}{\hbar^2}}\,\frac{l}{d}\gg 1,$$

since $l/d \gg 1$, and all other factors are of the order of unity. Thus, only the asymptotic value of the integral I at large values of a is of interest. It is easily found by neglecting the term t in the denominator compared with a. We similarly calculate the integral over the portion $(-l_2, 0)$. As a result we obtain

$$i=\frac{q\Gamma(1/\gamma)}{36\pi\hbar^3\gamma}\int\left[\frac{E_m}{E(p_\perp)}\right]^{1/\gamma}\exp\left\{\frac{E(p_\perp)}{E_m}\right\}\{f_n(W)-$$
$$-f_p(W)\}\,\delta(p'_\perp-p_\perp)\,\delta(W'-W)\,d^2p'_\perp d^2p_\perp\,dW'dW. \tag{12}$$

In the calculation of the integral (12) we can neglect the dependence on $p_\perp$ in the factor $[E_m/E(p_\perp)]^{1/\gamma}$ (but not in the exponent!). Actually, in the important region of values of $p_\perp$ we have $p^2_\perp/\epsilon_0 m_r \sim (\mu - E_c)/\epsilon_0 \ll 1$.

We introduce the notation

$$E_0=\frac{\pi}{2}\,\frac{\varepsilon_0}{qd}\left(\frac{\varepsilon_0 m_r d^2}{\hbar^2}\right)^{1/2}. \tag{13}$$

This is the intensity of a field of atomic magnitude. The ratio E_0/E_m is on the order of 10. Integrating with respect to W' and $p'_\perp$ in (12) we obtain

$$i=\frac{q\Gamma(1/\gamma)}{36\pi\hbar^3\gamma}\left(\frac{E_m}{E_0}\right)^{1/\gamma}\int\{f_n(W)-f_p(W)\}\,e^{-\frac{E(p_\perp)}{E_m}}\,dW\,d^2p_\perp. \tag{14}$$

In the case of complete degeneracy the statistical factors enter through the limits of integration. To establish the latter we note that

$$\frac{p_\perp^2}{2m_n}\leqslant W \tag{15a}$$

and by virtue of the constant energy of the transition

$$\frac{p_\perp^2}{2m_p}\leqslant\Delta-q\Phi-W,\ \Delta\equiv\Delta_n+\Delta_p. \tag{15b}$$

Thus,

$$0\leqslant p_\perp^2\leqslant p^2_{\max}=\min\{2m_nW,\ 2m_p(\Delta-q\Phi-W)\}. \tag{16}$$

We further obtain for W (the zero value of energy is aligned with the bottom of the conduction band):

$$\max\{\Delta_n-q\Phi,\ 0\}\leqslant W\leqslant\min\{\Delta_n,\ \Delta-q\Phi\}. \tag{17}$$

We introduce the notation

$$p_0^2=\frac{E_m}{E_0}\,\varepsilon_0 m_r,\ W_i=\frac{p_0^2}{2m_i}\quad(i=n,\ p,\ r). \tag{18}$$

These quantities are, strictly speaking, dependent on Φ. However, as a rule, this dependence is slight and we can approximate the expressions (18) by means of their values at $\Phi = 0$. Then

$$W_i = \frac{m_r}{m_i} \frac{\varepsilon_0}{2\beta}, \quad i = n, p, r, \quad \beta = \frac{E_0}{E_{m,0}}. \tag{19}$$

The parameter β is of the order of 10, from which it follows that the quantities W_n, W_p, W_r are of the order of several hundred electron volts.

Integrating with respect to $p_\perp$ in (14) we obtain

$$i = \frac{q\Gamma(1/\gamma)}{36\hbar^3\gamma} \left(\frac{E_m}{E_0}\right)^{1/\gamma} p_0^2 e^{-\frac{E_0}{E_m}} \int dW \left\{1 - e^{-\frac{p_{\max}^2}{p_0^2}}\right\}. \tag{20}$$

The factor preceding the integral will be denoted briefly by A:

$$A = \frac{q\Gamma(1/\gamma)}{36\hbar^3\gamma} \left(\frac{E_m}{E_0}\right)^{1/\gamma} p_0^2 e^{-\frac{E_0}{E_m}}. \tag{21}$$

The integral with respect to W in (20) will be calculated under the assumption that $\Delta_p > \Delta_n$, i.e., the degree of degeneracy is greater in the p region than in the n region* (see the figure). As applied to germanium, this case is apparently of greatest interest experimentally. Depending on the doping conditions, two cases can occur, $\Delta_p m_p > \Delta_n m_n$ and $\Delta_p m_p < \Delta_n m_n$, which we shall examine separately (the second case is apparently characteristic of germanium). Here, by virtue of the intermittent character of the functions f_n and f_p at $T = 0$, the volt-ampere characteristic must be written out separately for several portions. It is easy to verify, however, that the expressions given below go over into each other continuously and with continuous derivatives at the boundary points.

1) $\Delta_p m_p - \Delta_n m_n < 0$.

$$\text{a) } 0 \leqslant q\Phi \leqslant \Delta_n - \Delta_p \frac{m_p}{m_n}: \tag{22a}$$

$$i = A \left\{ q\Phi + W_p e^{-\frac{\Delta_p}{W_p}} - W_p e^{-\frac{\Delta_p - q\Phi}{W_p}} \right\}; \tag{23a}$$

$$\text{b) } \Delta_n - \Delta_p \frac{m_p}{m_n} \leqslant q\Phi \leqslant \Delta_n: \tag{22b}$$

$$i = A \left\{ q\Phi + W_r e^{-\frac{\Delta - q\Phi}{W_r}} - W_p e^{-\frac{\Delta_p - q\Phi}{W_p}} - W_n e^{-\frac{\Delta_n - q\Phi}{W_n}} \right\}; \tag{23b}$$

$$\text{c) } \Delta_n \leqslant q\Phi \leqslant \Delta_p: \tag{22c}$$

$$i = A \left\{ \Delta_n - W_n + W_r e^{-\frac{\Delta - q\Phi}{W_r}} - W_p e^{-\frac{\Delta_p - q\Phi}{W_p}} \right\}; \tag{23c}$$

$$\text{d) } \Delta_p \leqslant q\Phi \leqslant \Delta: \tag{22d}$$

$$i = A \left\{ \Delta - q\Phi + W_r \left(e^{-\frac{\Delta - q\Phi}{W_r}} - 1\right) \right\}. \tag{23d}$$

When $q\Phi \geq \Delta$ the tunnel current vanishes.

2) $\Delta_p m_0 - \Delta_n m_n > 0$.

---

*This condition is actually not a limitation. The formulas from the opposite case are obtained from those given below by obviously interchanging the notation.

This case differs from the first case only at the very start of the characteristic. Namely, when

$$0 \leqslant q\Phi \leqslant \Delta_p - \frac{m_n}{m_p}\Delta_n \tag{24a}$$

we have

$$i = A\left\{q\Phi + W_n e^{-\frac{\Delta_n}{W_n}} - W_n e^{-\frac{\Delta_n - q\Phi}{W_n}}\right\}. \tag{25}$$

When

$$\Delta_p - \frac{m_n}{m_p}\Delta_n \leqslant q\Phi \tag{24b}$$

the current density is given by formulas (23b), (23c), and (23d). When using formulas (23a)—(24b) it must be remembered that the value of A also depends on Φ.

$$A = A_0\left(1 - \frac{\Phi}{U_c}\right) e^{-\beta\left(1 - \frac{\Phi}{U_c}\right)^{-\frac{\gamma}{\gamma+1}}} \tag{26}$$

(A_0 is a constant). Therefore in the general case the volt-ampere characteristic is given by rather complicated expressions. These, however, simplify appreciably if we take into consideration that in a region that is not close to the minimum of the current we have $\Phi \ll U_c$. In addition, the values of W_p, W_n, and W_r are small compared with ϵ_0.

Let us calculate under these conditions the derivative of the current density with respect to Φ, and readily verify that the voltage Φ_m corresponding to the maximum of the current is $\leq \Delta_n/q$. Explicit formulas for Φ_m can be readily obtained by noticing that under conditions of strong degeneracy we have

$$\Delta_n \gg W_i, \quad i = n, p, r. \tag{27}$$

Depending on the relationship between the parameters of the problem (i.e., in final analysis, on the properties of the basic material and on the conditions of doping), Φ_m can be expressed in different fashion. Namely, we introduce the notation

$$\Phi_0 = \frac{\gamma+1}{\gamma}\frac{U_c}{\beta} \equiv \frac{\gamma+1}{\gamma}\frac{\Delta E + \Delta_p + \Delta_n}{q\beta}. \tag{28}$$

When $q\Phi_0 \gg \Delta_n$ we have

$$q\Phi_m \simeq \Delta_n. \tag{29}$$

When $q\Phi_0 < \Delta_n$ three cases are possible, depending on the relation between $q\Phi_0$ and Δ_n. If the inequalities

$$q\Phi_0 \gg \Delta_n, \quad \exp\left(-2\frac{\Delta_p - \Delta_n}{W_p}\right) \ll 1 \tag{30}$$

are satisfied, then, similar to (29),

$$q\Phi_m = \Delta_n - W_n e^{-\frac{\Delta_p - \Delta_n}{W_p}} \simeq \Delta_n. \tag{31}$$

The same is also obtained if

$$\Delta_p - \Delta_n \lessapprox W_p. \tag{32}$$

On the other hand, if

$$\frac{q\Phi_0}{W_n}\left\{e^{-\frac{\Delta_n - q\Phi_0}{W_n}} + e^{-\frac{\Delta_p - q\Phi_0}{W_p}}\right\} \ll 1, \tag{33}$$

but $q\Phi_0 \ll \Delta_n$, then

$$\Phi_m \simeq \Phi_0\left\{1 - e^{-\frac{\Delta_p - q\Phi_0}{W_p}} - e^{-\frac{\Delta_n - q\Phi_0}{W_n}}\right\} \simeq \Phi_0. \tag{34}$$

3. INDIRECT TRANSITIONS WITH PARTICIPATION OF PHONONS

In considering transitions in which phonons participate, it must be kept in mind that we are justified under certain conditions in equating to zero the temperature involved in the electron distribution function, but not the phonon temperature contained in the formula for the transition probability. Actually, the former merely denotes that T is small compared with the degeneracy temperature, while the latter would denote neglect of the phonon absorption process.

Inasmuch as the derivation is in principle quite similar to that described in Section 2, we give here only the final result (obtained with the aid of the formulas of reference [10]). We introduce the following notation: M — mass of element result; ρ — density of the crystal; M_{vc} — matrix element of the electron-phonon interaction energy, connecting the states of the valence band and the conduction band (this quantity has the dimensionality of energy); ω — frequency of the phonon participating in the process

$$A_F = \frac{\Gamma(1/\gamma)\, q^{5/2} E_m^{3/2} (m_n m_p)^{3/2} M}{2^{9/2}\gamma \pi^{5/2} \hbar^{9/2} (2m_r)^{5/4} \Delta E^{7/4} \rho}\left(\frac{E_m}{E_0}\right)^{1/\gamma} |M_{vc}|^2; \tag{35}$$

$N = \frac{1}{e^{\hbar\omega/kT} - 1}$ — average number of phonons of frequency

$$D_+ = (N+1)\exp\left\{-\frac{4\sqrt{2m_r}\,(\Delta E - \hbar\omega)^{3/2}}{3q\hbar E_m}\right\}; \tag{36a}$$

$$D_- = N\exp\left\{-\frac{4\sqrt{2m_r}\,(\Delta E + \hbar\omega)^{3/2}}{3q\hbar E_m}\right\}; \tag{36b}$$

i_+ — density of the tunnel current connected with emission of the phonon; i_- — density of tunnel current connected with the absorption of the phonon;

$$W_0^{\pm} = \frac{q\hbar E_m}{2\sqrt{2m_r}\,(\Delta E \mp \hbar\omega)^{1/2}}. \tag{37}$$

We confine ourselves as in Section 3 to the case $\Delta_p > \Delta_n$. As before, by virtue of the discontinuity of the functions f_n and f_p, it becomes necessary to write out the volt-ampere characteristic separately for the individual portions. We obtain

a) $0 \leq q\Phi \leq \Delta_n$: (38a)

$$i_- = A_F D_-\left\{\left[1 + \exp\left(-\frac{\Delta - q\Phi - \hbar\omega}{W_0^{(-)}}\right)\right][\min(\Delta_n, \Delta - q\Phi - \hbar\omega) -\right.$$

$$- (\Delta_n - q\Phi)] + W_0^{(-)}\left[\exp\left(-\frac{\min(\Delta_n, \Delta - q\Phi - \hbar\omega)}{W_0^{(-)}}\right) - \exp\left(-\frac{\Delta_n - q\Phi}{W_0^{(-)}}\right) -\right.$$

$$-\exp\Big(-\frac{\Delta-q\Phi-\hbar\omega-\min(\Delta_n,\ \Delta-q\Phi-\hbar\omega)}{W_0^{(-)}}\Big)+\exp\Big(-\frac{\Delta_p-\hbar\omega}{W_0^{(-)}}\Big)\Big]\Big\}, \tag{39a}$$

$$i_+ = A_F\,D_+\,\Big\{\Big[1+\exp-\frac{\Delta-q\Phi+\hbar\omega}{W_0^{(+)}}\Big)\Big](q\Phi-\hbar\omega)+$$

$$+W_0^{(+)}\Big[\exp\Big(-\frac{\Delta_n}{W_0^{(+)}}\Big)-\exp\Big(-\frac{\Delta_n-q\Phi+\hbar\omega}{W_0^{(+)}}\Big)-$$

$$-\exp\Big(-\frac{\Delta_p-q\Phi+\hbar\omega}{W_0^{(+)}}\Big)+\exp\Big(-\frac{\Delta_p}{W_0^{(+)}}\Big)\Big]\Big\}; \tag{40a}$$

b) $\Delta_n \le q\Phi \le \Delta_p$: (38b)

$$i_- = A_F\,D_-\,\Big\{\Big[1+\exp\Big(-\frac{\Delta-q\Phi-\hbar\omega}{W_0^{(-)}}\Big)\Big]\min(\Delta_n,\Delta-q\Phi-\hbar\omega)+$$

$$+W_0^{(-)}\Big[\exp\Big(-\frac{\min(\Delta_n,\ \Delta-q\Phi-\hbar\omega)}{W_0^{(-)}}\Big)-1+\exp\Big(-\frac{\Delta-q\Phi-\hbar\omega}{W_0^{(-)}}\Big)-$$

$$-\exp\Big(-\frac{\Delta-q\Phi-\hbar\omega-\min(\Delta_n,\ \Delta-q\Phi-\hbar\omega)}{W_0^{(-)}}\Big)\Big]\Big\}, \tag{39b}$$

$$i_+ = A_F\,D_+\,\Big\{\Big[1+\exp\Big(-\frac{\Delta-q\Phi+\hbar\omega}{W_0^{(+)}}\Big)\Big][\Delta_n-\max\ (0,\Delta_n-q\Phi+\hbar\omega)]+$$

$$+W_0^{(+)}\Big[\exp\Big(-\frac{\Delta_n}{W_0^{(+)}}\Big)+\exp\Big(-\frac{\Delta-q\Phi+\hbar\omega-\max(0,\Delta_n-q\Phi+\hbar\omega)}{W_0^{(+)}}\Big)-$$

$$-\exp\Big(-\frac{\Delta_p-q\Phi+\hbar\omega}{W_0^{(+)}}\Big)-\exp\Big(-\frac{\max(0,\Delta_n-q\Phi+\hbar\omega)}{W_0^{(+)}}\Big)\Big]\Big\}; \tag{40b}$$

c) $\Delta_p \le q\Phi \le \Delta$: (38c)

$$i_- = A_F\,D_-\Big\{(\Delta-q\Phi-\hbar\omega)\Big[1+\exp\Big(-\frac{\Delta-q\Phi-\hbar\omega}{W_0^{(-)}}\Big)\Big]+$$

$$+2W_0^{(-)}\Big[\exp\Big(-\frac{\Delta-q\Phi-\hbar\omega}{W_0^{(-)}}\Big)-1\Big]\Big\}, \tag{39c}$$

$$i_+ = A_F\,D_+\,\Big\{\Big[1+\exp\Big(-\frac{\Delta-q\Phi+\hbar\omega}{W_0^{(+)}}\Big)\Big][\Delta-q\Phi-\max\ (0,\Delta_n-q\Phi+$$

$$+\hbar\omega)]+W_0^{(+)}\Big[\exp\Big(-\frac{\Delta-q\Phi}{W_0^{(+)}}\Big)-\exp\Big(-\frac{\max(0,\Delta_n-q\Phi+\hbar\omega)}{W_0^{(+)}}\Big)-$$

$$-\exp\Big(-\frac{\hbar\omega}{W_0^{(+)}}\Big)+\exp\Big(-\frac{\Delta-q\Phi+\hbar\omega-\max(0,\Delta_n-q\Phi+\hbar\omega)}{W_0^{(+)}}\Big)\Big]\Big\}. \tag{40c}$$

The total tunnel current is given by the sum of i_+ and i_- :

$$i = i_- + i_+. \tag{41}$$

Formulas (38a) — (40c) are rather cumbersome. It is easy to notice, however, the following two circumstances.

a) At small voltages (on the rising branch of the curve) there exists a structure connected with the need for consuming part of the energy of the external field to form a phonon; this structure was experimentally observed by different authors many times.

b) The structure of formulas (38a) — (40c) is essentially the same as in the corresponding expressions of Section 2 [formulas (22a) — (25)]; we must merely put formally $W_n = W_p = W_r = W_0 \equiv W_0^{\pm}|_{\omega\to 0}$ in the latter* (here we recognize that in our case $\hbar\omega \ll \Delta_n$).

---

*It is possible to proceed in the same fashion also on the descending branch of the curve.

Consequently the basic qualitative conclusions of Section 2 remain in force. In particular, formulas (30) — (34) for Φ_m remain valid (except that W_n and W_p are replaced by W_0, and ϵ_0 is replaced by ΔE).

4. INDIRECT TRANSITIONS IN SCATTERING BY A CHARGED IMPURITY

We introduce the notation

$$A_t = \frac{\Gamma(1/\gamma)\, q^{5/2} E_m^{3/2} (m_n m_p)^{3/2} (E_m/E_0)^{1/\gamma}}{2^{9/2} \gamma \pi^{5/2} \hbar^{9/2} (2m_r)^{5/4} \Delta E^{7/4}} |N_{cv}\varphi|^2 N_{\text{lim}} \exp - \frac{4\sqrt{2m_r}\,\Delta E^{3/2}}{3qE_m\hbar}, \tag{42}$$

$$W_t = \frac{q\hbar E_m}{2\sqrt{2m_r \Delta E}}. \tag{43}$$

Then, using the formulas of [12] and the procedure of Section 2, we obtain

a) $0 \leq q\Phi \leq \Delta_n$: (44a)

$$i = A_t \left\{ \left(1 + e^{-\frac{\Delta - q\Phi}{W_t}}\right) q\Phi + W_t \left[e^{-\frac{\Delta_n}{W_t}} + e^{-\frac{\Delta_p}{W_t}} - e^{-\frac{\Delta_n - q\Phi}{W_t}} - e^{-\frac{\Delta_p - q\Phi}{W_t}} \right] \right\}; \tag{45a}$$

b) $\Delta_n \leq q\Phi \leq \Delta_p$: (44b)

$$i = A_t \left\{ \left(1 + e^{-\frac{\Delta - q\Phi}{W_t}}\right) \Delta_n + W_t \left[e^{-\frac{\Delta_n}{W_t}} - 1 - e^{-\frac{\Delta_p - q\Phi}{W_t}} + e^{-\frac{\Delta - q\Phi}{W_t}} \right] \right\}; \tag{45b}$$

c) $\Delta_p \leq q\Phi \leq \Delta$: (44c)

$$i = A_t \left\{ \left(1 + \exp\left(-\frac{\Delta - q\Phi}{W_t}\right)\right) (\Delta - q\Phi) + 2W_t \left[\exp\left(-\frac{\Delta - q\Phi}{W_t}\right) - 1 \right] \right\}. \tag{45c}$$

For the maximum of the current we again obtain formulas (30) — (34) (with W_n, W_p and W_r replaced by W_t, and ϵ_0 replaced by ΔE).

5. NEGATIVE RESISTANCE

The expression obtained in the preceding sections for the volt-ampere characteristics enable us, in particular, to investigate the negative resistance of the tunnel diode. By definition we have (in the region where the derivative $\partial i/\partial \Phi < 0$)

$$\frac{1}{R} \equiv \sigma = -\frac{\partial i}{\partial \Phi}. \tag{46}$$

In accordance with formulas (23a) — (23d) and (45a), (45b) we obtain (using as before the strong degeneracy condition $\Delta_n \gg W_n, W_p, W_r \ldots$):

a) Direct transitions.

When

$$\Phi_m \leqslant \Phi \leqslant \frac{\Delta_n}{q} \tag{47a}$$

$$\sigma(\Phi) = \frac{Aq}{\Phi_0} \left\{ \Phi - \Phi_0 + \Phi_0 e^{-\frac{\Delta_n - q\Phi}{W_n}} \right\}. \tag{48a}$$

When

$$\frac{\Delta_n}{q} \leqslant \Phi \leqslant \frac{\Delta_p}{q} \tag{47b}$$

$$\sigma(\Phi) = \frac{Aq}{\Phi_0}\left\{\frac{\Delta_n}{q} + \Phi_0 e^{-\frac{\Delta_p - q\Phi}{W_p}}\right\}. \tag{48b}$$

When

$$\frac{\Delta_p}{q} \leqslant \Phi \leqslant \frac{\Delta}{q} \tag{47c}$$

$$\sigma(\Phi) = \frac{Aq}{\Phi_0}\left\{\frac{\Delta}{q} - \Phi + \Phi_0 - \Phi_0 e^{-\frac{\Delta - q\Phi}{W_r}}\right\}. \tag{48c}$$

b) Indirect transitions with scattering on the impurity

$$\Phi_m \leqslant \Phi \leqslant \frac{\Delta_n}{q}, \tag{49a}$$

$$\sigma(\Phi) = \frac{A_t q}{\Phi_0}\left\{\Phi - \Phi_0 + \Phi_0 \exp - \frac{\Delta_n - q\Phi}{W_t}\right\}. \tag{50a}$$

When

$$\frac{\Delta_n}{q} \leqslant \Phi \leqslant \frac{\Delta_p}{q} \tag{49b}$$

$$\sigma(\Phi) = \frac{A_t q}{\Phi_0}\left\{\frac{\Delta_n}{q} + \Phi_0 \exp - \frac{\Delta_p - q\Phi}{W_t}\right\}. \tag{50b}$$

When

$$\frac{\Delta_p}{q} \leqslant \Phi \leqslant \frac{\Delta}{q} \tag{49c}$$

$$\sigma(\Phi) = \frac{A_t q}{\Phi_0}\left\{\frac{\Delta}{q} - \Phi + \Phi_0\left[-\left(1 + \frac{\Delta - q\Phi}{W_t}\right)\exp - \frac{\Delta - q\Phi}{W_t} + 1\right]\right\}. \tag{50c}$$

We recall that in this case it is necessary to substitute in place of ϵ_0 in the formula for E_0 (and consequently for Φ_0) the thermal width ΔE of the forbidden band.

Formulas (48a) — (48c) and (50a) — (50c) have a very similar structure. Analogous (but somewhat more cumbersome) expressions are obtained also in the case of indirect transitions with scattering by phonons. It is seen that the negative resistance depends in a sufficiently complicated manner on the external voltage Φ. This dependence is not even monotonic. By calculating the derivatives $\partial\sigma/\partial\Phi$ and $\partial^2\sigma/\partial\Phi^2$, we can readily verify that the absolute value of the negative conductivity $\sigma(\Phi)$ reaches a maximum in the interval $\Phi_m < \Phi \le \Delta_n/q$, can have (under certain conditions) a minimum in the second portion ($\Delta_n \le q\Phi \le \Delta_p$), and monotonically decreases when $q\Phi > \Delta_p$, vanishing when $q\Phi = \Delta$.

For the minimum point of Φ'' we obtain

$$q\Phi'' \simeq \Delta_p - 2W_p \ln \frac{q\Phi_0}{\sqrt{\Delta_n W_p}} \tag{51}$$

in the case of direct "transitions" and

$$q\Phi'' \simeq \Delta_p - 2W_t \ln \frac{q\Phi_0}{\sqrt{\Delta_n W_t}} \tag{52}$$

in the case of indirect transitions in scattering by a charged impurity. These expressions are valid so long as $q\Phi_0 > \sqrt{\Delta_n W_p}$ or, accordingly, $q\Phi_0 > \sqrt{\Delta_n W_t}$. If these inequalities are not satisfied (which is possible at sufficiently large values of Δ_n), then the function $\sigma(\Phi)$ has no minimum, but decreases monotonically in the interval $\Delta_n \leq q\Phi \leq \Delta$.

Calculation of the voltage Φ' at which σ reaches a maximum is made complicated by discontinuities of the derivative $\partial\sigma/\partial\Phi$ on the boundaries of the regions. The presence of these discontinuities is apparently connected with the complete degeneracy approximation; consequently, to resolve ultimately the question of the maximum of the negative conductivity it is necessary to consider the case of non-zero temperatures. We shall note here merely that for direct transitions under the conditions

$$2q\Phi_0 < \Delta_n < \frac{2q\Phi_0 + W_n}{1 - 2\frac{W_n}{q\Phi_0}} \tag{53}$$

we have

$$q\Phi' \simeq \Delta_n - 2W_n \ln \frac{q\Phi_0}{\sqrt{W_n(\Delta_n - 2q\Phi_0)}}. \tag{54}$$

Similar formulas (with W_n replaced by W_t and ϵ_0 replaced by ΔE) are valid also for indirect transitions with scattering on the impurity; the same results are obtained in scattering on phonons.

CONCLUDING REMARKS

Summarizing, we note three circumstances.

First, the formulas for the different observed quantities (Φ_m, Φ', Φ'') are essentially the same (apart from a small variation of certain parameters) for different mechanisms of the tunnel current. The only exception is in the form of the volt-ampere characteristic at low lattice temperatures when formulas (39a) — (39c) and (40a) — (40c) described a characteristic "phonon" structure, which was already observed experimentally many times [13].

Second, an account of the inhomogeneity of the field in the junction is essential* (particularly when calculating the absolute value of the current). Actually, we can formally proceed to the case of a homogeneous field by putting $\gamma \to \infty$ everywhere. As can be readily seen from formulas (4), (21), (35) and (42), the exponents and the expressions for A, A_F, $D_\pm$, A_t can change by a factor of two as γ changes from 1 to ∞. In this case the absolute values of the exponents change from approximately 10 to approximately 20; i.e., the magnitude of the tunnel current changes quite noticeably. Changes occur also (but to a considerably lesser extent) in the point Φ', Φ'', Φ_m. The reason for this is obvious and lies in sharp dependence of the tunnel current on the field intensity, as a result of which even a small region where the field is locally increased can make an important contribution (not proportional to the dimensions of this region) to the current.

Third, all the expressions obtained above depend essentially on the parameters Δ_n and Δ_p, which reflect the doping conditions of the specimen. When these quantities change, a change may take place not only in the numerical value of some particular voltage (Φ_m, Φ', Φ''), but also in the form of the functional dependence of this voltage on the parameters of the system. Moreover, even the very fact of presence or absence of a minimum in the negative conductivity, as we have seen in the preceding section, depends on the doping conditions. Thus, the tunnel diode is technologically a very "flexible" system, the properties of which can be controlled to a considerable extent.

REFERENCES

1. V.L. Bonch-Bruevich. Radio Engineering and Electronic Physics. 1960, 5, 12, 2033.
2. E.O. Kane. J. Appl. Phys. 1961, 32, 1, 83.

---

* The authors are grateful to S.G. Kalashnikov, who called their attention to the importance of this consequence of the theory developed above.

3. Yu.I. Ivanchik. Solid State Physics. 1961, 3, 1, 103.
4. H.L. Frisch, S.P. Lloyd. Phys. Rev. 1960, 120, 4, 1175.
5. Nick Holonyak, Jr. J. Appl. Phys. 1961, 32, 2, 130.
6. V.L. Bonch-Bruevich, A.G. Mironov. Solid State Physics. 1961, 3, 10.
7. R.C. Klander. Phys. Rev. (in press)**.
8. B.N. Vul. Proceedings, Academy of Sciences USSR. 1954, 96, 2, 257.
9. L.V. Keldysh. ZhETF. Journal of Experimental and Theoretical Physics. 1957, 33, 4, 994.
10. L.V. Keldysh. ZhETF 1958, 34, 4, 962.
11. E.O. Kane. Phys. Chem. Sol. 1960, 12, 2, 181.
12. P.S. Serebrennikov. Radio Engineering and Electron Physics (in press).
13. N. Holonyak et al. Phys Rev. Letters. 1959, 3, 4, 167.

Received by editor 11 July 1961

CONCERNING THERMIONIC CONSTANTS

L.N. Dobretsov

The paper considers the question of the thermionic constants contained in various equations for the density of thermionic current in the case of the homogeneous electrodes.

Recently, in connection with the problem of thermionic converters of heat into electricity, interest in the question of the so-called thermionic constants has again resumed. We have become convinced that many persons engaged in this problem are not completely clear in their minds concerning this question. In this connection it seems to us that it would be useful to consider again the question of the thermionic constants involved in various equations that determine the density of thermionic currents. We confine ourselves to homogeneous electrodes only.

Assume that the state of the electron in the conduction band of a cubic crystal with volume L^3 is characterized by a wave function $\psi(\vec{r}) = f_{\vec{p}}(\vec{r}) \times \exp\left[\frac{2\pi i}{h}(\vec{p}\,\vec{r})\right]$, i.e., is determined by three quasi-momentum components $p_x = \frac{h}{L} S_x$, $P_y = \frac{h}{L} S_y$, $p_z = \frac{h}{L} S_z$, where S_x, S_y, S_z are integers. If the x axis is directed along the normal to some surface of the body, then the coefficient of passage of this electron above the potential threshold at the surface D and the coefficient of reflection from the threshold $R = 1 - D$, as is well known from quantum mechanics, depends only on one component of the quasi momentum p_x, i.e.,

$$D = D(p_x) = 1 - R(p_x).$$

** The authors are grateful to M. Lax for a preprint of this paper.

If the numerical density of the current of electrons incident from the outside of the body on surface, with a given value of p_x, is defined by a distribution function $\nu(p_x)$, then the density of the thermionic emission saturation current j flowing through this emitter surface will be

$$j = \varepsilon \int D(p_x) \nu(p_x) \, dp_x, \tag{1}$$

where the integration must be carried out only over those values of p_x which correspond to the total energy E_x connected with the motion of the electron along the x axis and greater than zero, i.e., $E_x > 0$ (in the absence of an external field at this emitter surface, the value of D is zero for those values of p_x for which $E_x < 0$). The values of E_x are referred to the energy of an electron at rest outside the body.

Formula (1) can be represented in the form

$$j = \varepsilon \overline{D} \int \nu(p_x) \, dp_x, \tag{1a}$$

where

$$\overline{D} = \frac{\int D(p_x) \nu(p_x) \, dp_x}{\int \nu(p_x) \, dp_x}, \tag{2}$$

i.e., $\overline{D}$ is the value of the coefficient of passage above the barrier, averaged over the portion of the distribution $\nu(p_x)$ corresponding to $E_x > 0$.

Sommerfeld's theory of metals, where the states of the electrons inside the body are described by plane de Broglie waves $\psi(\vec{r}) = \exp\,[\frac{2\pi i}{h}(\vec{p}\,\vec{r})]$ and the quasi-momentum is equal to the momentum, the total energy is $E = E_a + \frac{1}{2m}(p_x^2 + p_y^2 + p_z^2)$ and $E_x = E_a + \frac{1}{2m} p_x^2$ (see Fig. 1). With this, $p_x = \sqrt{2m(E_x - E_a)}$, i.e., p_x is simply expressed in terms of E_x, and therefore $D(p_x)$ and $\nu(p_x)$ can be represented in the form $D(E_x)$ and $\nu(E_x)$, while (1) and (1a) can be rewritten:

$$j = \varepsilon \int_0^\infty D(E_x) \nu(E_x) \, dE_x, \tag{1b}$$

$$j = \varepsilon \overline{D} \int_0^\infty \nu(E_x) \, dE_x, \tag{1c}$$

where

$$\overline{D} = \frac{\int_0^\infty D(E_x) \nu(E_x) \, dE_x}{\int_5^\infty \nu(E_x) \, dE_x} \tag{2a}$$

is the coefficient of passage above the barrier, averaged over the distribution $\nu(E_x)$ in the interval of values of E_x from zero to infinity.

As is well known, the coefficients $D(E_x)$ and $D'(E_x)$ of passage above some potential threshold, for electrons with given value of E_x, incident on the threshold from one side (for example, for emitter electrons incident from the outside on its boundary) or from the other side (for example, for electrons emitted by a second emitter, or for electrons from the electron gas above the surface of the given emitter, incident on the same boundary from the outside), are equal to each other. Assume that there exists above the surface of the emitter an equilibrium electron gas, in which the distribution of the electrons in the current, relative

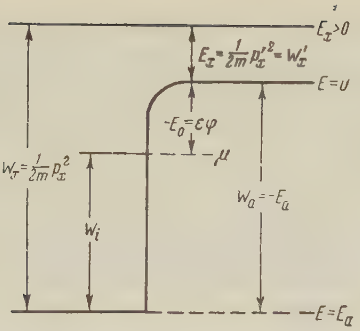

Fig. 1

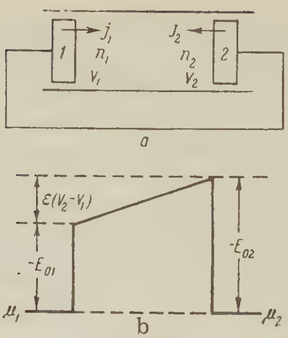

Fig. 2

to $E_x = W'_x$, is given by the function $\nu'(E_x)$. In the inverval dE_x, the current of electrons flowing from the gas inside the emitter with energies E_x will be $D'(E_x)\,\nu(E_x)dE_x$, while the current flowing from the emitter, with the same values of E_x, is equal to $D(E_x)\,\nu(E_x)dE_x$, According to the principle of detailed balance these currents should equal each other, i.e., $D'(E_x)\nu'(E_x)\,dE_x = D(E_x)\,\nu(E_x)\,dE_x$. Recognizing that $D(E_x) = D'(E_x)$, we obtain $\nu'(E_x) = \nu(E_x)$. It follows therefore that

$$\overline{D} = \frac{\int_0^\infty D(E_x)\,\nu(E_x)\,dE_x}{\int_0^\infty \nu(E_x)\,dE_x} = \frac{\int_0^\infty D'(E_x)\,\nu'(E_x)\,dE_x}{\int_0^\infty \nu'(E_x)\,dE_x} = \overline{D}',$$

i.e., not only $D(E_x)$ and $D'(E_x)$ are identical, but also their averaged values $\overline{D}$ and $\overline{D}'$ are identical for the current of the electrons incident from inside the emitter with $E_x > 0$ on some surface of the emitter, and for the current of electrons incident from the outside from the equilibrium electron gas. If we substitute in (1c) $\nu(E_x) = \frac{4\pi kT}{h^3}\exp\left[\frac{W_i - W_x}{kT}\right] = \frac{4\pi kT}{h^3}\exp\left[\frac{E_0 - E_x}{kT}\right]$ (see Fig. 1), which follows from Sommerfeld's theory for the case $E_0 = W_a - W_i \gg kT$, then, this equation goes over, as is well known, into the equation

$$j = A_0\overline{D}\,T^2\exp\left[\frac{W_a - W_i}{kT}\right] = A_0\overline{D}T^2\exp\left[\frac{E_0(T)}{kT}\right]. \tag{3}$$

The quantity A_0 is called the thermionic constant. According to Sommerfeld it is the same for all metals and has a value

$$A_0 = \frac{4\pi m\varepsilon k^2}{h^2} = 120\ \text{amp/cm}^2\ \text{deg}^2$$

One might think that the statement that A_0 is universal would be a consequence of the simplifying assumptions contained in Sommerfeld's "free electron" theory. In this case, for emitters to which Sommerfeld's theory cannot be applied, the statement of the universality of the thermionic constant does not necessarily hold true and the factor preceding $\overline{D}T^2\exp\left[\frac{E_0(T)}{kT}\right]$ may be different, not equal to A_0. Let us show that this is not the case.

We write down the equation for the thermionic current density in the form

$$j = f(T)\exp\left[\frac{E_0(T)}{kT}\right]. \tag{3a}$$

Since no assumptions are made concerning the function f(T), this notation implies no loss of generality.

We consider an equilibrium isothermal system, containing two different emitters, connected with each other by a conductor (Fig. 2a). The electrons inside both emitters, which are electrically connected with each other, will be in equilibrium when the levels of the electrochemical potentials μ_1 and μ_2 become equalized in both emitters (see Fig. 2b). Let the distance between the emitters be such that above each there is an electron gas whose state is determined by the properties of each emitter separately. The equilibrium between the electron gas inside the first emitter and the electron gas above its surface will occur when the density of the thermionic electron current flowing from the emitter into the gas with value j_1/ϵ becomes equal to the density of the current of thermionic electrons flowing from the gas inside the emitter. The latter has a value $\overline{D}'_1\nu_1 = \overline{D}'_1 \frac{1}{4} n_1\overline{v}_1$ where ν_1 — density of the current of electrons incident on the first emitter, n_1 — numerical concentration of the the electrons above the surface of the first emitter; $\overline{v}_1$ — average thermal velocity of these electrons. Therefore $j_1/\epsilon = \frac{1}{4}\overline{D}'_1 n_1 v_1$ or, taking (3a) into account

$$n_1 = \frac{4j_1}{\varepsilon \overline{D}'_1 \overline{v}_1} = \frac{4f_1(T)}{\varepsilon \overline{D}'_1 \overline{v}_1} \exp\left[\frac{E_{01}(T)}{kT}\right]. \tag{4}$$

A similar expression is obtained for the equilibrium numerical concentration of the electrons in the gas above the surface of the second emitter

$$n_2 = \frac{4j_2}{\varepsilon \overline{D}'_2 \overline{v}_2} = \frac{4f_2(T)}{\varepsilon \overline{D}'_2 \overline{v}_2} \exp\left[\frac{E_{02}(T)}{kT}\right]. \tag{4a}$$

From (4) and (4a), recognizing that $\overline{v}_1 = \overline{v}_2$ because T is constant, we obtain

$$\frac{n_1}{n_2} = \frac{f_1(T)}{f_2(T)} \frac{\overline{D}'_2}{\overline{D}'_1} \exp\left[\frac{E_{01} - E_{02}}{kT}\right]. \tag{5}$$

Finally, if the electron gases above the surfaces of the first and second emitters are degenerate (which occurs for all known emitters with a great margin) and the relative potential energy of the electrons in these emitters is sufficiently small compared with kT (which is also true for all known emitters [1]), then these gases will turn out to be in equilibrium with each other if the ratio of the electron concentrations in the gases satisfies the Boltzmann equation

$$\frac{n_1}{n_2} = \exp\left[\frac{\varepsilon(V_2 - V_1)}{kT}\right], \tag{6}$$

where $\epsilon(V_2 - V_1)$ is the difference in the potential energies of the electrons above the surfaces of the second and first emitters in the field of the contact potential difference: $\epsilon(V_2 - V_1) = E_{01} - E_{02}$ (Fig. 2b). Taking this into account, we obtain from (5) and (6)

$$\frac{f_1(T)}{\overline{D}'_1} = \frac{f_2(T)}{\overline{D}'_2} = F(T). \tag{7}$$

Since we made no limiting assumptions whatever concerning the properties of the emitters under consideration, except for assuming that the electron gases above them are perfect, F(T) in (7) is a universal function of the temperature for all emitters for which the last assumption is valid. Therefore (3a) can be represented in the form

$$j = F(T)\,\overline{D} \exp\left[\frac{E_0(T)}{kT}\right]. \tag{8}$$

However, for a Sommerfeld emitter $F(T) = A_0T^2$, in accordance with (3). Therefore for an emitter of any nature (and not only for metals) equation (3) is valid with the same value of the thermionic constant A_0. Recognizing that $E_0(T) = -\epsilon\varphi(T)$, we rewrite (1a) in the more customary form

$$j = A_0 \overline{D} T^2 \exp\left[-\frac{\varepsilon\varphi(T)}{kT}\right]. \tag{9}$$

If in some temperature interval near the value of T_0 we can represent $\varphi(T)$ with sufficient accuracy by means of a linear function, i.e., if

$$\varphi(T) = \varphi(T_0) + \alpha(T - T_0), \tag{10}$$

then the temperature dependence of the saturation current can be represented in the form

$$j = A_1 T^2 \exp\left[-\frac{\varepsilon\psi}{kT}\right], \tag{11}$$

where $\psi = \varphi(T_0) - \alpha T_0$ is a constant for the given emitter (effective or Richardson work function) which is independent of T; $A_1 = A_0\overline{D}\exp[-\frac{\epsilon\alpha}{kT}]$. The plot of the function $\ln\frac{j}{T^2} = F(\frac{1}{T})$ will be a straight line (the Richardson line) in this temperature interval, its slope $\frac{d(\ln\frac{j}{T^2})}{d(\frac{1}{T})}$ has a value $\epsilon\psi/k$, while the intercept of the Richardson line with the ordinate axis has a value $\ln A_1$. The constant A_1 in (11) is also customarily called a thermionic constant, just as A_0 is in (9). In order to distinguish between these two constants, we shall call A_0 the Sommerfeld thermionic constant of the emitter, while A_1 in (11), determined from the Richardson curve, will be called the Richardson thermionic constant of the emitter.

As shown above, the Sommerfeld thermionic constant is universal for all emitters and is independent of the temperature. The Richardson thermionic constants of different emitters may vary, first owing to the inequality in both the sign and in the temperature coefficient of the work function α, and second because of differences in the values of $\overline{D}$ for these emitters. From a purely theoretical point of view, the thermionic constant can be temperature dependent even in the vicinity where (10) is valid, owing to the dependence of the coefficient of transmission of the electrons on E_x. Indeed, if $D = D(E_x)$, then averaging over the electron distributions with respect to E_x, which are different for different temperatures, we get $\overline{D} = \overline{D}(T)$, i.e., $A_1 = A_1(T)$.

The fact that the work function $\varphi(T)$ depends on the temperature, and the presence of reflection on the boundary between the emitter and the vacuum, taken into account by the factor $\overline{D}$, lead, as is well known, to difficulties in determination of the true work functions as compared with the readily measured values j and T. Indeed, it follows from (9) that $\varphi(T) = \frac{kT}{\epsilon}[\ln A_0 + \ln\overline{D} - \frac{j}{T^2}]$; if $\overline{D}$ were known for a given emitter, then by measuring j at a second temperature T one could calculate $\varphi(T)$. In the "total current" method one calculates the work function from the equation $\varphi_{tc} = \frac{kT}{\epsilon}[\ln A_0 - \ln\frac{j}{T^2}]$; i.e., the term $\frac{kT}{\epsilon}\ln\overline{D} < 1$ is discarded. Thus, this method yields somewhat excessive values of the work function. These values are not "spoiled" by failure to account for the temperature dependence of $\varphi(T)$, but by failure to account for reflection. The work function determined from the slope $\frac{d(\ln\frac{j}{T^2})}{d(\frac{\epsilon}{kT})}$ of the Richardson curve, as can be seen from (11), is not as spoiled by failure to include reflection, but differs from the true work function by an amount αT_0, which can be both greater than zero or less than zero for various emitters. The choice of method depends on the ratio of the quantities $\frac{kT}{\epsilon} \ln \overline{D}$ and αT_0 (for emitters with $\alpha > \sim 5 \cdot 10^{-5}$ v/deg, the total-current method yields small error if $D > \sim 0.5$).

Let us examine the passage of a current of electrons emitted by one of the electrodes of a flat diode, for example by the electrode 1 of Fig. 2a. We shall assume that the distance between the electrodes is such that the space charge in the interelectrode space can be disregarded and the scattering of electrons in this stage can be neglected. Let us take into account the multiple scattering of the electrons both on the surface of emitter 1, and on the surface of collector 2.

We denote the quantity $E_x - E_0$ by W_x (see Fig. 3); the coefficients of passage above the potential barriers of the first and second emitters will obviously depend on W_{x1} and W_{x2} respectively; $D_1(W_{x1})$ and $D_2(W_{x2})$. Let the distribution of the electrons in the beam incident from inside the first emitter on its boundary over W_{x1} be given by the function $\nu(W_{x1})$. The flux of electrons of the given interval $dE_x = dW_{x1}$ leaving the emitter and reaching the collector will be $D_1(W_{x1})\, \nu\, (W_{x1})\, dW_{x1}$. The flux going into the collector after the first incidence on it will be $D_1(W_{x1})\, \nu_1\, (W_{x1})\, dW_{x1}\, D_2(W_{x2})$, where $W_{x2} = W_{x1} - \epsilon V$ (see Fig. 3). It is easy to see that the flux going into the collector during the second incidence on the collector, after reflection on both electrodes, will be

$$D_1(W_{x1})\, \nu\, (W_{x1})\, dW_{x1} R_2\, (W_{x2})\, R_1\, (W_{x1})\, D_2\, (W_{x2});$$

in the third incidence we get

$$D_1(W_{x1})\, \nu_1\, (W_{x1})\, dW_{x1}\, [R_2\, (W_{x2})\, R_1\, (W_{x1})]^2\, D_2\, (W_{x2}),\ \text{etc.}$$

The total number of electrons from among the $\nu_1\, (W_{x1})\, dW_{x1}$ that have reached the boundary of the emitter from the inside and have gone into the collector after all the reflections on the electrodes, equal to the sum of the individual currents, will be

$$d\nu_{12} = \frac{D_1\, (W_{x1})\, D_2\, (W_{x2})}{1 - R_1\, (W_{x1})\, R_2\, (W_{x2})}\, \nu_1\, (W_{x1})\, dW_{x1}. \tag{12}$$

It is easy to verify that the current of electrons going from the second emitter into the first, with the same value of E_x, will be

$$d\nu_{21} = \frac{D_1\, (W_{x1})\, D_2\, (W_{x2})}{1 - R_1(W_{x1})\, R_2\, (W_{x2})}\, \nu_2\, (W_{x2})\, dW_{x2}. \tag{12a}$$

We shall call the quantity $[D_1(W_{x1})\, D_2\, (W_{x2})]/[1 - R_1(W_{x1})\, R_2\, (W_{x2})]$ the combination coefficient of passage of the diode, and we shall denote it by $D_{12}(E_x, V)$. This quantity, as can

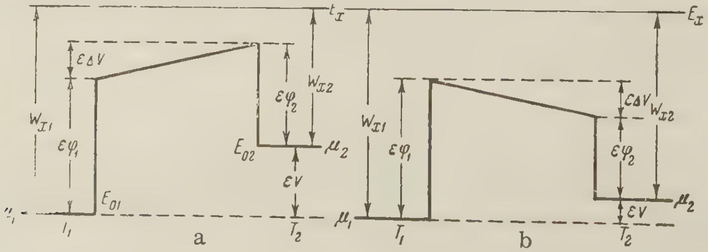

Fig. 3

be seen, depends on the properties of both electrodes of the diode, but for electrons with given E_x for any value of the external potential difference V, it is the same for the currents flowing from both electrodes of the given diode:

$$D_{12}(E_x, V) = D_{21}(E_x, V). \tag{13}$$

From this we get an important conclusion of importance for the understanding of the laws governing thermionic emission.

Let us examine again an equilibrium isothermal system, i.e., $T_1 = T_2$ and $V = 0$. In accordance with the principle of detailed balance, the electron currents $d\nu_{12}$ and $d\nu_{21}$ should be equal to each other in such a system. Therefore, using (12), (12a) and (13), we obtain

$$\nu_1(E_x - E_{01}) = \nu_2(E_x - E_{02}) \text{ when } T = \text{const}, \tag{14}$$

i.e., the densities of the electron currents flowing from the inside of any emitter to its boundary, at identical temperatures and for identical values of E_x, reckoned from the levels of the electrochemical potentials in these emitters, are the same. Since the distribution functions $\nu(E_x - E_0)$ are determined by the properties of the emitters (and the temperature), equation (14) holds true independently of whether the emitters form an equilibrium system or not.

At first glance this is an unexpected result, since the density of these states, corresponding to a certain value of $E_x - E_0$, and consequently the number of electrons with this value of E_x in different bodies, are naturally different.

Let us resolve the question of the current density in different bodies, using as an example a one-dimensional model of the crystal. The density of states dZ/dE corresponding to a certain value of E has in a one-dimensional crystal a value $2dp_x/dE$, where dp_x is the number of values of the quasi-momentum corresponding to the energy interval from E to $E + dE$. The number of electrons in this energy interval is $dn(E) = 2\frac{dp_x}{dE}[\exp(\frac{E-E_0}{kT}) + 1]^{-1}\,dE$, and the current is $d\nu = v_{gr}\,dn(E)$, where v_{gr} is the group velocity ($v_{gr} = dE/dp$); therefore $d\nu = 2[\exp(\frac{E-E_0}{kT}) + 1]^{-1}$. Thus, although $Z(E) = 2\frac{dp_x}{E}$ is different in different bodies, the product of $Z(E)$ and v_{gr}, which determines $\nu(E)$, is the same in all bodies for identical $(E-E_0)$ when T is constant. But the expressions (1a) are the same for all bodies, thus explaining the universality of equation (3) and its independence of the band structure of the emitter. We note that these considerations, which lead to the universality of (3), are not based on the assumption that the equilibrium electron gas over the surface of the emitter is perfect.

Let us return to the question of the density of the currents flowing from one electron into another in a planar diode. We consider first mode a in Fig. 3. In the electron current $A_0T^2\exp[-\frac{\epsilon}{kT_1}\varphi_1(T_1)]$, incident from inside the emitter 1 on its boundary, only a fraction $\gamma(\Delta V, T_1)$ of the electrons, for which $W_{x1} - \epsilon\varphi_1 = W'_{x1} \geq \epsilon\Delta V$, will reach the electrode 2, i.e.,

$$\gamma(T_1, \Delta V) = \frac{\int\limits_{\varepsilon\Delta V}^{\infty} \nu'_{T_1}(W'_{x1})\,dW'_{x1}}{\int\limits_{0}^{\infty} \nu'_{T_1}(W'_{x1})\,dW'_{x1}}. \tag{15}$$

Of this fraction, owing to reflections on the electrodes 1 and 2, there will enter into the second electrode a current with density

$$j_{12}^{(a)} = A_0 T_1^2 \overline{D_{12}^{(a)}}(T_1, \Delta V)\,\gamma(T_1, \Delta V)\exp\left[-\frac{\varepsilon}{kT_1}\varphi_1(T_1)\right], \tag{16}$$

where $\overline{D_{12}^{(a)}}(T_1, \Delta V)$ is the value of the combined coefficient of transmission of the diode averaged over W'_{x1} and $W'_{x2} = W'_{x1} - \epsilon V$ is the combined transmission coefficient of the diode. In this case the averaging of $D_1(W'_{x1})$ and $R_1(W'_{x1})$ in the expression for $D_{12}^{(a)}$ must be made over the distribution function $\nu_{T_1}(W'_{x1})$ corresponding to the temperature T_1 in the interval $\infty > W'_{x1} > \epsilon\Delta V$, while the averaging of $D_2(W'_{x2})$ and $R_2(W'_{x2})$ must be made over the same distribution function but in the interval $\infty > W'_{x2} > 0$. Equation (16) can be rewritten in the form

$$j_{12}^{(a)} = A_{12}^{(a)} T_1^2 \gamma(T_1, \Delta V) \exp\left[-\frac{\varepsilon}{kT_1}\varphi_1(T_1)\right], \tag{16a[12]}$$

where $A_{12}^{(a)} = A_0\overline{D_{12}^{(a)}}$ will be called the combined thermionic constant of electrode 1 in mode a of Fig. 3. In this mode the current density $j_{21}^{(a)}$ flowing from electrode 2 into electrode 1, as can be readily seen, will be

$$j_{21}^{(a)} = A_{21}^{(a)} T_2^2 \exp\left[-\frac{\varepsilon}{kT_2}\varphi_2(T_2)\right], \tag{16a[21]}$$

where $A_{21}^{(a)}$ is the combined thermionic constant of electrode 2 in mode a of Fig. 3: $A_{21}^{(a)} = A_0\overline{D_{21}^{(a)}}$, with the averaging carried out over $\nu_{T_2}(W'_x)$ in the same limits as in $D_{12}^{(a)}$. When $T_1 = T_2$, obviously, $A_{12}^{(a)} = A_{21}^{(a)}$. In mode b of Fig. 3, we can write similarly

$$j_{12}^{(b)} = A_{12}^{(b)} T_1^2 \exp\left[-\frac{\varepsilon}{kT_1}\varphi_1(T_1)\right], \tag{16b[12]}$$

$$j_{21}^{(b)} = A_{21}^{(b)} \gamma(T_2, \Delta V) T_2^2 \exp\left[-\frac{\varepsilon}{kT_2}\varphi_2(T_2)\right], \tag{16b[21]}$$

where $A_{12}^{(b)} = A_0\overline{D_{12}^{(b)}}$ and $A_{21}^{(b)} = A_0\overline{D_{21}^{(b)}}$, with the averaging in $D_{12}^{(b)}$ carried out over $\nu_{T_1}(W'_x)$, while the averaging in $\overline{D_{21}^{(b)}}$ is over $\nu_{T_2}(W'_x)$ within the limits $\infty < W'_{x2} < \epsilon\Delta W$ and $\infty < W'_{x1} < 0$. When $T_1 = T_2$ we also have in this case $A_{12}^{(b)} = A_{21}^{(b)}$. When $T_1 \neq T_2$, the combined thermionic constants of the two electrodes of the diode can differ from each other on purely theoretical grounds, owing to the difference between $\nu_{T_1}(W'_x)$ and $\nu_{T_2}(W'_x)$, over which the averaging takes place.

Let us now take account of the Maxwellian distribution of the thermionic electrons over the kinetic energies W'_x:

$$\nu'(W'_x) = C\exp\left[-\frac{W'_x}{kT}\right]. \tag{17}$$

With such a distribution (and only with such) $\gamma(T_1, \Delta V)$ has given (15) the form

$$\gamma(T_1, \Delta V) = \exp\left[-\frac{\varepsilon\Delta V}{kT}\right]. \tag{18}$$

It is known that for a metal with $\epsilon\varphi \gg kT$ (after Sommerfeld) the distribution of the electrons that can go out of the emitter (i.e., with $W_x > W_a$) relative to W_x is Maxwellian. But then, in accordance with (14), it is Maxwellian also for all other emitters. The distribution remains Maxwellian for the thermionic electrons leaving the emitter, in W'_x, only if the reflection coefficient is independent of W'_x (and therefore W_x), i.e., when $D'(W'_x) = D(W_x) =$ const. But in this case, averaging over different distributions $\nu'(W'_x)$, for example, corresponding to different temperatures T, and in different limits of W'_x, yields the same value $\overline{D}_i = D_i$. But then all four combined thermionic constants are equal to each other:

$$A_{12}^{(a)} = A_{21}^{(a)} = A_{12}^{(b)} = A_{21}^{(b)} \cdot \frac{D_1 D_2}{1 - R_1 R_2} = A_{1,2}^{*}. \tag{19}$$

We shall call $A_{1,2}^{*}$ the combined thermionic constants of the diode. We note A_{12} is equal to A_{21} in this diode for all temperatures, but the thermionic constant of the diode is not universal and can have different values in diodes with different cathodes or anodes, owing to their different values of D_1 and D_2. Taking (18) and (19) into account, we can write the expressions for the densities of the currents flowing from any one electrode to the other, in identical form

$$j = A_{1,2}^{*} T^2 \exp\left[-\frac{\varepsilon}{kT}\Phi(T)\right], \tag{20}$$

where T is the temperature of the emitting electrode; $\Phi(T)$ is its "effective" work function, equal to the true work function $\varphi(T)$ in the absence of the field that retains the emitted electrons and equal to $[\varphi(T) + \Delta V]$ in the presence of a retaining potential difference ΔV.

Theoretically, of course, $D'(W_x)$ cannot be independent of W'_x. In practice, the Maxwellian distribution of the thermionic electrons is evidence only that $D'(W'_x)$ is sufficiently constant for values of W'_x from zero to several times kT. One could cite several considerations to explain the practical independence of D' from W'_x in this region, based on an account of the forces of the electric image at the surface of the emitter (see, for example, [2]). One could also refine the expressions for A_{12} and A_{21} for different cases, by accounting for the dependence $D'(W'_x)$, which although weak does nevertheless exist. Such a refinement of the expressions for A_{12} and A_{21} is, however, inefficient, at any rate for polycrystalline emitters, since the presence of "spots" with different work functions leads to greater deviations from the idealized case considered above than the neglect of the dependence $D'(W'_x)$.

The dependence $D'(W'_x)$ at large values of W'_x enables us to motivate the use of (3) in an analysis of the results of measuring the saturation current in planar diodes. Strictly speaking, in this case, too, we should take in place of D_1 the quantity $\overline{D}_1\overline{D}_2^*/(1-\overline{R}_1\overline{R}_2^*)$ where D_2^* is the average transmission coefficient for the anode and $R_2^* = 1 - D_2^*$. But here the averaging must be carried out not over W'_{x0} with which the thermionic electrons leave the cathode, but over the energies $W''_x = W'_{x0} + \epsilon V_0$, with which the electrons arrive at the anodes. Since $R(W'_x)$ decreases with increasing W'_x, we have $\overline{R}_2^* \ll \overline{R}_1$ and we can set $\overline{R}_2^*$ equal to zero with sufficient accuracy. In the case of a cylindrical diode construction (the cathode is a filament), owing to the small probability of a thermionic electron being reflected from the anode and again falling on the cathode, one can assume $\overline{R}_a^* = 0$ with even greater justification.

REFERENCES

1. A.L. Reimann. Thermionic Emission. Wiley, New York, 1934 [Russian translation, GITTL, 1940, pp. 39-42].
2. H. Bethe and A. Sommerfeld. Electron Theory of Metals (translated from German), ONTI, 1938, p. 106-108.

Received by editor 21 March 1961

EFFECT OF DRAIN OF THERMIONIC CURRENT ON THE TEMPERATURE MODE OF A SEMICONDUCTOR CATHODE

A.A. Ostroukhov

The cooling or heating of a cathode coating due to drain of thermionic current is considered. The use of the literature values of the heat conductivity and electric conductivity of the oxide coating shows that whether the coating is fine or coarse grained, the cooling after a time $t \lesssim 10^{-4}$ sec is appreciably only at very large emission current densities and evidently does not play an appreciable role in the fall-off of relatively small pulse currents during the time $t \lesssim 10^{-4}$ sec.

INTRODUCTION

It is stated in [1] that for a qualitative explanation of the experimentally observed peculiarities of pulsed thermionic emission one can advance various physical hypotheses: the time variation of the degree of coating of the surface of the cathode by the atoms, which influence the thermionic emission (increase in the external work function) [2, 3]; reduction in concentration of the volume donors in the region of the coating next to the surface (increase in the internal work function) [4, 5, 6]; change in the values of the volume and surface charges, which screen the external field, during the anode-voltage pulse. As shown by an estimate of the characteristic times of these processes [1], based on the values of the diffusion coefficients of heavy particles (atoms, vacancies, ions) in the oxide taken from the literature [7, 8, 9], the first two hypotheses can be used for a quantitative explanation of only the slowly decreasing component of the current pulse. The last hypothesis, which leans on the existence of many semiconductor surface levels on the surface, with effective time of recombination with the carriers on the order of 10^{-4} and 10^{-6} second, enables us to explain the experimentally observed singularities in the fall-off of the current pulse during times on the order of 10^{-4} sec [1, 10, 11]. The fall-off of the current takes place in this case for all values of the drawn current; the limits of variation of the current in the pulse depend on the state of the surface and the degree of ionization of the volume donors, and on the applied anode voltage. It turns out here that the change in the surface charge influences the magnitude of the fall-off of the current much more strongly than the change of the charge on the volume donors.

In the present paper we consider the influence of cooling or heating of the coating during the current drain on pulsed emission. This fact has been known experimentally for a long time; an approximate theory for it is proposed in [12]. We deem it advantageous to dwell once more on this question in connection with the more recent data on the resistance of the outside coating at large current and on its distribution over the thickness of the layer, and also new measurements of the coefficient of heat conduction of the oxide layer [13, 14, 15]. We have formulated the problem more mathematically in the present case and give the final results in a form suitable for comparison with the experiment.

The physical picture of cooling or heating of the cathode by the emission current is as follows. At the instant when the drain of the emission current $I(t)$ starts ($t = 0$), a heat flux $I(\chi + 2kT_0/e)$ begins to move away from the surface of the cathode, along with the energy flux due to thermal radiation; here $e\chi$ — external work function of the electrons from the layer; T_0 — temperature of the free surface of the layer. The semiconductor layer of thickness on the order of the mean free path of the electron l is now continuously depleted of fast electrons, with energy sufficient to go out to the vacuum; the time required to leave the layer under consideration is $t \sim l/\bar{v} \sim 10^{-12}$ sec, where $\bar{v}$ is the mean thermal velocity of the electrons. The slow electrons remaining in this layer again enter into thermal equilibrium with the lattice within a time on the order of the time of temperature relaxation of the electron gas in the volume, $t \lesssim 10^{-10}$ sec, and can go out into the vacuum in the form of ordinary thermionic electrons. If we neglect such short times, we can assume that at each given instant of time the temperature of the electron gas and of the lattice are equal to each other (we disregard the heating of the electron gas by the electric field in the layer). Thus, the lattice gives up its thermal energy to the vacuum with the aid of the electronic emission current with almost no time delay. The cooling surface receives also from inside the cathode an additional heat flux, due to the heating of the layer of the cathode by the flowing current. Depending on the value of the current drained at different instants of time the surface temperature of the layer will be either higher or lower than the temperature in the absence of emission current.

In examining the cooling effect, we shall make use of the ordinary equations of the phenomenological theory of semiconductors. An exact solution of the problem within the framework of this theory is obviously very difficult, since the initial equations contain coefficients that are functions of the temperature, and this temperature dependence is not sufficiently well known. One can, however, obtain the correct order of magnitude of the considered effect, and also the order of magnitude of its time lag, by using this approach. In addition, the phenomenological character of these equations enables us to apply them to a polycrystalline porous coating. It is necessary here merely to consider the coefficients in the initial equations as being certain effective parameters, characterizing the layer in the mean, and obtain these parameters from the experimental data. The influence of the microcrystalline structure of the coating on this effect will be discussed in greater detail in the next section.

In calculating the temperature variation ΔT, it is sufficient to confine oneself to small relative values $\Delta T/T$. Indeed, since the external work function is $\chi \sim 1$ volt and $kT_0/e \sim \sim 0.1$ volt, even when $|\Delta T/T| \sim 0.1$ the current changes by approximately a factor e.

1. MAGNITUDE AND TIME DELAY OF THE COOLING OR HEATING OF THE EMITTING LAYER BY THE EMISSION CURRENT

We consider a semiconductor layer of thickness d, situated on a metal core; the x axis is directed inside the layer; then x = 0 corresponds to the free surface, and x = d corresponds to the boundary with the core. The law of heat conservation in the case of quasi-stationary currents ($\operatorname{div} l = 0$) and in the case of a homogeneous layer leads to the following equation [16]

$$\rho c \frac{\partial T}{\partial t} = \operatorname{div} \varkappa_0 \nabla T + \tau \vec{I} \nabla T + \frac{I^2}{\sigma}, \tag{1}$$

where ρ is the density of the coating; c is the specific heat capacity; $\varkappa_0$ is the coefficient of heat conduction; τ is the Thomson coefficient; and σ is the specific electric conductivity. We shall henceforth assume these coefficients, as well as the current I, to be constant, so as to simplify the calculations. In this case (1) can be rewritten as:

$$\frac{\partial T}{\partial t} - a^2 \frac{\partial^2 T}{\partial x^2} - b \frac{\partial T}{\partial x} = F, \tag{2}$$

where

$$a^2 = \frac{\varkappa_0}{\rho c}; \quad b = \frac{I\tau}{\rho c}; \quad F = \frac{I^2}{\rho c \sigma}. \tag{3}$$

On the boundary between the layer and the core, depending on the heat-exchange conditions, we can fix either the heat flux or the temperature. As will be shown in the next section, the temperature mode on the boundary with the core does not have great significance for the effect under consideration in the range of time intervals in which the temperature changes appreciably upon considerable variation of the parameters. For the sake of being specific, we fix the temperature:

$$T(x, t)|_{x=d} = T_d = \text{const.} \tag{4}$$

On the boundary with the vacuum we have

$$\varkappa_0 \frac{\partial T}{\partial x} + (\Pi + \zeta) I \Big|_{x=0} = r\sigma_0 T_0^4 + I\left(\chi + 2\frac{kT_0}{e}\right), \tag{5}$$

where Π — Peltier coefficient, ζ — chemical potential of the electrons in the layer, σ_0 — the Stefan-Boltzmann constant, r — the reflection coefficient, and $e\chi$ — the work function of the electrons leaving the layer. As is well known [17],

$$\Pi + \zeta \approx \frac{kT}{e}(2 + n), \tag{6}$$

where n — exponent in the dependence of the mean free path of the electron l on the energy E: $l \sim E^n$. Taking this into account, as well as the fact that, as indicated, we can confine ourselves to small $|\Delta T/T| \ll 1$, we linearize the boundary condition (5), whereupon it assumes the form

$$\varkappa_0 \frac{\partial T}{\partial x}\Big|_{x=0} = k_0 + k_1 T_0, \tag{7}$$

$$k_0 = -3W + I\chi, \quad k_1 = \frac{1}{T_0^0}\left(4W - n\frac{kT_0^0}{e} I\right), \; W = r\sigma_0 T_0^{04}, \tag{8}$$

where T_0^0 is the temperature of the surface of the layer in the absence of current.

The initial distribution of the temperature can be readily obtained, and it has the form

$$T(x, t)|_{t=0} = T^0(x) = T_0^0 + \frac{W}{\varkappa_0} x. \tag{9}$$

Thus, an approximate solution of the problem reduces to a solution of equation (2) with boundary and initial conditions (4), (7), (9).

We seek the solution in the form

$$T(x, t) = u_1(x, t) + u_2(x). \tag{10}$$

The stationary part $u_2(x)$ is

$$u_2(x) = T_0^0 + \frac{W}{\varkappa_0} d + R\left(e^{-y\frac{x}{d}} - e^{-y}\right) + \frac{I^2 d^2}{\varkappa_0 \sigma y}\left(1 - \frac{x}{d}\right), \tag{11}$$

where

$$R = -[y + (1 - 6^{-y}) A]^{-1}\left\{\frac{d}{\varkappa_0}(I\chi - 3W) + \frac{I^2 d^2}{\varkappa_0 \sigma y} + A\left(T_0^0 + \frac{Wd}{\varkappa_0} + \frac{I^2 d^2}{\varkappa_0 \sigma y}\right)\right\},$$

$$y = \frac{bd}{a^2} = \frac{I\tau d}{\varkappa_0}; \quad A = \frac{d}{\varkappa_0 T_0^0}\left(4W - n\frac{kT_0^0}{e} I\right). \tag{12}$$

The value of $u_2(x)$ for x = 0 is

$$u_2(0) = T_0^0 + \left[\frac{1}{y}(1 - e^{-y}) A + 1\right]^{-1}\left\{\frac{d}{\varkappa_0}\left[W - \left(W + I\chi - \right.\right.\right.$$

$$-n\frac{kT_0^0}{e}I\Big)\frac{1}{y}(1-e^{-y})\Big]+\frac{I^2d^2}{\sigma\varkappa_0}\frac{1}{y}\Big[1-\frac{1}{y}(1-e^{-y})\Big]\Big\}. \tag{13}$$

The nonstationary component $u_1(x, t)$ is expressed by the series

$$u_1(x, t)=\sum_{m=1}^{\infty} C_m X_m(x)\, e^{-\frac{xy}{2d}-\left(\frac{y^2}{4}+v_m^2\right)z}, \tag{14}$$

where

$$X_m(x)=\cos v_m\frac{x}{d}+\frac{H}{v_m}\sin v_m\frac{x}{d};\; z=\frac{a^2t}{d^2},$$

and v_m are the positive roots of the equation

$$\cos v_m+\frac{H}{v_m}\sin v_m=0;\; H=A+\frac{y}{2}. \tag{15}$$

In order of magnitude when $H \lesssim 1$, $v_m \sim \frac{\pi}{2}(2m-1)$, $m = 1, 2, \ldots$ the coefficients C_m are equal to

$$C_m=\frac{2v_m^2}{v_m^2+H+H^2}\,\frac{1}{d}\int_0^d [T^0(x)-u_2(x)]\, e^{\frac{xy}{2d}}X_m(x)\,dx. \tag{16}$$

The nonstationary parts of the solution $u_1(x, t)$ attenuate exponentially with time. A direct calculation of the coefficients C_m by means of formula (16) shows that $|C_m| \sim 1/v_m^2$ as $m \to \infty$ and therefore the series (14) converges. At small currents, when $|y| = |I\tau d/\varkappa_0| \ll 1$, the coefficients C_m are equal to

$$C_m=\frac{2}{v_m^2+H+H^2}\left\{\frac{Id}{\varkappa_0}\left(\chi-n\frac{kT_0^0}{e}\right)-\frac{I^2d^2}{\varkappa_0\sigma}\frac{1}{v_m}\left[\frac{H}{v_m}+\left(1+\frac{H^2}{v_m^2}\right)\sin v_m\right]\right\}. \tag{17}$$

It is seen from (17) that at sufficiently small currents, when the effect of cooling at the surface predominates over the effect of release of Joule and Thomson heat in the volume, all the C_m have the same sign and the time dependence of $T(x, t)$ is a monotonically decreasing function of t. As the current I increases, some of the first coefficients C_m may reverse sign, and the dependence of $T(x, t)$ on t ceases to be monotonic. Under definite values of $\varkappa_0$ and σ, this can occur when $|y| \ll 1$, so that (17) still holds true for C_m.

Let us see now how the temperature of the surface $x = 0$ changes as the current drawn I increases, in the case of sufficiently long anode-voltage pulses. From (13) with $|y| \ll 1$ we obtain

$$\Delta T=T(0,\infty)-T_0^0=\frac{Id}{\varkappa_0}\left[-\left(\chi-n\frac{kT_0^0}{e}\right)+\frac{Id}{2\sigma}\right](1+A)^{-1}. \tag{18}$$

If (18) is valid for the current

$$I_0=\frac{2\sigma}{d}\left(\chi-n\frac{kT_0^0}{e}\right), \tag{19}$$

i.e., $|y| = |I_0\tau d/\varkappa_0| \ll 1$ then it follows from (18) that when $I < I_0$ the surface of the layer is cooled by the emission current drain, and when $I > I_0$ the surface is heated. If we can neglect the dependence of A on I, i.e., $4W \gg n\frac{kT_0^0}{e}I$, then we obtain from (18) that the maximum cooling of the surface occurs at a current $I_{\min} \approx I_0/2$, with

$$\Delta T_{\min} \simeq -\frac{\sigma}{2\varkappa_0}\left(\chi - n\frac{kT_0^0}{e}\right)^2 (1+A)^{-1}. \tag{20}$$

It is seen from (19) and (20) that in the case we are currently considering, that of relatively low currents, the current $I_{\min}$, which guarantees maximum cooling of the surface in the new stationary state, is determined essentially by the resistance of the coating d/σ, while the amount of cooling $\Delta T_{\min}$ is determined by the ratio $\sigma/\varkappa_0$. With further increase in current, when $|y| \sim 1$, the Thomson effect greatly influences the value of $T(0, \infty)$. However, the case $|y| \sim 1$ is probably not realized in practice, since the relation $|y| \sim 1$ is obtained in a wide interval of values of the parameters $\varkappa_0$, σ, and τ at very large currents, which in accordance with (18) result in a considerable overheating of the surface and a destruction of the coating. Thus, in the stationary mode, when the current drain is relatively small, the influence of the Thomson effect on the surface temperature is generally speaking insignificant.

Let us examine the behavior of T(x,t) at small t, satisfying the inequality

$$z^{\frac{1}{2}} = \frac{a\sqrt{t}}{d} \ll 1. \tag{21}$$

It is easiest to obtain an asymptotic expression for T(x,t) when (21) is satisifed by solving, by operator methods, the initial equations (4), (2), (7), and (9) and neglecting all the terms that contain factors of order exp $(-d^2/a^2t)$ after taking the inverse Laplace transform.

In this case we obtain for the temperature T(x,t) the following expression

$$T(x, t) = T^0(x) + \frac{I^2d^2}{\sigma\varkappa_0}\left(1 + \frac{\tau\sigma W}{\varkappa_0 I}\right)\left[\frac{a^2t}{d^2} - e^{-\frac{xy}{2d}} f_2(x, t)\right] - \\ - \frac{Id}{\varkappa_0}\left(\chi - n\frac{kT_0^0}{e}\right) e^{-\frac{xy}{2d}} f_1(x, t), \tag{22}$$

where

$$f_1(x, t) = e^{-\frac{xy}{2d}}(2H + y)^{-1} \operatorname{erfc}\left[\frac{1}{2a}\left(\frac{x}{\sqrt{t}} - b\sqrt{t}\right)\right] - \\ + e^{\frac{xy}{2d}}(2H - y)^{-1} \operatorname{erfc}\left[\frac{1}{2a}\left(\frac{x}{\sqrt{t}} + b\sqrt{t}\right)\right] - 4H(4H^2 - y^2)^{-1} \exp \times \\ \times\left[H\frac{x}{d} + \left(H^2 - \frac{y^2}{4}\right)\frac{a^2t}{d^2}\right] \operatorname{erfc}\left[\frac{x}{2a\sqrt{t}} + H\frac{a\sqrt{t}}{d}\right]; \tag{23}$$

$$\operatorname{erfc}(x) = 1 - \frac{2}{\sqrt{\pi}}\int_0^x e^{-u^2}du; \quad H = A + \frac{y}{2}; \tag{24}$$

$$A = \frac{k_1 d}{\varkappa_0} = \frac{d}{\varkappa_0 T_0^0}\left(4W - n\frac{kT_0^0}{e} I\right); \quad y = \frac{bd}{a^2} = \frac{I\tau d}{\varkappa_0}.$$

The expression for f_2 has a similar structure; we do not cite it here because of its complexity. We note only that both f_1 and f_2 change at a fixed point $x > 0$ from values $f_1|_{t=0} = f_2|_{t=0} = 0$ to a certain new stationary value, within a time which is approximately determined by the conditions

$$\frac{1}{2a}\left(\frac{x}{\sqrt{t}} \pm b\sqrt{t}\right) \sim 1; \quad \frac{x}{2a\sqrt{t}} + H\frac{a\sqrt{t}}{d} \sim 1. \tag{25}$$

Thus, the cooling wave, brought about by the start of the current drain at the instant $t = 0$ and propagating from the surface $x = 0$ inside the layer, causes an appreciable change in the temperature at the point $x > 0$ at the instant of time t, determined by the conditions (25).

The temperature of the surface $x = 0$, if (21) is satisfied, has a value

$$\Delta T' = T(0, t) - T_0^0 = -\frac{Id}{\varkappa_0}\left(\chi - n\frac{kT_0^0}{e}\right)\left(\frac{a\sqrt{t}}{d}\right)\frac{2}{\sqrt{\pi_1}} + \frac{I^2d^2}{\varkappa_0\sigma}(1 + B)\left(\frac{a\sqrt{t}}{d}\right)^2 + \ldots, \tag{26}$$

$$B = \left(I\frac{d}{\sigma}\right)^{-1}\left[H\left(\chi - n\frac{kT_0^0}{e}\right) + \frac{Wd}{\varkappa_0}\tau\right]. \tag{27}$$

From this we obtain the position of the minimum $t_{\min}$ on the curve $T(0,t)$:

$$t_{\min} = \frac{\rho c d^2}{\pi\varkappa_0}\left(I\frac{d}{\sigma}\right)^{-2}\left(\chi - n\frac{kT_0^0}{e}\right)^2(1 + B)^{-2}. \tag{28}$$

In this case the inequality (21) should be satisfied for $t_{\min}$. The depth of the minimum is

$$\Delta T'_{\min} = T(0, t_{\min}) - T_0^0 = -\frac{\sigma}{\pi\varkappa_0}\left(\chi - n\frac{kT_0^0}{e}\right)^2(1 + B)^{-1}. \tag{29}$$

It follows from (27) and (29) that the explicit dependence of $\Delta T'_{\min}$ on the current I is generally speaking insignificant. The Thomson coefficient τ enters into (26), (27), and (29) via B and H; in the case of small t the influence of the Thomson heat on the values of $\Delta T'_{\min}$ and $t_{\min}$ is also insignificant. We can verify further that ΔT vanishes when $t \simeq 4t_{\min}$, i.e., the temperature of the surface $x = 0$ becomes greater than T_0^0 already within a time $\gtrsim 4t_{\min}$ after the start of the current drain.

We now compare $\Delta T_{\min}$ from (20) with $\Delta T'_{\min}$ from (29). Expression (20) has been obtained subject to condition $|I_0\tau d/\varkappa_0| \ll 1$, where $I_0 = \frac{2\sigma}{d}\left(\chi - n\frac{kT_0^0}{e}\right)$; expression (29) has been obtained subject to condition (21) for $t_{\min}$. It follows from (28) that $t_{\min}$ is all the smaller, the smaller I_0 and the greater I. It is therefore possible that when $t \to \infty$ and at small currents $I \sim I_0$ expression (20) will hold for the same layer for which expressions (28) and (29) hold when $t \to 0$ and the currents I are large (it must also be taken into account that the other parameters of the layer can change with increasing I).

From (20) and (29) we obtain $\Delta T'_{\min}/\Delta T_{\min} \sim \sigma'/\sigma$, where the conductivity for the large current is denoted by σ'. Thus, drawing of very large pulse currents leads to a cooling of the surface within a time $t \sim t_{\min}$; the extent of this cooling can be of the same order as the maximum possible cooling in stationary drain of relatively small currents, provided the conductivity σ does not change strongly with changing I.

Using (28) and (29) we obtain the connection between $t_{\min}$ and $\Delta T'_{\min}$

$$t_{\min} = -\Delta T'_{\min}\frac{\rho c d}{I^2\frac{d}{\sigma}(1 + B)}. \tag{30}$$

From the foregoing expressions (13), (14), (18), (22), and (26) for $T(x,t)$ when $|y| \ll 1$ we get the qualitative time variation of the temperature of the free surface $T(0,t)$ as shown in the figure. In the range of current values $0 \lesssim I \lesssim I_0/2$, $T(0,t)$ decreases monotonically with increasing t; maximum cooling takes place at $I \sim I_0/2$ (curve 1). When $I_0/2 \lesssim I \lesssim I_0$ we obtain curve 2; when $I \gg I_0$ and the position of the minimum shifts toward t, the surface begins to heat up strongly after a brief cooling (curve 3).

In solving equation (2) we assumed the coefficients a^2, b, and F to be constant. If we make use of the orders of magnitude of the parameters given below, then according to (20), (28), and (29) the magnitude and the time lag of the cooling effect will be determined essentially by the parameters I, σ, $\varkappa_0$, χ, and ρc. These parameters depend themselves on the

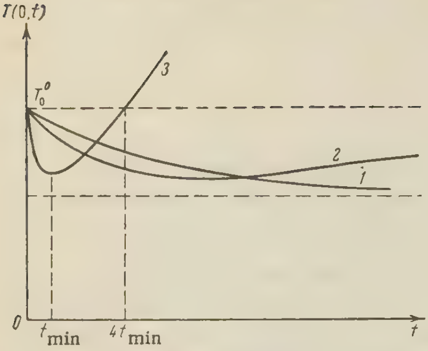

temperature, and consequently should change when the surface is cooled, with only I and σ changing most radically when $|\Delta T| / T \ll 1$. The decrease in σ upon cooling should lead, according to (20) and (29), to a decrease in the cooling effect itself. Since usually experience shows that I/σ increases with increasing temperature, $t_{\min}$ can shift with decrease in temperature, in accordance with (28), toward the larger t, and the effect of cooling will decrease after a time $t \lesssim 10^{-4}$ sec. Thus, an account of the dependence of the coefficients a^2, b, and F on the temperature in equation (2) will apparently not bring about an increase in the cooling effect.

2. DISCUSSION OF RESULTS AND COMPARISON WITH EXPERIENCE

We first note the following. The reduction in the temperature of the layer of the coating next to the surface influences the emitting ability of the cathode in two ways. First, the current from the surface of the cathode I' (this current generally speaking is not equal to the through current I) changes because of the change in the concentration of the current carriers in this region; for an appreciable change in concentration it is necessary that the cooling extend over a depth on the order of the screening length; this process will last a time $t \gtrsim t_{rec}$, t_{prop}, where t_{rec} is the time necessary to establish recombination equilibrium between the conduction band and the volume donors, and t_{prop} is the time necessary for the cooling wave to propagate inside by a length of order of the screening length. Second, the current I' changes because of a change in the average kinetic energy of the electrons; for this purpose it is necessary that the cooling extend over a region of thickness on the order of the length l_T, at which temperature equilibrium is established between the carriers and the lattice. The length l_T is generally speaking smaller than the screening length, and the duration of this process obviously will be less than the times t_{rec} and t_{prop}. The initial phenomenological equations are incapable of accounting for the change in temperature at distances less than or of the order of l_T. We can therefore assume that the temperature in the region $0 \lesssim x \lesssim l_T$ is T(0,t). Thus, the change of the current from the surface of the cathode I' with time, in such an analysis, is determined by the dependence of the temperature of the surface T(0,t) on the time t. On the other hand, the change in the through current I with time will in this case depend appreciably on the magnitude of the applied anode voltage U_a. If U_a is sufficiently small, so that the current drain I occurs under space charge conditions in vacuum, then the change in the current I with time will be small so long as the current from the surface is $I'(t) > I(t)$, and consequently the concentration of the electrons at the surface of the cathode in the vacuum does not differ greatly from its equilibrium value. As noted in [10], an analogous small change in current I occurs when the cathode operates in the space-charge mode, and also in the mechanism of current fall-off considered in [1, 10]. At large U_a, when all the emitted electrons are carried to the anode, I' = I and the time dependence of the current is determined by the change in the surface temperature T(0,t) during the time of the pulse of U_a; i.e., it will depend on the values of the layer parameters $\varkappa_0$ and σ, and also on I itself. In the estimates below we confine ourselves to only this case of large voltages U_a.

We neglect for the time being the polycrystalline structure of the coating and choose parameters $\varkappa_0$, σ, and τ, etc., which characterize the layer on the average. Let $d = 10^{-2}$ cm, $\chi = 1$ v, $kT_0^0/e = 0.1$ v, $T_0^0 = 1160$°K, $W = r\sigma_0 T_0^{04} = 2.8$ w/cm^2, since $r = 0.25 - 0.30$ [18], $\rho c = 2$ J/cm$^3 \cdot$ deg [18, 12], n = 1. As for the majority of semiconductors, for an oxide coating we get $T\tau = T^2 \frac{\partial \alpha}{\partial T} \approx T\alpha \simeq 0.1$ in [19] at $T \approx 1000$°K; α — specific thermal emf.

The data for $\varkappa_0$ are highly scattered [18, 15]: $\varkappa_0 = 10^{-3} - 5 \cdot 10^{-5}$ w/cm $\cdot$ deg, the latter value being the most likely, since it is obtained by direct measurement with the aid of thermal probes [15].

At the values chosen, we have $\varkappa_0 z^{\frac{1}{2}} = a\sqrt{t}/d \simeq (2-0.5)\sqrt{t}$. We confine ourselves to an examination of the temporal changes in the quantities, occurring after $t \lesssim t_0 = 10^{-4}$ sec. For such values of t, the inequality (21) is well satisfied: $z^{1/2} \ll 1$. Establishment of a new stationary state, as can be seen from (14), occurs after a time $t \sim d^2/a^2$, which in this case is considerably greater than t_0. Thus, the cooling wave traveling from the surface inside the layer can propagate after a time $t \lesssim t_0$ over a distance $x_0 \ll d$. It follows therefore that in the effect considered only the values of the parameters for the near-surface layers of the coating are of importance, and also that the boundary conditions for the temperature at the core do not play an appreciable role. The latter can also be readily traced by examining the asymptotic behavior of the Laplace transform of the temperature $T(x, s)$.

The coating resistance was measured in [13] over a wide range of currents $0 \lesssim I \lesssim 50$ a/cm^2. For the internal layer the value obtained was $d/\sigma \simeq 1$ ohm · cm^2. In [14], a direct measurement has shown (at relatively small currents) that the near-surface layers of the coating have a larger resistance than the internal layers. In addition, it is known that the near-surface layer (with thickness $\sim 10^{-4}$ cm) of a mixed coating is enriched with strontium oxide, the resistance of which is considerably greater than the resistance of barium oxide [13, 20]. Thus, it appears to us more realistic to take for the surface layer resistance a value $d/\sigma \simeq 1$ ohm · cm^2, and not $d/\sigma = 0.01$ ohm · cm^2, as was done in [12].

Thus, for the chosen values of the parameters, using (19) and (20), we obtain for $\varkappa_0 = 10^{-3}$ w/cm · deg values $A \sim 10^{-1}$, $y \sim 10^{-3}\, I$ (a/cm^2), $I_0 \sim 2$ a/cm^2, $\Delta T_{min} \sim -4$K°; and for $\varkappa_0 = 5 \cdot 10^{-5}$ w/cm · deg we get $A \sim 2$, $y \sim 2 \cdot 10^{-2}\, I$ (a/cm^2), $I_0 \sim 2$ a/cm^2, $\Delta T_{min} \sim -30$K°. In both cases the maximum cooling takes place at relatively small stationary currents I_0.

It is seen from this estimate that by drawing sufficiently long pulses ($t_{pulse} \gtrsim d^2/a^2$) of relatively small currents the surface can become appreciably cooled, and thus the drawn current itself reduced.

Let us examine expressions (28) and (29) for Δt_{min} and $\Delta T'_{min}$, obtained by solving the nonstationary equations. As was already noted, for the times considered here the inequality (21) is fulfilled over a wide range values of $\varkappa_0$, and expansion (26) can be used. When $\varkappa_0 = 10^{-3}$w/cm · deg we have $t_{min} \sim 5 \cdot 10^{-2}\, I^{-2}$ (a/cm^2) sec, $\Delta T'_{min} \sim -3$K°; when $\varkappa_0 = 5 \cdot 10^{-5}$ w/cm · deg, we obtain $t_{min} \sim I^{-2}$ (a/cm^2) sec, $\Delta T'_{min} = -60$K°; in order to satisfy the condition $\frac{a\sqrt{t_{min}}}{d} \ll 1$ it is necessary in this case to have $I \gg 1$ a/cm^2. Thus, at the first value of $\varkappa_0$, we get $t_{min} \lesssim t_0$ when $I \gtrsim 30$ a/cm^2, but $\Delta T'_{min}$ is small. For the second value of $\varkappa_0$ small t_{min} and large $\Delta T'_{min}$ can exist simultaneously only for large currents; at small values of I the position of t_{min} shifts toward the larger t and the cooling effect to $t \lesssim t_0$ becomes small. From (30) with $\Delta T'_{min} = -100$K°, $t_{min} = 10^{-4}$ sec we obtain $I = 140$a/cm^2.

Thus, for a polycrystalline coating with mean values of the parameters $\varkappa_0 \approx 5 \cdot 10^{-5}$ w/cm · deg and $d/\sigma \simeq 1$ ohm · cm^2 for near-surface layers, the cooling effect after a time $t \lesssim 10^{-4}$ sec is appreciably only at very large currents ($I \gtrsim 100$ a/cm^2). This result was obtained in [12] for a value of $\varkappa_0$ which is ten times greater, owing to the somewhat arbitrary reduction in the resistance d/σ.

One can sometimes find in the literature values of $\varkappa_0$ which are smaller than the value which we have used [15]. At such small values of $\varkappa_0$ we obtain from (25) that after $t \simeq 10^{-4}$ sec the cooling extends to a depth $x_0 \lesssim 10^{-4}$ cm, i.e., in practice a value smaller than or equal to the dimensions of the microcrystals. It follows therefore that one cannot substitute into the resultant expressions parameter values that characterize the coating in the mean, which are determined in experiments on the measurement of $\varkappa_0$ and σ. In the case of coarse-grain coatings, obviously one comes closer to reality by estimating the order of magnitude and time lag of the effect by considering the cooling of a monocrystalline layer of thickness d. Since for a single crystal of barium oxide the values of T, ρc, d, χ, and τ are the same as before, and values $\varkappa_0 \simeq 10^{-3}$ w/cm · deg and $1/\sigma \simeq 0.5$ ohm · cm have been assumed for $\varkappa_0$ and $1/\sigma$ [21], we obtain the following values: the depth of penetration of the cooling after $t \leq t_0$ is $x_0 \approx 4 \cdot 10^{-4}$ cm, $A \ll 1$, $|y| \ll 1$ for $1 \lesssim 100$ a/cm^2; the stationary current ensuring maximum cooling is $I_{\min} = 1/2\ I_0 \simeq 45$ a/cm^2; $\Delta T_{\min} \simeq -200K^{\circ}$. In the case of nonstationary current drain, $t_{\min}$ now shifts toward the larger t, and when $t \lesssim t_0$, $I \lesssim 100$ a/cm^2 we have from (26) $\Delta T' \simeq -20I$ (a/cm^2) $\sqrt{t(\text{sec})}$ K°, i.e., the effect is small even at large currents. If we take in this case $\varkappa_0 \simeq 10^{-4}$ w/cm · deg then $x_0 \lesssim 2 \cdot 10^{-4}$ cm, $\Delta T' \simeq -70\, I$ (a/cm^2) $\sqrt{t(\text{sec})}$ K° and the effect will be considerable only at currents $I \gtrsim 100$ a/cm^2. From our comparison of the theoretical and experimental data we can draw the following conclusion. Both in the case of minutely crystalline coating, which has low heat and electric conductivities $\varkappa_0$ and σ, as well as in the case of coarse-grain coatings, which have large values of $\varkappa_0$ and σ in the individual grains, the effect of coating after a time $t \lesssim 10^{-4}$ sec is appreciably only at large currents ($I \gtrsim 100$ a/cm^2) and obviously does not play an essential role in the observed fall-off of relatively small currents [2, 3]. Account of the inhomogeneity of the emitting surface could hardly change this result, since this would require that the ratio of the effective emitting surface to the surface of the cathode be on the order of 10^{-2}, which is little likely.

For a final clarification of the question of the influence of cooling of the layer by current drain on pulsed emission it is necessary to know simultaneously the coating parameters $\varkappa_0$, σ, and I. The coating must be either very finely crystalline or coarse grained, so as to be able to apply to it either the averaged parameters $\varkappa_0$ and σ or the parameters pertaining to each individual grain. In this case interest is attached to experiments with sufficiently large and long current pulses, at which one could observe the heating of the coating during the time of the pulse, and thus, estimate the values of $\Delta T'_{\min}$ and $t_{\min}$.

In conclusion, I thank K. B. Tolpygo for advice and interest in the work and I. M. Dykman for useful remarks made upon learning of the results obtained here.

REFERENCES

1. A.A. Ostroukhov, K.B. Tolpygo. Collection of Papers, Solid State Physics, II. Academy of Sciences USSR Press, 1959, p. 215
2. R.L. Sproull, Phys. Rev., 1945, 67, 5, 166.
3. S.G. Kalashnikov, G.A. Kubetskii, V.N. Osher. ZhTF. Journal of technical phsics. 1946, 16, 12, 1369. (See collection The Oxide Cathode edited by L.N. Dobretsov, GEI, 1957, p. 5).
4. L.S. Nergaard. RCA Rev., 1952, 13, 4, 464
5. Collection, The Oxide Cathode, edited by B.M. Tsarev, Foreign Literature Press, 1957, p. 211.
6. G.A. Haas. J. Appl. Phys., 1957, 28, 4, 1486.
7. R.W. Redington. Phys. Rev., 1952, 87, 1066.
8. R.S. Bever. J. Appl. Phys., 1953, 24, 8, 1008.
9. R.L. Sproull, R.S. Bever, G. Libovitz. Phys. Rev., 1953, 92, 77.
10. A.A. Ostroukhov. Collection of Papers, Solid State Physics, II. Academy of Sciences USSR Press, 1959, p. 224.
11. A.A. Ostroukhov. Solid State Physics. 1961, 3, 1, 3.
12. S.V. Ptitsyn. Physical Phenomena in Oxide Cathodes, GITTL, 1949.
13. W.E. Danforth, D.L. Joldwater. J. Appl. Phys., 1949, 20, 2. 163.
14. Ya.P. Zingerman. Transactions, Institute of Physics, Academy of Sciences, Ukrainian SSR. 1949, No. 2, p. 57.
15. Ya.P. Zingerman. Ukrainian Physics Journal. 1956, 1, 3, 308.

16. A. Sommerfeld. Thermodynamics and Statistical Physics. Translated from the German, Foreign Literature Press, 1955, p. 193.
17. K.B. Tolpygo. Transactions, Institute of Physics, Academy of Sciences, Ukrainian SSR, 1952, No. 3, p. 52.
18. G. German, S. Vagener. The Oxide Cathode, GTI, 1949.
19. P.A. Zel'tsman, N.D. Morgulis, V.S. Yagovdik. ZhTF. Journal of Technical Physics, 1951, 21, 9, 1035.
20. A. Eisenstein. J. Appl. Phys., 1946, 17, 8, 654.
21. R.T. Dolloff. J. Appl. Phys., 1956, 27, 1418.

Received by editor 30 January 1961

PHYSICAL PROPERTIES OF THE CESIUM PLASMA IN A THERMIONIC ENERGY CONVERTER

N.D. Morgulis, Yu.P. Korchevoi

Results are given of an experimental investigation of the physical properties of a plasma produced in cesium vapor during the operation of a thermionic converter of heat into electricity [4]. It is shown that such a converter can operate in two essentially different modes: "quasi-vacuum" at low pressures and "arc" at increased cesium vapor pressures. The properties of the plasma and all its parameters (distribution of potential and the jumps of the potential near the electrode, the temperature and concentration of the electrons, etc.) are noticeably different in the two cases. In particular, in the former case the plasma is predominantly thermal and in the latter it is predominantly gas-discharge. A direct correspondence is shown to exist between the output voltage of the converter and the change in the contact potential difference between its electrodes, etc. All these data enable us to draw several interesting conclusions concerning the nature and the role of phenomena in the plasma of such converters.

INTRODUCTION

The problem of direct and highly efficient conversion of heat into electricity assumes at present great national economic significance [1]. From among the different methods of such conversion, great physical interest attaches to the thermionic method, the general principles of which are described in the reviews [2], and which has prospect of practical feasibility. The most widely used thermionic energy converter is at the present time a vacuum two-electrode electronic device filled with cesium vapor at low pressure. The purpose of this vapor is to neutralize the electron space charge by means of the thermionic ions of the cesium obtained at the cathode, and to produce contact potential difference to accelerate the electrons. However, the presence of cesium vapor inside the device may lead to the occurrence of a cesium plasma, i.e., a gaseous semiconductor; the latter, in turn, can exert an appreciably influence on the characteristics of the operation of the converter. At the present time there is no complete understanding of the mechanism of the operation of the thermionic converter and of the role of the cesium plasma produced in it. Thus, for example, some researchers [3], emphasizing the predominant role of the latter, have also called it a "plasma thermocouple", although there are grounds for assuming that the main role in the operation of such a converter is played by electrode phenomena, i.e., the thermionic emission of its cathode and the contact potential difference between its electrodes.

In this connection, the need arises for a detailed investigation of the physical properties of the cesium plasma under real operating conditions of the device. With this in mind, we started suitable investigations, the preliminary results of which we published in [4]. The data cited there enable us to make tentatively some new interesting physical conclusions concerning the properties and the role of the phenomena in a cesium plasma of a thermionic converter. At the present time the necessary measurements have been to a certain degree completed and their results are reported in the present article.

1. INVESTIGATION PROCEDURE

The investigation of the question considered here was carried out with the aid of the experimental vacuum tube shown schematically in Fig. 1 and filled with cesium vapor. These tubes had the following: a cathode (1), consisting of a tungsten ribbon coated with thorium bicarbide ThC$_2$, and an anode (2) made of tantalum (coated with a film of cesium during the time of the experiments). The latter had both guard rings (to be able to measure the parameters of the converter only from the central uncooled part of the cathode), and a radiator, not shown in Fig. 1, to improve its cooling; the interelectrode distance was 5 mm. The use of a ThC$_2$ cathode guaranteed good electronic emission and good conversion power in a medium range of temperatures, on the order of 2000°K [5].

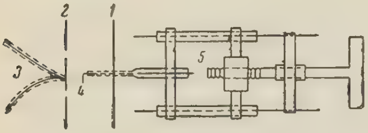

Fig. 1

The temperature of the cathode was determined with the aid of an optical micropyrometer, and that of the anode by means of a tungsten-platinum thermocouple (3); the leads to the latter were enclosed in quartz tubes. A probe (4), consisting of a tungsten wire 0.1 mm in diameter and ~1—1.5 mm long was inserted in the interelectrode space; the lead to the probe was enclosed in a double quartz sheath, preventing surface leakage. The probe was fastened on glides (5), connected with a frame on a screw which permitted it to be displaced along the cathode-anode distance and thereby determine the parameters of the investigated plasma at different points of the interelectrode space. To eliminate the distorting action of the electric and magnetic fields of the cathode filament current, the latter was fed by the well known procedure of using alternating current with rectifier [6]. All the measurements in the tube and probe circuits were made oscillographically only during that half cycle in which the filament current of the cathode was cut off by the rectifier. To prevent the probe from overheating by the electron current flowing through its circuit, a special commutator was included in this circuit, which reduced the average value of this current to approximately one tenth. All the measurements were carried out in four operating modes of the thermionic converter: 1) short circuit; 2) considerable converter power delivered to an external load; 3) maximum conversion power delivered; and 4) nearly open circuit. In addition, these measurements were made over a wide range of values of the pressure p or of the saturation temperature t of the cesium vapor in the tubes.

A typical example of a family of probe characteristics obtained under such conditions is shown in Fig. 2a for the case of relatively low values t = 120°C (p = $2\cdot10^{-3}$ mm Hg) and in Fig. 2b for increased values of t = 210°C (p = 0.1 mm Hg) at one definite position of the probe. The ordinates represent the values of log I_{pr} + C. The numbers on the curves denote the sequence of the operating modes listed above. All the basic probe characteristics, including those shown in Fig. 2, have been plotted relative to the converter anode; to determine the potential of the cathode (see below), similar characteristics were plotted in addition also with respect to this electrode. All these characteristics have a perfectly normal form, which enables us to determine with their help the distribution of the potential in the converter space, and the concentrations and temperatures of the electrons, as was indeed done.

An important factor in such measurements is the constancy of the contact potential difference $\Delta U'_c$ between the probe and the anode of the converter. One might think that the data below show convincingly that in our case the condition $\Delta U'_c \simeq 0$ is satsified almost all the time, since both the anode and the probe should be covered with a film of cesium with nearly equal degrees of coating. Nevertheless, to verify this circumstance we constructed a special tube, duplicating the construction of the preceding tube, except that above-described probe was replaced by a point-like tungsten-platinum thermocouple, which made it possible to determine its temperature in the near-cathode and near-anode regions of the working converter with account of the heat rise produced in the probe by the electron current flowing through its circuit. Using the data of [7], we could therefore ascertain whether a film of cesium could exist on the probe, since such a film, judging from the temperature, was always present on the anode. These experiments together with the data of the probe measurements over the entire distance from the cathode to the anode lead us to conclude that even in the most dangerous case of the lowest temperature t = 120°C the value of $\Delta U'_c$ was practically constant and probably close to zero.

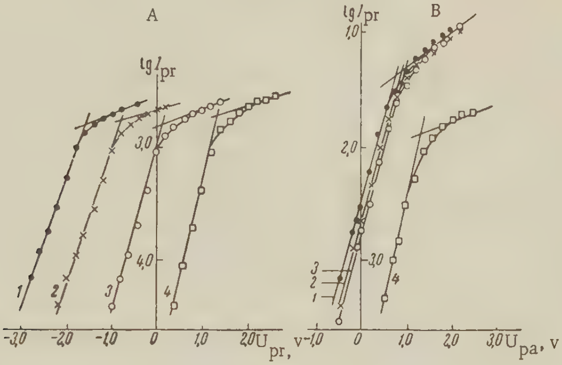

Fig. 2

In the additional case of probe measurements relative to the cathode, the value of $\Delta U''_c$ between the latter and the coldest probe was assumed to be ≈ 1.6 v (see below). Finally, we point out that a noticeably high interelectrode distance (relative to the case of a normal converter, where $d \lesssim 1$ mm), namely d = 5 mm, was necessary to obtain the curve for the distribution of the plasma parameters in this space. Although this circumstance has caused a certain decrease in the output power of the thermionic converter, the values obtained here for the plasma parameters should be normal, as can be seen in part, for example, from a comparison with the data of [4].

2. RESULTS OF THE MEASUREMENTS

The probe characteristics shown in Fig. 2 were plotted by us in a wide range of values of the temperature 100—250°C and under the aforementioned operating modes of the converter. In examining these characteristics, we call attention first of all to one of the most interesting questions, namely the distribution of the potential in the interelectrode space. Similar curves U = f(x) for the two most typical cases t = 120 and 210°C shown in Fig. 2 are plotted in Figs. 3 and 4; the numbering of the curves corresponds to the converter operating modes indicated above (1 — short circuit, etc.). The data of Fig. 3 correspond to a short-circuit current $I_0 = 2.2$ a/cm^2 and an optimum output power and voltage $W_m = 3.2$ w/cm^2 and $U_m = 1.6$ v; corresponding to the data of Fig. 4 are values $I_0 = 10$ a/cm^2, $W_m = 2.7$ w/cm^2, and $U_m = 0.5$ v. In addition, the dashed curves of Figs. 3 and 4 show data for t = 140 and 200°C obtained with a different tube. All these data fully confirm the conclusions given in [4], on the basis of a much more limited material, namely that there exist two manifestly different and practically usable operating modes of the thermionic converter, namely the quasi-vacuum mode at low temperature and the arc mode at increased temperatures. The first mode must be distinguished from the true vacuum mode, which calls for the distance between the converter electrodes to be made very small [2]. At the same time, all these potential-distribution curves of Figs. 3 and 4 show clearly that in both cases the interelectrode space of the converter contains a plasma with a typical distribution of potential and resultant equality of the electron and ion concentrations. The character of this plasma, however, and the positions of the adjacent near-electrode potential jumps turn out to be quite different in the two extreme cases.

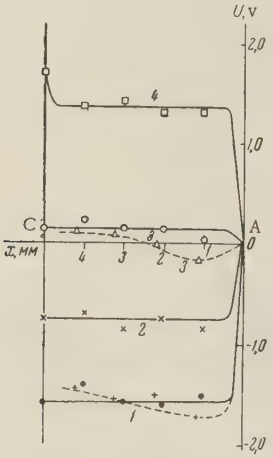

Fig. 3

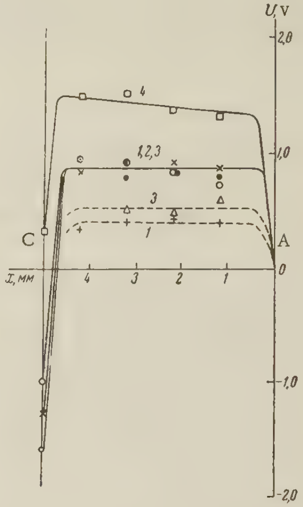

Fig. 4

In the first, quasi-vacuum mode, the electron gas-kinetic free path λ_e, determined on the basis of [8], turns out to be considerably greater than the interelectrode distance d, i.e., $\lambda_e \gg d$. The plasma obtained in this case is directly in contact with the cathode and is separated from the anode by a potential jump U_a. In the short-circuit mode the value of U_a is close to the value of the contact potential difference ΔU_c between the converter electrodes; in our case with electron work functions $\varphi_c = 3.2$ ev and $\varphi_a = 1.6$—1.8 ev for the cathode and anode respectively we should obtain $\Delta U_c = 1.4$—1.6 volts.

As we go over from the short-circuit mode to modes with external load, and finally as we go to open-circuit operation, the value of U_a decreases gradually, passes through zero (at approximately the optimum-power mode), and then reverses sign. Incidentally, curve 1 of Fig. 3, as expected, is quite close in character both to the curve obtained experimentally in [9], and to curve III of Fig. 61 of [10], but for cases where anode voltage is present. The electrons and the ions in the interelectrode space were obtained essentially by thermal means on the surface of the cathode; such a plasma, of course, hardly produces any glow. Although in this case the condition $\lambda_e \gg d$ is satisfied, there occurs here, as in many other similar cases, a strong electron-ion volume interaction of a specific nature [11]; this interaction brings about an undoubted occurrence of a typical plasma in this case, with all the characteristic features of such a plasma.

In the second, arc mode, the inverse relation holds true, namely $\lambda_e \ll d$. The plasma obtained in this case is separated from the cathode by a considerable potential jump U_c; it is separated from the anode by a small negative potential jump U_a, i.e., a jump that slows down the plasma electrons. In the short-circuit case, when the current flowing is always close to saturation, the value of U_c relative to the plasma should be $U_c \simeq (\Delta U_c + U_a)$, i.e., $U_c \gtrsim 2$ volts.

On going over from the short-circuit mode to the mode with the external load, the distribution of the potential in the plasma remains unchanged; in this case, however, a corresponding reduction takes place in the cathode potential jump. When the thermionic converter operates under these conditions, the plasma glows intensely. All this convinces us that this operating mode is quite close to the case of an ordinarily low-voltage arc discharge with an incondescent cathode in a gas at reduced pressure; the ignition potential of such a discharge may be even lower than the potential necessary to excite the atoms of the gas (see curve II of Fig. 61 of [10]). A similar discharge in cesium vapor was investigated in detail by us in the past [12]; we give below additional arguments in favor of this analogy. The plasma obtained has in this case an undoubtedly mixed character (thermal to a lesser degree and gas-discharge to a greater degree), since the jump in the potential in the interelectrode space $\sim U_c$ can noticeably exceed in this case the excitation potential of the cesium atoms, the value of which is 1.5 volts. Consequently, and also owing to the great density of the electron current, all the conditions necessary for a noticeable excitation and for a stepwise ionization of the cesium atoms are present.

In parallel with the data of Figs. 3 and 4, we show in Fig. 5 the distribution of the electron concentration in the interelectrode space, on a logarithmic scale, for the short-circuit mode in the cases t = 120°C (curve I) and 210°C (curve II). We observe here not only the difference, natural under these conditions, in the absolute values of this quantity n_e, but also an appreciably difference in the character of its distribution in space. Whereas in the arc mode n_e is approximately constant [12], as is characteristic of this case, in the quasi-vacuum mode there is a clearly pronounced gradient of this quantity. The latter is obviously connected with the occurrence of electrons and ions essentially only on the surface of the cathode and their subsequent diffusion from there into the remaining space.

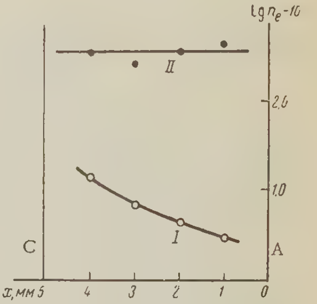

Fig. 5

An appreciable change occurs on going from the quasi-vacuum to the arc mode in all the parameters of the plasma and the thermionic converter as a whole. This is seen from Fig. 6, which shows the dependence on the cesium vapor saturation temperature t of the following quantities: the logarithm of the concentration of the electrons, n_e(I); the potential of the plasma relative to the anode, U_{pa} (II); the temperature T_e (III) of the electrons corresponding to the short-circuit mode with current I_0 (IV); and also the optimum converter power W_m (V). The region of transition from the first mode to the second is approximately at 140°C, corresponding to $p \simeq 5 \cdot 10^{-3}$ mm Hg and $\lambda_e \simeq 2$ mm (at an approximate electron energy of one volt [8]), i.e., when $\lambda_e \simeq d$.

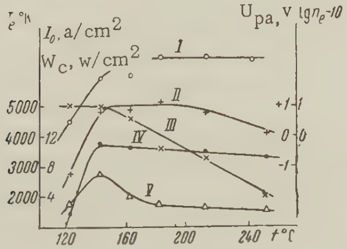

Fig. 6

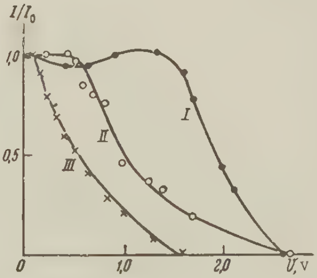

Fig. 7

It is interesting to note that in a similar changeover to the arc mode of the conversion, there occur, in particular, a reduction in T_e and an increase in n_e to values typical for the cases of a low-voltage arc discharge in cesium vapor [12]. Under these conditions, the changeover from the short-circuit mode to the optimum-power mode does not change the values of T_e and n_e appreciably.

We do not give the numerical values of these quantities for the different cases, since they have been published in [4]. Finally, the important role of such a transition from the quasi-free to the diffusion [13] mode of electron motion is seen also in Fig. 7, which shows the characteristic delays in the electron current for 120°C ($\lambda_e > d$) — curve I; 140°C ($\lambda_e \simeq d$) — II; and 210°C ($\lambda_e \ll d$) — III. A gradual and understandable deformation of these characteristics is seen clearly in this figure [7]; to obtain a maximum output voltage and conversion power (with I_0 = const), as can be readily seen, it is best to employ the quasi-vacuum characteristic I.

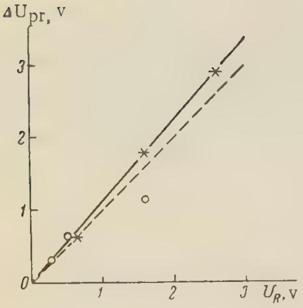

Fig. 8

It is well known [2] that the effective operation of a thermionic converter is connected essentially with the use of the contact potential difference between its electrodes ΔU_C. A convincing proof of this statement follows from a comparison of the parallel shift in the probe characteristics ΔU_{pr}, which determines the change in ΔU_C, and the simultaneously measured output voltage of the converter U_R across an external resistor. In connection with the specific (see Figs. 3 and 4) distribution of the potential it is easy to understand that to resolve this question it is necessary to plot similar probe characteristics for 120°C with respect to the anode, and for 210°C with respect to the cathode of the converter. The results of such measurements are shown in Fig. 8, where the asterisks pertain to 120°C and the circles to 210°C. The points obtained (with one exception) fit well on a straight line, almost coinciding with the 45° dashed line, i.e., actually $\Delta U_{pr} = U_R$. This circumstance offers undoubted evidence that the output voltage of the converter is due to the use of the contact difference of potential between its electrodes, as follows from the "electrode" notions concerning the operation of this device [2].

In connection with what was said above with respect to the arc mode of the operation of the converter, it is interesting to compare it directly with the usual low-voltage arc discharge with incandescent cathode in cesium vapor under approximately identical experimental conditions. For this purpose Fig. 9 shows plots of the distribution of the potential for cases of thermionic converter in the short-circuit mode (1) and a similar arc discharge (2), according to the data of [12] under identical conditions $I_0 = 4 a/cm^2$ (on the cathode) and $t = 250°C$; in this case the interelectrode distance was different, $d_1 = 5$ mm and $d_2 = 30$ mm. We see that both curves (the near-electrode regions of which are shown schematically) are quite close to each other in character. Moreover, the values of the parameters of the plasma obtained under these cases are also quite close to each other, namely: in the former case $n_e \simeq 5 \cdot 10^{12}\,cm^{-3}$, $T_e \simeq 2600°K$, $U_c = 1.8$ volt and $U_a = -4$ volt, and in the latter case $n_e \simeq 7 \cdot 10^{-2}\,cm^{-3}$, $T_e \simeq 2600°K$, $U_c = 1.3$ volt and $U_a = -0.3$ volt; only the potential gradients in the plasma are somewhat different.

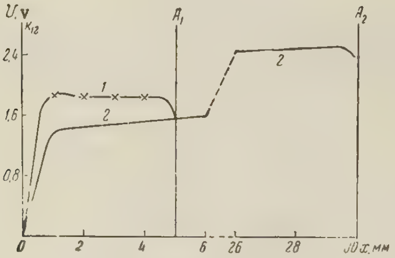

Fig. 9

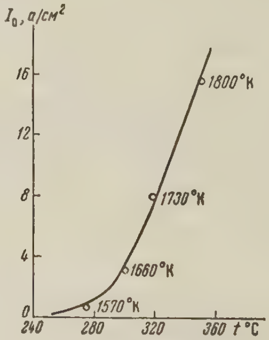

Fig. 10

Thus, all this is additional serious evidence in favor of the close analogy, indicated above, between the thermionic converter in the arc mode of operation and the ordinary low-voltage arc discharge in cesium vapor.

From an examination of Figs. 7 and 9 we also make certain additional conclusions, on top of those made in [8], with respect to the effective transverse scattering $q = 1/\lambda$ of the slow electrons by the cesium atoms. As the cesium vapor pressure p increases, the quasi-vacuum delay curve I of Fig. 7 goes gradually over into curve II, which obviously characterizes single scattering of electrons, and finally into the limiting curve III, which characterizes multiple scattering. Comparison of curves I and II makes it possible to estimate the order of magnitude of Q; thus, for example, for electrons with "thermal" velocities ($T_e \simeq 300°K$) we obtain $Q_1 \simeq 40\ cm^{-1}$ (for p = 1 mm Hg).

On the other hand, the same quantity can be estimated also from curve 2 of Fig. 9 on the basis of the value obtained from that curve for the plasma conductivity $\sigma = I/E$ and the mobility of the electrons in the plasma

$$\mu = \sigma / en_e \simeq \frac{e}{mv} Q^{\ 1};$$

in this case we obtain for the plasma electrons with $T_e = 2600°K$ a value $Q_1 \simeq 100\ cm^{-1}$. Both values of Q pertain to the scattering of electrons by the cesium atoms, because the relative concentration of the ions of the cesium is quite small in both cases (on the order of 10^{-3}); these values of Q are quite approximate and undoubtedly need serious revision.

In light of the statements made above concerning the arc mode of operation of the thermionic converter, it becomes understandable why we and the author of [14] observed the possibility of obtaining very large emission densities I_0 for metal cesium cathodes in the short-circuit mode without the use of an additional ionizer [7]. Fig. 10 shows the dependence of the optimum value of I_0 on t for the case of a tantalum cathode with a distance d = 0.3 mm. Each point of the curve corresponds to dynamic equilibrium of the cathode with the cesium vapor at the maximum of the dependence $I_0 = f(T_c)$ with t = const. We observe a strong increase in the quantity I_0, which reaches 15.5 a/cm^2 at 350°C (p = 6 mm Hg) and $T_c = 1800°K$. To all the points on the curve of Fig. 10 there corresponds approximately the same state of the cathode, and on the basis of the Richardson formula (assuming the entire current to be purely electronic), identical values of the electron work function $\varphi_c \simeq 2.8$ ev with the value $A \simeq 320\ a/cm^2 \cdot deg^2$ for the constant. Thus, there should exist here a noticeable interelectrode contact potential difference, sufficient to maintain a powerful low-voltage arc discharge in the cesium vapor, for the indicated values of I_0, p, and d.

3. CERTAIN DEDUCTIONS AND CONCLUSION

This circumstance can impose definite limitations both on the methods and on the analysis of the results of investigations on the phenomena in such somewhat unusual plasma; the latter, in particular, can be regarded as a gaseous semiconductor [15]. It must be remembered that the nature of the plasma in the thermionic converter will have a different character, depending on the relationship between λ_e and d. By virtue of this factor, the phenomena in the plasma of the converter can have noticeably different character under the two indicated modes, and can therefore require different analysis.

Thus, in the operation of a thermionic converter filled with cesium vapor, regardless of the vapor pressure, there occurs in the interelectrode space a typical plasma. The plasma is characterized by the well known conditions $dU/dx = E \simeq const$, i.e., $n_e \simeq n_p$, and then $x_D \ll d$ and $\tau_L \ll \tau$; here $x_D = \sqrt{\frac{kT_e}{8\pi e^2 n_e}} \approx 10^{-4}$ cm is the screening length and $\tau_L = \sqrt{\frac{\pi m}{e^2 n_e}} \simeq 10^{-10}$ sec is the period of the Langmuir oscillations; τ is the duration of the possible instabilities (oscillations) of our plasma. It can be easily shown that in all the cases described here these conditions do take place. However, unlike the ordinary plasma, the large densities of the current I that flows through the converter cause as a result the unusual inequality $I \gtrsim j_M$, where $j_M = en_e \sqrt{kT_e/2\pi m}$ is the density of the random current in the plasma.

In determining the cesium vapor pressure p_0', at which ($\lambda_e \simeq d$) a transition takes place from the quasi-vacuum into the arc mode ($p_0' = A/\lambda_e \simeq A/d$), it must be remembered that this pressure also determines the transient density of the electronic short-circuit current of the converter I_0'. In fact, the condition of dynamic equilibrium between the surface of the incandescent cathode and its surrounding atmosphere of atoms and thermionic ions of cesium [16], with concentrations n_a and n_p, can be represented under conditions of short circuit of a device such as a converter operating in the quasi-vacuum mode (for a plane-parallel system) in the form

$$\alpha n_a \sqrt{\frac{kT_0}{2\pi M}} = n_p \left[\sqrt{\frac{kT_c}{2\pi M}} \left(\beta + e^{-\frac{eU_a}{kT_c}} \right) + \gamma n_e d \right]. \tag{1}$$

Here α and β are the coefficients of ionization of the atoms and neutralization of the ions on the surface of the cathode, heated to a temperature T_c; $T_0 = (t + 273°)$ U_a — the jump in potential at the anode; γ — coefficient of volume recombination. In our case, on the basis of [17], the last number in equation (1) is very small. Hence, the limiting cesium vapor pressure necessary to neutralize the electronic space-charge current I_e, i.e., for $n_p = n_e = I_e/eu_e$ (with $U_a \ll kT_c/e$), will have in the indicated mode a value

$$p_0 = \frac{(1+\beta)}{e\alpha} I_e \sqrt{2\pi mkT_0}. \tag{2}$$

Thus, for example, when $I_0 = 20$ a/cm^2 and $T_0 = 500$°K in the case $\alpha = 0.05$ and $\beta = 0.95$ (corresponding approximately to a ThC_2 cathode [5]), we obtain $p_0 \simeq 2 \cdot 10^{-2}$ mm Hg, i.e., $t \simeq 170$°C ($\lambda_e \ll d$); in the case $\alpha = 0.95$ and $\beta = 0.05$ (approximating a tantalum cathode) we obtain $p_0 \simeq 1 \cdot 10^{-3}$ mm Hg, i.e., $t \simeq 115$°C ($\lambda_e \gg d$). On the other hand, knowing the value of p_0' from the expression $p_0' \simeq A/d$, we determine on the basis of (2) the value of I_0' for the limiting case of transition from the quasi-vacuum mode to the arc mode, etc.; all this is in satisfactory agreement with the experimental data.

In the development of the arguments given in [3, 7, 13] one can, using the experimental data obtained in the present investigation, calculate in the Maxwellian distribution the near-electrode potential jumps of the converter in the open-circuit mode (curves 4 of Figs. 3 and 4), i.e., at a current $I = 0$. Under these conditions one can expect the presence of two potential jumps at the electrodes: U_a' at the anode and U_c' at the cathode. The behavior of the cold anode is in this case equivalent to the behavior of an isolated ($\Sigma I = 0$) probe in a plasma, with a potential jump produced at the surface of the probe and retarding the plasma electrons

$$U_a' = \frac{kT_e}{e} \ln \frac{u_e}{u_p} = \frac{kT_e}{e} \ln \sqrt{\frac{T_e}{T_p} \frac{M}{m}}. \tag{3}$$

On the other hand, the potential jump near the cathode is also determined from the condition $\Sigma I = 0$; since in both cases $t = 120$ and 210°C the saturation current of the cathode I_0 is greater than the sum of the random current in the plasma j_M and the thermionic current I_p, this potential jump will slow down the cathode current; its value is

$$U_c' = \frac{kT_c}{e} \ln \frac{I_0}{(j_M + I_p)}. \tag{4}$$

In similar fashion we obtain for $t = 120$°C the values $U_c' = 0.8$ v and $U_a' = 1.4$ v and at $t = 210$°C the values $U_c' = 0.3$ v and $U_a' = 1.6$ v. A comparison of these data with the experimental curves of Figs. 3 and 4 shows that they are in satisfactory qualitative agreement, with exception of one case, the near-cathode jump at 210°C, which for some reason has a sign opposite to that expected.

In the second extreme case of short-circuit (curves 1 on Figs. 3 and 4) we observe the occurrence of large potential jumps U_a at the anode in the quasi-vacuum mode and U_c at the cathode in the arc mode. Obviously, both potential jumps are due to the concentration of excess space charge of suitable sign near these electrodes; i.e., in this case one can employ the "two-thirds" law:

$$I = I_e = \frac{1}{9\pi} \sqrt{2 \frac{e}{m}} \frac{U_a^{3/2}}{x_a^2}; \quad I_p = \frac{1}{9\pi} \sqrt{2 \frac{e}{M}} \frac{U_c^{3/2}}{x_c^2}. \tag{5}$$

Here I_e and I_p are the densities of the electron and ion currents in the anode and cathode;

x_a and x_c are the thicknesses of their space-charge zones. Thus, for example, according to the data of Fig. 3, for t = 120°C, $I_e = 2.2$ a/cm^2 and $U_a = 1.6$ v we obtain $x_a \simeq 1 \cdot 10^{-3}$ cm and $E_a \simeq U_a/x_a \simeq 10^3$ v/cm; according to the data of Fig. 4, for t = 210°C, assuming $I_p = I_e\sqrt{m/M}$, where $I_e = 10$ a/cm^2 and $U_c = (\Delta U_c + U_a) = 2.3$ v, we obtain approximately the same values of x_c and E_c. In the latter case, however, where the converter operates in the arc mode, it must be remembered that the ionic component of the current in the arc can have a different value, depending on the circumstances, and for the time being it is quite difficult to determine [12].

Great interest is attached to the fact that, in analogy with the case of low-voltage arc discharge [10], the near-anode potential jump U_a in a thermionic converter operating in the arc mode has a sign that prevents the drift of the electrons from the plasma toward the anode. Such a drift of the electrons against the electric field can occur only by diffusion; for this purpose it is necessary to have a sufficient gradient of electron concentration n_e, corresponding (in the Maxwellian approximation) to the condition

$$D_e \frac{\Delta n_e}{\Delta x} > n_e \mu_e E \quad \text{or} \quad \frac{\Delta n_e}{n_e} > \frac{\mu_e}{D_e} E \Delta x \simeq \frac{eU_a}{kT_e}, \tag{6}$$

where μ_e and D_e are the mobility and coefficient of diffusion of the electrons; E — intensity of the electric field. This means that in our case $T_e \simeq 3300$°K and the concentration of the electrons in the central region of the plasma is $n_e \simeq 4 \cdot 10^{12}$ cm^{-3}; at the very surface of the anode, the last quantity should be $n_e' \simeq 1 \cdot 10^{12}$cm^{-3}. The last figure, however, brings us to the density of the random current $j_M \simeq 2$ a/cm^2, which for some reason is noticeably less than the current in the converter circuit $I_0 \simeq 10$ a/cm^2.

Finally, the data given in [4] and here concerning the concentration and temperature of the electrons in the plasma enable us to calculate the coefficient of the Seebeck thermal emf [3] for different operating modes of the thermionic converter. It seems to us that there is no need for giving these values and comparing them with the experimental data, since evidence against such a "plasma" notion concerning the operation of the converter is afforded, for example, by such serious facts as: 1) the lack of correspondence between the near-electrode electron temperature and the temperatures of the hot cathode and the colder anode (see above and [4]); 2) the practical independence of the emf of the thermionic converter of the cesium vapor pressure in the wide interval t = 25 — 250°C [7]; 3) the presence of a correspondence between the output voltage of the converter and the change in the interelectrode contact potential difference (see Fig. 8). All this manifestly favors the "electrode" (see above) and not the plasma nature of the operating principle of the converter, although the phenomena in the plasma can leave a serious imprint [13] on its properties. The latter, as can be seen from Fig. 7, can manifest itself, for example, on the internal resistance and consequently on the output parameters of the converter, such as the voltage and power and meaning also the efficiency. Thus, the phenomena in the plasma of a thermionic converter should obviously have a secondary and not a primary character that decides its operating principle.

REFERENCES

1. N. Morgulis. Herald of the Academy of Sciences, USSR. 1961, 31, 9, 25.
2. N. Morgulis. Advances of Physical Sciences. 1960, 70, 679; L. Dobretsov, ZhTF Journal of Technical Physics. 1960, 30, 365.
3. H. Lewis, J. Reitz. J. Appl. Phys. 1959, 30, 1439, 1838; J. Grover, Nucleonics. 1959, 7, 54; W. Ranken, G. Grover, E. Salmi, J. Appl. Phys. 1960, 31, 2140.
4. N. Morgulis, Yu. Korchevoi. Proceedings, Academy of Sciences USSR. 1961, 136, 336.
5. N. Morgulis, Yu. Korchevoi. Atomic Energy. 1960, 9, 49.
6. P. Marchuk. Transactions, Institute of Physics, Academy of Sciences, Ukrainian SSR. 1956, 7, 3.
7. P. Marchuk. Ibid. 1956, 7, 17; N. Morgulis, Yu. Korchevoi, Yu. Chutov, ZhTF. 1961, 31, 835.
8. R. Brode, Phys. Rev. 1929, 34, 673.

9. S. Ptitsyn, I. Tsukkerman. Collection Devoted to the 70th Birthday of Academician A.F. Ioffe. Academy of Sciences USSR Press, 1950, p. 173.
10. M. Druyvesteyn, F. Penning. Rev. Mod. Phys. 1940, 12, 148.
11. V. Granovskii. Electric Current in a Gas, 1, GITTL, 1952, p. 244.
12. N. Morgulis, P. Marchuk. Ukrainian Physics Journal. 1956, 1, 59.
13. B. Moizhes, G. Pikus. Solid State Physics. 1960, 2, 756.
14. R. Hirsch. J. Appl. Phys. 1960, 31, 2064.
15. A. Ioffe. Semiconductor Thermocouples. Academy of Sciences USSR Press, 1960, p. 160.
16. N. Morgulis. ZhETF, Journal of Experimental and Theoretical Physics, 1946, 16, 489.
17. F. Mohler. J. Res. Nat. Bur. Standards. 1937, 19, 447.

T.G. Shevchenko
Kiev State University

Received by editor 27 May 1961

NEUTRALIZATION OF ION SPACE CHARGE BY ELECTRONS

V.P. Ignatenko, A.S. Myasinkov

We consider the process of propagation of one-dimensional ion beam, the space charge of which is compensated by introducing electrons at a certain cross section of the beam.

INTRODUCTION

At the present time long beams of charged particles with large current density are finding an ever increasing application. The characteristic feature of such beams is the interaction between the charged particles comprising the beam, which imposes a limit on the possible current density and the length of the beam [1]. It is possible to obtain long intense charged-particle beams by neutralizing the space charge of the beam through the introduction of particles of opposite charge. The particles necessary for such neutralization can be obtained either by using the residual gases always present in a vacuum system [2], or by introducing particles of opposite sign into the beam.

The purpose of the present investigation was to study the simultaneous motion of one-dimensional beams of differently charged particles under different initial conditions, when the electrons are introduced in a certain cross section of the ion beams and are dragged into the beam by the forces of the ion space charge.

All the investigations were carried out under the following assumptions: 1) the motion of the electron-ion beam was assumed steady in the external stationary electrostatic fields; 2) the presence of residual gases in the vacuum system and the associated ion charge-exchange processes were neglected; 3) recombination of charged particles in the beam was disregarded; 4) in the case when grid-like electrodes were used, we neglected the current loss on such electrodes, and the electric field was assumed constant in the plane of the grids; 5) all the initial velocities of the charged particles were assumed to be equal.

1. FORMULATION OF THE PROBLEM

Figure 1 shows the arrangement of the electrodes necessary to produce an electron-ion beam. The ion current, limited by its own space charge at the anode, is produced by the potential difference V_i. Owing to the energy obtained in the accelerating gap d, the ion beam reaches an electron emitter in the form of a grid, at a potential $0 \le V_0 \le V_i$, and then propagates in the drift space behind the electron emitter. The interelectrode gap l can be chosen such as to make the potential due to the space charge of the ions greater than the potential of the electron emitter V_0. Under the influence of the potential difference $V_m - V_0$, the electrons will be drawn into the ion beam, thus reducing the space charge of the ions. If $V_0 > 0$, then the electron current becomes circulating; i.e., the electrons execute vibrational motion about the maximum of the potential V_m in the space (x_1, l). Under certain conditions the electrons can be dragged by the ion beam also in the drift space beyond the electron emitter.

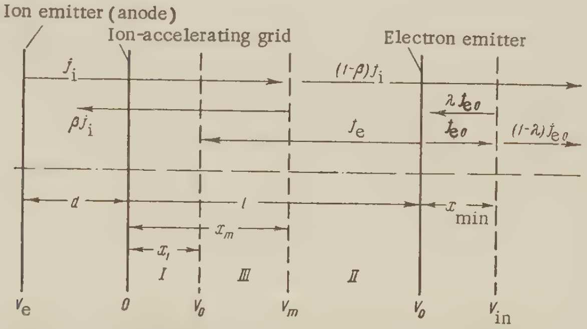

Fig. 1. Arrangement of the electrodes necessary to obtain an electron-ion beam. Region III exists only in the case when $\beta > 0$ ($V_m = V_i$); λ corresponds to the fraction of the reflected electron current j_{e0} from the virtual cathode.

However, the gap l may be so large that not all the ions reach the electron source, but some ions return to the accelerating gap d. Thus, the problem of obtaining a long electron-ion beam can be broken up into two: 1) the problem of bringing the ion beam to the electron emitter (internal problem); 2) the problem of propagation of the electron-ion beam beyond the electron emitter (external problem).

2. INTERNAL PROBLEM

The distribution of the potential in the space occupied by the electron-ion beam is determined, as is well known [1], by solving the following system of equations

$$\nabla^2 V = -4\pi(\rho_i - \rho_e), \tag{1}$$

$$\operatorname{div} \vec{j}_e = \operatorname{div} \vec{j}_i = 0,$$

$$\vec{j}_e = \rho_e \vec{v}_e, \quad \vec{j}_i = \rho_i \vec{v}_i, \tag{1'}$$

$$\begin{gathered} v_e^2 = 2\eta_e (V - V_0), \\ v_i^2 = 2\eta_i (V_i - V), \end{gathered} \tag{1''}$$

where ρ — charge density; η — specific charge of the particle; v — velocity of the particle; $\vec{j}$ — current density vector. The subscripts e and i pertain to the electrons and ions respectively.

We could write the continuity equation in the form of two separate terms only by assuming that there is no particle recombination in the system.

In the one-dimensional case, the system of equations (1) can be transformed to a single equation

$$\frac{d^2V}{dx^2} = \frac{4\pi j_{\mathrm{i}}}{\sqrt{2\eta_{\mathrm{i}}}}\left(\frac{\alpha}{\sqrt{V-V_0}} - \frac{1}{\sqrt{V_{\mathrm{i}}-V}}\right), \tag{2}$$

where $\alpha = \frac{j_e}{j_i}\sqrt{m/M}$; m and M are respectively the electron and ion masses.

In our formulation of the problem with a one-dimensional electron-ion beam, α will obviously be constant.

Equation (2) is best written in dimensionless coordinates, introducing for this purpose the notation

$$\frac{V}{V_{\mathrm{i}}} = \varphi, \quad \frac{V_0}{V_{\mathrm{i}}} = \varphi_0, \quad \frac{x}{l} = \xi.$$

Then

$$\frac{d^2\varphi}{d\xi^2} = A\left(\frac{\alpha}{\sqrt{\varphi-\varphi_0}} - \frac{1}{\sqrt{1-\varphi}}\right), \tag{3}$$

where

$$A = \frac{4\pi j_{\mathrm{i}} l^2}{\sqrt{2\eta_{\mathrm{i}} V_{\mathrm{i}}^3}}. \tag{4}$$

If there is no loss of ion current on the system elements and no recombination of particles, then in the case of total limitation of the ion current by the space charges (E = 0 on the surface of the ion source) the density of the ion current in the system is determined from the "two-thirds law" [1]:

$$j_{\mathrm{i}} = \frac{\sqrt{2\eta_{\mathrm{i}}}\, V_{\mathrm{i}}^{3/2}}{9\pi d^2}, \tag{5}$$

where d is the length of the accelerating gap. Substituting the value of j_i from (5) into (4) we get

$$A = \frac{4}{9}\sigma^2, \tag{6}$$

where $\sigma = l/d$.

It is easy to solve equation (3) in a region I where there is no electron current ($\alpha = 0$) by double integration:

$$\sigma(\xi_1 - \xi) = (2c_1 + \sqrt{1-\varphi})\sqrt{\sqrt{1-\varphi} - c_1} - (2c_1 + \sqrt{1-\varphi_0})\sqrt{\sqrt{1-\varphi_0} - c_1}, \tag{7}$$

where ξ_1 is the position of the turning point of the electrons in the interelectrode gap; c_1 is the integration constant. In region II the solution of (3) has the form

$$\pm\sigma(\xi_m - \xi) = I(\varphi_m, \varphi_0), \tag{8}$$

where

$$I(\varphi_m, \varphi_0) = \frac{1}{(1+\alpha^2)^2}\{(1-\alpha^2)(2c_2 + \sqrt{1-\varphi_0}) +$$

$$+ 2\alpha^2 \sqrt{(1-\varphi_0)\left(\sqrt{1-\varphi_0} - c_2\right)}\} + \frac{\sqrt{2}\,\alpha\,(1-\varphi_0)^{1/4}}{2\,(1+\alpha^2)^{7/4}}\{8c_2\,[E(\gamma, k) + \mathbf{E}(k)] -$$

$$- \left(4c_2 + \sqrt{(1-\varphi_0)(1+\alpha^2)}\right)[F(\gamma, k) + \mathbf{K}(k)]\}, \tag{9}$$

with

$$k^2 = \frac{1}{2}\left(1 - \frac{c_2}{\sqrt{(1-\varphi_0)(1+\alpha^2)}}\right);$$

$$\sin^2\gamma = \frac{\sqrt{(1-\varphi_0)(1+\alpha^2)} - \sqrt{1-\varphi_0}}{\sqrt{(1-\varphi_0)(1+\alpha^2)} - c_2},$$

where $\varphi_m = V_m/V_i$ is the relative magnitude of the potential maximum in the interelectrode space l; c_2 — integration constant; ξ_m — position of the potential maximum; $F(\gamma, k)$, $E(\gamma, k)$, $\mathbf{E}(k)$, and $\mathbf{K}(k)$ are elliptic integrals in the Legendre form.

To determine the integration constant we stipulate that the field intensity be continuous on the boundary between regions I and II. Then

$$c_1 = c_2 = \sqrt{1-\varphi_m} + \alpha\sqrt{\varphi_m - \varphi_0}$$

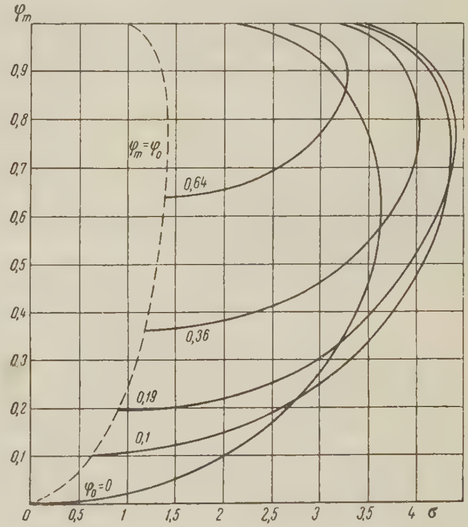

Fig. 2. Dependence of the maximum of the potential in the interelectrode space on the ratio σ at different potential biases on the electron emitter φ_0. The dashed curve corresponds to $\varphi_0 = \varphi_m$.

At sufficiently large electron emission from the source, the electron current becomes completely limited by its own space charge $\alpha = \alpha_m$ (the intensity of the electric field is equal to zero at the electron emitter). In this case

$$c_2 = \sqrt{1-\varphi_0},$$

$$\varphi_m = \frac{4\alpha_m^2}{(1+\alpha_m^2)^2} + \left(\frac{1-\alpha_m^2}{1+\alpha_m^2}\right)^2 \varphi_0 \tag{10}$$

and consequently

$$\sigma = \left(1 + 2\sqrt{1-\varphi_0}\right)\sqrt{1 - \sqrt{1-\varphi_0}} +$$

$$+ \frac{2\sqrt{2}\,\alpha_m\,(1-\varphi_0)^{3/4}}{(1+\alpha_m^2)^{7/4}}\{8\mathbf{E}(k) - \left(4 + \sqrt{1+\alpha_m^2}\right)\mathbf{K}(k)\}, \tag{11}$$

$$\xi_1 = \sigma (1 + 2\sqrt{1-\varphi_0}) \sqrt{1 - \sqrt{1-\varphi_0}},$$

$$\xi_m = (1 + \xi_1)/2,$$

$$k^2 = \frac{1}{2}\left(1 - \frac{1}{\sqrt{1+\alpha_m^2}}\right).$$

The dependence of the maximum of the potential φ_m on the ratio σ is shown in Fig. 2 for different biases of the potential φ_0. In the region $\varphi_m < \varphi_0$ there is no solution, for in this case the electrons can be drawn into the ion beam. The dragging of the electrons into the ion beam becomes possible when

$$\sigma \geqslant \sigma_0 = (1 + 2\sqrt{1-\varphi_0}) \sqrt{1 - \sqrt{1-\varphi_0}}.$$

It is clear from Fig. 2 that starting with a certain value $\sigma_0 \geq \sigma_1 = \sigma_0 + 2.73\,(1 - \varphi_0)^{3/4}$ there exist two values of φ_m for one and the same value of σ. This case corresponds to the phenomenon of ionic hysteresis [3]. It is seen from Fig. 2 that for a given value of φ_0 we have $\sigma \leq \sigma_{max}$, where σ_{max} is determined from the expression (6) with $\alpha_m = 0.516$:

$$\sigma_{\max} = \sigma_0 + 4.05\,(1 - \varphi_0)^{3/4}.$$

At values $\sigma > \sigma_{max}$ there exists a solution with partial reflection of the ion current from the virtual anode produced in the interelectrode gap, to the true anode. If we denote the reflected part of the ion current by βj_i, and the point of reflection in relative units is denoted by ξ_m, then

$$\beta = \frac{1-\alpha_m}{1+\alpha_m}, \tag{12}$$

where α_m is determined for the specified values of σ from the expression

$$\begin{aligned} \sigma = {} & (1 + 2\alpha_m \sqrt{1-\varphi_0}) \sqrt{1 - \alpha_m \sqrt{1-\varphi_0}} + \\ & + (1-\varphi_0)^{3/4} \left[\frac{1.365}{\sqrt{\alpha_m}} - \frac{\alpha_m^2 (1 + 6\alpha_m + \alpha_m^2 + 2\alpha_m^3)}{(1+\alpha_m^2)^2} \sqrt{1-\alpha_m^2} \right] + \\ & + \frac{\sqrt{2}\,\alpha_m (1-\varphi_0)^{3/4}}{2(1+\alpha_m^2)^{7/4}} \{8\alpha_m [\mathbf{E}(k_1) + E(\gamma_0, k_1)] - \\ & - (4\alpha_m + \sqrt{1+\alpha_m^2}) [\mathbf{K}(k_1) + F(\gamma_0, k_1)]\}, \end{aligned} \tag{13}$$

with

$$\sin^2 \gamma_0 = \frac{\sqrt{1+\alpha_m^2} - 1}{\sqrt{1+\alpha_m^2} - \alpha_m};$$

$$k_1^2 = \frac{1}{2}\left(1 - \frac{\alpha_m}{\sqrt{1+\alpha_m^2}}\right).$$

From (12) and (13) we see that for a given value of φ_0 the ion current is reflected when $\sigma \geq \sigma_1$; i.e., in the range of values $\sigma_1 \leq \sigma \leq \sigma_{max}$ there exist three different solutions, corresponding to different stationary modes of propagation of the electron-ion beam.

It is interesting to note that $\alpha \to 0$ and $\beta \to 1$ when $\sigma \to \infty$; i.e., the values of the electron current and the transmitted part $(1 - \beta) j_i$ of the ion current decrease with increasing interelectrode distance l. The position of the virtual anode is determined from the expression

$$\xi_m = 1 - \frac{1.365}{\sigma \sqrt{\alpha_m}} (1 - \varphi_0)^{3/4}. \tag{14}$$

In addition, if $\varphi_0 > 0$, then the electrons can not penetrate the accelerating interval d but are returned to the electron emitter by the forces of the ionic space charge from a certain section ξ_1. The position of the turning point of the electron current can be determined from the following relation

$$\sigma\xi_1 = (1 + 2\alpha_m \sqrt{1 - \varphi_0}) \sqrt{1 - \alpha_m \sqrt{1 - \varphi_0}} - \\ - (2\alpha_m + 1) \sqrt{1 - \alpha_m} (1 - \varphi_0)^{3/4}. \tag{15}$$

If $\varphi_0 = 0$, then the electron current that enters the accelerating interval causes an increase in the ion current, which in our case will correspond to a reduction of all values of σ by an amount $\sqrt{j_i/j_{i0}}$, which is determined from the well known Langmuir relation [4] as a function of α.

Fig. 3. Dependence of σ on the potential bias φ_0 of the electron emitter, for different modes of propagation of the electron-ion beam. The dash-line cross hatched area corresponds to total passage of the ion current without entrainment of the electrons into the interelectrode interval. The unshaded area corresponds to one possible stationary electron-ion beam with complete passage of the ion current. The doubly-hatched region corresponds to two possible stationary electron-ion beams with total passage of the ion current (region of ion hysteresis) and one stationary mode with partial reflection of the ions. The singly-hatched region corresponds to a stationary electron-ion beam with partial reflection of the ion current.

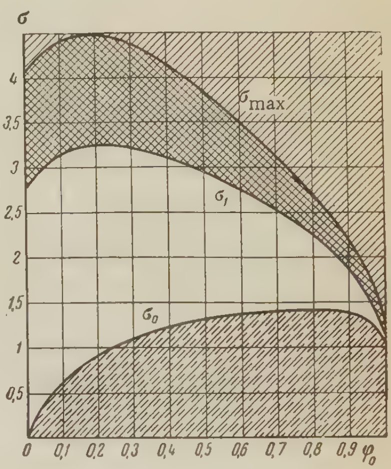

Figure 3 shows the limits of the possible values of σ for given values of $\varphi_0 > 0$. If $0 < \varphi_0 < 1$ and $0 < \sigma < \sigma_0$, then there is no potential maximum in the interelectrode space and the electrons are not drawn into this space. On the other hand, if $\sigma_0 < \sigma < \sigma_1$, then a single potential maximum is possible in the interelectrode space and the electrons are drawn into this space by the potential difference $\Delta\varphi = \varphi_m - \varphi_0$. When $\sigma_1 < \sigma < \sigma_{max}$ three values of the potential maximum φ_m are possible in the interelectrode space, corresponding to three possible stationary electron-ion beams, wherein the realization of any particular beam depends on the specific experimental conditions (for example, on the time of establishment of the stationary mode); when $\sigma \geq \sigma_{max}$ only a stationary electron-ion beam with partial (or complete) reflection of the ions back to the source is possible.

As was already indicated, in the presence of a positive potential bias on the electron emitter relative to the accelerating electrode, the electrons execute oscillation motion in the interelectrode space about the potential maximum, with a frequency

$$\nu_m = \frac{1}{2}\left(\int_{l}^{(1-\xi_1)l} \frac{dx}{v_e}\right)^{-1} = \frac{\sqrt{2\eta_e V_i}}{2d}\bar{\nu}_m, \tag{16}$$

where

$$\bar{\nu}_m = \frac{(1 + \alpha_m^2)^{3/4}}{6\sqrt{2}(1 - \varphi_0)^{1/4}[2\mathbf{E}(k) - \mathbf{K}(k)]};$$

η_e — specific charge of the electron; $\alpha = \alpha_m$ (case of total limitation of the electron current by its own space charge).

For example, when $V_i = 10$ kv, $d = 1$ cm, and $\varphi_0 = 0.1$ we get $\nu_m \simeq 220$ mc.

Thus, at specified values $\varphi > 0$ we can choose σ such as to cause the ion beam to reach the electron emitter in its entirety.

3. THE EXTERNAL PROBLEM

After reaching the electron emitter, the ions penetrate beyond it by inertia into the drift space, imparting to this space a positive potential, which in turn will cause electrons to move from the emitter into the drift space. The presence of the electrons reduces the potential of the space, contributing to further propagation of the ion beam. Thus, the physical possibility is produced of obtaining long electron-ion beams. If we neglect the initial velocities of the electrons, then we can determine the potential distribution in the drift space by using equation (3), the solution of which is a periodic function with period

$$d_0 = \frac{2\sqrt{2}\,\alpha_m (1-\varphi_0)^{3/4}}{(1+\alpha_m^2)^{7/4}} \{8\,\mathbf{E}(k) - (4 + \sqrt{1+\alpha_m^2})\,\mathbf{K}(k)\}\, d. \qquad (17)$$

In this case, when the electron current is completely limited by its own space charge ($\alpha = \alpha_m$) we can show that the space charge density, averaged over the period of the potential distribution function, is equal to zero. The quantity $\alpha_m = \frac{j_e}{j_i}\sqrt{m/M}$ depends on the specific experimental conditions and is contained in the range $0 \leq \alpha_m \leq 1$.

Thus, as follows from (17), even when the electron and ion currents do not have equal densities there exists a finite quasi-mutual volume, corresponding to the period d_0 of the potential distribution function. In particular, if $j_e = j_i$ and $M \gg m$, then

$$d_0 \simeq 3\pi (1-\varphi_0)^{3/4} d \sqrt{\frac{2m}{M}}. \qquad (18)$$

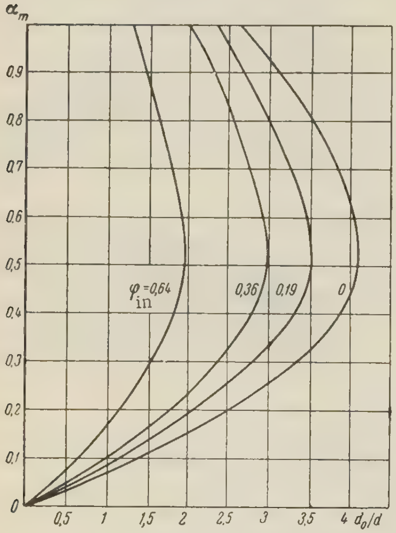

Fig. 4. Dependence of the period on the potential distribution function on the quantity α_m, which characterizes the transmitted part of the electron current at different values of φ_{in}.

In the case when the current densities are equal, it follows from (10) that $\varphi_m - \varphi_0 \simeq 4\ m/M$, i.e., the potential difference, which determines the velocity of the electrons in the ion beam when the ion-accelerating voltage is $V_i < 30$ kv, is commensurate with the thermal velocities of the electron. Simultaneous account of the electron distribution function over the initial velocities and the space-charge effect in the Poisson equation leads to serious mathematical difficulties. However, in the first approximation we can replace the electron distribution function over the initial velocities by a constant quantity corresponding to the average electron velocity. In this case equation (3) and its solution will remain the same if we replace in these equations φ_0 by $\varphi_{in} = \varphi_0 - \frac{mv_{in}^2}{2eV_i}$, where V_{in} is the initial velocity of the electrons, determined by the emitter temperature.

Figure 4 shows the dependence of the ratio d_0/d on α_m for different values of φ_{in}. The double-valued nature of the curves corresponds to two possible stationary modes of propagation of the electron-ion beam, the establishment of which depends on the conditions through which the particular mode is reached.

When the initial electron velocities are thus taken into account for the case when the

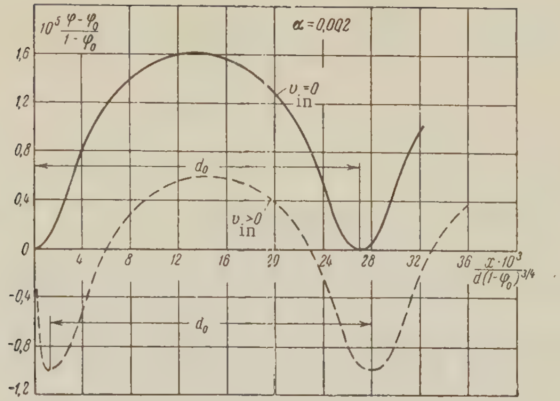

Fig. 5. Distribution of the potential in the drift space when the electrons have no initial velocity ($\varphi_{in} = \varphi_0$) and for the case when the electrons do have an initial velocity.

electron current entering into the ion beam is completely limited by its own space charge, part of the electrons are reflected back to the emitter from a certain distance x_{min} (occurrence of a virtual cathode). Starting with the distance $x > x_{min}$, the potential distribution function will be periodic with a period d_0, determined from (17), whereas α_m should account in this case for only the portion of the electron current entering into the ion beam, while φ_0 must be replaced by φ_{in}. Fig. 5 shows the characteristic distribution of the potential in the drift space for different values of initial electron velocities.

We see that the presence of initial electron velocities changes the period of the potential distribution function very little, while the average potential of the drift space decreases.

REFERENCES

1. J.R. Pierce. Theory and Design of Electron Beams. Van Nostrand, New York, 1949, (Russian Translation).
2. M.M. Bredov. Automatic Neutralization of Space Charge in Electron Beams. Collection Devoted to the Seventiety Anniversary of Academician A.F. Ioffe. Academy of Sciences USSR Press, 1950.
3. F. Wentzl. Ionen und elektronen einheitlicher Anfangsgeschwindigkeiten in Vakuum. Z. Angew. Phys. 1952, 4, 3, 94.
4. I. Langmuir. The interaction of electron and positive ion space charges in cathode Sheaths. Phys. Rev. 1929, 33, 6, 954.

Received by editor 4 April 1961

BRIEF COMMUNICATIONS

CONCERNING THE ACCUMULATION OF NOISE AND FADING IN RADIO RELAY COMMUNICATION LINE WITH LONG-DISTANCE TROPOSPHERIC PROPAGATION

Yu.B. Sindler

In the investigation of processes occurring in radio relay lines with long-distance tropospheric propagation, it may be of interest to obtain an asymptotic estimate of the distribution of the probabilities of output-noise fluctuation in the region where the noise is high, in the case when these fluctuations are due to fading of the signal on portions of the line.

Fading in radio relay lines with long-distance tropospheric propagation has the feature that one can clearly discern in it slow and fast fluctuations (the so-called slow and fast fadings).

Assume that we have a radio relay line with long-distance tropospheric propagation, consisting of n sections. Let us assume the following model of fading.

We assume that the radiowaves propagate exclusively by scattering on inhomogeneities of the troposphere, and that at the point of reception there arises a large number of elementary beams with a total power $2\sigma^2$. The phase shifts between the individual beams and the amplitudes of the beams vary continuously depending on the random structure of the scattering volume. This circumstance causes the rapid fading of the signal. The signal power $2\sigma^2$ changes slowly under the influence of changes in the average refraction conditions, the average turbulence intensity, etc.

We assume that at a fixed value of σ the amplitude of the field intensity has a Rayleigh distribution

$$W(E/\sigma) = \frac{E}{\sigma^2}\exp\left(-\frac{E^2}{2\sigma^2}\right). \tag{1}$$

We shall assume that the parameter σ is random, and it changes slowly, while its one-dimensional probability distribution is logarithmically normal

$$W(\sigma) = \frac{1}{\sqrt{2\pi}\sigma s}\exp\left[-\frac{(\ln\sigma - \overline{\ln\sigma})^2}{2s^2}\right], \tag{2}$$

where s — rms deviation of the parameter σ, in nepers. The parameter s will be called the depth of the slow fading. Formula (1) gives the conditional probability density of the quantity E for a fixed σ. The unconditional probability density of the field intensity W(E) can be represented in the form

$$W(E) = \int_0^\infty W(E/\sigma)\,W(\sigma)\,d\sigma = \frac{1}{\sqrt{2\pi}s}\int_0^\infty \frac{E}{\sigma^3}\exp\left[-\frac{E^2}{2\sigma^2} - \frac{(\ln\sigma - \overline{\ln\sigma})^2}{2s^2}\right]d\sigma. \tag{3}$$

Interest is attached to an estimate of the distribution of the field intensity E in the region of small values of this intensity. For small E we can readily obtain with the aid of (3)

$$W(E) \simeq E \exp [2 (s^2 - \overline{\ln \sigma})]. \tag{4}$$

The power of the fluctuation noise introduced by one section of the radio relay line is

$$y = \frac{B}{E^2}, \tag{5}$$

where B is a constant coefficient depending on the radio delay line apparatus.

The distribution function of the noise power in one section can be estimated, for large values of the noise, by means of the formula

$$F(y) \simeq 1 - \frac{B}{2y} \exp [2 (s^2 - \overline{\ln \sigma})]. \tag{6}$$

We make use of the results of [1], which contains formulas that permit an estimate of the distribution function of the total noise Y at the output of a radio relay line consistng of n identical sections. When the slow fading in the individual sections has independent values, the following relations hold true

$$F_n(Y) \simeq 1 - \frac{nB}{2Y} \exp [2 (s^2 - \overline{\ln \sigma})], \tag{7}$$

where $F_n(Y)$ — distribution function of the total noise power.

It is seen from formula (7) that the presence of slow fading with parameters s and $\overline{\ln \sigma}$ leads to an increase in the probability of exceeding the high-level noise by approximately $\exp [2 (S^2 - \overline{\ln \sigma})]$ times compared with the case when the only fading present is fast with a Rayleigh distribution and with a parameter $\sigma = 1$.

It is of interest to obtain an asymptotic estimate of the noise distribution when the slow fading in the neighboring sections is correlated. An analysis shows that the asymptotic formula (7) is valid also in the case when the slow fading is synchronous (i.e., the correlation coefficient is equal to unity). Thus, in the case of complete correlation of the slow fading in neighboring sections and when the values of the fadings in these sections are independent, the asymptotic properties of the distribution of the total noise turns out to be the same.

REFERENCE

1. Yu.B. Sindler. Accumulation of noise in FM radio relay communication lines, due to fading of the signal. Radio Engineering and Electronic Physics, 1956, 1, 5, 627. 1, 5, 627.

Received by editor 11 August 1961

REFLECTION OF CIRCULARLY POLARIZED RADIOWAVES BY METALLIC BODIES

P. Ya. Ufimtsev

In [1] there was proposed a method for directly measuring the "non-uniform" component of the field scattered by metallic bodies of revolution. In the present communication it is shown that this method is suitable for the measurement of the non-uniform component of the field scattered by arbitrary metallic bodies of finite dimensions.

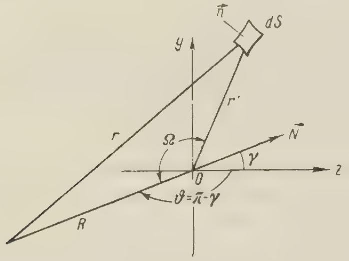

Assume that a plane electromagnetic wave strikes a metallic body of arbitrary shape situated in free space. A surface element of the body is shown in the figure. We choose a coordinate frame such that the normal $\vec{N}$ to the front of the incident wave, drawn through the origin, lies in the plane yoz. The angle between this normal and the z axis would be designated γ.

It is easy to show that in the case of E polarization ($\vec{E}_0 \perp$ yoz) of the incident wave, the current induced on the surface of the body is determined in the Kirchoff approximation by the following formulas

$$
\begin{aligned}
j_x &= -\frac{c}{2\pi} E_{0x} (n_y \sin\gamma + n_z \cos\gamma)\, e^{i\Psi},\\
j_y &= \frac{c}{2\pi} E_{0x} n_x \sin\gamma\, e^{i\Psi},\\
j_z &= \frac{c}{2\pi} E_{0x} n_x \cos\gamma\, e^{i\Psi},
\end{aligned}
\tag{1}
$$

while in the case of H polarization $\vec{H}_0 \perp$ yoz it is determined by the formulas

$$
\begin{aligned}
j_x &= 0,\\
j_y &= \frac{c}{2\pi} H_{0x} n_z e^{i\Psi},\\
j_z &= -\frac{c}{2\pi} H_{0x} n_y e^{i\Psi},
\end{aligned}
\tag{2}
$$

where c is the velocity of light in vacuum; E_{0x} and H_{0x} are the amplitudes of the electric and magnetic fields of the incident wave in E and H polarizations, respectively; $\Psi = k(y' \sin\gamma + z' \cos\gamma)$ — phase of the incident wave at the point (x'. y', z') on the surface of the body; n_x, n_y, and n_z — components of the normal to the surface at the same point. The time factor is given in the form $e^{-i\omega t}$.

Using the resultant current to calculate further the scattered field in the far zone, we obtain for E polarization

$$E_\varphi = H_\vartheta = \frac{ik}{2\pi} E_{0x} \frac{e^{ikR}}{R} \int [n_x \sin\gamma \cos\varphi + (n_y \sin\gamma + n_z \cos\gamma) \sin\varphi] \, e^{i\Phi} \, dS,$$

$$E_\vartheta = -H_\varphi = \frac{ik}{2\pi} E_{0x} \frac{e^{ik}}{R} \int [n_x (\sin\gamma \cos\vartheta \sin\varphi - \cos\gamma \sin\vartheta) - (n_y \sin\gamma + n_z \cos\gamma) \cos\varphi \cos\vartheta] \, e^{i\Phi} \, dS \tag{3}$$

and for H polarization

$$E_\varphi = -H_\vartheta = \frac{ik}{2\pi} H_{0x} \cos\varphi \frac{e^{ikR}}{R} \int n_z e^{i\Phi} \, dS,$$

$$E_\vartheta = H_\varphi = \frac{ik}{2\pi} H_{0x} \frac{e^{ikR}}{R} \int (n_y \sin\vartheta + n_z \sin\varphi \cos\vartheta) \, e^{i\Phi} \, dS, \tag{4}$$

where R, ϑ , φ — spherical coordinates of the point of observation; $\Phi = \Psi - kr' \cos\Omega$, and the integration is over the illuminated elements of the body surface. In the radar case, when the observation and illumination conditions coincide ($\vartheta = \pi - \gamma$, $\varphi = -\pi/2$) we obtain respectively

$$E_\varphi = H_\vartheta = \frac{iaE_{0x}}{2} \overline{\Sigma}_k \frac{e^{ikR}}{R}, \quad E_\vartheta = H_x = 0 \tag{3a}$$

and

$$H_x = E_\vartheta = \frac{ia\, H_{0x}}{2} \Sigma_k \frac{e^{ikR}}{R}, \quad E_x = H_\vartheta = 0. \tag{4a}$$

The quantity a contained in these formulas is some linear dimension of the body, while the functions Σ_k and $\overline{\Sigma}_k$ are given by

$$\Sigma_k = -\overline{\Sigma}_k = \frac{k}{\pi a} \int (n_y \sin\gamma + n_z \cos\gamma) \, e^{i\Phi} \, dS. \tag{5}$$

We have thus demonstrated that the equality $\Sigma_k = -\overline{\Sigma}_k$ is satisfied for bodies of arbitrary form. Consequently, the method described in [1] is universal and enables us to separate from the total field, scattered by arbitrary metallic bodies, that portion of the field due to the bending of the surface (flexure, kink, sharp point, projection, aperture, etc.).

REFERENCE

1. E.N. Maizel's, P.Ya. Ufimtsev. Radio Engineering and Electronic Physics, 1960, 5, 12, 1925.

Received by editor 10 June 1961

SYMMETRICAL DIAGRAMS REALIZED BY A ROUND RADIATING APERTURE

B.M. Minkovich

The conditions of realizability of a directivity pattern for a linear antenna of finite length are determined by the well known Wiener-Paley theorem [1]. The analogy between a linear antenna and a round aperture, established in [2], indicates the possibility of obtaining the conditions for the realizability of a symmetrical directivity pattern in a round aperture of finite dimensions. In the far zone the directivity pattern of a round aperture is expressed with the aid of the Hankel transformation [3]

$$F(u) = \int_0^1 A(\rho) J_0(u\rho)\, \rho d\rho, \tag{1}$$

where

$$A(\rho) = \int_0^\infty F(u) J_0(u\rho)\, u du, \tag{2}$$

and the connection established by expressions (1) and (2) is valid not for all arbitrary even or even continuous function F(u) and A(ρ).

Let us find the conditions that must be satisfied by the functions F(u) and A(ρ).

By means of expressions (1) and (2) we can readily find that the functions F(u) and A(ρ) are interrelated by an equation similar to the Parseval equation for the Fourier transformation

$$\int_0^\infty |F(u)|^2 u du = \int_0^1 |A(\rho)|^2 \rho d\rho. \tag{3}$$

For a physically realizable amplitude distribution we have

$$\int_0^1 |A(\rho)|^2 \rho d\rho < \infty \tag{4}$$

or

$$\int_0^\infty |F(u)|^2 u du < \infty, \tag{5}$$

and in the opposite case the directivity coefficient will vanish [3]. When F(0) is finite, then

$$\int_{-\infty}^{\infty} |F(u)|^2 du < \infty \tag{6}$$

is all the more valid. We now reduce the Hankel transformation (1) to a Fourier transformation, after which, with account of (6), we make use of the Wiener-Paley theorem for the Fourier transformation. Inasmuch as [4]

$$J_0(u\rho) = \frac{2}{\pi} \int_0^1 \frac{\cos u\rho y}{\sqrt{1-y^2}} dy,$$

(1) assumes the form

$$F(u) = \frac{1}{\pi} \int_{-1}^{1} I_1(y) e^{iuy} dy, \tag{7}$$

where

$$I_1(y) = \int_y^1 \frac{A(\rho)\rho}{\sqrt{\rho^2 - y^2}} d\rho$$

is an even function of the class $L_2(-1, 1)$. Consequently, the problem of realizability of a symmetrical directivity diagram in a round aperture reduces to a similar problem for a linear aperture. We now obtain the conditions that must be satisfied by the function F(u): The continuation of the function into the complex domain F(z) must be an entire transcendental function of exponential type with exponent ≤ 1; on the real axis the function F(z) must satisfy the condition (5) and not (6) as in the case of a linear aperture. It is seen from (5) that the functions that can still be realized as directivity patterns of a found aperture should decrease at infinity $\sqrt{u}$ times faster than the corresponding function for a linear aperture. This result was obtained earlier by Taylor [5]. This means that the directivity pattern, which has the form (sin u)/u at large values of u (the corresponding distribution functions in a linear aperture have a pedestal [5]), cannot be realized in a round aperture, since the integral (5) does not converge.

REFERENCES

1. N.I. Akhiezer. Lectures on the Theory of Approximations. GTI, 1947.
2. B.M. Minkovich, Yu.I. Davidchevskii. On the synthesis of an antenna with round aperture. Radio Engineering and Electronic Physics, 1961, 6, 8, 1935.
3. Microwave Antennas. Translated from the English, edited by Ya.N. Fel'd. Soviet Radio Press, Part I, 1950.
4. E.C. Titchmarsh. Introduction to the Theory of Fourier Integrals. Clarendon Press, Oxford, 1937 (translated from the English; OGIZ, 1948).
5. T.T. Taylor. Design of circular apertures for narrow beam width and low side lobes. IRE Trans. 1960, AP-8, 1, 17.

Received by editor 10 July 1961

DEPENDENCE OF THE PROPERTIES OF A CAVITY CHAIN ON THE DISPLACEMENT OF THE SLOTS IN ADJACENT DIAPHRAGMS

Ya. K. Trokhimenko

In electron-beam devices with longitudinal interaction, slow-wave systems are used in the form of chains of cylindrical cavities, inductively coupled through slots in the diaphragms.

A theoretical analysis of such systems, one sufficiently convenient for practical purposes, is developed in [1].

Dispersion equation (31) of reference [1], for modes close to TM_{010} in cavities separated by spin single-slot diaphragms, can be represented in the form

$$\frac{p^2-1}{p^3\,\mathrm{tg}\left(\frac{\pi S}{2p}\right)-\frac{\pi}{2}Sp^2}=\alpha, \qquad (1)$$

where $p = \lambda/\lambda_n$ — relative wavelength in free space; $S = \lambda_s/\lambda_n$ — relative resonant wavelength of the slot (for narrow peripheral slots $\lambda_s = 2b$, where b is the length of the slot); $\lambda_n = 2.615a$ — natural wavelength of a cylindrical cavity of radius a for the TM_{010} mode; $\alpha = \alpha_\pi \sin^2\frac{\varphi}{2}$ — coupling coefficient between cavities; $\alpha_\pi = 0.18\frac{aZ_0}{bZ_b}$ — static coupling coefficient; Z_0 — wave impedance of the transmission line equivalent to the slot [1]; $Z_b = \sqrt{\mu/\epsilon}$ — wave impedance of free space; φ — phase shift during one period of the system (per cavity).

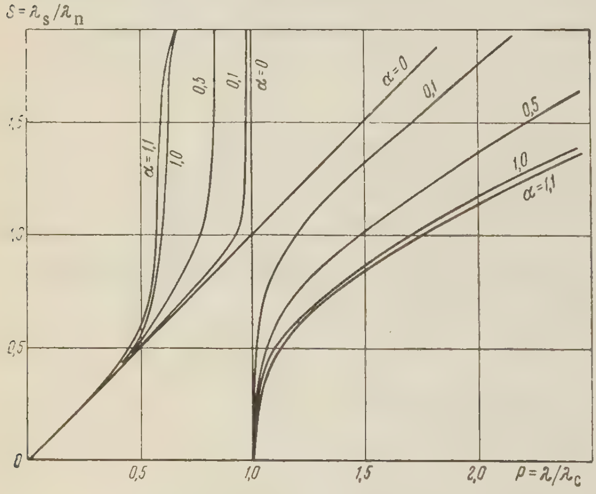

Fig. 1

The solution of dispersion equation (1) for the two pass bands of longest wavelength is shown in Fig. 1 in the form of slots $S = f(p, \alpha)$.

In the case of weak coupling ($s < 1$) the pass band connected with the natural cavity wavelength is located at longer wavelengths and is characterized by negative dispersion ($\lambda_0 < \lambda_\pi$). The pass band connected with the resonant wavelength of the slots has positive dispersion. An increase in the coupling with $S < 1$ leads to a broadening of both pass bands, with the band connected with λ_n broadening by an increase in λ_π at a constant value $\lambda_0 = \lambda_n$.

When $S = 1$ both pass bands come in contact at the point $p = 1$.

When $S > 1$, the cavity natural wavelength λ_n is connected with the shorter-wave pass band, while λ_s is connected with the longer-wave pass band. The sign of the dispersion in both pass bands is reversed when S = 1. With further increase in the coupling, the pass band connected with λ_n becomes somewhat narrower, while the pass band of the slots broadens and shifts towards the longer wavelengths.

Equation (1) is valid only for the case of weak coupling, when the influence of the longitudinal magnetic fields occurring near the coupling slots can be neglected. The influence of the longitudinal magnetic field manifests itself in a reduction in the resonant wavelength of the slots (owing to the occurrence of currents in the slots themselves) and in a change in the dispersion and the width of the pass band — essentially due to the mutual currents of the slots, determined by the direct coupling between the slots [1]. The magnitude of the mutual currents depends on the period of the system and on the placement of the slots in adjacent diaphragms.

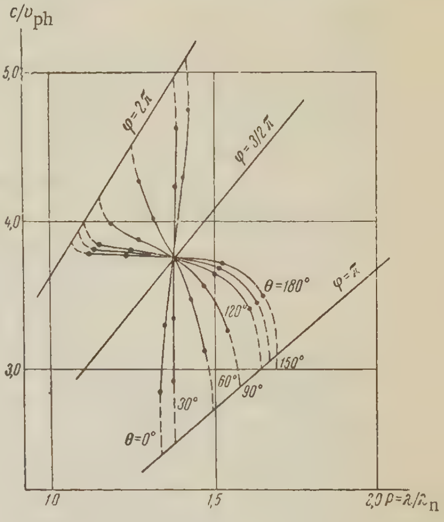

Fig. 2

The influence of the longitudinal magnetic field is accounted for quantitatively in [1] by means of formulas (46) which are valid for the case of identically situated single-slot diaphragms. For the case of practical importance of alternate displacement of the slots in neighboring diaphragms, the influence of the longitudinal magnetic field can be taken into account (as was confirmed experimentally) by replacing the parameters S and α_π in (1) respectively by

$$S' = \frac{S}{\sqrt{1 + P - Q\cos\varphi\cos\Theta}},$$
$$\alpha'_\pi = \alpha_\pi\sqrt{1 + P - Q\cos\varphi\cos\Theta}, \qquad (2)$$

where Θ — angle of relative rotation of the slots in the neighboring diaphragms (every other diaphragm); P and Q — coefficients that take into account the magnitudes of the self and mutual currents of the slot respectively. The coefficients P and Q (P > Q) are approximately calculated from formulas (44) of [1], which are valid for the simplest configuration of the coupling slots.

Formulas (2) differ from (46) of [1] in that they contain the factor $\cos\Theta$, which takes into account the alternate (every other diaphragm) shift of the diaphragms in the system by an angle Θ.

Calculation by means of (1) and (2) yields a good quantitative agreement with experiment in the case of narrow peripheral slots with angular lengths on the order of 90°. For the practically employed slots and cavities, of more complicated form, expressions (1) and (2) yield a quantitative estimate of the influence of the geometry of the slow-wave system on its properties.

Let us examine the case of practical importance $S > 1$, $p > 1$ (Fig. 1).

When the angular shift of the neighboring diaphragms is 90°, the mutual currents do not influence the properties of the system ($\cos\Theta = 0$), and the self-currents result in a reduction of the resonant wavelength of the slot

$$S'(0) = S'(\pi) = S/\sqrt{1+P},$$

which leads, as follows from the plots of Fig. 1, to a certain narrowing of the pass band, which is only partially offset by an increase in the coupling coefficient $\alpha'_\pi = \alpha_\pi\sqrt{1+p}$.

When the diaphragms are identically arranged ($\Theta = 0$) and $\varphi = 0$, the resonant wavelength of the slot increases $[S'(0) = S/\sqrt{1+P-Q}]$, and when $\varphi = \pi$ it decreases $[S'(\pi) = S/\sqrt{1+P+Q}]$. This leads to a sharp narrowing down of the pass band, and at certain large values of indirect coupling between the slots it reverses the sign of the dispersion in the long-wave pass band.

When $\Theta = 180°$, the resonant wavelength of the slot corresponding to $\varphi = 0$ decreases $[S'(0) = S/\sqrt{1 + P + Q}]$, while that corresponding to $\varphi = \pi$ increases $[S'(\pi) = S/\sqrt{1 + P - Q}]$. This leads to a broadening of the pass band compared with the case $\Theta = 90°$.

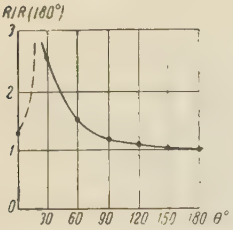

Fig. 3

The foregoing theoretical estimates are in good agreement with experiment. Fig. 2 shows the dispersion characteristics of a single-slot system for the first positive spatial harmonic, taken at different values of angle $\Theta (\alpha_\pi \simeq 0.4)$. As follows from (2), when Θ changes, the dispersion characteristics rotate about a point approximately to $\varphi = \frac{3}{2}\pi$.

The experimental investigations have also shown that the dependence of the coupling resistance R for the first spatial harmonic on the angle Θ is determined essentially by the change in the ratio v_{ph}/v_{gr}, since the distribution of the field near the axis of the system and the energy stored per unit length depend little on Θ. A plot of $R(\Theta)$, with the phase shifted by the period of the system $\varphi = \frac{3}{2}\pi$, is shown in Fig. 3.

In similar fashion we can estimate also the properties of a system having a different configuration of diaphragms. In particular, for two-slot diaphragms (slot symmetrical about the axis of the system), the maximum pass bands of the system correspond to a shift $\Theta = 90°$ between the adjacent diaphragms.

Thus, a change in the angle of rotation of the slots in neighboring diaphragms of a cavity chain with inductive coupling enables us to change, over a relatively wide range, the characteristics of the slow-wave system. This property can be used, in particular, for matching purposes, and also for gradual variation of the parameters of the slow-wave system, a factor which is important in certain applications. Great interest is also attached to an investigation of systems in which the coupling slots in the diaphragms are shifted along a helix.

REFERENCE

1. M.A. Allen, G.S. Kino. On the theory of strongly coupled cavity chains. IRE Trans. 1960, MTT-8, 3, 362.

Received by editor 8 May 1961

RADIO ENGINEERING AND ELECTRONIC PHYSICS

1961

CONTENTS

Number 1

Page

F. V. Bunkin: Thermal Fluctuations in Nonlinear Systems 1
M. F. Bakhareva: Cross Correlation of Field Fluctuations of Receiving Lenses with Finite Dimensions 6
A. V. Prosin: Calculation of Cross Noise Power in Long-Distance Scatter Communications Systems 9
N. K. Ignat'yev: Power Spectrum of a Signal Obtained by Scanning 19
L. A. Vaynshteyn and A. A. Fedorov: Plane and Cylindrical Wave Scattering on an Elliptical Cylinder and the Theory of Diffraction Waves 24
A. S. Goryainov: Diffraction of a Plane Electromagnetic Wave Propagating Along the Axis of a Cone 39
A. N. Sivov: Incidence of a Plane Electromagnetic Wave on a Plane Grid (Case in Which the H Vector is Parallel to the Wires) 49
Ya. A. Yashkin: π and T Ridged Waveguides uniformly bent in the E Plane 57
V. V. Nikol'skiy: Investigation of Cavity Systems with Anisotropic Regions by the Eigenfunction Method. Part III. Waveguides 64
B. M. Bulgakov, V. P. Shestopalov, L. A. Shishkin and I. P. Yakimenko: Unidirectional Propagation of Waves in a Helical Waveguide placed in a Ferrite Medium 70
V. P. Shestopalov and A. A. Bulgakov: Coaxial Bifilar Contra-Wound Helix Immersed in a Magneto-Dielectric Medium 80
Syuy Yan'-shen: Some Methods for the Solution of a Problem Concerning the Oscillations of a small Gyrotropic Sphere. Part II, Series Method 88
A. P. Fedotov and B. K. Shembel': Linear Accelerator Resonator as a Microwave Oscillator Load 95
G. D. Lobov: Gas Discharge Detector of Microwave Oscillations 103
S. B. Rubin: Some Theoretical Problems in the Operation of a Microwave Phasemeter 111
A. L. Igritskiy: Optimal Electron Beam Focusing in a Periodic Traveling-Wave Tube Focusing Device 121
N. L. Yasnopol'skiy, N. A. Karelina, V. S. Malysheva: Some Results of an Investigation of Transmission Secondary Electron Emission of MgO Emitters 129
Ya. M. Shvarts: Theory of Operation of the Electrostatic Fluxmeter in Plasma 134
N. A. Belova and A. N. Kovalev: Experimental Investigation of Tunnel Current in thin Germanium p-n Junctions 140
Ye. N. Bazarov and M. Ye. Zhabotinskiy: Fluctuations in a Reflex Klystron Oscillator due to Electron Velocity Spreading Shot and Heat Effects 145

BRIEF COMMUNICATIONS
M. B. Tseymlin, Ye. M. Il'ina: TWT Gain with Finite Values of the Gain Parameter C 148
V. V. Grigor'yants, M. Ye. Zhabotinskiy: Ammonia-Beam Maser operating without Liquid Nitrogen 153
LETTERS TO THE EDITOR
M. D. Gabovich: Excitation Mechanism of Electron Plasma Oscillations 155
Academician Abram Fedorovich Ioffe 157

Number 2

Yu.S. Lezin: Noise Storage in Delayed Feedback Devices 159
P. Ya. Nudel'man: Linear Correction of Transients in Systems with Finite Passband 165
Lin Hai-Ts'uan: Calculation of Channel Capacity in Two-Path Communication 168
Lin Hai-Ts'uan: Capacity of One-Path and Two-Path Communications Channels with Polarization Fading 172
A.V. Shabel'nikov: The Perturbation Method and its Relation to the Exact Diffraction Method in Solving Problems of Incoherent Scattering 176
N.G. Ponomarev: Graphical Method of Designing Aplanatic Antennas 185
O.N. Tereshin and A.Ye. Sokolov: Suppression of Currents Excited in Metal Shields by Diffraction Antennas of Finite Dimensions 191
B.Z. Katsenelenbaum, and Z.A. Malina: Transition Calculations for a Symmetrical Magnetic Wave in a Circular Waveguide 198
A.L. Fel'dshteyn: Synthesis of Stepped Directional Couplers 204
Yu.N. Kazantsev: Attenuation Measurements in Waveguides 210
V.I. Muromtsev and A.K. Piskunov: Some Problems of Microwave Channel Matching in Radio Spectroscopes 218
G.N. Rapoport: Large-Signal Operation of Backward-Wave Amplifier 227
L.V. Kasatkin: Amplification of Space-Charge Waves in the Passage of Electron Beams within Media with Inductive Susceptance 232
A.L. Igritskiy: Calculation of a Magnetic Periodic Focusing Device for TWT 239
G.D. Lobov, and V.I. Yeremeyev: Some Effects Accompanying Detection in a Gaseous Discharge 248
M.I. Elinson, G.V. Stepanov, and V.I. Pokalyakin: Emission of Hot Electrons from p-n Junctions in SiC Crystals 252
G.N. Fursei : Field Emission from Tungsten Single Crystals in the Prebreakdown Current Region 257
G.Ya. Myakishev: On the Theory of the Static Characteristics of a Planar Diode without an Incandescent Cathode taking into account Thermal Electron Velocity Distribution 262
Yu.R. Nosov: Transition Processes in Semiconductor Diodes Using Narrow Forward Current Pulses 271
V.V. Grigor'yants, and M.Ye. Zhabotinskiy: Molecular Frequency Standard with Subtraction of Reference Oscillator Error 279
BRIEF COMMUNICATIONS
L.K. Mikhaylovskiy: Wideband Amplification with Frequency Conversion . . 286
A.I. Yel'kind: Suppression of Harmonics in Coaxial Resonators 288
L.E. Bakhrakh and A.D. Sulimin: Calculation of Ribbon Stream Electron Guns 290

M.I. Elinson and V.A. Gor'kov: Some Special Features of Field Emission Cathode Operation in a Microwave Field 294
V.I. Makukha: Calcium Adsorption on Tungsten 298
V.I. Makukha: Adsorption of Strontium on Tungsten 301
V.P. Vasil'yev, and V.P. Pomazkov: Determining the Free Barium Content in an Oxide Cathode by a Radioactive Indicator Method 305

Number 3

V.I. Aksenov: Utilization of Kirchhoff's Approximation in the Problem of the Scattering of Radio Waves by Periodically Rough Surface with Finite Conductivity 307
G.A. Karpeyev: Utilization of a Two-Element Interferometer for the Investigation of Field Fluctuations 314
V.A. Malyshev and V.S. Mikhalevskiy: On the Theory of Traveling Wave Oscillators with Weak Feedback 322
N.M. Sovetov: Generalization of Impedance Circular Diagrams to the Case of Microwave Channels with Negative Resistance 329
S.I. Molokovskiy and A.D. Sushkov: Investigation of the Electric Field of a Dense Bunch of Charged Particles 332
Yu. V. Zubenko: Study of the Shape of W_2C Single Crystal Emitters Using an Electron Microscope 338
Yu.G. Ptushinskiy: Effect of Adsorption on the Resistance of Thin Metal Films Pt. II. Electropositive Atoms 340
G.N. Zastenker, G.S. Solntsev, et al.: On the Mechanism of Formation of a Low-Pressure, High-Frequency Discharge in Air 343
I.M. Polyak: Electric Current in Penning Tubes 349
Yu.F. Sokolov: Modified Four-Terminal Network Method for the Determination of Semiconductor Diode Contact Impedance at High-Frequencies 353
E.G. Solovyev and E.K. Karlova: Stub Delay Structure for Traveling-Wave Paramagnetic Amplifier of Centimeter Wavelength 359
N.V. Karlov, Yu.P. Pimenov, et al.: Saturation and Recovery Time of Paramagnetic Amplifiers 363
N.V. Karlov, Yu. P. Pimenov, et al.: On Sensitivity of Radio Receivers with Paramagnetic Amplifiers 368
P.D. Kalapchev and A.E. Salomonovich: Radio Telescope with a 22-Meter Parabolic Reflector (Physical Institute of the Academy of Sciences of the USSR) 373
A.M. Karachun, A.D. Kizmin, et al.: Investigations of Some Electrical Parameters of the Antenna of a 22-Meter Radio Telescope 379
A.K. Piskunov and V.I. Muromtsev: Influence of Signal Generator Frequency Fluctuations on the Sensitivity of Radio Spectroscopes with Transit and Reflector Cavities 385

BRIEF COMMUNICATIONS

M.V. Persikov: H_{02} Wave Filter in a Circular Waveguide 392
M.V. Persikov: On H_{01} Wave Excitation in a Circular Waveguide. 394

LETTERS TO THE EDITOR

S.I. Alber and V.I. Bespalov: On a Diffusion Equation for a Statistically Irregular Waveguide 396
M. E. Gertsenshteyn and V.B. Vasiliev: Concerning S.I. Alber and V.I. Bespalov's Letter "On a Diffusion Equation for a Statistically Irregular Waveguide". 397

REVIEWS AND BIBLIOGRAPHY

H.S. Lanzberg: Books on Radio Engineering and Electronics in 1961 399

CHRONICLE

Aleksandr Nikolaevich Shchukin (For His Sixtieth Birthday) 427

Number 4

A.N. Sivov: Electrodynamic Theory of a Dense Plane Grating of Parallel Conductors 429
S.I. Yevtyanov and V.N. Kuleshov: Fluctuations in Self-Excited Oscillators 440
N.K. Kul'man and P.S. Landa: Analog Investigation of Some Optimum Devices for Filtering of Random-Duration Pulse Signals 448
V.F. Pisarenko: Detection of Random Signals Against a Noise Background 455
Yu.S. Lezin: Influence of Storage Device Parameters on Operational Efficiency. 468
G. P. Tartakovskiy: Range Finder with Frequency Modulation in the Presence of Noise and Fluctuations in Reflected Signal 473
B.Ye. Kinber: Lateral Radiation of Parabolic Antennas 481
P.Ya. Ufimtsev: Symmetrical Illumination of Finite Bodies of Rotation 492
S. Dyad'kov: Resonance Transforms and Their Properties 500
G. P. Samuylov: Approximate Calculation of Eigenvalues of Higher Modes in Strip Transmission Lines 510
V.M. Dashenkov: Characteristic Impedance of Multiwire Lines with Circular Conductors . 514
G.F. Filimonov: Influence of Two Types of Longitudinal Periodic Modulation on the Properties of a Single-Beam Electron Stream 522
V.A. Malyshev: On A Theory of Diode Microwave Oscillators 532
A.I. Igritskiy: Calculation of Periodic Electrostatic Fields in Traveling-Wave Tubes with Bifilar Helices 539
A. L. Mikaelyan and A.A. Vasil'yev: Interaction of Magnetostatic Oscillations in Ferrite Specimen During Regeneration. Part I. Interaction of Simplest Modes 548
L.V. Kononchuk: Some Properties of a Thick-Layer Multialkaline Photocathode 556
M. Bakal, L.N. Dobretsov: Millikan Vacuum Capacitor, Part I 561
L.P. Afinogenov, et al.: Millikan Vacuum Capacitor, Part II 565

BRIEF COMMUNICATIONS

B.S. Tsybakov: Shannon Scheme for Gaussian Information with Uniform Spectrum and for A Channel with Fluctuation Noise 571
B.Ye. Kinber: Toward A Receiving Antenna Theory 573
V.P. Shestopalov and I.P. Yakimenko: Attenuation of Slow Electromagnetic Waves in a Plasma Rod in a Longitudinal Magnetic Field 575
F.G. Bass: On Electrodynamic Boundary Conditions at A Plane Surface with Arbitrary Value of Dielectric Constant 577
L.E. Bakhrakh: Evaluating the Influence of Thermal Velocities in Electron Beams 579
N.D. Porev: Calculation of Hollow Electron Beams 582
V.A. Libin: Polarization Analyzer 584
G.V. Bogdanov: Possible Application of Ferrites for Absolute Measurement of Microwave Power 587
D.D. Mishin and L.A. Kalyagina: Influence of Temperature Prehistory on Permeability of Nickel-Zinc Ferrites 591
I.M. Bronshteyn et al.: Energy Distribution of Field Emission Electrons in Semiconductors 594
A.G. Zhdan and M.I. Yelinson: Energy Spectrum of Slow Secondary Electrons in Adsorption of Beryllium onto Tungsten 595

LETTERS TO THE EDITOR

L.S. Miroshnichenko: Photoelectron Emission of LaB$_6$ 597
Yu. M. Aleskovskiy, et al.: Recombination Radiation of Cesium Plasma in Magnetic Field. 598

CHRONICLE

Symposium on Wave Diffraction 600
Venedikt Ivanovich Kalinin 603

Number 5

V.M. Lopukhin, The Kinetic Power Theorem and its Application to Electron Beam Devices 605
B.N. Mityashev, Interference Immunity of Two Methods of Reception of Pulse Signals 624
G.V. Druzhinin, Supply of Spare Parts for Electronic Circuits on the Basis of Load 635
A.I. Kalinin, Effect of Earth in UHF Tropospheric-Scatter Propagation 640
V.V. Novikov and G.I. Makarov, Propagation of Pulsed Signals over a Homogeneous Flat Earth 644
Yu.L. Kokurin, A.N. Sukhanovskiy et al., Investigation of a Model of Large-Scale Ionospheric Inhomogeneities by a Radio Astronomical Method 653
G.N. Krylov, Structure of Electromagnetic Field of Directional Antennas above a Flat Earth with Finite Conductivity 660
A.Ya. Yashkin, A Method of Calculation of Characteristic Modes and Dispersion in Straight and Bent Waveguides of Complex Cross Section 666
L.N. Loshakov, Coupling Coefficient between Electron Beam and Transverse Electromagnetic Field in a Microwave Waveguide 678
A.K. Musin, Plasma Motion in Crossed Electric and Magnetic Fields 681
M.D. Karasev, Influence of Parasitic Parameters of a Semiconductor Diode upon the Operation of a Parametric Amplifier 689
A.L. Mikaelyan and A.A. Vasil'yev, Interaction of Magnetostatic Oscillations in a Ferrite Sample in the Case of Regeneration. Part II—Conditions of Excitation of Oscillations in General 697
N.G. Basov, V.V. Nikitin, et al., Investigation of Maser Frequency Dependence upon Different Parameters. Part I—(Theory, Line J = 3, K = 2) 703
G.A. Siulina and G.A. Feshchenko, Fe^{3+} Spin Levels in Corundum 711

BRIEF COMMUNICATIONS

F.I. Khaytun, Increase in the Transmission Range of Pulse Signals of Given Energy in the Presence of Noise with an Arbitrary Spectrum 720
B.A. Dubinskiy, Method for Ideal Measurement of Oscillation Parameters 723
B.A. Sukhov, Characteristic Resistance and Attenuation of a TEM Wave Propagating along a Multiconductor Line Made Up of Rectangular Conductors 726
L.R. Yavich, Remarks on the Calculation of Cascade Connections of n-Similar Two-Ports 729
M.B. Tseytlin and Ye.M. Il'ina, On the Form of the Field in a Backward Wave Tube in the Presence of Distributed Attenuation 732
A.A. Shur and G.S. Maksimov, One Method of Measuring the Fluctuation of the Phase of Radio Waves in a Study of Tropospheric Scatter Propagation 734
Ye.M. Gershenzon, N.F. Ptitsyna, et al., Single-Loop Parametric Amplifier ... 735
A.N. Vakhrameyev, Experimental Investigation of Forces Oscillation in a Parametrically Regenerated Tank Circuit 741
Ye.M. Gershenzon and V.S. Etkin, Spectral and Amplitude-Frequency Characteristics of Superregenerative Parametric Amplifiers 744
Yu.Ye. D'yakov, Transfer Function of a Superregenerative Parametric Amplifier .. 747
Yu.Ye. D'yakov, An Error in the Analysis of a Two-Loop M Parametric Amplifier .. 749
Yu.A. Kravtsov, Consideration of Combination Frequencies in Systems with Periodically varying Reactance 750
G.N. Berestovskiy, Effect of Asymmetry on the Operation of Push-Pull Semiconductor Converters With External Excitation 753
N.V. Karlov, Yu.P. Pimenov, et al., Paramagnetic Amplifier for the Ten-Centimeter Band Using Fe^{3+} Ions in Corundum 755
A.L. Mikaelyan, A.A. Vasil'yev, et al., Microwave Regeneration in a Ferrite in Response to Longitudinal Pumping.............................. 765
V.G. Veselago, A Spin Generator 759

CHRONICLE

Third All-Union Conference on Electron Microscopy.................... 761
Interdepartmental Seminar on Cathode Electronics (17th Meeting)............. 772

Number 6

N.A. Armand, B.A. Vvedenskiy, Long-Range Tropospheric Propagation of Ultrashort Waves (Survey) . . . 775
N.D. Khaskind, Propagation of Electromagnetic Waves over a Gyrotropic Medium . . 791
A.N. Bruyevich, Asynchronous Oscillations in Self-Excited Oscillator with Two Degrees of Freedom in Overvoltage Operation . . . 799
B.Ye. Kinber, Decoupling of Two Closely-Spaced Reflectors . . . 809
R.V. Khokhlov, The Theory of Radio Shock Waves in Nonlinear Transmission Lines 817
L.S. Benenson, Induced Dipole Impedances in a Waveguide . . . 824
L.V. Kasatkin, Measurements of the Radial Admittance of Axially Symmetrical Systems with Inductive Walls . . . 831
O.A. Barmenkov, S.A. Kornilov, et al., Theoretical and Experimental Investigation of Frequency-Divider Klystrons with Preliminary Bunching . . . 838
V.I. Kanavets, Harmonics in an Electron Beam at the Output of a Traveling-Wave Tube . . . 848
A.L. Igritskiy, Focusing the Electron Beam in a Traveling-Wave Tube by a Periodic Electrostatic Field . . . 857
L.E. Bakhrakh, Yu.D. Zharkov, Geometric Parameters of Electron Beams in Ionic Focusing . . . 867
S.B. Gurevich, The Problem of Changing the Signal-to-Noise Ratio Produced by Camera Tubes in a TV System . . . 873
V.M. Breitman, V.S. Kuznetsov, Mathematic Formulation of Problems in Corpuscular Optics with Space Charge Taken into Account . . . 882
V.I. Shveykin, A Pulse Method of Determining the Parameters of Drift Transistors 887
L.S. Gorn, B.I. Khazanov, Conversion of a Current Pulse from a Photoelectric Multiplier into a Voltage Pulse by an Emitter Follower . . . 897
B.S. Mel'nikov, Electronic Control of Pulse Duration in L-Oscillator with Junction Transistor . . . 901
N.G. Basov, G.N. Strakhovskiy, et al. Study of the Dependence of the Frequency of Masers on Various Parameters. Part II. The J = 3, K = 3 Line . . . 905

BRIEF COMMUNICATIONS

N.V. Karlov, The Problem of Studies of Retarding Systems . . . 913

LETTER TO THE EDITOR

V.A. Malyshev, Concerning the Article "On a Magnetron Oscillator Theory" . . 914

CHRONICLE

Interinstitutional Seminar on Cathode Electronics, Eighteenth Session . . . 914

Number 7

A.E. Basharinov, Problems in the Statistics of Automatic Pattern Recognition by Multiframe Scanning . . . 917
B.S. Fleyshman, Nonstationary Method for Loading the Memory of a Control Device with Statistical Pattern Recognition . . . 922
V.A. Zyanitskiy, Model of the Memory Loading of a Control Device by the Method of Self-Analysis . . . 929
V.F. Nesteruk, The Theory of Optimal Detection of a Compound Signal with Correlated Noise . . . 934
R.L. Stratonovich, Optimal Reception of a Narrowband Signal of Unknown Frequency on a Background of Noise . . . 942
M.I. Dorman, The Spectrum of an Oscillation whose Frequency Passes through Zero . . . 955
V.I. Tikhonov, The Markov Nature of the Envelope of Quasi-Harmonic Oscillations 961
I.Kh. Rizvkin, The Characteristics of Nonlinear Elements of Frequency Dividers 971
V.I. Ivanchikov, Some Problems in the Theory of the Refraction of Magnetic Waves 979

P.P. Pavlov, The Electromagnetic Field and the Distribution of Current along an Infinitely Long Uninsulated Wire in a Conducting Medium 985
R.V. Khokhlov, Wave Propagation in Nonlinear Lines with Dispersion 993
L.S. Benenson, Calculation of the Phase Velocity of Waves in an Artificial Metal Dielectric when the Current Harmonics on the Elements of the Structure are Considered 1004
V.P. Shestopalov, A.A. Bulgakov, B.M. Bulgakov, Theoretical and Experimental Studies of Helical Dielectric Antennas 1011
L.D. Bakhrakh, I.V. Vavilova, Spherical Two-Mirror Antennas 1020
R.F. Matveyev, Calculation of Side Flow in a Long Waveguide Line 1029
S.B. Gurevich, Sensitivity of Television Systems with Different Scanning Parameters 1036
Ye.N. Petrov, Theory of a Flat-Electrode Triode with Negligibly Small Grid-Anode Space Charge. 1040
V.B. Braginskiy, V.A. Dianova, Ye.R. Mustel', Investigation of Frequency Multiplier Using the Nonlinear Capacitance of a p — n Junction 1043
L.K. Mikhailovskiy, et al., Nonlinear Nutation-Type Gyromagnetic Effects in Ferrites 1046
A.L. Mikaelyan, V.Ya. Anton'yants and Yu.G. Turkov, Phenomena of Mutual Coupling of Cavity Resonator and Ferrite 1052
M.I. Rodak, Calculation of the Polarization of an Alternating Magnetic Field Corresponding to Extreme Transition Probabilities in Electron Paramagnetic Resonance 1062

BRIEF COMMUNICATIONS

Wang Huan Cho, Calculation of a Matching Metallic Insert in a Circular Waveguide 1067
A.P. Fedotov and V.A. Teplyakov, Requirements of Amplitude and Phase Stability of Fields in Linear Accelerator Cavities 1070
V.N. Fetina, Excitation of Even Harmonics During Ferromagnetic Resonance . . . 1072
N.G. Nakhodkin and P.V. Melnik, Photoelectric Effect in the Region of Soft X-Rays 1074

LETTERS TO THE EDITOR

Concerning L.P. Kuklev and Yu.P. Ozerskiy's Article "Comparison of Interval Codes", I.M. Petrov and G.S. Tyslyatskiy 1076
Answer to the Letter of I.M. Petrov and G.S. Tyslyatskiy, L.P. Kuklev and Yu.P. Ozerskiy 1080
On the Problem of the Influence of Light Polarization upon the Photoeffect of Complex Cathodes, N.S. Klebnikov and A.E. Melamid 1080

Number 8

N.A. Armand and B.A. Vvedenskiy, Allowance for Antenna Directivity Pattern in the Calculation of Radio Wave Diffraction around the Earth 1083
P.Ye. Kubasov, Investigation of Space-Time Correlations of the Field Level of Centimeter Waves Propagating in a Turbulent Atmosphere 1091
Ya.D. Shirman, Statistical Analysis of Optimal Resolution 1098
G.D. Malyuzhinets and L.A. Vaynshteyn, Transverse Diffusion in Diffraction by an Impedance Cylinder of Large Radius. Part I. Parabolic Equation in Ray Coordinates 1106
M.D. Khaskind, Excitation of Waves on an Impedance Plane 1117
B.Ye. Kinber, Diffraction of Electromagnetic Waves by Concave Surface of Circular Cylinder 1130
R.B. Vaganov and V.V. Meriakri, Suppression of Resonance Phenomena in Multimode Waveguides 1139
P.P. Pavlov, Electromagnetic Field and Distribution of Current along an Infinitely Long Insulated Wire in a Conducting Medium. 1148
S.I. Viglin, Transient Characteristics of Coaxial System with Periodic Structure . . . 1161
A.B. Lazarev and G.F. Filimonov, Static Characteristics of a Plane Magnetron. 1169
G.A. Postnov, Possibility of Existence of Slow Waves in an Isotropic Plasma Waveguide 1176
G.P. Apushinskiy, Concerning the Sensitivity of Radiometers 1179

Z.S. Gribnikov, B.N. Kompan and L.V. Svyatogor, Investigation of Field Effect Transistors 1181
M.I. Yelinson, F.F. Dobryakova, et al., On the Theory of Field Emission and Thermionic Field Emission of Metals and Semiconductors 1191
Sh. M. Kogan, Thermal Radiation Produced by Hot Carriers in Semiconductors 1201
G.B. Der-Shvarts, Yu.M. Kushnir, et al., Certain Problems of Reflex Electron Microscopy, ... 1204
V.N. Vertsner, V.G. Nikiforova, et al., The EM-6 Light-Electron Microscope 1209
R.Ya. Berlaga, P.P. Konorov, M.I. Rudenok, Electron-Microscopic Investigations of Germanium Surface 1214
A.N. Pilyankevich, Calculation of the Characteristics of Scattering of Medium-Energy Electrons on Free Atoms 1217
P.A. Stoyanov, N.M. Grishina, Elimination of Astigmatism of the Intermediate Lens of an Electron Microscope with the Aid of a Stigmator During Microdiffraction . . 1220
P.A. Stoyanov, Alignment of an Electron Microscope by Means of Electromagnetic Fields 1225
Yu.V. Vorob'yev, Analysis of Aberrations Due to Defects in Manufacture and in Alignment of Electron Microscopes 1229
BRIEF COMMUNICATIONS
A.V. Prosin, On the Calculation of the Bandwidth in UHF Tropospheric Scatter Propagation 1234
B.M. Minkovich, Yu.I. Davidchevskiy, On the Synthesis of an Antenna with Circular Aperture 1237
Yu.A. Il'inskiy, M.D. Karasev, Transients in a Two-Circuit Parametric Amplifier 1239
A.M. Strashkevich, Simulation and Calculation of Trajectories of Relativistic Charged Particles in Electrostatic Fields 1243
Yu.V. Troitskiy, Two-Anode Electron Gun for Electronic Microwave Devices 1245
S.N. Ivanov, Distribution of Impurities in the Region of a Welded Contract on Gallium Arsenide 1247
V.S. Fomenko, Thermionic Properties of Carbides of Hafnium and Niobium and of Borides of Scandium and Thulium 1249
CHRONICLE
A.A. Yasnopol'skaya, et al., Joint Seminar on Cathode Electronics (Nineteenth Session) 1251

Number 9

Yu.B. Kobzarev, A.Ye. Basharinov: Effectiveness of Search Algorithms Based on the Use of Trial Steps of Controlled Duration 1253
V.V. Vitkevich, A.D. Kuz'min, et al.: Radio Astronomic Observations of Soviet Space Rockets 1261
N.D. Filipp: Character of Fluctuations of a UHF Radio Signal Propagating over an Inhomogeneous Surface 1270
N.K. Kul'man, R.L. Stratonovich: Certain Optimal Devices for Detection of a Pulse Signal of Random Duration in the Presence of Noise 1279
V.V. Shirokov: Effect of Signal Fluctuations on a Receiver with AGC 1288
V.K. Turkin, G.A. Levin: On the Detection of Frequency Modulated Oscillations . . 1296
G.A. Levin, V.K. Turkin: On the Theory of Detection of Complex Frequency Modulated Oscillations 1301
V.A. Shpolyanskiy, L.S. Tyufyakin, P.P. Korsakov: Automatic Phase Control with Delay 1304
B.M. Minkovich, Yu.I. Davidchevskiy: Analysis of Antennas with Plane Apertures . . 1317
L.A. Vaynshteyn G.D. Malyuzhinets: Transverse Diffusion in Diffraction by an Impedance Cylinder of Large Radius. II. Asymptotic Laws of Diffraction in Polar Coordinates 1324

B.N. Morozov: Influence of Bending on the Properties of Periodically Diaphragmed Waveguides of Rectangular Section 1331
Yu.N. Pchel'nikov: Interaction between an Electron Beam and the Field of a Helix in the Region of an Absorbing Insert 1335
G.F. Filimonov: Excitation of a Delay Line by Means of a Periodic Sequence of Ideally Focused Electron Bunches 1341
V.N.Shevchik, A.A. Kurayev, General Dispersion Equation of a Traveling Wave Tube with Periodic Slow-Wave System 1351
A.M. Starik: Propagation of Microwave Oscillations in a Waveguide Containing the Cathode Parts of a Glow Discharge 1365
T.F. Loginova: Hollow Electron Beam of Conical Shape in a "Conical" Magnetic Field 1372
G.S. Misezhnikov, V.B. Shteynshleyger: Contribution to the Theory of a Traveling-Wave Quantum Paramagnetic Amplifier 1377
A.S. Maydankovskiy: Investigation of a Transistorized Low-Frequency Self-Oscillator 1385
A.M. Strashkevich: Investigation of Non-Gaussian Trajectories in the Field of an Electrostatic Quadrupole Lens 1392
V.N. Lutskiy: Procedure for Energy Analysis of Thermionic Electrons under Pulsed Emission Conditions 1396

BRIEF COMMUNICATIONS

V.I. Bunimovich, V.A. Morozov: Estimate of Frequency of Narrowband Signal against a White-Noise Background 1403
A.V. Prosin: Calculation of Reliability of Tropospheric Communications System in the Presence of Correlated Fading 1407
A.L. Fel'dshteyn: Cascaded Bridges 1411
V.V. Nikol'skiy: Variational Principle for Hollow Systems with Anisotropic Medium 1413
A.I. Denisov: Effect of Sectionalization on the Saturation Power of a Traveling Wave Tube 1416
T.M. Murina: Radio Spectroscope with Disk Resonator 1417
A.G. Berkovskiy, Chia Kao: Electron Focusing in the Cathode System of Photomultipliers with Semitransparent Cathodes 1419
Yu.M. Aleskovskiy, V. L. Granovskiy: Spectroscopic Determination of the Deionization Rate of Cesium Vapor in a Magnetic Field 1421

Number 10

A.I. Sharov, Ideal Reception of Optimum-Code Signals 1425
P.A. Perepelyatnik, Oscillations in an Oscillator with Delay 1430
V.P. Yakovlev, Synchronization of an Oscillator by a Weakly Modulated External Signal 1437
Yu.V. Grigor'yev, R. V. Khokhlov, Oscillator Parametrically Coupled with a Linear Network 1444
A.V. Men', Time (Spectral) Characteristics of Phase-Difference Fluctuations Occurring in the Propagation of Radio Waves in the Troposphere 1451
M.F. Bakhareva, Frequency Correlation of Amplitude and Phase of Fluctuations in the Use of a Sharply Directional Antenna 1460
Hsu Yen-Sheng, Effect of a Metallic Wall on Magnetostatic Oscillations of a Small Gyrotropic sphere 1468
B.Ye. Kinber, Diffraction of Electromagnetic Waves on a Concave Spherical Surface 1474
V.V. Kolpakov, Diffraction of Surface Electromagnetic Waves on an Impedance Step of a Circular Cylinder 1479
V.Ya. Smorgonskiy, The Determination of the Natural Frequencies of the Higher Modes in a Coaxial Cable with Elliptical Conductors 1486

Yu.N. Dnestrovskiy, D.P. Kostomarov, Concerning a Nonlinear Problem in the Theory of Electromagnetic Waves in a Plasma 1488
A.N. Didenko and L.N. Bezmaternykh, Contribution to the Design of Rectangular Waveguides Loaded with Dielectric Diaphragms 1491
V.V. Nikol'skiy, V.G. Sukhov, On the Ritz Method for Hollow Systems with Anisotropic Media 1497
L.N. Loshakov, Advisable Form of the Expression for the Coupling Coefficient in the Interaction between an Electron Beam and Spatial Harmonics of a Slow-Wave System 1505
V.B. Glasko, A.A. Zyuzin-Zinchenko, et al. Influence of Pulsations of the Cross-Section of the Electron Beam on the Noise Factor of a Traveling-Wave Tube . . . 1507
V.N. Lugovoy, Molecular Oscillator with Two Resonator Natural Frequencies within the Width of the Emission Line 1518
V.A. Fabrikov, New Principle of Microwave Amplification with Ferrites. 1524
A.I. Sokolik, Equivalent Circuits of the Deflecting Plates of a Cathode Ray Tube 1533
A.M. Strashkevich, Electrostatic Quadrupole Lens, the Field of Which Has Two Anti-Symmetry Planes and No Symmetry Plane 1538
N.Ya. Basalayeva, et al. Investigation of Some Properties of Cold Magnesium Oxide Cathodes with Self Maintaining (Molter-Type) Emission 1541
G.F. Vasil'yev, Penetration of an Electric Field into a Semiconductor 1551
L.Ya. Pervova, Determination of the Lifetime of Nonequilibrium Current Carriers in Semiconductors from the Spectral Distribution of the Noise 1553
Yu.L. Kurkin, N.S. Kurkina, Precision Transistor Amplifiers for Electronic Analogs with High Input (or Output) Resistance 1557

BRIEF COMMUNICATIONS

A.Ya. Yashkin, Connection Between the Method of Undetermined Coefficients and the Integral-Equation Method 1563
M.Ya. Mandel'shtam, Adjustable Directional Coupler with Constant Phase Shift . . . 1566
Ye.B. Zaltsman, V.E. Poyarkov, "Perturbation" of a Resonator in the H_{01n} Mode by a Cylindrical Rod 1570
O.E. Shushpanov, Coupling Coefficients for a Bent Coaxial Waveguide of Round Cross Section 1573
I.M. Bronshteyn, et al. Secondary and Photoelectronic Emission in the Adsorption of Beryllium and Silver on Barium 1575
V.N. Yakovlev, Investigation of Transistor Pulse Generators with Delayed Feedback 1577
B.V. Bondarenko, et al. Thermionic Properties of Barium Hafnates and Rhenates . . 1579
F.J. Nagy, Anomalous Volt-Ampere Characteristic of Alloyed Germanium 1582

Number 11

Yu.I. Vorontsov and K.S. Rzhevkin, Tunnel Diodes in Amplifier Circuits (Review) . . 1585
A.N. Radchenko and E.T. Mironchikov, Sequential Methods of Correcting Single and Multiple Closely-Spaced Errors in Group Codes. 1606
S.A. Akhmanov and R.V. Khokhlov, Transformation of Random Signals in Nonlinear Lines 1613
O.N. Litvinenko, Synthesis of Inhomogeneous Lines on the Basis of an Input Impedance Specified in the Form of a Rational Fraction of the Frequency 1624
P.A. Perepelyatnik, Biharmonic Oscillations in a Self-Oscillator with Delay at a Non-Synchronous Frequency Ratio. 1631
A.I. Rutkas, Chain Synthesis of a Reactance Multi-Port Network. 1637
Ya.S. Shifrin, Correlation Characteristics of the Field of a Linear Antenna. 1643
M.D. Khaskind, Diffraction of Waves on a Slot and on a Ribbon Oriented Perpendicular to an Impedance Plane. 1656
L.A. Lyubimov, G.I. Veselov, and N.A. Bei, Dielectric Waveguide With Elliptical Cross Section. 1668

V.N. Shevchik and N.I. Sinitsyn, Effect of Variation of Electron Velocities on the Operation of a Backward Wave Tube 1677
V.D. Ivanova and V.S. Mikhalevskii, Plasma Control of Frequency of a Traveling Wave Oscillator 1683
L.A. Birger, Bandwidth and Noise Figure of Tunnel-Diode Tuned Amplifier 1688
B.A. Trigubenko, B.M. Tsarev, Thermionic Properties of Hexaborides and other Interstitial Compounds 1694
I.A. Rezgol', Optimum Operating Points on the Volt-Ampere Characteristic of a Thermoelectric Converter 1699
F.M. Yablonskiy, Current Control of the Ignition of a Discharge in a Dekatron. 1706
N.A. Belova and A.N. Kovalev, Some Special Features of the Volt-Ampere Characteristics of Narrow Germanium p-n Junctions 1712
L.S. Lototskii, Comparison of Static and Dynamic Characteristics of Germanium Diodes Under Negative Bias 1717

BRIEF COMMUNICATIONS

A.V. Prosin, Transient Noise in Two-Path Radiowave Propagation 1722
A.N. Shusterovich, Concerning One Case of Determination of the Statistical Characteristics of the Phase of a Vacuum-Tube Self-Oscillator in Response to a Low-Amplitude Voltage 1727
L.I. Artemenkov and I.V. Galkin, High-Frequency Rotating Field in Cylindrical Cavity 1730
S.A. Kornilov and M.V. Lavrov, Measurement of the Power of Amplitude Fluctuations of Reflex Klystron. 1732
S.I. Molokovskii, Conditions for Obtaining Minimum Pulsations of Electron Beams Focused by a Homogeneous Magnetic Field in Systems with Partially Screened Cathode 1734

LETTERS TO EDITOR

V.G. Kononov, Storage of Noise in an Accumulator with Delayed Feedback 1736

Number 12

N.A. Esepkina et al., Investigation of the Radiation Characteristics of Highly Directional Mirror Antennas with Reflector of Alternating Profile 1739
N.A. Armand, Fluctuations of the Thermal Radiation of the Atmosphere at Centimeter and Millimeter Wavelengths 1753
V.N. Yakovlev, Use of the Method of Slowly Varying Parameters for an Investigation of Nonlinear Self-Oscillating Systems with Delay 1766
M.I. Kontorovich, V.Yu. Petrun'kin, Smallest Number of Controllable Elements in an Antenna with Electric Beam Scanning. 1774
N.A. Kuz'min, T.V. Makarov, Electromagnetic Waves in a Rectangular Cross-Shaped Waveguide. 1781
Hsu Yen-cheng, Magnetostatic Oscillations of a Small Gyrotropic Spheroid Magnetized Perpendicular to the Axis of Rotation 1790
I.P. Kotik, A.N. Sivov, Propagation of H_{0n} Modes in Annular Waveguide with Dielectric Sheath and Metal Braid 1796
L.N. Loshakov, Use of Lorentz Lemma for Approximate Calculation of the Propagation Constants in an Electronic Device such as a Tube with Transverse Interaction 1802
S.N. Kornilov, Combination Noise in a Transit Klystron. 1807
S.N. Ivanov, N.E. Skvortsov, Yu.F. Sokolov, Frequency Properties of Negatively Biased Germanium Diodes with Welded Contacts 1817
V.S. Bagaev, A.A. Zherebtsova, V.A. Pavlenko, Capacitance and Series Resistance of Germanium Diodes 1824
V.L. Bonch-Bruevich, P.S. Serebrennikov, Volt-Ampere Characteristic of Tunnel Mode 1828
L.N. Dobretsov, Concerning Thermionic Constants. 1841

A.A. Ostroukhov, Effect of Drain of Thermionic Current on the Temperature Mode of a Semiconductor Cathode 1850
M.D. Morgulis, Yu.P. Korchevoi, Physicsl Properties of the Cesium Plasma in a Thermionic Energy Converter 1859
V.P. Ignatenko, A.S. Myasinkov, Neutralization of Ion Space Charge by Electrons . . 1868

BRIEF COMMUNICATIONS

Yu.B. Sindler, Concerning the Accumulation of Noise and Fading in Radio Relay Communication Line with Long-Distance Tropospheric Propagation 1876
P.Ya. Ufimtsev, Reflection of Circularly Polarized Radiowaves by Metallic Bodies 1878
B.M. Minkovich, Symmetrical Diagrams Realized by a Round Radiating Aperture 1880
Ya.K. Trokhimenko, Dependence of the Properties of a Cavity Chain on the Displacement of the Slots in Adjacent Diaphragms 1882
CONTENTS FOR 1961 1885

ERRATUM

Volume 6, No. 4, 1961, p. 434, line 4 should read:

$$E_{x2}-E_{x1}=ik\left[l\,(H_{\xi 2}+H_{\xi 1})-\frac{i}{k}\,L\,\frac{\partial}{\partial\xi}\,(E_{y2}+E_{y1})\right]. \qquad (20)$$

RADIO ENGINEERING AND ELECTRONIC PHYSICS

Institute of Radio Engineering and Electronic Physics,
Academy of Sciences of the USSR

EDITORIAL BOARD

Editor-in-Chief: V.A. Kotel'nikov
Associate Editors: D.V. Zernov, Yu.B. Kobzarev

A.I. Berg
B.A. Vvedenskiy
I.S. Gonorovskiy
V.L. Granovskiy
L.A. Zhekulin
N.D. Devyatkov

L.N. Dobretsov
A.N. Kazantsev
S.G. Kalashnikov
P.L. Kapitsa
V.V. Migulin
A.L. Mikaelyan
A.A. Pistol'kors

A.M. Prokhorov
S.M. Rytov
V.I. Siforov
Ya.N. Fel'd
S.E. Khaykin
B.M. Tsarev

Scientific Secretary of Editorial Board: G.A. Bernashevskiy

The English Edition of Radio Engineering and Electronic Physics is mailed to subscribers within 18 weeks after the publication of the original Russian issue.

Russian electronic journals published by the
American Institute of Electrical Engineers
Translated by Royer and Roger, Inc.

Subscription rates

	Individuals		Libraries	
	$	£	$	£
Radio Engineering and Electronic Physics	28.50	10	57.00	20
Radio Engineering	14.25	5	28.50	10
Telecommunications	14.25	5	28.50	10

Royer and Roger translates and produces
the following Russian scientific journals:

Biophysics
Entomological Review
Geochemistry
Geodesy and Cartography
Izvestiya, Academy of Sciences of the USSR, Geologic Series
Pavlov Journal of Higher Nervous Activity
Problems of Oncology
Radio Engineering
Radio Engineering and Electronic Physics
Refractories
Sechenov Physiological Journal of the USSR
Soil Science
Telecommunications

Comments and inquiries regarding *Radio Engineering and Electronic Physics* and other translation journals should be sent to:

International Division
Royer and Roger, Inc.

1000 Vermont Avenue, N.W.
Washington 5, D.C.

41 East 28th Street
New York 16, New York

RADIO ENGINEERING AND ELECTRONIC PHYSICS

РАДИОТЕХНИКА И ЭЛЕКТРОНИКА

NUMBER 12 1961

CONTENTS

N.A. Esepkina et al., Investigation of the Radiation Characteristics of Highly Directional Mirror Antennas with Reflector of Alternating Profile 1739
N.A. Armand, Fluctuations of the Thermal Radiation of the Atmosphere at Centimeter and Millimeter Wavelengths 1753
V.N. Yakovlev, Use of the Method of Slowly Varying Parameters for an Investigation of Nonlinear Self-Oscillating Systems with Delay 1766
M.I. Kontorovich, V.Yu. Petrun'kin, Smallest Number of Controllable Elements in an Antenna with Electric Beam Scanning. 1774
N.A. Kuz'min, T.V. Makarov, Electromagnetic Waves in a Rectangular Cross-Shaped Waveguide. 1781
Hsu Yen-cheng, Magnetostatic Oscillations of a Small Gyrotropic Spheroid Magnetized Perpendicular to the Axis of Rotation 1790
I.P. Kotik, A.N. Sivov, Propagation of H_{0n} Modes in Annular Waveguide with Dielectric Sheath and Metal Braid 1796
L.N. Loshakov, Use of Lorentz Lemma for Approximate Calculation of the Propagation Constants in an Electronic Device Such as a Tube with Transverse Interaction 1802
S.N. Kornilov, Combination Noise in a Transit Klystron. 1807
S.N. Ivanov, N.E. Skvortsova, Yu.F. Sokolov, Frequency Properties of Negatively Biased Germanium Diodes with Welded Contacts 1817
V.S. Bagaev, A.A. Zherebtsova, V.A. Pavlenko, Capacitance and Series Resistance of Germanium Diodes 1824
V.L. Bonch-Bruevich, P.S. Serebrennikov, Volt-Ampere Characteristic of Tunnel Diode 1828
L.N. Dobretsov, Concerning Thermionic Constants 1841
A.A. Ostroukhov, Effect of Drain of Thermionic Current on the Temperature Mode of a Semiconductor Cathode 1850
N.D. Morgulis, Yu.P. Korchevoi, Physical Properties of the Cesium Plasma in a Thermionic Energy Converter 1859
V.P. Ignatenko, A.S. Myasinkov, Neutralization of Ion Space Charge by Electrons . . 1868

BRIEF COMMUNICATIONS

Yu.B. Sindler, Concerning the Accumulation of Noise and Fading in Radio Relay Communication Line with Long-Distance Tropospheric Propagation 1876
P.Ya. Ufimtsev, Reflection of Circularly Polarized Radiowaves by Metallic Bodies 1878
B.M. Minkovich, Symmetrical Diagrams Realized by a Round Radiating Aperture 1880
Ya.K. Trokhimenko, Dependence of the Properties of a Cavity Chain on the Displacement of the Slots in Adjacent Diaphragms 1882
CONTENTS FOR 1961 1885
ERRATUM 1896